



UWL REPOSITORY
repository.uwl.ac.uk

INVESTIGATIONS INTO THE DUCTILITY OF LAP JOINTS IN LOW-STRENGTH
REINFORCED CONCRETE BEAMS

Karkarna, Yakubu Mustapha (2023) INVESTIGATIONS INTO THE DUCTILITY OF LAP JOINTS IN LOW-STRENGTH REINFORCED CONCRETE BEAMS. Doctoral thesis, University of West London.

<https://doi.org/10.36828/xvqy0384>

This is the Published Version of the final output.

UWL repository link: <https://repository.uwl.ac.uk/id/eprint/10384/>

Alternative formats: If you require this document in an alternative format, please contact: open.research@uwl.ac.uk

Copyright:

Copyright and moral rights for the publications made accessible in the public portal are retained by the authors and/or other copyright owners and it is a condition of accessing publications that users recognise and abide by the legal requirements associated with these rights.

Take down policy: If you believe that this document breaches copyright, please contact us at open.research@uwl.ac.uk providing details, and we will remove access to the work immediately and investigate your claim.



INVESTIGATIONS INTO THE DUCTILITY OF LAP JOINTS IN LOW-STRENGTH REINFORCED CONCRETE BEAMS

By

Yakubu Mustapha Karkarna

A thesis submitted for the degree of Doctor of Philosophy School of
Computing and Engineering

University of West London

March 2023

Supervisors and advisory team:

Professor Ali Bahadori-Jahromi - University of West London

Dr Hamid Zolghadr Jahromi - University of Westminster

Mrs Emily Halliwell and Mr Charles Goodchild -The Concrete Centre

Abstract

The most current standardised design guidelines for tension laps originated from the Fib Model Code 2010. These guidelines have had a significant impact on the newly proposed version of Eurocode 2, set to be published in 2023. The existing Eurocode 2 detailing guidelines can result in significantly longer lap joints than earlier design guidelines, such as the replaced British Code (BS 8110-1). Furthermore, the Model Code 2010 necessitates lengthier laps than Eurocode 2.

This research describes the analytical and experimental investigations conducted at the University of West London concrete laboratory to investigate the influence of rebar laps on the ductility of lapped sections. The tests were designed specifically to evaluate the effectiveness of longer tension laps in transmitting forces between the two-lap splice rebars.

The work described in this thesis is conducted in two stages. The first stage is an experimental test conducted on simply supported reinforced concrete beams with lap splices under four points bending with varying lap lengths and two reinforcement bar types. The analyses and experimental results for all the samples are described, with the deflection at the midspan of the beam measured using a built-in AEP TC4 transducer, and the result stored in a LabVIEW-based software attached to the actuator. In addition to the in-built displacement transducer, one variable displacement transducer was placed at the centre of the bottom face of the beam to record displacement for more accuracy. The test showed that variation in lap splice length increases the stiffness and resistance of the sample. The results demonstrated how the samples' behaviour changed, when transverse cracks initially appeared as lap joint failure approached. The detailed examination of the modelled and experimental results entails a comparison of the splice length's ultimate performance with current Eurocode design recommendations.

The second section describes the numerical model, which is based on nonlinear analysis. The samples are replicas of the simply supported concrete beams. The model allows the stress-strain behaviour of structural concrete to be simulated to failure and also considers the nonlinear behaviour in compression, tension, cracking and crushing of concrete. The simulation findings were then compared to the laboratory test results. Based on the analysis conducted, it was observed that increasing the lap splices beyond 50ϕ has no additional benefit for increasing its strength.

The findings also showed that the stainless steel reinforced concrete beam deformations, which coincide with 35% and 62% of the maximum bending moment were higher than those of mild steel reinforced concrete beam. Moreover, the research also concluded that there is sufficient ductility and rotation at lap ends. However, designing the lap with a factor of 1.2 would lead to rebar congestion and unsustainable design practices in terms of sustainability.

1. Contents

1.	Introduction.....	1
1.1	Background.....	1
1.2	Research motivation	4
1.3	Research aim	5
1.4	Study scope	5
1.5	Study objectives	5
1.6	Research questions	6
1.7	Thesis structure	6
2.	Review of Lap Joint in RC beams	8
2.1	Lap joint/splices.....	8
2.2	Type of lap joints/splices.....	10
2.2.1	Mechanical Splices.....	10
2.2.2	Welded Splices.....	12
2.2.3	Lap Splices.....	13
2.3	Bond in concrete	15
2.4	Application of the theory of bond to tension lap joint	16
2.5	The use of finite Element Method in RC beams	20
2.6	Current Design methodology	22
2.6.1	Parameters affecting lap strength.....	22
2.6.2	Design models for lap joints	29
2.6.3	PTI Working Draft.....	44
2.6.4	Canbay and Frosch (2005)	45
2.7	Structural Application of stainless steel.....	47
2.7.1	Composition	47
2.7.2	Classification	48
2.7.3	The American iron and steel institute system	48
2.7.4	The European standard.....	48
2.8	Material properties	50
2.8.1	Recycle	52

2.8.2	Cost	52
2.9	Stainless steel reinforcing bars in concrete structures	52
2.9.1	Life cycle cost	53
2.9.2	Durability.....	55
2.9.3	Mechanical behaviour.....	56
2.9.4	Use of stainless-steel reinforcement	57
2.9.5	Fire behaviour	59
2.9.6	Corrosion behaviour	61
2.9.7	Bond behaviour.....	62
2.10	Analysis and summary.....	63
2.10.1	Lapped bars of different diameter.....	64
2.10.2	Interaction between shear and bond requirement.....	64
2.10.3	Location of lapped joints	66
2.10.4	Continuity of reinforcement in lap joints	68
2.10.5	Minimum confining reinforcement	74
2.10.6	Comment and summary	80
3.	Research Methodology.....	83
3.1	Research design.....	83
3.2	Health and safety considerations.....	83
3.3	Ethical Considerations	83
3.4	Laboratory Experiments.....	84
3.4.1	Details of the reinforcing bars	84
3.4.2	Casting procedure.....	84
3.4.3	Testing procedure	86
3.5	Finite element simulations with LUSAS, (2021)	94
3.5.1	Element type	96
3.5.2	Material Model	99
3.5.3	Material nonlinearity	106
3.5.4	The von Mises yield criterion.....	106
3.5.5	The Prandtl-Reuss flow rule.....	108
3.5.6	Isotropic Strain Hardening	108
3.5.7	Geometric Nonlinearity	110
3.6	Modelling of steel rebar	110

3.6.1	Embedded modelling	110
3.6.2	Distribution modelling	111
3.6.3	Discrete modelling	112
3.7	Model Interface Behaviour	113
3.8	Nonlinear solution procedure	113
3.9	Convergence criteria	116
3.10	Solution approach	117
4.	Comparative study of factors influencing tension lap joints.....	119
4.1	Introduction.....	119
4.2	Database evaluation and design models	119
4.3	Results and Discussion	121
4.3.1	Effect of lap-length to bar-diameter ratio on lap strength.....	121
4.3.2	Influence of design models on estimating bar stress	122
4.3.3	Effect of effective bond length on splice strength	124
4.3.4	Effect of bar spacing on splice strength.....	125
4.3.5	Effect of concrete strength on lap splice strength	126
4.3.6	Effect of stirrup confinement on lap splices strength	128
4.3.7	Effect of side cover on lap splice strength.....	129
4.4	Concluding remark	129
5.	Development and validation of the finite element model.....	131
5.1	Introduction.....	131
5.2	Validation of experimental results.....	131
5.3	Mesh analysis	132
5.4	Beam failure	133
5.5	Finite element model validation	142
5.5.1	Load displacement	142
5.5.2	Crack formation	144
5.6	Concluding remarks.....	144
6.	A numerical and experimental study into the tension lap joints.....	145
6.1	Introduction.....	145
6.2	Range of parameters.....	145
6.3	Methodology	146
6.4	Experimental Program	149

6.5	Finite Element Model	150
6.6	Results and Discussions.....	151
6.7	Impact of lap length on bar stress.....	153
6.8	Influence of shear links spacing	155
6.9	Bar forces versus strain	157
6.10	Concluding remarks.....	159
7.	Tension lap joints in reinforced concrete beams	161
7.1	Introduction.....	161
7.1.1	Material characteristics	162
7.2	Results and discussion.....	168
7.2.1	Load displacement behaviour.....	168
7.2.2	Deformation.....	169
7.2.3	Crack development.....	174
7.2.4	Maximum bending capacity.....	175
7.3	Tension lap joints	177
7.3.1	Strain distribution in longitudinal bars	177
7.3.2	Transverse strain distribution	180
7.4	Lapped bar stress	182
7.4.1	Lapped bar stress distributions.....	182
7.4.2	Ultimate lapped bar stresses	184
7.5	Concluding remarks.....	186
8.	Conclusions and Recommendations	187
8.1	Conclusion	187
8.2	Suggestions for future studies	191
9.	References.....	192
10.	Appendix	202

Table of Figures

FIGURE 2.1. (A) CONTACT LAP SPLICES (PREFERRED) AND (B) NON-CONTACT LAP SPLICES.....	9
FIGURE 2.2. COLD-SWAGED COUPLING SLEEVE (SOURCE: ALEANO, 2019).	11
FIGURE 2.3. SPLICING BARS BY WELDING (A) FORGING, (B) HEAD- TO HEAD, (C) LAP SPLICES (SOURCE: CRSI, 2013 AND ALEANO, 2019).	13
FIGURE 2.4. LAP SPLICES IN COLUMN (NIAMUL AND MOHAMMED, 2013).....	14
FIGURE 2.5. TEPFERS' ASSUMPTION FOR DISTRIBUTION AROUND A TENSILE LAPPED SPLICE (TEPFERS, 1980).	18
FIGURE 2.6. REYNOLDS AND BEEBY'S ASSUMPTION FOR THE DISTRIBUTION OF STRESS AROUND TENSION LAP JOINT (REYNOLDS AND BEEBY, 1982).....	19
FIGURE 2.7. SPLIT FAILURES (MODEL CODE, 2010).....	23
FIGURE 2.8. (A) INCREASING THE BOND STRESS SLIP CURVES ALONG THE BOND LENGTH AND (B) BOND STRESS OVER BOND LENGTH FOR DIFFERENT BOND LENGTHS (KRELLER, 1989).....	25
FIGURE 2.9. BOND STRENGTH CONTRIBUTION, FRICTION, ADHESION, AND INTERLOCK (MODEL CODE, 2010).	28
FIGURE 2.10. SPLITTING FAILURE MODES (REPRODUCED FROM (ELIGEHAUSEN, 1979) BASED ON (FERGUSON AND BRICENO, 1969).....	30
FIGURE 2.11. COEFFICIENT kd FOR EFFICIENCY OF STIRRUPS (SOURCE: [MODE CODE, 2010]).....	35
FIGURE 2.12. LAP AND ANCHORAGE LENGTH FOR CONCRETE CLASS C25/30 (MM) (EXTRACT FROM (BOND ET AL., 2018).....	40
FIGURE 2.13. FACE SPLITTING (LEFT), SIDE-SPLITTING (MIDDLE), AND FORCE DISTRIBUTION AT BOND FORCES (RIGHT) [ADAPTED FROM (CANBAY 2006)].....	45
FIGURE 2.14. STRESS-STRAIN CURVES FOR STAINLESS STEEL AND CARBON STEEL (BADDOO AND BURGAN, 2012).	53
FIGURE 2.15. LIFE CYCLE ANALYSIS FOR SWEDEN'S OLAND BRIDGE (MCGURN, 1998)	55
FIGURE 2.16. GATWICK BRIDGE IN AUSTRALIA (STAINLESSREBAR, 2021).....	58
FIGURE 2.17. STONECUTTERS BRIDGE (MARK, 2021).....	59
FIGURE 2.18. ALLT CHONOGLIAS BRIDGE IN SCOTLAND (STAINLESSREBAR, 2021)	59
FIGURE 2.19. COMPARISON OF CARBON STEEL AND STAINLESS-STEEL STRENGTH RETENTION FACTOR (BADDOO, 2008)	60
FIGURE 2.20. COMPARISON OF CARBON STEEL AND STAINLESS-STEEL STIFFNESS RETENTION FACTOR (BADDOO, 2008).....	60
FIGURE 2.21. CORROSION PERFORMANCE OF VARIOUS STAINLESS STEEL COMPARED TO CARBON STEEL.	62
FIGURE 2.22. DEVELOPMENT LENGTH TYPE TEST SAMPLE (JIRSA ET AL., 1995).	65
FIGURE 2.23. REDUCTION IN LAP LENGTH PERMITTED FOR EXCESS REINFORCEMENT (MODEL CODE, 1990).....	66
FIGURE 2.24. REDUCTION IN LAP LENGTH PERMITTED FOR EXCESS REINFORCEMENT, EC2 (METELLI, CAIRNS AND PLIZZARI, 2015).	67
FIGURE 2.25. REDUCTION IN LAP LENGTH PERMITTED FOR EXCESS REINFORCEMENT (ACI 318, 2011).	68
FIGURE 2.26. CHANGE IN BAR STRESS ALONG LAP (A) 100% LAPPED (B) 50% LAPPED (C) 33% LAPPED (CAIRNS, 2014).....	71
FIGURE 2.27. INFLUENCE OF PROPORTION OF BARS LAPPED AT THE SECTION ON STRESS AT MID-LENGTH OF LAP AND INFLUENCE OF PERCENTAGE (μ) OF LAPPED BARS ON JOINT POST-PEAK STRENGTH (JPPs), (METELLI ET AL., 2016).	72
FIGURE 2.28. INFLUENCE OF PROPORTION LAPPED ON LAP STRENGTH (CAIRNS AND JONES, 2012).	74
FIGURE 2.29. INFLUENCE OF STAGGERING LAPS ON LAP STRENGTH, (CAIRNS, 2011)	74
FIGURE 2.30. BURSTING STRESS AROUND THE BAR (CAIRNS AND JONES, 2012).	75
FIGURE 2.31. DIRECT STRAIN MEASUREMENTS (CHINN JAMES PHIL M., FERGUSON PHIL M., AND THOMPSON J NEILS., 1955).....	77
FIGURE 2.32. TYPICAL LOAD-DEFORMATION PLOT OF LAP CONFINED BY LINKS, $K_{TR}=2.3\%-3.9\%$ (METELLI ET AL., 2010)	78
FIGURE 2.33. WEAKNESS OF COVER CONCRETE AFTER SPLITTING CRACK FORMATION (FIB BULLETIN, 2014)	78
FIGURE 2.34. BOND DUCTILITY WITH TRANSVERSE REINFORCEMENT WELL CONFINED INTO COVER (CAIRNS AND JONES, 1996).	79
FIGURE 2.35. SPLITTING FAILURE MODES (TEPFERS, 1973).	80
FIGURE 3.1. SLUMP TEST.	84
FIGURE 3.2. SAMPLE CASTING.....	85
FIGURE 3.3. VIBRATING CYLINDER SAMPLES WITH SHAKE TABLE, (B) CYLINDERS SAMPLES IN CURING TANK.	86
FIGURE 3.4. COMPRESSIVE STRENGTH APPARATUS AND TESTED SAMPLES	87
FIGURE 3.5. ARRANGEMENT OF LOADING TEST SPECIMEN (FOUR-POINT LOADING).	88
FIGURE 3.6. EXPERIMENTAL SET-UP WITH LINEAR VARIABLE DISPLACEMENT IN POSITION.	89
FIGURE 3.7. STRESS- STRAIN GRAPHS FOR 12 MM MILD STEEL REINFORCEMENT	90
FIGURE 3.8. STRESS-STRAIN GRAPHS FOR 8 MM MILD STEEL REINFORCEMENT.	91
FIGURE 3.9. STRESS-STRAIN GRAPHS FOR 8 MM STAINLESS STEEL REINFORCEMENT.....	91

FIGURE 3.10. STRESS-STRAIN GRAPHS FOR 12 MM STAINLESS STEEL REINFORCEMENT.....	92
FIGURE 3.11. A FLOWCHART DEPICTING THE STEPS REQUIRED IN DEVELOPING THE NUMERICAL MODEL.	95
FIGURE 3.12. DETAILS OF BAR ELEMENT BAR (A) AND (B) PLANE STRESS ELEMENT QPM8 (LUSAS, 2018).	97
FIGURE 3.13. SIDE VIEW OF 2D MODEL.....	97
FIGURE 3.14. DETAILS OF BAR ELEMENT BRS3 (A) AND (B) PLANE STRESS ELEMENT HX20 (LUSAS, 2018).	98
FIGURE 3.15. <i>LOADING AND BOUNDARY CONDITION OF THE 3D MODEL</i>	99
FIGURE 3.16. DAMAGE EVALUATION FUNCTION (SOFTENING CURVE) (LUSAS, 2016).	101
FIGURE 3.17. <i>POST-FAILURE STRESS-STRAIN RELATIONSHIP (LUSAS, 2016)</i>	103
FIGURE 3.18. ISOTROPIC HARDENING MODEL USED IN THE NONLINEAR MATERIAL MODEL (VERSION, 2014).....	109
FIGURE 3.19. EMBEDDED REINFORCING BAR ELEMENT: IN THE LOCAL AND GLOBAL COORDINATE SYSTEM (A) AND (B) (LUSAS, 2014).	111
FIGURE 4.1. INFLUENCE OF LAP LENGTH TO BAR DIAMETER RATIO ON MAXIMUM BAR STRESS MEASURED IN THE TEST.	122
FIGURE 4.2. COMPARISON OF MAXIMUM BAR STRESS IN TEST TO THE CALCULATED BAR STRESS ACCORDING TO FIB BULLETIN 72 (A) AND MODEL CODE (2010) (B).	124
FIGURE 4.3. EFFECTIVE BOND LENGTH AGAINST SPLICE STRENGTH.	125
FIGURE 4.4. EFFECT BAR SPACING ON THE SPLICE STRENGTH.	126
FIGURE 4.5. INFLUENCE OF COMPRESSIVE STRENGTH ON THE SPLICE STRENGTH (A) FIB BULLETIN 72 AND (B) MODEL CODE 2010.	127
FIGURE 4.6. INFLUENCE STIRRUP CONFINEMENT ON THE SPLICE STRENGTH.	128
FIGURE 4.7. EFFECT OF SIDE COVER ON SPLICE STRENGTH.	129
FIGURE 5.1. DETAILS REINFORCEMENT AND GEOMETRY USED IN VALIDATING THE STUDY.	131
FIGURE 5.2. MESH SENSITIVITY ANALYSIS FOR EC2 BEAM WITH LAP.	133
FIGURE 5.3. EXPERIMENTAL AND ANALYTICAL FAILURE FOR CONTROL SAMPLE (A) AND (B).....	135
FIGURE 5.4. EXPERIMENTAL AND ANALYTICAL FAILURE FOR 30Ø LAP SAMPLE (A) AND (B).	137
FIGURE 5.5. EXPERIMENTAL AND ANALYTICAL FAILURE FOR 40Ø LAP SAMPLE (A) AND (B).	139
FIGURE 5.6. EXPERIMENTAL AND ANALYTICAL FAILURE FOR 50Ø LAP SAMPLE (A) AND (B).	140
FIGURE 5.7. EXPERIMENTAL AND ANALYTICAL FAILURE FOR EC2 CALCULATED LAP (62Ø) SAMPLE (A) AND (B).....	142
FIGURE 5.8. LOAD DISPLACEMENT GRAPHS FOR EXPERIMENTAL BEAMS	143
FIGURE 5.9. LOAD DISPLACEMENT GRAPHS FE.	143
FIGURE 6.1. TYPICAL LABORATORY FOUR-POINT LOADING ARRANGEMENT.	147
FIGURE 6.2. DETAILS OF CONCRETE MATERIALS AND CASTING.	150
FIGURE 6.3. DETAILS OF BEAM END ELEVATION (A), SIDE ELEVATION (B), AND (C) REINFORCEMENT LAYOUT.....	151
FIGURE 6.4. LOAD VERSUS DISPLACEMENT RESPONSE OF THE CONTROL BEAMS.....	152
FIGURE 6.5. INFLUENCE OF LAP LENGTH-TO-BAR DIAMETER RATIO AND CONCRETE GRADE ON LAPPED BAR STRESS (A) AND (B).....	154
FIGURE 6.6. EFFECT OF ZERO SHEAR SPAN DISTANCE ON CONCRETE AND BAR STRESS.	155
FIGURE 6.7. EFFECT OF SHEAR LINK SPACING ON BAR STRESS AND CONCRETE GRADE.	156
FIGURE 6.8. EFFECT OF LAP LENGTH TO BAR DIAMETER RATIO ON BAR FORCE AND STRAIN.....	158
FIGURE 6.9. EFFECT OF CONCRETE GRADE ON BAR FORCE.	158
FIGURE 7.1. BEAM SAMPLES CONFIGURATION INCLUDING (A) THE GEOMETRICAL AND REINFORCEMENT DETAILS AND (B) REINFORCEMENT ARRANGEMENT AND FORMWORK.	165
FIGURE 7.2. LOAD DISPLACEMENT GRAPHS FOR MILD STEEL AND STAINLESS STEEL	167
FIGURE 7.3. REINFORCEMENT STRAIN DISTRIBUTION SAMPLE 30Ø, 40Ø, 50Ø, AND 62Ø [EC2] LAPS	179
FIGURE 7.4. REBAR STRAIN DISTRIBUTIONS ALONG THE LAP SPLICE 30Ø, 40Ø, 50Ø, AND 62Ø [EC2].....	182
FIGURE 7.5. REBAR STRESS DISTRIBUTIONS ALONG THE LAP SPLICE 30Ø, 40Ø, 50Ø, AND 62Ø [EC2].....	184
FIGURE 7.6. REINFORCEMENT STRESS DISTRIBUTION SAMPLE 30Ø, 40Ø, 50Ø, AND 62Ø [EC2] LAPS.....	186
FIGURE 10.1. REBAR STRAIN DISTRIBUTION ALONG LAP SPECIMEN 40Ø	202
FIGURE 10.2. REBAR STRESS DISTRIBUTION ALONG LAP SPECIMEN 30Ø	203
FIGURE 10.3. REBAR STRAIN DISTRIBUTION ALONG LAP SPECIMEN 40Ø	204
FIGURE 10.4. REBAR STRESS DISTRIBUTION ALONG LAP SPECIMEN 40Ø	206
FIGURE 10.5. REINFORCEMENT STRAIN DISTRIBUTION SAMPLE 40Ø.....	207
FIGURE 10.6. REINFORCEMENT STRESS DISTRIBUTION SAMPLE 40Ø LAPS	208
FIGURE 10.7. REBAR STRAIN DISTRIBUTION ALONG LAP SPECIMEN 50Ø	209
FIGURE 10.8. REBAR STRESS DISTRIBUTION ALONG LAP SPECIMEN 50Ø	210

FIGURE 10.9. REINFORCEMENT STRAIN DISTRIBUTION SAMPLE 50Ø LAPS.....	211
FIGURE 10.10. REINFORCEMENT STRESS DISTRIBUTION SAMPLE 50Ø LAPS.....	213
FIGURE 10.11. REBAR STRAIN DISTRIBUTION ALONG LAP SPECIMEN 62Ø[EC2 DESIGN RECOMMENDATION].....	214
FIGURE 10.12. REBAR STRESS DISTRIBUTION ALONG LAP SPECIMEN 62Ø[EC2 DESIGN RECOMMENDATION].....	215
FIGURE 10.13. REINFORCEMENT STRAIN DISTRIBUTION SAMPLE 62Ø [<i>EC2 design recommendation</i>] LAPS.....	216
FIGURE 10.14. REINFORCEMENT STRESS DISTRIBUTION SAMPLE 62Ø [<i>EC2 design recommendation</i>] LAPS.....	217

List of Tables

TABLE 2.1. COEFFICIENT η_4	35
TABLE 2.2. BOND SLIP RELATIONSHIP BASED ON (MODEL CODE, 2010).....	37
TABLE 2.3 SPLICED LENGTH COEFFICIENT FOR THE PERCENTAGE OF LAPPED BARS AND THE PROVIDED REINFORCEMENT (ACI COMMITTEE 318, 2011).	43
TABLE 2.4 GERMAN NATIONAL ANNEX FOR THE PERCENTAGE OF SPLICED BAR UNDER TENSION BASED ON (NA/EC2).....	44
TABLE 2.5. THE CHEMICAL COMPOSITION OF VARIOUS STAINLESS-STEEL GRADES (MARKESSET ET AL.,2006).....	49
TABLE 2.6. MECHANICAL PROPERTIES OF STAINLESS STEELS GRADES (EN 10088-2, 2014).....	51
TABLE 2.7. MECHANICAL PROPERTIES OF STAINLESS-STEEL REINFORCEMENT (MCGEE, 2017).....	57
TABLE 3.1. AVERAGE COMPRESSIVE STRENGTH OF THE CYLINDERS.....	86
TABLE 3.2. AVERAGE RESULTS FOR MILD STEEL REINFORCING BAR (12 MM).....	90
TABLE 3.3. AVERAGE RESULTS FOR MILD STEEL REINFORCING BAR (8 MM).....	92
TABLE 3.4. AVERAGE RESULTS FOR STAINLESS STEEL REINFORCING BAR (8 MM).....	93
TABLE 3.5. AVERAGE RESULTS FOR STAINLESS STEEL REINFORCING BAR (12 MM).....	94
TABLE 4.1. SUMMARY OF FILTERED SPECIMENS CONSIDERED IN THIS STUDY.....	121
TABLE 5.1. MATERIAL PROPERTIES OF REINFORCED CONCRETE BEAMS.....	132
TABLE 6.1. PARAMETERS STUDIES.....	146
TABLE 6.2. CONCRETE MIXTURE.....	150
TABLE 7.1. MEAN COMPRESSIVE OF THE CYLINDERS.....	162
TABLE 7.2. BEAM TEST RESULTS AND MATERIAL PROPERTIES.....	163
TABLE 7.3. BEAM TEST RESULTS AND MATERIAL PROPERTIES.....	164
TABLE 7.4. DESIGN DEFLECTION VALUES.....	173

List of notations:

A_s	Cross sectional area
E	Young modulus of elasticity
c_{min}	Minimum concrete cover
c_{max}	maximum cover concrete
d	effective depth
r	radius
s_t	longitudinal spacing of confining reinforcement (mm)
u	perimeter
s_{st}	Transverse bar spacing
A_{st}	cross-sectional area of one leg of a confining bar (mm^2)
n_{st}	number of stirrups in the lap length
l_o	design lap length
n_l	shear link leg number
k_m	coefficient of efficiency of shear link
f_{cm}	measured concrete cylinder compressive strength
l_b	anchorage length
k_{tr}	density of shear link
\emptyset	diameter
n_b	number of lapped bars at a section
f_y	yield stress
f_{bd}	design bond strength
$f_{st,0}$	average stress formed by bond for the base conditions of confinement with
p_{tr}	average compression stress perpendicular to the potential splitting failure surface
f_{stm}	mean estimated stress developed in the bar
$f_{bd,0}$	basic bond strength
f_c	compressive strength
n_1	coefficient taken 1.75 for ribbed bars (including stainless and galvanised reinforcement)
n_2	casting position of the bar during concreting
n_2	good bond condition.
γ_{cb}	partial safety factor for bond
α_t	coefficient for the bar diameter;
n_3	represent the bar diameter:
n_4	characteristics strength of steel reinforcement that is being lapped
n_g	number of items of confining reinforcement within the bond length
$A_{s,cal}$	area of reinforcement
n_t	number of stirrups crossing a potential splitting failure surface at a section

$A_{s,prov}$	area of reinforcement provided
n_g	number of items of confining reinforcement within the bond length
$l_{b,min}$	minimum accepted design value for lap length
σ_{sd}	design stress of the bar
f_{yd}	design yield strength of the reinforcement
$A_{s,ef}$	actual area of reinforcement
$A_{s,cal}$	required area of reinforcement
$l_{0,min}$	minimum accepted design value for lap length
Ω_{cyc}	effect of cyclic loading
Ω_{cr}	effect of longitudinal cracking
Ω_y	effect of yielding
$\Omega_{p,tr}$	effect of transverse pressure
n_1	coefficient associated with the bar position and bond conditions during concreting
f_{ctd}	concrete design strength
α_{ct}	coefficient which takes into consideration the loading and long-term effect of tensile strength
γ_c	partial safety factor
$l_{b,rqd}$	required basic anchorage length
α_1	coefficient associated to bars shape
α_2	coefficient associated cover concrete
α_3	coefficient of shear link if present
k	accounts for the transverse reinforcement's efficacy in relation to its position inside the section
ψ_c	coefficient for coated reinforcement (for uncoated bars $\psi_c = 1.0$)
λ	Coefficient of transverse reinforcement along the anchorage length
α_1	proportion of bar lapped
ρ_1	proportion of lapped bars at a section
ψ_s	coefficient for bar diameter (1.0 for bars ≥ 22 mm, otherwise 0.8)
ψ_t	coefficient for bond (for good bond condition $\psi_t = 1.0$)
k_{tr}	shear link index
σ_{ctd}	design value of the mean compression stress perpendicular to the potential splitting plane
K_{conf}	effectiveness factor
θ	inclination of struts commencing at the rib flanks (20 ° provided optimal results)
F_{st}	splitting resistance by a shear link [kip]
F_{split}	splitting resistance by cover concrete along the lap length [kip]
F_{sp}	bursting force perpendicular to crack plane
f_b	bond force transmitted along the transmission length
m	bending moment
ρ	reinforcement ratio

f_s	fracture stress
F_l	longitudinal force transmitted by bond
J_1	first deviatoric stress variant
J_2	the second deviatoric stress variant
J_3	third deviatoric stress variant
σ^-	von Mises stress
$\delta\varepsilon$	iterative strain
$\delta\varepsilon_p$	iterative plastic strain
$\delta\varepsilon_e$	elastic strain increment
ν	poison's ratio
G	modulus of shear
$\partial\sigma$	iterative stress
k	amount of work done during plastic deformation
$\delta\varepsilon_p$	iterative local plastic strain
δk	iterative hardening parameter
D_{ep}	elasto-plastic modulus matrix
D	damage parameter
H	slope of the curve at a certain stress
$\Delta\delta_n$	incremental displacement
δ_n	current displacement
Δp_n	load increment
K_T	tangent matrix of stiffness
g_n	residual correctness
p_n	applied load
Δp_n	displacement load
g_1	out-of-balance force

Acknowledgements

First and foremost, I would like to thank my principal supervisor, Professor Ali Bahadori-Jahromi, for his extensive knowledge, and encouragement. His support was invaluable during the research and laboratory work of this thesis. I also wish to thank Dr Hamid Zolghadr Jahromi, my second supervisor, for his excellent advice, guidance, and motivation throughout my research. This thesis would not have been possible without their feedback and continuous support.

I would like to thank Mrs Emily Halliwell and Mr Charles Goodchild, for their invaluable comments, and insightful suggestions for this research. Despite their commitments, they often take a great deal of time to discuss technical issues together.

Exceptional thanks to my parents Prof. Mustapha and Maimunat for their encouragement and endless support, without them, I would not have been able to accomplish this. Last but not the least, many thanks to all my colleagues and friends for their kindness and encouragement.

List of Publications

Journal papers:

- Karkarna, Y.M., Bahadori-Jahromi, A., Jahromi, H., Bonner, E. and Goodchild, C.(2020) *Comparative study of factors influencing tension lap splices in reinforced concrete beams*. Advances in Concrete Construction, 10(4), pp.279-287
- Karkarna, Y.M., Bahadori-Jahromi, A., Jahromi, H., Bonner, E. and Goodchild, C.(2023) *An experimental and analytical investigation into reinforced concrete beams with lap joint*. Engineering Future Sustainability Journal.

Book Chapter

- Karkarna, Y.M., Ali Bahadori-Jahromi, Hamid Zolghadr Jahromi, Emily Halliwell, and Musab Mohammad Rabi (2022). In: H. M. Saleh, M.M. & A.I. Hassan, eds. Reinforced Concrete Design with Stainless Steel. London: TechOpen.

Journal drafted:

- Karkarna, Y.M., Bahadori-Jahromi, A., Jahromi, H., Bonner, E. (2022) Comparative study of mild and stainless steel with laps splices, Advanced cement-based materials. London.

Abstract submission:

- Karkarna, Y.M., Bahadori-Jahromi, A., Jahromi, H., Bonner, E. Comparative study of stainless steel and mild steel with lap splices in reinforced concrete. The 31st Biennial National conference of the Concrete Institute of Australia.

1. Introduction

1.1 Background

Reinforced concrete beams are commonly used in construction due to their ability to withstand bending moments and support loads. In many beam designs, lap joints are employed to connect reinforcement bars, ensuring structural integrity and load transfer. The lap joint length, which refers to the distance over which the reinforcement bars overlap, is a critical parameter that directly influences the bond strength and overall performance of the beam. Laps are essential in reinforced concrete beams for several reasons. Firstly, laps facilitate the transfer of tensile forces across the beam's length, ensuring that load-bearing capacity is distributed effectively. By overlapping reinforcing bars, the laps enable the development of continuity and reduce the risk of structural failure under applied loads. This continuity is particularly critical in large-span structures or areas subjected to significant bending moments and shear forces. Understanding the behavior of laps is crucial for justifying their use in reinforced concrete beams. Laps experience a range of forces and deformations during loading conditions, and their behavior directly impacts the overall performance of the beam. One key aspect of lap behavior is the transfer of tensile forces between the overlapping bars. When subjected to tension, the bars engage in bond stress distribution across the lap length, ensuring load transfer and preventing bar slippage. This bond stress distribution is critical for maintaining the structural integrity of the beam. Another important consideration is the ductility of laps. Ductility refers to the ability of a material or structural element to undergo substantial plastic deformation before failure. In the case of laps, sufficient ductility ensures that the beam can undergo plastic deformations beyond the lap length, preventing brittle failure and enhancing overall structural safety. The behavior of laps, including their ability to provide ductility and resist crack propagation, is influenced by factors such as the type and quality of reinforcing bars, concrete strength, and lap length.

The determination of an appropriate lap length is crucial for the effective performance of reinforced concrete beams. The lap length is influenced by various factors, including the design requirements, applied loads, and structural configurations. The primary justification for specifying a particular lap length is to ensure adequate development length, which

allows the reinforcing bars to develop their full tensile strength within the concrete beam. Insufficient lap length can lead to reduced load transfer capacity, increased risk of bar slippage, and compromised structural integrity. Conversely, excessively long laps can result in congestion of reinforcing bars, increased costs, and potential constructability issues. Furthermore, the choice of lap length is closely related to the desired level of ductility. Longer lap lengths can enhance the ductility of the beam by providing a greater zone for plastic deformation and rotation. However, it is important to strike a balance between lap length, ductility, and constructability considerations to ensure a practical and efficient design.

Numerous studies have investigated the effects of lap joint length on the behavior and performance of reinforced concrete beams. The optimal lap joint length is crucial to ensure sufficient bond strength and prevent premature failure or excessive deflection in the beam. One of the primary factors affecting the choice of lap joint length is the bond strength between the reinforcement bars and the surrounding concrete. The bond strength plays a vital role in transferring loads from the reinforcement bars to the concrete, enabling the beam to resist bending and shear forces effectively.

Several standards and codes provide guidelines for determining the minimum lap joint length based on various factors, including the diameter of the reinforcement bars, the concrete strength, and the specific design requirements. For example, Eurocode 2 offers designers three possibilities: (a) to stagger the laps to increase the residual strength, (b) to provide confinement reinforcement to increase the deformation capacity, (c) to design the lap for $1.2 \sigma_{sd}$ in order to make sure that brittle failures occur only after large plastic deformations outside the lap length. However, Eurocode 2 further recommends that where tension laps have to be located across plastic hinge location, tension laps may be designed for design strength (σ_{sd}) if they are staggered so that the area of lapped bars $\leq 35\%$ of the total cross-section area of the reinforcing steel bars in linear members such as beams, and columns, tension laps should be designed for $1.2 \sigma_{sd}$. The issue is that 35% is impractical, and some UK practitioners believe that there is sufficient ductility at the lapped section and increasing the laps' length causes rebar congestion and makes the design costly. This research has been performed as a direct consequence of the above-mentioned issues. It is essential to note that the minimum lap joint length specified by codes may not always

ensure optimal bond strength and structural performance. Factors such as concrete quality, curing conditions, and construction practices can influence the bond behavior and may require adjustments to the recommended lap length. Furthermore, researchers have conducted experimental investigations and numerical simulations to evaluate the influence of lap joint length on the behavior of reinforced concrete beams. These studies have examined various aspects, including bond stress distribution, bond slip, cracking behavior, and load-carrying capacity. The results of these studies have provided valuable insights into the relationship between lap joint length and beam performance. For instance, Smith and Johnson (2008) conducted experimental tests on reinforced concrete beams with different lap joint lengths and observed that increasing the lap length significantly improved the bond strength and load-carrying capacity of the beams. Similarly, Zhang et al. (2015) used finite element analysis to investigate the effect of lap joint length on crack propagation and observed that shorter lap lengths resulted in larger crack widths and reduced beam stiffness.

In recent years, advancements in computational modeling techniques, such as finite element analysis, have allowed for more detailed and accurate predictions of the behavior of reinforced concrete beams with varying lap joint lengths. These numerical models can provide valuable insights into the bond behavior, stress distribution, and overall performance of the beams under different loading conditions.

One might wonder which coefficient should be used in the equation for laps according to Fib Bulletin 72 (2014), elaborated by Fib task group 2.5 for laps to safely estimate the required bond length. Cairns and Eligehausen (2014) recently discovered that the lap design following Eurocode 2 has a lower safety of margin than expected. Even though many earlier national codes required shorter lap lengths, there has never been a major lap failure. Any increase in lap lengths is a concern to the UK designers who already find the reinforcement detailing of the current Eurocode 2 unsustainable in terms of project cost and complexity of construction.

Depending on the code consulted, the factor to apply to a 'base' bond length to get the design lap length differs in Figure 1.1. To encourage the designers to stagger the locations of lapped bars, the ACI committee 318 (2011) states that the splice should be at 1.3 times the

anchorage length when the percentage of bars lapped is greater than 50%. Eurocode 2, on the other hand, is more conservative, requiring the lengths to be increased by up to 1.5 times the anchorage length, based on the proportion of bars spliced at the location. When all bars are spliced at the same section in Fib Model Code (2010), the lap length required could be up to twice the base anchorage.

1.2 Research motivation

The motivation for this research stems from significant concerns raised by industry professionals regarding the practical implementation of existing Eurocode 2 detailing guidelines for reinforced concrete construction. The adherence to these guidelines has been associated with various challenges such as sustainability implications, increased costs, and congestion of reinforcement, without clear justification. Consequently, this PhD project aims to address the ongoing disagreement between UK practitioners and continental professors regarding the design of lap joints in reinforced concrete, particularly in the context of revising Eurocode 2.

Currently, Eurocode 2 clause 11.5.2(4) recommends designing laps near plastic hinges or sections expected to experience maximum moments with a factor of 1.2 times the design strength (σ_{sd}). This provision intends to ensure that brittle failures occur only after significant plastic deformations outside the lap length. While some academics support this recommendation, UK practitioners argue that sufficient ductility exists at the lapped section and that increasing lap lengths leads to rebar congestion, higher costs, and unsustainable design practices.

Research conducted by Micallef et al. (2017) and Tarquini et al. (2019) has suggested the presence of rotation capacity and ductility in lap joints using reinforcing bars of sizes 40Ø and 60Ø. However, the question arises: is this rotation and ductility adequate at the lap joints? Furthermore, does it enable the statistical analysis of lap lengths to be based on multiple lap locations instead of relying solely on single-lap location failure?

The novelty of this research lies in investigating the influence of rebar laps on the ductility of the lapped section and determining the minimum lap length required for the development of rebar rotation prior to the formation of the plastic hinge. To achieve this, a

comprehensive approach combining laboratory testing and finite element modeling was employed. Laboratory tests were conducted on a series of beams subjected to four-point bending to examine the ductility along the lap joints. Subsequently, finite element modeling was carried out using LUSAS software to validate the laboratory findings and enhance the understanding of the lap joint behavior.

The outcomes of this study will have direct implications for the construction industry. By identifying the optimal lap length that maintains structural integrity while reducing costs, the research contributes to the development of more economical concrete structures. Additionally, it provides insights into improving design practices and potentially revising the Eurocode 2 guidelines, bridging the gap between theoretical recommendations and practical implementation in reinforced concrete construction.

1.3 Research aim

The research aimed to advance the understanding of lap joint behavior in reinforced concrete beams and contribute to the development of more efficient and reliable design guidelines in the field of structural engineering.

1.4 Study scope

The scope of this research was focused on investigating the ductility of lap splice tension bars in low-strength concrete beams, specifically those lapped at the same section. However, certain aspects were excluded from this investigation due to limited time. These included the analysis of compression lap bars and the staggering of lap splices. While these were important considerations in lap joint design, they were not addressed in this particular study.

1.5 Study objectives

1. Undertook a critical review of currently available literature on lap joints in reinforced concrete beams. This objective was crucial for establishing a strong foundation of knowledge and understanding of the subject matter. It helped identify gaps, and areas requiring investigation.
2. Developed a holistic methodology for evaluating lap joint performance within structural elements. This objective aimed to establish a systematic approach that considered various factors influencing lap joint behavior, including material properties, loading conditions, and structural configurations. The methodology

provided a robust framework for assessing the effectiveness and reliability of lap joints in practice.

3. Investigated the impact of lap joint length on structural performance under ultimate load. This objective helped determine the relationship between lap joint length and key performance indicators such as ductility, load-carrying capacity, and failure modes. By understanding this relationship, optimal lap joint lengths were recommended to enhance structural performance.
4. Investigated and discussed the potential impact of existing regulations on lap joint design. This objective aimed to assess the compatibility of current design codes, such as Eurocode 2, with the findings of the study. It identified areas where revisions or additional provisions may be necessary to optimise lap joint design.
5. Investigated the current state of lap joint design in UK buildings and how it could potentially be affected by changes in the design code. This objective sought to understand the prevailing approaches, challenges, and limitations faced by practitioners in lap joint design. It provided insights into the practical implications of implementing revised design codes and the necessary adaptations required in construction practices.

1.6 Research questions

- What is the effect of increasing lap length on the ductility of the lapped section?
- What is the impact of the ultimate load on the structural performance of lap joints?
- What is the minimum lap length for rotation to occur?
- What are the impacts of current regulations on lap joint design?

1.7 Thesis structure

The analytical and experimental investigations into the ductility of lap joints in reinforced concrete beams are addressed in this thesis.

This thesis contains chapters one to eight. Chapter one introduced the background and motivation of the study. It further highlights the research aims, objectives, questions, and significance. Chapter two introduced and reviewed the principles of lapped joints/splices in reinforced concrete elements, as well as the fundamental concept of a bond between ribbed reinforcing bars and concrete. General trends of factors affecting bond strength as

well as the application of the theory of bond to tension lap joint were discussed. Moreover, the most important parameters affecting lap strength and the expressions for lap strength were also described. Lastly, lap joint detailing issues were highlighted and analysed. Chapter three addressed the research design, ethical concern, and research paradigm. Moreover, the method employed in this study to carry out laboratory experiments and finite element modelling using LUSAS software was described. Chapter four explained the model development and validation, the material behaviour, mesh type, solution approach, loading and boundary condition for the finite element model. Moreover, the reason for choosing a 3D model over 2D is discussed and justified. Lastly, the chapter also discusses the numerical model's validation using the laboratory experimental results. Chapter five examines the influence of various parameters such as concrete cover, lap splice length, shear links confinement and concrete strength on the structural performance of lap splices based on an extensive experimental database of laps and anchorage, which is gathered by Task Group 2.5. A parametric study was conducted in chapter six to investigate the impact of varying lap joint lengths on the structural performance of RC beams under ultimate load by using the LUSAS finite element software (LUSAS). The variables utilised in this computational study conforming to Eurocode 2 are the reinforcement bar diameter (d_b), concrete design tensile strength (f_{ctd}), concrete cover (c_d) and yield strength of the steel (f_y). Chapter seven evaluates and compares the behaviour of stainless and mild steel reinforced concrete with and without lap splices. The chapter further described and analysed the stress and strain distribution of tension lap joints.

2. Review of Lap Joint in RC beams

2.1 Lap joint/splices

Transportation constraints and the construction process of reinforced concrete structures require steel rebars to be spliced in some sections. While alternate rebar coupler systems such as welded bars, loop joints and mechanical splices are available, they are not extensively employed. In all reinforced concrete designs, it is often necessary for practical reasons, e.g., handling long lengths of bars and/or changing bar diameter, to provide reinforcement in several sections rather than continuous length. When this is necessary, it is important that the force is transferred consistently from one section of the bar to the next adjacent continuing section. This transfer may be achieved by lap length/joint, welding, or joining them with mechanical connectors like Unitec (CARES, 2019).

The stress of reinforcing bars embedded in concrete is transferred to concrete in reinforced concrete structures through the steel and concrete bond. As a result, sufficient lap splices and development lengths should be provided to develop the desired strength of reinforcing bars. The bonded length of reinforcing bars that are lap spliced is called lap splice length or lap length, whereas the bonded length of reinforcing bars that are not spliced with another reinforcing bar is called development length.

In the construction industry, lap splices of reinforcing bars are frequently required because of the requirements at construction joints, changes from larger bars to smaller bars, and the limitation of bar length. Although steel manufacturers often stock reinforcing bars from 6m to 18m in length, it is usually convenient to work in the field with bars of shorter length, therefore requiring rather frequent use of lap splices.

The usual traditional method of lap splicing of bars is simply by lap splicing them one over the other. Overlapped bars may be either placed in contact or non-contact, as shown in Figures 2.1(a) and 2.1(b), with contact lap splices (Figure 2.1(a)) being more favoured for practical reasons because the bars can be tied together and due to ease of fixing. Such bars also hold their position better against displacement during the placing of the concrete.

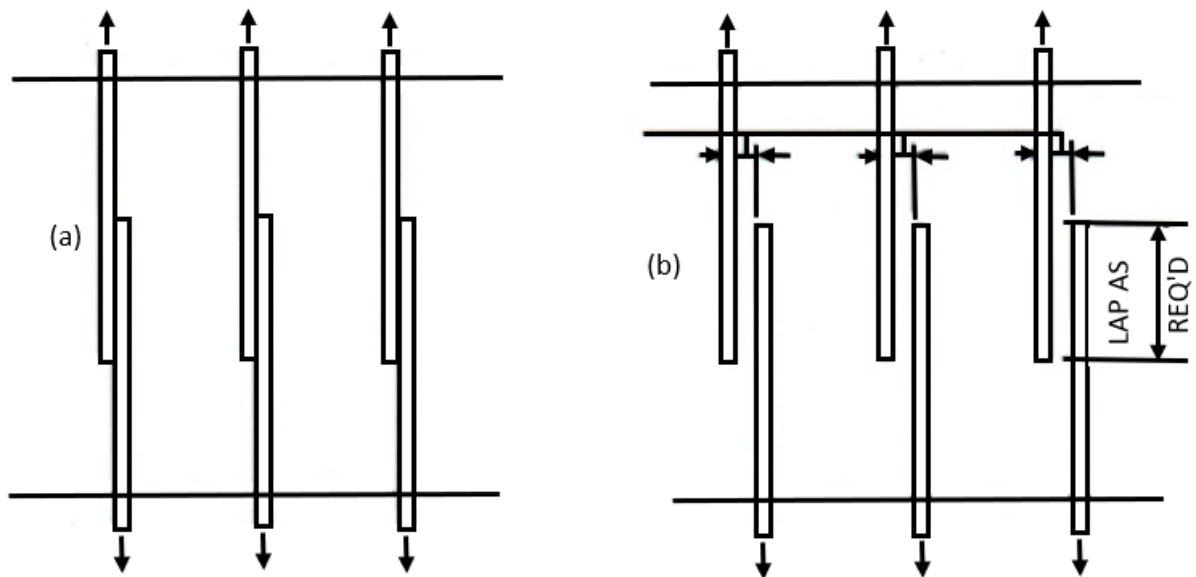


Figure 2.1. (a) contact lap splices (preferred) and (b) non-contact lap splices.

Even though lap splices are simple to make, the resulting stress transfer is complicated and can lead to local cracks in the vicinity of the bar ends. Bond stresses play a vital role in transferring forces from one bar to another. According to Park and Pauley (1975), adhesion stress is the shear stress on the concrete surface and the place where the load is transferred between the surrounding concrete and the reinforcing steel, thus changing the reinforcing steel stress. The crucial parameters that impact the bond strength between concrete and steel reinforcing bars are well-known. Important among these parameters are splice length, compressive strength, concrete cover, the diameter of the reinforcing bar, type of concrete and the number of stirrups in the lap joints (David *et al.*, 1996; Zuo & Dawin, 2000).

Existing design standards, such as BS EN 1992-1-1 (2004), ACI Committee 408 (2003), Fib Model Code (2010), and ACI committee 318 (2011), establish criteria for lap splice and development lengths based on experimental findings from the splice test (ACI Committee 408, 2003). The design codes, however, base their development length ideal on the achievable mean bond stress across the embedment length (ACI committee 318, 2011). Significant efforts have been made to achieve more economical and accurate design. Hwang and Yi (2017) proposed a nonlinear bond stress distribution model to estimate tension bar development length, which addressed the bond stress distribution along the development length and the bond strength per unit length, and the model was also applied to the development length of compression bars, headed bars and hooked bars. Metelli *et al.*

(2022) performed nonlinear regression analysis using existing splice test results with a transverse bar, cover concrete, clear bar spacing, bar diameter and concrete strength as the main factors. Canbay and Frosch (2005) used split tension cracking failure to investigate the bond strength effects of transverse bars and concrete cover. Zuo and Darwin (2000) examined the influence of bar rib area on bond stress and recommended using $\sqrt[4]{f'_c}$ instead of $\sqrt{f'_c}$, which was adopted in the ACI Committee 408 (2003) guidelines.

2.2 Type of lap joints/splices

There are three methods to splice bars in a reinforced concrete structure: welded splice, mechanical splices, and lap splices. Of the three methods, lap splicing/joint is usually preferred because it is the most common and least expensive compared to the others.

2.2.1 Mechanical Splices

Mechanical splices, as shown in Figure 2.2, normally comprise some sort of sleeve splice, which fits over the ends of the bars to be joined and into which a metallic grout filler is placed to interlock the grooves inside the sleeve with the bar deformations. From the viewpoint of stress transfer, good mechanical connectors are next best to welded splices. However, they do have the disadvantage that some slippage may occur in the connections; as a result, there may be some concrete cracks in the area of the splices (McCormac, 2005).

Three major parameters can be considered for the use of mechanical splices: (i) Number of splices in a section; splicing all the bars at the same location can lead to poor behaviour under cyclic load, (ii) Coupler's shape: all the investigations conclude that high, long, and slender couplers can lead to inappropriate performance by reducing seismic parameters such as load capacity and ductility, (iii) Type of splice: in terms of plastic hinge location, strain capacity and ductility of reinforced concrete elements, shorter couplers may provide more appropriate outcomes than slender and long couplers.

In mechanically spliced bars, failure might happen in the bar-coupler bond or the coupler. The latter failure type might be caused by the brittle material of the coupler. The couplers crack and fail when the spliced bars are subjected to cyclic or monotonic tensile load. Coupler failure under tension is shown in Figure 2.2. Failure of the bar-to-coupler bond results in the bar sliding in the coupler sleeve, resulting in longitudinal cracks in the reinforcing bars. This type of failure happens when the sleeves or bars are not correctly

positioned. Parameters such as inadequate pressure and bar sleeve (in swaged couplers), length and depth of threads in both bars, and inappropriate screws in shear screw couplers can lead to bond failure.

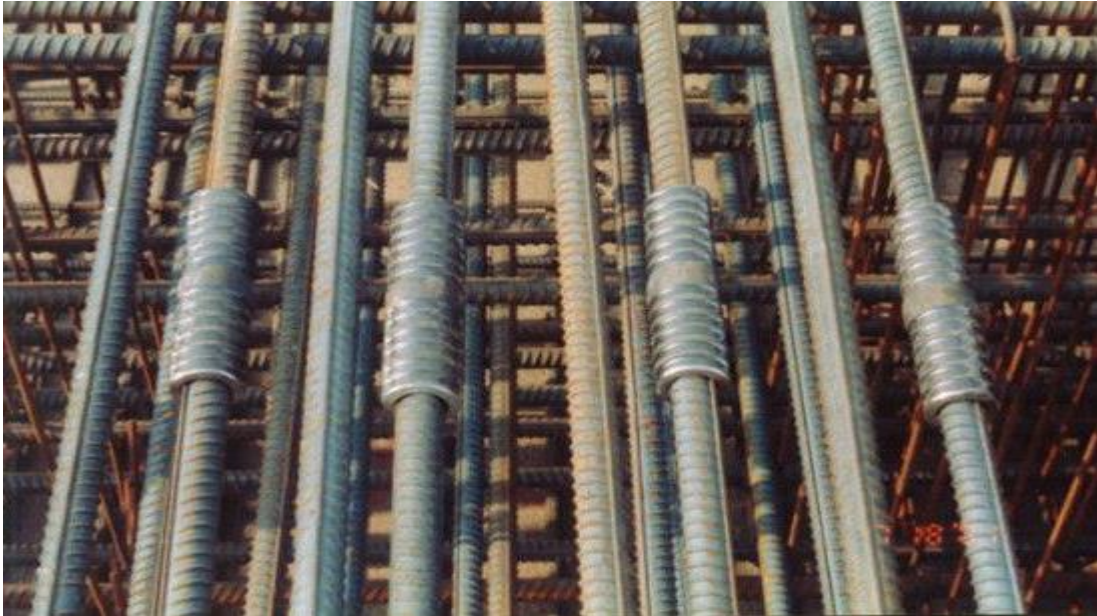


Figure 2.2. Cold-swaged coupling sleeve (source: Aleano, 2019).

Three critical factors that can undeniably affect the performance of mechanical splices are:

- (a) Number of splices in a section
- (b) Coupler shape
- (c) Type of mechanical splice

Similarly, studies recommend a maximum coupler of 15db since this length minimizes the detrimental influence of couplers on structural elements' rotational capacity, whereas longer couplers affect the plastic hinging of reinforced concrete members (Tazarv and Saiidi, 2016; Bompa and Elghazouli, 2018; Dahal and Tazarv, 2020). Moreover, splicing all of the bars in the same section is strongly discouraged. According to the results of the experiments, this might be due to the non-uniform behavior of mechanically spliced couplers, which results in poor reinforced concrete elements' performance (Kheyroddin et al., 2020; Ali and Hamed, 2020).

The first advantage of mechanical splices is that they eliminate bar congestion caused by lap splices. This enhances the performance of structural elements and construction quality by

properly pouring concrete and vibrating it to eliminate voids in concrete. Furthermore, mechanical splices are independent of concrete strength in comparison to lap splices. It simply implies that mechanical couplers might be used in structural elements with low concrete strength. Moreover, because the lap splices are eliminated, additional dead load and construction costs might be decreased by reducing the purchase demand for reinforcement bars and reusing a considerable portion of wasted bars.

The most significant disadvantage of mechanical splices is that some of them are practically difficult to fit into bars with limited access. For example, inserting a portable pressing machine between the bars of a column with closely spaced reinforcing bars is not feasible. Furthermore, threading bars for the installation of coupler decreases their cross-section area. Thus, alternative techniques such as headed, swaged, and grouted bars might be employed instead. It is important to note that the use of some techniques needs technical inspections and knowledge. As such, standards for controlling the depth and length of threads on bars spliced by threaded couplers have been established (Radovanović, 2019). Stricter construction planning, which is essential when using a coupler, should also be considered.

2.2.2 Welded Splices

Welded splices/joints, as shown in Figure 2.3, are usually used where very long bar lengths would be left protruding from existing structures for future expansion. Welded splices, from the viewpoint of force transfer, are the best splices/joint, but they may be expensive and may cause metallurgical problems (McCormac, 2005). The result may be particularly disastrous in high seismic zones. It should be realized that welded splices are usually expensive due to the high labour costs and due to the cost of proper inspection. Welded connections are classified into three main methods: (i) gas pressure or forging, (ii) welding head-to-head, (iii) welding bars along the bars' direction (welded overlapped splices). Figure 4 depicts the above-mentioned methods.

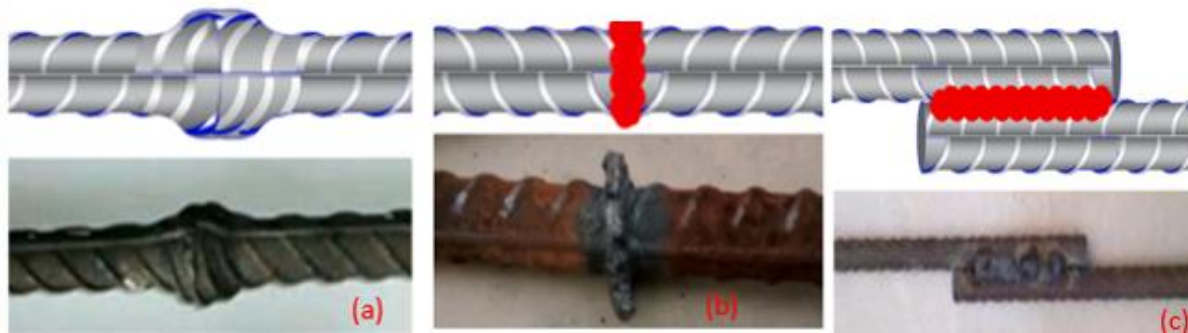


Figure 2.3. Splicing bars by welding (a) forging, (b) head- to head, (c) lap splices (source: CRSI, 2013 and Aleano, 2019).

2.2.3 Lap Splices

Lap splices/joint, as shown in Figure 2.4, is the predominant method of lapping bar in a reinforced concrete structure. They are usually produced by the overlapping of two parallel bars with sufficient length and are commonly used in slabs and beams. This is mainly because they are regarded as an economical and effective splicing method and due to their cheap and ease of use. The most common failure mode in the lap splice technique is debonding, which takes place in the splice region and is caused mostly by insufficient transverse reinforcement or inadequate lapped length. It has been confirmed by previous studies that shear links improve the lap splice performance by providing confinement for longitudinal bars. When debonding deteriorates, longitudinal cracks spread in the cover concrete and the concrete spalls as a result, reducing the flexural strength of the member (Figure 2.4).



Figure 2.4. Lap splices in column (Niamul and Mohammed, 2013).

The lap splice failures generally occur at the end of bars in the splice region, according to the failure modes identified in earlier research and taking into account Figure 2.4. As a result, the following recommendations could be made to enhance the performance of lap splice:

- a) Small bar diameters behave better than large-diameter bars. Thus, providing smaller longitudinal bars may lead to more appropriate lap splice performance in comparison to large-diameter bars (Mabrouk and Mounir, 2018).
- b) At the lap splice region, longitudinal bars should be confined by providing adequate shear links. When compared to other shear link types, rectangular closed shear links placed at 60 mm spacing may provide better performance (Mabrouk and Mounir, 2018). Similarly, the more shear links provided, the better the behaviour of lap splices (Mabrouk and Mounir, 2018; Tarabia et al., 2016; Hassan and Rizkalla, 2012; Chen et al., 2019).
- c) Hooks at the bar ends can considerably improve lap splices' performance (Karabinis, 2014; Goksu et al., 2014; Mousa, 2015).
- d) In addition to the above-mentioned considerations, the spacing between the bars should be limited to 15.24 mm when using non-contact lap splices (Masud, 2020).

Bar congestion is the major issue with the lap splice technique, especially in structural elements such as reinforced concrete slabs or beam-column joints. Bar congestion in the

above-mentioned members hinders effective pouring of concrete and vibrating. As a result of remaining air bubbles, the quality of construction and the performance under dynamic and static loads may be affected. It should also be noted that while lap splicing is known as the simplest splice technique, requiring no additional skills or instruments, the lapping length of the reinforcing bars may raise construction costs. More crucially, the performance of lap splices is largely dependent on the strength of concrete. It implies that even if the lap splice is accurately designed and placed, it might fail due to low concrete strength.

Conducting a suitable evaluation of various splice techniques involves a thorough analysis of identical elements using the same specimens and test setup that differ solely in terms of splice technique.

2.3 Bond in concrete

The term "bond" is used to describe the force transmission between concrete and reinforcement. Traditionally, a bond is defined as the variation of force along a reinforcing bar divided by the nominal area of the bar surface (equation 2.1). This simple concept represents a major simplification. However, as the ultimate limit state approaches, the bond depends more on the bearing of the ribs on the concrete. Moreover, friction and adhesion along the whole bar surface are also important for force transmission between concrete and reinforcement at relatively low stress (Model Code ,2010).

$$f_b = \Delta\sigma_s * A_s / \pi\phi l_b \quad (2.1)$$

Where

ϕ is the nominal diameter of the bar

A_s is the cross-sectional area of the bar

l_b is the bond length over which $\Delta\sigma_s$ takes place

$\Delta\sigma_s$ is the change in stress over l_b

f_b is the average bond stress over length l_b

The simplicity of equation 2.1 may be misleading. The assessment of bond resistance is complicated, even though there is broad consensus on the factors that affect bond

resistance. Quantifying the contribution magnitude attributed to each parameter differs considerably. There are no less than ten parameters in the CEB-FIP Model Code (1990) for calculating lap splice length. Individual researchers' detailed numerical models for analysing the impact of bonds on structural behaviour generally incorporate additional parameters. The one general deduction made by all is that bond is a quantity influenced by stress state, material characteristics, geometry, bar, and concrete section, rather than a fundamental property of the bar, as originally believed.

Bond has several influences on the performance of concrete structures. At the Serviceability Limit State, bond influences curvature, tension stiffening, transverse crack width, and spacing. While at the Ultimate State, bond is responsible for the resistance of lapped joints of reinforcement, as well as influencing the rotation capacity of plastic hinge zones. While it is evident that bond affects structural behaviour under service condition, bond properties of deformed reinforcement are not an influencing factor. Certainly, the change in tension stiffening and crack control between reinforcing bars with markedly differing bond-slip behaviour is almost unnoticeable in certain cases. Other aspects of performance, most notably the spacing between bars and percentage of reinforcement in the cross-section, are far more important. The effect of bond on rotation capacity is subject to similar considerations.

Bond failure of lap might occur in one of two different ways. Failure of ribbed bars is characterized by shearing of the concrete on a surface along the tops of the ribs when confinement is greater, usually when cover concrete around the reinforcing bar is excessive of four to five times the bar diameter, or where compressive stresses act in the transverse direction or where there is a high percentage of transverse reinforcement (Fib Bulletin 72, 2010).

2.4 Application of the theory of bond to tension lap joint

The tension lap joints, which transfer tensile force between the two bars through the bond between concrete and reinforcing bars, are the engineering section most prone to longitudinal bond splitting. Evidence demonstrates that the failure of such a section is generally complete and sudden (when a shear link is not provided), and because of this, as well as a failure to understand the splitting behaviour of the section, it gives rise to very

conservative permissible bond stress value being used in design guidelines, with correspondingly lengthy lap joints.

Tepfers (1973) investigated the splitting and bond stress distribution both around and along the tensile lap splices using the fundamental theory of bond. Tepfers asserts that the splitting bond stress components for the individual bar are independent of the direction of the shear bond stress in each bar because the reinforcing bars are placed side by side. Therefore, the splitting bond stress component is proportional to the absolute value of bond stress at any point in the section. Tepfers concluded that each bar could be analysed as a single anchorage, with stresses resulting in longitudinal cracking determined, utilizing the ring theory for cover cracking along the individual bar in the lap joint.

Tepfers identified two extreme instances for the mean distribution of splitting forces produced around the tension lap joint based on these assumptions and the distribution of the angle of the compressive strut around the bars (Figure 2.9). In the first scenario, Tepfers assumed that the tangential bond transfer between the bars would be destroyed by increasing relative slip, thus doubling the splitting bond stress component to 90 degrees (Figure 2.9(b)). In the second case, Tepfers assumed that the splitting bond stress component would be equal to 45 degrees and constant around the perimeter of both bars, and the splitting stress equal in magnitude to bond stress (Figure 2.9(a)).

Eligehausen et al. (1983) used a three-dimensional finite element model to investigate the distribution of splitting forces around a tension-lapped joint. They concurred with Tepfers' second suggestion for bond stress distribution around the lap joint and proposed a different viewpoint for the enhanced radial bond stress component. Eligehausen et al. (1983) asserted that due to the concrete between the reinforcing bars being crushed far beyond its compressive strength, the resultant radial deformations would be confined, creating a horizontal force that would incline to force the rebars away leading to radial stress distribution like that obtained by (Tepfers, 1980), as shown in Figure 2.9(b).

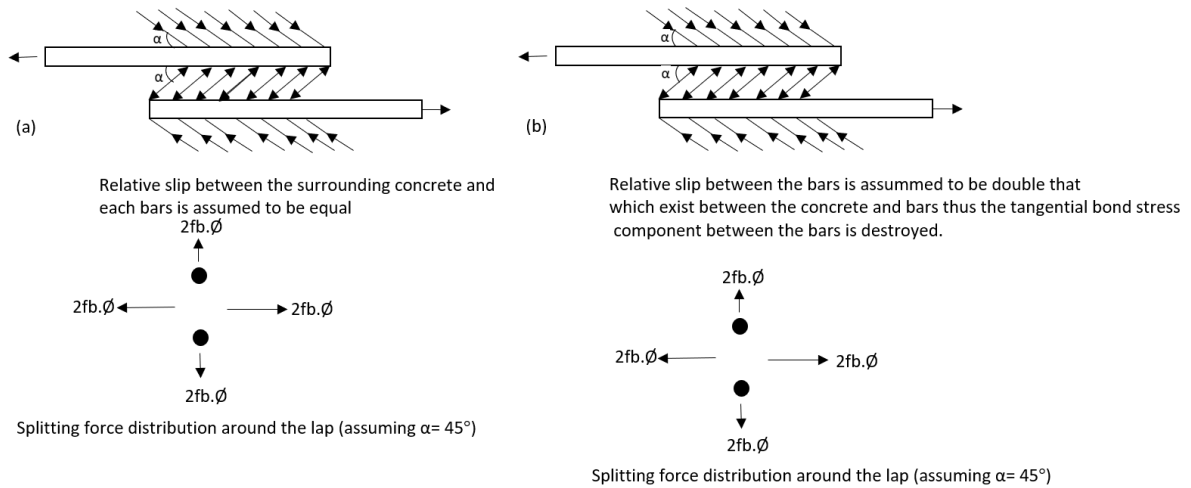


Figure 2.5. Tefpers' assumption for distribution around a tensile lapped splice (Tefpers, 1980).

When the splitting stress distribution illustrated in Figure 2.9(b) is applied to the tension lap joint, it becomes evident that the force exerted on the surrounding concrete "oval" ring by the lapped bars is twice that of a single bar anchorage. Thus, the length of anchorage required to transmit the bond forces would be double that of a single reinforcing bar if the failure resulted from concrete cover splitting. Reynolds and Beeb (1982) questioned this assumption, stating that the tangential bond does not go directly between the rebars, but rather follows the stiffest available path, which is directly between rebars. They asserted that this would result in a similar equivalent decrease in the splitting bond stress component and lead to the distribution of bond stress depicted in Figure 2.10. Reynolds and Beeb (1982) provided experimental outcomes demonstrating that the splitting bond forces created by a single bar anchorage and those developed in tension lap joints are identical.

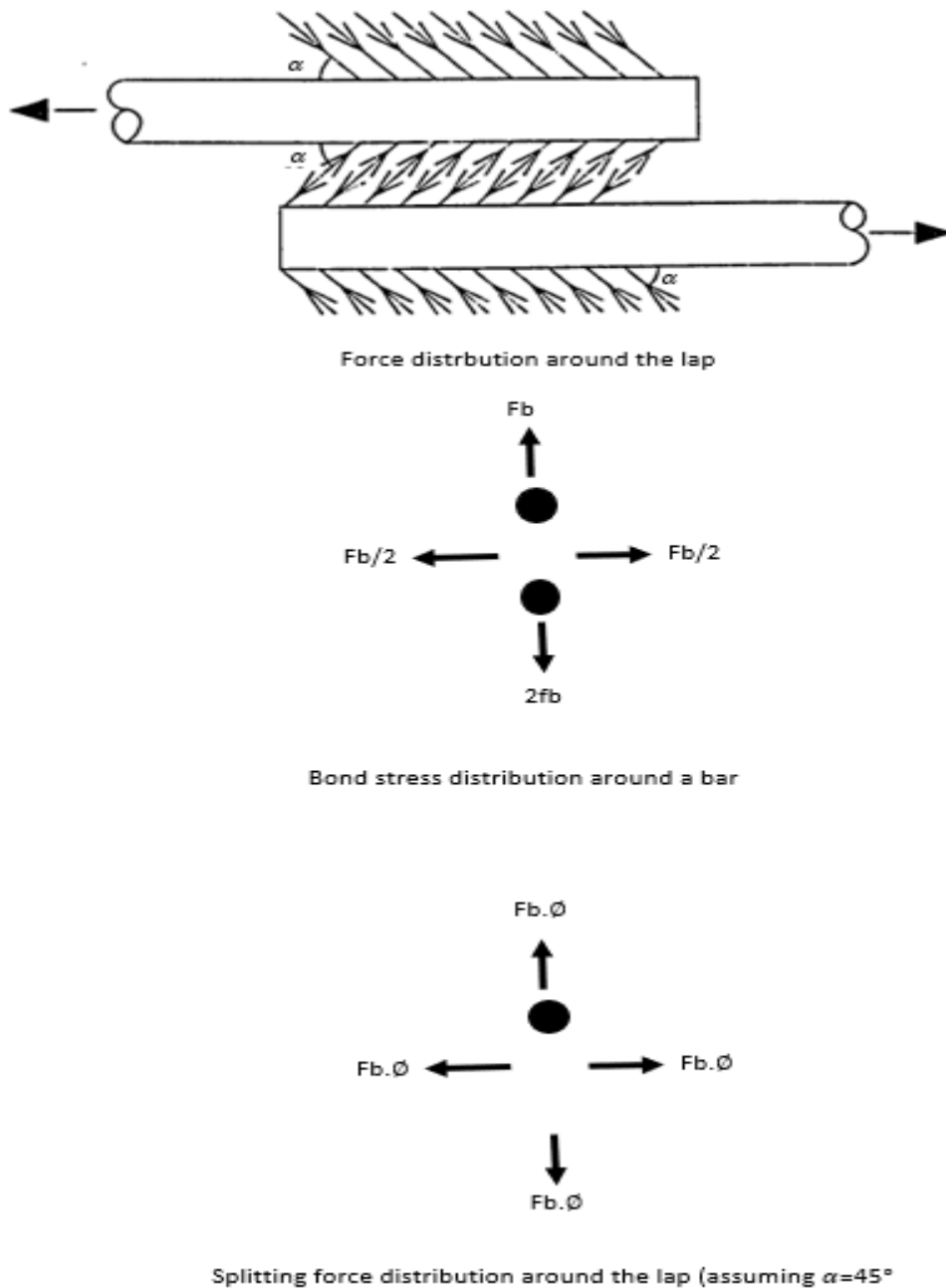


Figure 2.6. Reynolds and Beeby's assumption for the distribution of stress around tension lap joint (Reynolds and Beeby, 1982).

Apart from the problems highlighted regarding the splitting force distribution around a tension lap joint, there has been extensive discussion about how splitting and bond stress are distributed across the lap joint. Due to the abrupt tension failure linked to tensile lap joints, their strength has usually been anticipated by employing plastic theory, assuming that the section will collapse when the mean splitting stress produced by the entire reinforcing bar surpasses the section's permissible concrete tensile strength. It is possible to

predict a lower bound to the bond stress that a tensile lap joint can withstand by connecting the splitting bond stress to the bond stress by the angle (α) or by applying this assumption to some possible failure plane and assuming a value for the concrete's tensile strength.

Tepfers (1973) used this approach to analyse six possible failure planes and develop equations that predicted the ultimate bond strength that the lap could sustain, as well as predicting the most likely failure plane (for bar parameters and a given section). Tepfers used the modulus of displacement theory to test the validity of the uniform splitting forces assumption across the lap. Although Tepfers found that the splitting forces changed across the lap at lower loads, he deduced that, as long as the strength forecasts were associated with the slip observed at failure, the presumption of a constant distribution of splitting stress along the reinforcing bar just before failure was valid.

Similarly, Eligehausen et al. (1983) examined several methods of evaluating lap strength based on the non-uniform distribution of splitting stress along the lap joints and discovered that the estimated strengths were smaller than those determined using the mean plastic failure criteria. Despite these outcomes, Eligehausen et al. (1983) deduced that the plastic approach of analysis may be utilised to accurately estimate the lap strength.

2.5 The use of finite Element Method in RC beams

Reinforced concrete beams are fundamental structural elements in civil engineering and construction. Accurate analysis and design of these beams are essential to ensure their safe and efficient performance. The Finite Element Method (FEM) has gained significant attention as a powerful numerical technique for analysing the behavior of reinforced concrete beams (Zienkiewicz et al., 2005). The Finite Element Method is a numerical technique that approximates the behavior of complex structures by dividing them into smaller, interconnected elements. By applying the principles of mechanics and numerical analysis to these discrete elements, the overall behavior of the structure can be approximated. This method has been widely used to analyse reinforced concrete beams due to its ability to capture complex phenomena such as material nonlinearity, cracking, and interaction between concrete and reinforcement.

In FEM-based analyses of reinforced concrete beams, accurate modeling of both the concrete and reinforcement is crucial. Several approaches have been proposed to model

concrete, ranging from simple linear elastic models to more sophisticated nonlinear material models that account for concrete cracking and crushing behavior (Park and Paulay, 1975; Hordijk and Beenhakker, 2004). Reinforcement is typically modelled using beam or truss elements, considering its mechanical properties such as yield strength, modulus of elasticity, and bond-slip relationships (Vecchio and Collins, 1986). The FEM allows for the application of various loading conditions to simulate real-world scenarios. Different types of loads, including point loads, distributed loads, and moments, can be accurately applied to the beam elements (DeWolf and Hajjar, 2005). Boundary conditions, such as supports and restraints, can also be defined to mimic real structural configurations. The FEM enables engineers to study the response of reinforced concrete beams under different loading and support conditions, thereby assessing their structural behavior and performance.

Reinforced concrete beams often exhibit nonlinear behavior, particularly in the post-cracking phase. The FEM facilitates the consideration of nonlinear effects such as concrete cracking, steel yielding, and bond-slip behavior (Kachakev and Maekawa, 2001; Hordijk et al., (2010). Researchers have employed various nonlinear analysis techniques, including plasticity-based approaches, smeared cracking models, and discrete crack models, to accurately capture the failure modes and load-deformation response of reinforced concrete beams (Eligehausen et al., 1993; Zhan and Hsu, 2012). Validation of the FEM models is essential to ensure the accuracy and reliability of the analysis results. Researchers have conducted experimental tests on reinforced concrete beams to obtain benchmark data for validation purposes (Nilson et al., 2006). Comparisons between experimental and numerical results help validate the FEM models and assess their predictive capabilities. Furthermore, researchers have developed calibration techniques to improve the accuracy of FEM predictions by adjusting material parameters based on experimental data (Faria and Camoes, 2013).

While the FEM has proven to be a powerful tool for analysing reinforced concrete beams, certain challenges remain. These include accurately modeling material behavior, capturing local phenomena such as bond-slip effects, softening, and addressing computational efficiency.

2.6 Current Design methodology

Tension lap joints play a critical role in reinforced concrete structures, providing continuity and strength between reinforcing bars. The design of these lap joints is crucial to ensure structural integrity and adequate load-carrying capacity. Over the years, significant research and advancements have been made to develop methodologies for the design of tension lap joints. This section discussed the current methodology employed in the design of tension lap joints, highlighting the key considerations, factors, and design approaches involved.

2.6.1 Parameters affecting lap strength.

2.6.1.1 *Shear links confinements*

Shear links play an important role in reducing the width of splitting failure and preventing abrupt splitting. To be effective, shear links must be spaced appropriately to decrease longitudinal crack widths. Only reinforcing bars within their vicinity can effectively minimise crack widths, which means that the spacing between shear links cannot be excessively large. However, the spacing must be sufficient to allow for adequate compaction of concrete.

Shear links are particularly effective in heavily used sections of the lap length where the bond stress distribution is nonlinear across its length. It's important to note that while shear links can reduce the width of longitudinal cracks, they are incapable of yielding (Burkhardt, 2000; Hegger et al. 2015; Eligehausen, 1979). Nonetheless, researchers have discovered that the diameter of the shear link can have an influence on the lap strength that can be achieved. Plizzari et al. (1998) found that the longitudinal crack widths decreased with increasing shear link diameter in anchorage experiments with longer lap lengths. They also discovered a linear relationship between lap strength and shear link diameter.

The position of the shear link inside the cross-section heavily influences the bond strength increase. While continuous bars within structural members do not cross potential splitting planes, shear links inside the cover concrete can and therefore add to lap strength. In a series of beam tests conducted by Sakurada et al. (1993) to examine the influence of inner transverse reinforcement on the dynamic behavior of lap splices, they noted that inner supplementary ties reduced crack width. They also observed that the main reinforcement in the intermediate section combined with inner supplementary ties showed greater bond stress than the main reinforcement without inner supplementary ties. Their research agreed

with that of Chinn et al. (1996), who found that the inclusion of a shear link within the splice section improved the performance of the splice and reduced cracking.

The impact of the shear link is also dependent on the cover dimensions, as the splitting planes are determined by the bar spacing and concrete cover. Only vertical legs enhance bond strength if the splitting plane is strictly horizontal. Side and corner split failures with effective vertical shear link legs are illustrated in Figure 2.7, as well as face split failure in which the horizontal transverse bar crosses the cracks.

In addition to crack prevention, shear links cause multi-axial concrete compression at lapped bars or anchored in bending structural elements. The bursting forces of longitudinal bars at the lap ends provide additional tensile stress on the concrete cover in such elements. Shear links confine the lap's end, resulting in an increase in lap stress. Finally, shear links have a positive effect on both beams and direct tension members (Burkhardt, 2000).

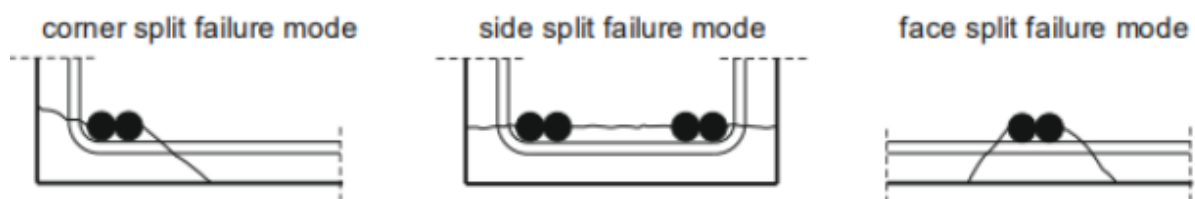


Figure 2.7. Split failures (Model Code, 2010)

A straight transverse bar can reduce crack width when splitting cracks occur in the bottom cover of slabs with wide bar spacing, according to studies by Orangun et al. (1977), Canbay and Frosch (2005), and Zuo and Darwin (2000) Jukka et al. (2023).

Azizinamini et al. (1995) studied the minimum shear link requirement over the splice region and concluded that including a minimum amount of shear link over the lap splice is a better method than increasing lap splice length. They observed that the strain distribution over the splice region is not uniform near the maximum midspan displacement. As the splice length reduces, strain distribution shows a more uniform value. In general, only the outer-most stirrup over the splice region reaches the yield strain at maximum midspan displacement, with the remaining shear links over the splice region reaching strain values below yielding.

Hamad et al. (2003) performed two series of beam experiments with high-strength concrete. In the first series, shear links were placed in various amounts. In the second series,

steel fibres of different volumes percentages were used. In both series, twelve full-scale beams were tested with three different bar sizes (20, 25, and 32 mm). They concluded that the presence of hoop shear links in the splice zone produces a relatively more ductile and gradual mode of failure than beams with fibre reinforcement. Moreover, increasing the number of stirrups or the amount of steel fibres in the splice zone enhances the ductility of the mode of failure of the high-strength concrete samples. Additionally, they observed that increasing the fibre content in the spliced zone increases the mean bond strength of tension lap splices. Mousa (2015) investigated the bond strength of lap splices in RC beams with a concentrated load at the middle. A total of eighteen specimens were tested using two different longitudinal bar diameters (12 mm and 16 mm). The variables in the study were the shape of the anchor at the splices, concrete grade, concrete cover, and the amount of transverse reinforcement within the splice zone. They concluded that shear links at the end of the lap splice or hooked end splice enhanced bond strength, ductility, and crack propagation remarkably.

Karabinis (2014) studied the performance of RC beam-column joints incorporating lap splices. Twenty-four specimens were tested with three different longitudinal bar diameters (4, 8, and 10 mm). All samples were designed based on Eurocode 2 and tested under reversed cyclic loading. The effect of lap splice length, axial load, the geometry of the reinforcing bar extension, the cover of lap splices, loading history, confining reinforcement, percentage, and shape of shear link confining the lap splice zone were studied. The outcome of the study showed that the existence of hooked splices reduced reinforcement sliding. Shear links at the splice zone increased load-carrying capacity, ductility, and absorbed energy.

Tarabia et al. (2016) investigated the behaviour and strength of reinforced concrete slabs with lap splice under monotonic and cyclic loading. The main variables in the study were cracking behaviour, bond strength, ultimate load, and failure mode. Their results showed that providing confinement in the splice region increased the strength and ductility of the slab.

2.6.1.2 Lap length

The distribution of bond stress along reinforcing bars is nonlinear. When the bond length is longer, the bond stress decreases gradually towards an asymptote (see Figure 2.8(b) bottom

right). However, when the bond length is shorter, the bond stress decreases rapidly as it approaches the loaded end (see Figure 2.8(b) top right) (Wildermuth, 2013). The non-linear behaviour is influenced by several factors such as the softening of the concrete around the reinforcing bar due to crack formation around the tips of the lugs, the formation of cracked shear planes, concrete crushing, and the development of longitudinal and radial splitting cracks (Fib Bulletin, 2013).

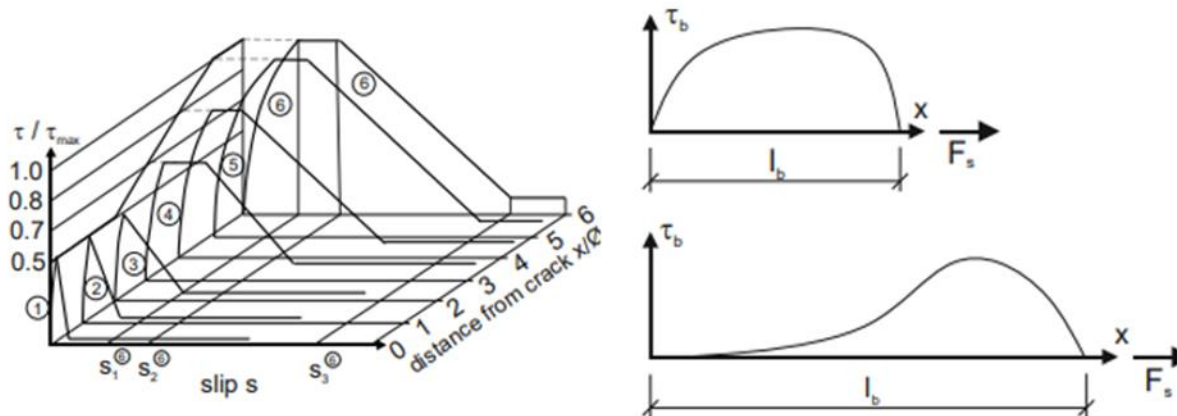


Figure 2.8. (a) Increasing the bond stress slip curves along the bond length and (b) Bond stress over bond length for different bond lengths (Kreller, 1989).

At various locations along the lap length, different stress states emerge (see Figure 2.8(b) on the right). The bond between the concrete and reinforcement deteriorates in the vicinity of cracks, and complete bond strength is only available at a specific distance from the crack (see Figure 2.8(a) on the left) (Kreller, 1989).

When loads are low, the rear position along the lap length does not achieve full lap strength. The bond between concrete and reinforcement at the rear locations of the bond length is triggered as soon as the maximum bond strength is reached at the loaded end. Sozen and Moehle (1990) developed a design method to examine splice lengths for deformed steel rebars. Their study included a total of 233 experimental results. They observed a descending trend between the lap-length-to-bar diameter ratio, l_s/db and normalized bond strength, $u/\sqrt{f'c}$. They also noted a plausible trend for strength, $\sqrt{f'c}$, to increase with cover, db/C_{min} . For as-rolled deformed bars (without epoxy coating) with less than 12 inches of concrete cast beneath them, the proposed method required a

development length of 40 bar diameters using a specified yield stress of 60,000 psi (413 MPa) and a concrete compressive strength of 4,000 psi (27 MPa).

Micallef and Vollum (2018) observed that samples with longer splice lengths generally showed less splitting over their length, whereas shorter splices showed splitting over a large part of their length. Longer splice lengths appeared to stabilize, with a considerable center length remaining unsplit until the last abrupt failure occurred. Similarly, Najafgholipour et al. (2018) evaluated the behavior of lap splices in RC beams. They tested nine specimens with two different bar diameters (12 mm and 16 mm) under revised cyclic loading. The main variables were the transverse reinforcement, splice length, and grade of longitudinal steel bars. The objective of their study was to determine the global behavior of the splice, as well as the axial strain in the longitudinal bars. Their study showed that beams with ACI lap splice length did not exhibit reliable performance under cyclic load, while beams with a 25% increase in lap length survived under cyclic load with adequate flexural ductility.

Tarquini et al. (2019) investigated the deformation capacity of lap splices in RC wall boundary elements under uniaxial tension-compression cyclic loading. They tested twenty-four samples with loading history, confining reinforcement, and lap splice length as the main study variables. The results of the study showed that the deformation capacity of lap splices increased with increasing lap splice length and confining reinforcing was larger for bottom casted compared to top-cast lap splices.

The cyclic behavior of lightly reinforced concrete columns with short lap splices was investigated by Lee and Han (2019). They conducted tests on four specimens under unidirectional and bidirectional loadings. All samples were designed based on ASCE guidelines, with the loading types and axial load levels as the main variables. They concluded that unidirectional loading increased the maximum bond strength of spliced bars, while bidirectional loading decreased it.

2.6.1.3 Bar diameter

The bond strength is related to the reinforcing circumference, while the maximum bar force depends on the cross-sectional area of the reinforcing bar. The relative rib area, concrete cover, and lap length must all be taken into account when evaluating the effect of bar diameter. However, the effects of bar diameter on lap splices reported in the literature are

conflicting. For instance, Rehm and Martin (1968) and Steuck et al. (2007) observed no effect, while Chinn et al. (1996) found a small reduction in lap strength as the diameter of the bar increased. Nevertheless, the influence of bar diameter is negligible when the lap length and the cross-sectional dimensions are multiples of the bar diameter (Eligehausen et al., 1983).

In an extensive experimental program on laps, Tepfers (1973) found that increasing bar diameters at a constant lap length resulted in a decrease in developable bar stress. However, the influence of bar diameter is not visible when looking at the lap length-to-bar diameter ratio in the test results conducted by Tepfers. As the bar diameter increases, the bond stiffness reduces, resulting in softer bond behavior (Viwathanatepa et al., 1979; Schenkel, 1998).

Regarding the influence of bar diameter on crack width, some studies (Ferguson and Breen, 1965; Rezaiee et al., 2021) have asserted that crack width is not related to bar diameter. Hassan and Feldman (2012) investigated the influence of confinement on large lap spliced diameter bars. They aimed to understand the bond characteristics of larger bar diameter on lap splices. They tested 20 samples under a four-point bending setup using two different bar diameters (28 mm and 63.5 mm) in accordance with the ACI code requirements for lap splice. The main variables they considered were the amount of reinforcement provided within the splice region, bar size, concrete strength, and splice length. Their study showed that transverse reinforcement in the splice zone affected large bars more than regular size bars. They recommended a 25% increase in ACI development length for 63.5 mm bars.

Nawaz and Yehia (2020) evaluated the performance of confined lap splices in self-compacting lightweight concrete. They tested 24 samples with three different bar diameters (12, 20, and 25 mm) under tensile load. The main variables in the study were the lap length, bar diameter, and splicing detail. They observed that bond stress increased by increasing the bar diameter.

2.6.1.4 Concrete compressive strength

The bond mechanism relies on the shear component of the interfacial forces induced by the localized pressure under the ribs, as well as the tensile stress in the concrete due to the

diffusing compressive struts. The tensile capacity of concrete and its multi-axial response to compression can affect the bond behavior (FIB Bulletin 2013).

In practical situations, bond failures often occur at the concrete cover due to splitting, and in cases where the bond is confined by shear reinforcement, the secondary bar may be pulled out. Therefore, the splitting forces are often the controlling factor, and the bond strength is related to the tensile strength of concrete (FIB Bulletin 72, 2014).

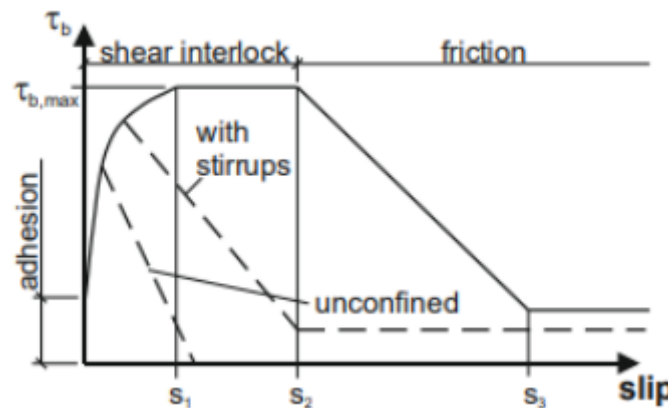


Figure 2.9. Bond strength contribution, friction, adhesion, and interlock (Model Code, 2010).

Both the bond strength and bond stiffness, denoted as $\Delta\tau / \Delta s$ in Figure 2.9, increase nonlinearly with concrete strength. To prevent the formation of wide crack widths, most codes prescribe bond strength for modest slip values. As a result, bond strength is generally described by the relation $\tau_b \sim f_c^x$ for initial stiffness, with an exponent x between $1/4$ and $2/3$. Since the lap strength distribution differs throughout the lap length, the lap strength of short lap lengths increases with $f_c^{2/3}$, whereas the increase in lap strength for longer lap lengths is considerably smaller. Lap strength is roughly constant for low concrete strength and short lap length. Darwin et al. (1996) statistically developed an expression for the force bond strength of unconfined and confined splices. The expression includes bar spacing, lap splices, concrete cover, concrete strength, shear link, and the geometric properties of the spliced bars. They recommended the use of the power $1/4$ instead of $1/2$ for the concrete compressive strength to accurately represent the effect of concrete strength on bond strength.

Azizinamini et al. (1993) investigated the bond performance of reinforcing bars embedded in high-strength concrete. They concluded that the assumption of a uniform bond stress

distribution at the ultimate stage may not hold for high-strength concrete, and the nonuniform bond stress distribution could be more pronounced as the concrete cover decreases or splice length increases. For high-strength concrete with small covers, increasing the splice length is not an efficient method for enhancing bond capacity. A better approach would be to require a minimum amount of shear link over the spliced length. They also noticed that for small covers, top cast bars appear to perform better with respect to bond, which is in contrast to the performance of such bars in normal strength concrete.

Goksu et al. (2014) evaluated the effect of lap splice length on the behavior of low-strength RC columns under cyclic lateral load. They tested five specimens with spliced lengths. Their results showed that 180-degree hooked lap splices reduced the negative effects of inadequate lap splice length, even in the case of low-strength concrete.

2.6.2 Design models for lap joints

Design models for required lap length are used in design codes for structural members to account for stress formed in bond regions. With each new code reissue, the design models are regularly updated. For instance, Eurocode 2, which has been in use since 2004, includes a lap design model that was originally published in the Model Code 1990. For the next generation of Eurocode 2, the project team has developed a new proposal (PTI working draft prEN 1992-1-1:2018). The lap design model was derived from Fib Bulletin 72, which is the background document for Model Code 2010. The Eurocode 2 project team provides preliminary calibration factors for changes from average values provided in Fib Bulletin 72 to design values that are still to be verified (PTI working draft prEN 1992-1-1:2018) for lap design models.

Models with and without bond strength definitions are differentiated in code provisions for laps. Earlier design codes specified lap lengths for different concrete classes based on bond strength (for example, Model Code 2010 and Eurocode 2). The ACI and Fib Bulletin models, on the other hand, were developed from statistical analysis of experimental data that took into consideration the maximum bar strength in laps without determining bond strength. The bond strength for Model Code 2010 was determined from the Fib Bulletin 72 design model. Bond strength is an optional parameter that simplifies the design, but it is not required for lap design.

Experimental and partially computational studies with finite element analysis are used to develop models for estimating developable stresses in laps. The processes for finding calibration factors, the influencing parameters, and the composition of equations differ. The major impacting parameters for all the models are compressive strength and lap length, however, their components differ. Some models introduce a summand for shear link contribution, while others consider the shear link contribution by a coefficient. A cover-to-bar diameter ratio is used in all models to account for the influence of concrete cover. The models take into account the influence of shear links differently. Some models comprise the transverse bar spacing s_{st} , while others consider the number of shear link bars n_{st} . The correlation is provided by expression (2.2).

$$\sum A_{st} = n_{st} A_{st} = \left(\frac{l_0}{s_{st}} + 1 \right) A_{st} \approx \frac{A_{st} l_0}{s_{st}} \quad (2.2)$$

Where;

A_{st} is the area of reinforcement

l_0 is the lap or anchorage

s_{st} is the longitudinal spacing of confinement ultimate slip

n_{st} is the number of stirrups in the lap length

The horizontal cracking plane is crossed by the number of shear link leg in side-splitting. As a result, if side-splitting is assumed, the shear link leg number n_l is included in the lap design models. The shear link cross-section is only evaluated once in face-splitting design models because it only provides tensile resistance in one face crack. The number of shear link leg is not considered in this case (see Figure 2.7).

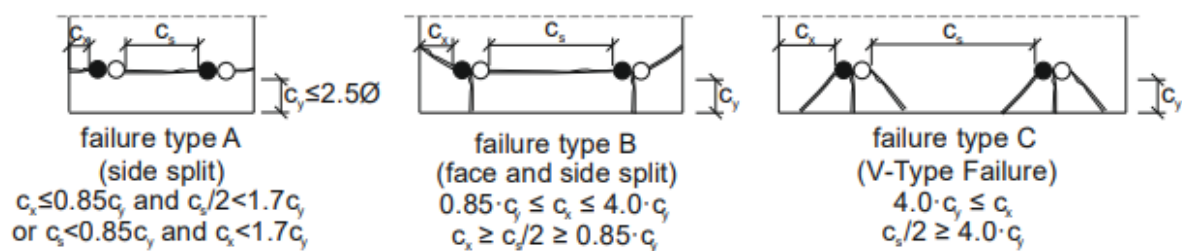


Figure 2.10. Splitting failure modes (reproduced from (ELIGEHAUSEN, 1979) based on (Ferguson and Briceno, 1969))

The design expression for laps based on Eurocode, National Annex, and ACI are provided in this section. The origin of the design expressions in the proposal for the next generation of Eurocode 2 from Fib Bulletin 72 and in the Model Code 2010 are discussed.

2.6.2.1 Fib Bulletin 72

Fib Bulletin 72 (2014) describes the background of bond strength established in Model Code 2010. The semi-empirical expression for estimating the average bar stress in tension lap joints was obtained from 800 tests performed in Asia, Europe, and United States.

The expression for average lap stress representing the authenticated affecting factors is provided as follows:

$$f_{stm} = 54(f_{cm}/25)^{0.25} \cdot (25/\phi)^{0.2} \cdot (l_b/\phi)^{0.55} \cdot [(c_{min}/\phi)^{0.25} \cdot (c_{max}/c_{min})^{0.1} \cdot k_m k_{tr}] \leq f_y \quad (2.3)$$

Where;

f_{cm} is the measured concrete cylinder compressive strength

c_{min} is the minimum cover concrete

k_m is the coefficient of efficiency of shear link

c_{max} is the maximum cover concrete

l_b is the lap or anchorage

k_{tr} is the density of shear link

$$k_{tr} = n_l n_{st} A_{st} / (n_b \phi l_b) \leq 0.05$$

n_b is the number of lapped bars at a section

n_{st} is the number of stirrups in the lap length

f_y is the yield stress

n_l is the number of stirrups legs that crosses the potential splitting failure plane

The bond strength does not increase with a shear link ratio k_{tr} above 0.05. The parameter k_m compensates for the efficacy of the shear link depending on possible failure planes and their position. The shear link is particularly effective when the lap or an anchored bar has a

lesser spacing to the next shear link leg across a splitting crack. When the horizontal spacing between bars is greater than 5ϕ or 125 mm, the efficiency is decreased by 50%. There is zero effect on bond strength if the shear link does not cross the splitting crack.

Since test results outside of these boundaries hardly exist, Equation (2.3) is restricted to the following boundary conditions.

- Good bond condition

$$\frac{l_0}{\phi} \geq 10$$

$$\frac{15}{\phi} \leq 5$$

$$\frac{25}{\phi} \leq 2$$

$$\frac{c_{\max}}{c_{\min}} \leq 5$$

$$0.5 \leq c_{\min}/\phi \leq 3.5$$

The stress developed by bond increases when the transverse pressure is present to

$$f_{\text{stm,tr}} = f_{\text{stm}} + 6(l_b/\phi)p_{\text{tr}} < 1.75f_{\text{st},0} + 0.8(l_b/\phi)p_{\text{tr}} < 8.0(l_b/\phi)f_{\text{cm}}^{0.5} \quad (2.4)$$

Where:

$f_{\text{st},0}$ average stress formed by bond for the base conditions of confinement with

$$f_{\text{st},0} = 54(f_{\text{cm}}/25)^{0.25}(l_b/\phi)^{0.55}(25/\phi)^{0.2} \quad (2.5)$$

p_{tr} average compression stress perpendicular to the potential splitting failure surface

f_{stm} is the mean estimated stress developed in the bar

2.6.2.2 Model code 2010

The International Federation for Structural Concrete (known as the Federation Internationale du Beton or Fib) offers advice for the design of prestressed and reinforced concrete in the Model Code 2010. In order to establish the required lap length, Model Code 2010 like Eurocode 2, necessitates the calculation of the design bond strength (f_{bd}).

The design bond strength f_{bd} provided in Model Code 2010 was determined by rewriting ACI express for transverse reinforcement index Equation. (34) with a lead coefficient of 41 to enable the formation of the reinforcement design strength $f_{yd} = 435 \text{ MPa}$. The basic bond strength $f_{bk,0}$ was determined by rearrangement of Equation (2.3) with a coefficient of 41. The shear link stress f_{stk} was set to $\frac{500}{1.5} = 435 \text{ MPa}$ and

$$\begin{aligned} l_{b,0}/\phi &= (f_{yk}/\gamma_c \cdot 41)^{1.82} \cdot (f_{cm}/25)^{-0.45} \cdot (25/\phi)^{-0.36} & 2.6 \\ &= 73.5 \cdot (f_{cm}/25)^{-0.45} \cdot (25/\phi)^{-0.36} \end{aligned}$$

$$f_{bk,0} = f_{yd} \cdot \phi/4 \cdot l_{b,0} = 1.5 \cdot (f_{cm}/25)^{0.45} \cdot (25/\phi)^{0.36} \quad 2.7$$

The coefficient, as well as the indices, were approximated to more practical values, and the confining reinforcement and cover values equivalent to the least detailing requirements were established. The coefficient π_1 1.5 was modified to $\pi_1 = 1.6$ for the calculation of the basic bond strength without stirrups. The coefficient π_1 was modified to 1.75 and the values of basic bond strength were increased by 10% to account for the increase in bond strength if minimal confining reinforcement is provided (Model Code for Concrete, 2013). The design bond strength is calculated using equation (2.8).

$$f_{bd} = (\alpha_2 + \alpha_3) \cdot f_{bd,0} - 2P_{tr}/\gamma_{cb} < 2f_{bd,0} - 0.4P_{tr}/\gamma_{cb} < 1.5\sqrt{f_{ck}}/\gamma_{cb} \quad (2.8)$$

Where:

$f_{bd,0}$ is the basic bond strength, which is derived using equation (2.9) and is a function of the characteristic compressive strength (f_c)

$$f_{bd,0} = \pi_1 \pi_2 \pi_3 \pi_4 \left(\frac{f_c}{25} \right)^{0.5} \quad (2.9)$$

π_1 is a coefficient taken 1.75 for ribbed bars (including stainless and galvanised reinforcement)

π_2 represents the casting position of the bar during concreting: $\pi_2 = 1.0$ for good bond condition.

γ_{cb} is the partial safety factor for bond $\gamma_{cb} = 1.5$

The influence of passive confinement from transverse reinforcement and concrete cover are represented as α_2 and α_3 . Where; $\alpha_2 = \left(\frac{c_{min}}{\phi}\right)^{0.5} \cdot \left(\frac{c_{max}}{c_{min}}\right)^{0.15}$ and $\alpha_3 = k_d \cdot (k_{tr} - \alpha_t/50) \geq 0.0, k_{tr} \leq 0.05$.

Where:

c_{min} is the minimum cover concrete: $c_{min} = \min\left\{c_x; c_y; \frac{c_s}{2}\right\}$

c_{max} is the maximum cover concrete: $c_{max} = \min\left\{c_x; c_y; \frac{c_s}{2}\right\}$

α_t is the coefficient for the bar diameter;

$\alpha_t = 1.0$ for $\phi = 25$ mm

$\alpha_t = 0.5$ for $\phi = 50$ mm

$k_{tr} = \pi_t \cdot \frac{A_{st}}{(n_b \phi s_t)}$ is the density of transverse reinforcement, relative to the lapped bars;

π_t is the number of legs of confining reinforcement crossing a potential splitting failure surface at a section;

A_{st} is the cross-sectional area of one leg of a confining bar (mm^2);

s_t is the longitudinal spacing of confining reinforcement (mm);

ϕ is the bar diameter;

n_b is the number of pairs of lapped bars in the potential splitting failure section;

π_3 represent the bar diameter: $\pi_3 = 1.0$ for $\phi \leq 25$ mm

π_4 represents the characteristics strength of steel reinforcement that is being lapped (see Table 2.2).

Table 2.1. Coefficient η_4

η_4	Characteristic strength of steel reinforcement f_{yk} (MPa)
1.2	400
1.0	500
0.85	600
0.75	700
0.68	800

k_d is an effective factor dependent on the reinforcement details and accounts for the stress developed and the nonlinear behaviour between the lap length in the bar (see Figure 2.8).

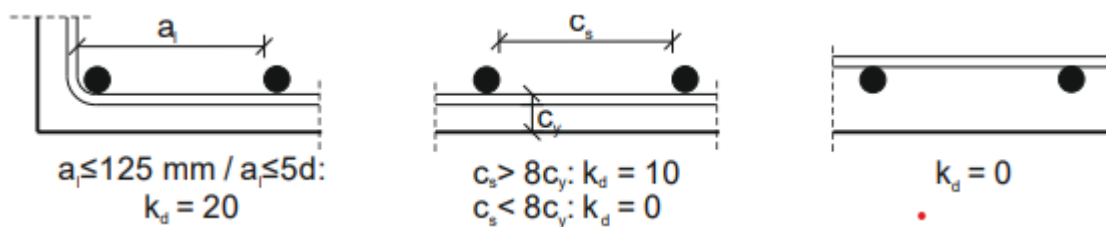


Figure 2.11. Coefficient k_d for efficiency of stirrups (Source: [Mode Code, 2010])

In case the concrete class is grade C60 or below and the anchored bar's diameter is less than 20 mm, the stirrup added for other reasons can be deemed to be adequate to meet the least criteria for confined reinforcement without additional explanation (Model Code, 2010). Therefore, the minimum stirrup has to be located with:

$$\sum A_{st} = n_g n_t A_{st} \geq \frac{\alpha_t A_{s,cal}}{A_{s,prov}} \cdot n_b A_s \quad (2.10)$$

Where;

$A_{s,cal}$ calculated area of reinforcement

n_t is the number of stirrups crossing a potential splitting failure surface at a section

$A_{s,prov}$ area of reinforcement provided

n_g number of items of confining reinforcement within the bond length

The design anchorage length l_b can be calculated from equation (2.11):

$$l_b = \frac{\sigma_{sd}}{4f_{bd}} \geq l_{b,min} \quad (2.11)$$

$l_{b,min}$ is the minimum accepted design value for lap length, calculated as:

$$l_{b,min} > \max \left\{ \frac{0.3\sigma_{sd}}{4f_{bd}}; 10\phi, 100 \text{ mm} \right\} \quad (2.12)$$

Where σ_{sd} is the stress in the bar that will be anchored by bond across the length of the lap, and is calculated as:

$$\sigma_{sd} = \alpha_1 \cdot f_{yd} \quad (2.13)$$

$$\alpha_1 = \frac{A_{s,cal}}{A_{s,ef}}$$

Where $A_{s,ef}$ and $A_{s,cal}$ are the actual area of reinforcement and the required area of reinforcement determined in design, f_{yd} is the design yield strength of the reinforcement.

The design lap length is calculated as follows:

$$l_0 = \alpha_4 \frac{\sigma_{sd}}{4f_{bd}} \geq l_{0,min} \quad (2.14)$$

$l_{0,min}$ is the minimum accepted design value for lap length, calculated as:

$$l_{0,min} > \max \left\{ \frac{0.7\sigma_{sd}}{4f_{bd}}; 15\phi, 200 \text{ mm} \right\} \quad (2.15)$$

The coefficient $\alpha_4 = 0.7$ may be used if no more than 34% of the bars are lapped at the section or the reinforcement stress estimated at the limit state does not surpass 50% of the reinforcement's characteristic strength, otherwise $\alpha_4 = 1.0$ may be used.

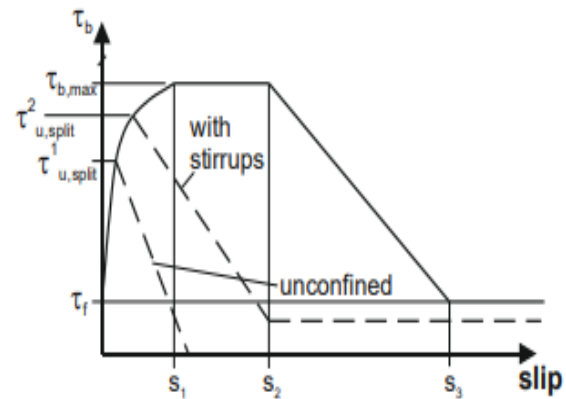
According to Model Code 2010, the stress developed in a lap may be taken as:

$$\sigma_{sd} = l_0/\phi \cdot 4/\alpha_4 \cdot [(\alpha_2 + \alpha_3) \cdot 1.75 \cdot (25/\phi)^{0.3} \cdot (f_{ck}/25)^{0.5} - 2P_{tr}]/\gamma_{cb} \quad (2.16)$$

Model Code 2010 specifies two distinct design bond stress-slip relationships in addition to the lap length and design bond strength. The designer determines the suitable relationship to use according to the mode of failure, which is confinement or bond failure. Table 2.3 depicts the general bond stress-slip model.

Table 2.2. Bond slip relationship based on (Model Code, 2010)

	Splitting		Pull-out
	Stirrups	Unconfined	
τ_{max}	$8(F_{cm}/25)^{0.25}$	$7(F_{cm}/25)^{0.25}$	$2.5\sqrt{f_{cm}}$
s_1	$s(\tau_{max})$	$s(\tau_{max})$	1 mm
s_2	s_1	s_1	2 mm
s_3	$0.5c_{clear}$	$1.2s_1$	c_{clear}
α	0.4	0.4	0.4
τ_f	$0.4\tau_{max}$	0	$0.4\tau_{max}$



Where:

$$\tau_0 = \tau_{max}(s/s_1)^\alpha \text{ for } 0 \leq s \leq s_1$$

$$\tau_0 = \tau_{max} \text{ for } s_1 \leq s \leq s_2$$

$$\tau_0 = \frac{\tau_{bmax}(\tau_{max}-\tau_f)(s-s_2)}{(s_3-s_2)} \text{ for } s_2 \leq s \leq s_3$$

$$\tau_0 = \tau_f \text{ for } s_3 < s$$

c_{clear} is the clear distance between the ribs

τ_f is the residual bond stress

2.6.2.3 Eurocode 2

The Eurocode 2 design model for laps is based on CIB-FIP (1991). In order to determine the design lap length in Eurocode 2, the design bond strength must first be determined, then

the anchorage length. The bond strength is used to calculate the anchorage length with the following expression:

$$f_{bd} = 2.25\eta_1\eta_2f_{ctd} \quad (2.21)$$

In this equation, η_1 is a coefficient associated with the bar position and bond conditions during concreting, with 0.7 representing all other conditions and unity indicating good bond condition. The bond strength to tensile concrete strength ratio is described by the coefficient 2.25. When the diameter of the bar is smaller than 32 mm, the coefficient η_2 is considered as unity; otherwise, the following equation is used:

$$\eta_2 = \frac{132-\emptyset}{100} \text{ for } \emptyset > 32 \text{ mm} \quad (2.22)$$

The concrete design strength is f_{ctd} is obtained from $\frac{f_{ctk,0.005}}{\gamma_c}$ where is $f_{ctk,0.005}$ restricted to concrete grade C60/75. The concrete tensile strength is determined as a function of the compressive strength of concrete:

$$f_{ctd} = \frac{f_{ctk,0.005}}{\gamma_c} = \alpha_{ct} = 0.21(f_{ck})^{\frac{2}{3}}/\gamma_c \quad (2.23)$$

The coefficient α_{ct} which takes into consideration the loading and long-term effect of tensile strength is a nationally defined factor, the value recommended is 1.0. Equation (1.32) give the safety considered in the Eurocode 2 anchorage design model. The bond strength is calculated using a 5%- fractile of the concrete tensile strength divided by the concrete's partial safety factor $\gamma_c = 1.5$. Therefore, the average bond strength required for comparing the test results is:

$$f_{bm} = 2.25\eta_1\eta_20,3f_{ck}^{\frac{2}{3}} \quad (2.24)$$

The required basic anchorage length is obtained as:

$$l_{b,rqd} = \left(\frac{\emptyset}{4}\right) \left(\frac{\sigma_{sd}}{f_{bd}}\right) \quad (2.25)$$

The stress at the cross section in which the anchorage length begins is the design stress of the bar σ_{sd} . The design length of the anchorage is determined as:

$$l_{bd} = \alpha_1 \cdot \alpha_2 \cdot \alpha_3 \cdot \alpha_4 \cdot \alpha_5 \cdot l_{b,rqd} \geq l_{b,min} \quad (2.26)$$

α_1 and α_2 are coefficient associated to bars shape and cover concrete, respectively.

$\alpha_1 = 1.0$ for straight rebars.

$$\alpha_2 = 1 - 0.15 \left(\frac{(c_{min} - \emptyset)}{\emptyset} \right) \leq 1.0$$

α_3 is the coefficient of shear link if present, with

$$0.7 \leq \alpha_3 = 1 - k\lambda = 1 - \frac{k(\sum A_{st} - \sum A_{st,min})}{A_s} \leq 1.0 \quad (2.27)$$

If there is no transverse pressure and welded transverse reinforcement, α_4 and α_5 can be taken as unity. However, when transverse pressure is present, the anchorage length can be decreased by:

$$0.7 \leq \alpha_5 = 1 - 0.004p \leq 1.0 = 1.0 \quad (2.28)$$

K accounts for the transverse reinforcement's efficacy in relation to its position inside the section. The difference in cross-section area between the minimum transverse reinforcement $\sum A_{st,min}$ and the transverse reinforcement provided along the anchorage length is described by the coefficient λ with $\sum A_{st} = 0.25A_s$ for anchorage and $\sum A_{st,min} = 1.0A_s \left(\frac{\sigma_{sd}}{f_{yd}} \right) \geq 1.0A_s$ for laps.

Eurocode 2 recommended that laps should be positioned in a low-moment region and staggered. The clear lapped spacing between bars should not exceed 50 mm or $4\emptyset$. If all bars are in layer, the permissible proportion of lapped bars in tension is 100% and should not exceed 50% for lapped bars in several layers.

The basic required anchorage length and the coefficients are included in the design of lap length $l_{b,rqd}$, which takes into account the key impacting parameters.

$$l_0 = \alpha_1 \cdot \alpha_2 \cdot \alpha_3 \cdot \alpha_4 \cdot \alpha_5 \cdot \alpha_6 l_{b,rqd} \geq l_{0,min} \quad (2.29)$$

The coefficient α_1 to α_5 described above. For the proportion of bars lapped at a section, the coefficient α_6 can be taken from Figure 2.9 below.

		Bond condition, (see Figure 1)	Reinforcement in tension, bar diameter, ϕ (mm)								Reinforcement in compression
			8	10	12	16	20	25	32	40	
Anchorage length, l_{bd}	Straight bars only	Good	230	320	410	600	780	1010	1300	1760	40ϕ
		Poor	330	450	580	850	1120	1450	1850	2510	58ϕ
	Other bars	Good	320	410	490	650	810	1010	1300	1760	40ϕ
		Poor	460	580	700	930	1160	1450	1850	2510	58ϕ
Lap length, l_o	50% lapped in one location ($\alpha_6 = 1.4$)	Good	320	440	570	830	1090	1420	1810	2460	57ϕ
		Poor	460	630	820	1190	1560	2020	2590	3520	81ϕ
	100% lapped in one location ($\alpha_6 = 1.5$)	Good	340	470	610	890	1170	1520	1940	2640	61ϕ
		Poor	490	680	870	1270	1670	2170	2770	3770	87ϕ
Notes											
1 Nominal cover to all sides ≥ 25 mm, [i.e. $a_2 \leq 1$]. At laps, clear distance between bars ≤ 50 mm.											
2 $\alpha_1 = \alpha_3 = \alpha_4 = \alpha_5 = 1.0$. For the beneficial effects of shape of bar, cover and confinement see Eurocode 2, Table 8.2.											
3 Design stress has been taken as 435 MPa. Where the design stress in the bar at the position from where the anchorage is measured, σ_{sd} , is less than 435 MPa the figures in this table can be factored by $\sigma_{sd}/435$. The minimum lap length is given in cl 8.7.3 of Eurocode 2.											
4 The anchorage and lap lengths have been rounded up to the nearest 10 mm.											
5 Where 33% of bars are lapped in one location, decrease the lap lengths for '50% lapped in one location' by a factor of 0.82.											
6 The figures in this table have been prepared for concrete class C25/30; refer to Table 13 for other classes or use the following factors for other concrete classes.											
Concrete class	C20/25	C28/35	C30/37	C32/40	C35/45	C40/50	C45/55	C50/60			
Factor	1.16	0.93	0.89	0.85	0.80	0.73	0.68	0.63			

Figure 2.12. lap and anchorage length for concrete class C25/30 (mm) (Extract from (Bond et al., 2018)).

The coefficient α_6 may also be determined as follows:

$$1.0 \geq \alpha_6 = \left(\frac{\rho_1}{25}\right)^{0.5} \leq 1.5$$

With

ρ_1 is the proportion of lapped bars at a section

The placing of shear links at the outer section of the lap length is required by Eurocode 2 for the concentration of splitting forces at lap ends. Shear links required for other reasons might be assumed sufficient if the proportion of lapped bars is less than 25%. The cross-sectional area of the shear link must not be lower than the cross-sectional area of one lapped bar for laps with a diameter higher than or equal to 20ϕ .

Equation (2.29) must be rearranged to obtain the bar developable stress. This enables the computation of experimental data and compared the various design model.

$$\sigma_{sd} = (l_o/\phi) \left(\frac{4f_{bd}}{\alpha_1 \alpha_2 \alpha_3 \alpha_4 \alpha_5 \alpha_6} \right) \quad (2.30)$$

For straight bars without shear pressure and good bond condition, the average bar stress may be calculated as:

$$\sigma_{sd} = (l_0/\phi) \left(\frac{2.7f_{ck}^{2/3} \eta_2}{\alpha_2 \left(1 - k \left(\frac{\sum A_{st} - \sum A_{st,min}}{A_s} \right) \right) \alpha_6} \right) \quad (2.31)$$

2.6.2.4 American Concrete Institute (ACI)

Orangun et al. (1977) developed the design model that is used in ACI Code (2011). The design anchorage length is determined as:

$$\sigma_{sd} = \left(\frac{3}{40} \right) (f_y / \lambda \sqrt{f'_c}) \left(\frac{\psi_t \psi_c \psi_s}{c_b + k_{tr}} \right) \phi \quad (2.32)$$

f_y is the bar yield stress

$c_b = \min \left\{ \frac{(c_s + \phi)}{2}; c_y + \frac{\phi}{2}; c_x + \frac{\phi}{2} \right\}$, because the cover values are connected to the bar centre in ACI, the values $\frac{\phi}{2}$ have to be added to comply with the notion.

f'_c is the cylinder concrete strength limited to 69 MPa

ψ_c is the coefficient for coated reinforcement (for uncoated bars $\psi_c = 1.0$)

ψ_s is the coefficient for bar diameter (1.0 for bars ≥ 22 mm, otherwise 0.8)

ψ_t is the coefficient for bond (for good bond condition $\psi_t = 1.0$)

k_{tr} is the shear link index

$$k_{tr} = \frac{40A_{st}[\text{in.}^2]}{s[\text{in.}]n_b} \quad (2.33)$$

$$\frac{c_b + k_{tr}}{\phi} \quad (2.34)$$

Where

S is the shear link spacing

A_{st} is the cross-sectional area of all shear links within the spacing

n_b are the number of lapped bars

Pull-out failure becomes more probable for confinement ratios $\frac{(c_b+k_{tr})}{\phi}$ above 2.5 and increasing transverse reinforcement or concrete cover does not result in enhanced bond capacity. Darwin et al. (1995) reported that for $\frac{c_b+k_{tr}}{\phi} > 3.75$, the bond capacity did not increase, thus the limit of 2.5 provides extra safety (ACI Committee 408, 2003).

For normal-weight concrete, uncoated reinforcement, and good bond conditions, equation (3.8 first) can be simplified to

$$l_b = \left(\frac{3}{40}\right) \left(\frac{f_y}{\sqrt{f'_c}}\right) \left(\frac{\psi_s}{\frac{c_b+k_{tr}}{\phi}}\right) \phi (\text{in.}) \quad (2.35)$$

Rearranging for the anchorage strength gives

$$\sigma_s = \left(\frac{40}{4}\right) \left(\frac{l_b}{\phi}\right) \sqrt{f'_c} \left(\frac{c_b+k_{tr}}{\phi}\right) \left(\frac{1}{\psi_s}\right) (\text{psi}) \quad (2.36)$$

If confinement by compressive reaction is present at the simple support, the development length can be decreased by around 30%. It is worth noting that the ACI design guide permits bar diameters of up to 57 mm. For reinforcing bars with 43 mm and 57 mm diameters, the minimum allowable cover concrete is 38 mm in beams and 19 mm in slabs.

It must be noted that ACI [14] allows for bar diameters up to 57 mm. The minimum permissible concrete cover is 38 mm in beams and 19 mm in slabs (for ϕ 43 mm and ϕ 57 mm reinforcing bars: 38 mm). The smaller of the two values, the bar diameter or 25 mm, is the minimum clear bar spacing.

Due to a lack of sufficient experimental evidence, ACI does not allow laps of 43ϕ and 57ϕ . Table 8 shows the relation between the required and provided reinforcement and the coefficient for the proportion of bars lapped based on ACI recommendations. The coefficient 1.3 is not established on bond stress investigations; however, it is intended to promote the placement of laps away from high tensile stress regions to places where the reinforcement cross-sectional area provided as a minimum is twice that required by analysis. As a result, this coefficient contains a level of safety.

Table 2.3 Spliced length coefficient for the percentage of lapped bars and the provided reinforcement (ACI committee 318, 2011).

Lap length	$A_{s,prov}/A_{s,req.}$	Percentage of A_s spliced
$\max \{1.0 \cdot l_b; 305 \text{ mm}\}$	≥ 2.0	50
$\max \{1.3 \cdot l_b; 305 \text{ mm}\}$		100
		< 2.0

Smaller bar diameters with short lap lengths, the majority of which were less than 300 mm, were used to validate the design model. As a result, a factor for bar size γ is 1.0 and 0.8 for larger bar diameters and smaller bars not more than 22 mm were introduced. The ACI committee 408 advised against a size effect factor of less than 1.0.

2.6.2.5 German National Annex

The minimum permissible bar spacing coefficient (c_s) and the tensile strength coefficient (α_{ct}) are nationally determined parameters used for lap and anchorage calculation according to Eurocode 2. The National Annex defines the spacing of the bars as $c_s = 1.0$ and the tensile strength $\alpha_{ct} = 1.0$ for bond strength calculation.

The anchorage length at direct supports may be computed using $\alpha_5 = 2/3$, taking transverse pressure into consideration. For anchorages, the National Annex suggests using a simple cover concrete coefficient of $\alpha_2 = 1.0$. The cover concrete orthogonal to the lap plane (c_y) is not taken into consideration for spliced rebars with straight ends, based on the National Annex.

For laps, the cover used for the calculation of the coefficient α_2 is $c_{min} = \min(c_s/2, 0, c_x)$. The lap factor α_6 is determined by the bar diameter and the proportion of bars lapped at a location. The recommended values for α_6 are shown in Table 2.9.

Table 2.4 German National Annex for the percentage of spliced bar under tension based on (NA/EC2).

Percentage of bars lapped at a section in one layer		Bar diameter \emptyset
$\geq 33\%$	$\leq 33\%$	
1.4 (1.0)	1.2 (1.0)	$< 16 \text{ mm}$
2.0 (1.4)	1.4 (1.0)	$\geq 16 \text{ mm}$
The values in brackets are valid for $c_s \geq 8\emptyset$ and $c_x \geq 4\emptyset$		

According to Eurocode 2, if more than 50% of the reinforcement is spliced at one location, transverse reinforcement in laps must be made by links. However, the National Annex relaxes this requirement by specifying that the transverse reinforcement does not need to have a longitudinal spacing of $0.5l_0$ between adjacent lap centres or consist of links with distances between adjacent laps greater than $10\emptyset$.

2.6.3 PTI Working Draft

The PTI working draft proposes a revised design model for the next generation of Eurocode 2 based on Fib Bulletin 72. To make the model easier to use, the exponents have been simplified. The required bond strength for good bond conditions comes from

$$l_{bd,req.} = 40(25 \text{ MPa}/f_{ck})^{1/2} \left(\frac{\sigma_{sd}}{435 \text{ MPa}} \frac{\gamma_c}{1.5} \right)^{3/2} (\emptyset/20 \text{ mm})^{1/3} (1.5\emptyset/c_{d,conf})^{1/2} \quad (2.37)$$

$$\leq l_{b,min}$$

With

$l_{b,min}$ is the minimum lap length with $20\emptyset$ for laps

$$c_{d,conf} = c_d + \left(30k_{conf} \frac{n_l A_{st}}{n_b \emptyset S_{st}} + 8\sigma_{ctd}/\sqrt{f_{ck}} \right) \emptyset \leq 3.75\emptyset \quad (2.38)$$

σ_{ctd} is the design value of the mean compression stress perpendicular to the potential splitting plane

K_{conf} is the effectiveness factor. K_{conf} is taken as 0.25 for shear links within the cover c_y with cover spacing greater than 8ϕ , and 1.0 for confinement reinforcement crossing the potential splitting plane (the maximum recommended distance from the leg to the lapped bar is less than 5ϕ). In other circumstances, K_{conf} is taken as zero.

The PTI working draft recommended the laps be designed for $1.2 \times \sigma_{sd}$ if tension laps are located in regions where the yield strength may be exceeded. Therefore, a reduction of lapped bars or confining reinforcement is required. Reliability analysis of the coefficients 8,30, and 40 in Fib Bulletin 72 expression (1.45) and (1.46). Rearranging for the developable stress in anchorages gives

$$f_{std} = 435(1.5/\gamma_c)^{1/3}(20/\phi)^{2/9}(l_b/40\phi)^{2/3}(c_{d,conf}/1.5\phi)^{1/3} \quad (2.39)$$

2.6.4 Canbay and Frosch (2005)

Four hundred and eighty experiments with and with shear links were used by Canbay and Frosch (2005) to verified their model for ultimate lap load. The ultimate lap strength at splitting failure, taking shear link into account is defined as

$$\sigma_{sd} = F_{split} + F_{st}/n_b A_s \tan\beta = 2.75/n_b A_s (F_{split} + F_{st})(ksi) \quad (2.40)$$

Where

θ inclination of struts commencing at the rib flanks (20° provided optimal results)

F_{st} is the splitting resistance by a shear link [kip]

F_{split} is the splitting resistance by cover concrete along the lap length [kip]

Canbay and Frosch (2005) distinguish side (Figure 2.10, middle) and face splitting types (Figure 2.10 left).

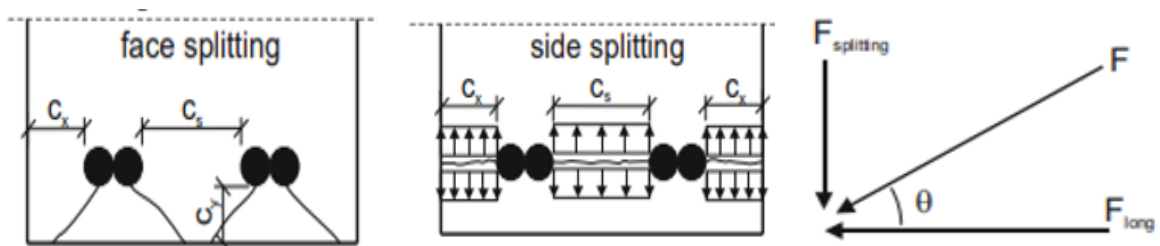


Figure 2.13. face splitting (left), Side-splitting (middle), and force distribution at bond forces (right) [adapted from (Canbay 2006)]

It is assumed that the tensile concrete stress surrounding the bars is linear along the lap length. The bond strength nonlinearity along the splice length is taken into account by using an efficient lap length l_0^* . The side-splitting force $F_{split,side}$ is

$$F_{split,side} = l_0^* [2c_x^* + 2c_x^*(n_b - 1)] 6f_c^{1/2} \text{ (kip)} \quad (2.41)$$

For face-splitting, the splitting force $F_{split,face}$ is

$$F_{split,face} = l_0^* \left[2c_y^* \left(0.1 \frac{c_x}{c_y} + 0.9 \right) + 2c_y^*(n_b - 1) \left(0.1 \frac{c_s}{2c_y} + 0.9 \right) \right] 6f_c^{1/2} \quad (2.42)$$

With

c_x^* , c_x^* , $\left(\frac{c_s}{2}\right)^*$ coefficients for the efficiency of concrete cover at linear stress distribution

$$l_0^* = l_0 \frac{9.5l_1}{\sqrt{l_0/\phi} f_c^4} \leq l_0$$

l_0 coefficient for the efficiency of lap length at linear stress distribution

In the failure of splitting, shear links provides extra resistance. The splitting force $F_{st,side}$ provided by the shear link, is given by expression (2.43). For side splitting, this expression includes the number of legs crossing the splitting plane in

$$F_{st,side} = n_{st} n_l A_{st} f_{yt} \left[\frac{n_b f_c^{1/2}}{170} \right] \text{ (kip)} \quad (2.43)$$

Because the shear link crosses the splitting plane at each bar in face split failure, expression (1.52) incorporates the bar number instead of the leg number in determining the splitting force.

$$F_{st,face} = n_{st} n_b A_{st} f_{yt} \left[\frac{n_b f_c^{1/2}}{170} \right] \text{ (kip)} \quad (2.44)$$

62 MPa is the suggested transverse bar yield strength. A safety factor of 1.2 was utilised to develop the design expression (2.40). 50% of the calculated strength were unsafe without the safety factor. Only 16% of the confined and 10% of the unconfined test meet their yield strength when the factor of 1.2 was used. This takes into consideration the lap length designed based on the proposed model and a nominal yield strength of 414 MPa.

2.7 Structural Application of stainless steel

In the field of structural engineering, stainless steel is a popular choice for load-bearing applications due to its exceptional corrosion resistance, good formability, and recyclability, as well as its outstanding mechanical properties and long lifespan, requiring minimal maintenance (Shamass and Cashell, 2018). Compared to mild steel, stainless steel has superior strain-hardening capacity and ductility, making it an ideal choice for use as a ductile section that warns of impending collapse. Initially, stainless steel was used in building construction during the 1920s for façade and roofing purposes (Baddoo, 2008). Recently, stainless steel has gained popularity in load-bearing applications that require strength, ductility, durability, stiffness, and high resistance. Various forms of stainless steel are manufactured, including tubes, plates, sheets, bars, fasteners, fixings, and rolled and cold-formed structural sections. Among these, cold-formed sections made from steel plates are the most widely utilised materials for structural components, as they are readily available and relatively easy to produce (Gardner, 2005).

2.7.1 Composition

Stainless steel is a type of corrosion-resistant alloy steel with a maximum carbon content of 1.2% and a minimum chromium concentration of 10.5% (EN 10088-1, 2014). The unique properties of stainless steel are determined by its constituent elements, so choosing the right grade for each purpose is essential. In all stainless steel alloys, chromium is one of the most important elements as it provides corrosion resistance by forming a thin chromium oxide film on the surface of the material when exposed to oxygen, creating a passive protective layer (Evans, 2002). Other alloying elements also play a crucial role in determining the characteristics of stainless steel. For instance, nitrogen significantly enhances the mechanical properties of the material, molybdenum improves its resistance against uniform and localized corrosion, and nickel improves its formability and ductility (Markeset et al., 2006). Other commonly present alloying elements include sulfur, carbon, phosphorus, copper, and silicon. The European Standard EN 10088-1 (2014) provides comprehensive information on the chemical composition of various stainless steel grades. Table 7.1 shows the chemical composition of some commonly used stainless steel reinforcement grades.

2.7.2 Classification

Stainless steels are classified using various international categorisation systems, with the American Iron and Steel Institute (AISI) specification and European standards being the most commonly used. For more information on these classification systems, please refer to the sub-sections below.

2.7.3 The American iron and steel institute system

Stainless steels are categorised into different types by the AISI. For example, ferritic and austenitic stainless steels are classified as 400 series alloys (e.g., 403, 409) and 300 series alloys (e.g., 316, 304), respectively. However, one of the drawbacks of this system is that it does not provide detailed information about the chemical composition of each grade. To address this issue, Table 2.5 provides a list of some commonly used stainless-steel reinforcement grades, along with their equivalents.

2.7.4 The European standard

Stainless steel's chemical composition is classified by the European standard EN 100088-1 (2014). An individual number is assigned to correspond to the nominal alloy composition, and then a generic number is assigned to each grade to identify it as part of a group. For example, in grade 1.4436, the number 1 represents the standard, 44 represents the stainless-steel group, and 36 represents the individual material ID. To provide more information about a grade's chemical composition, the grade number is also given the corresponding grade name. Grade 1.4436, for instance, is designated as X3CrNiMo 17-13-3. The X represents high alloy steel, 3 represents the % of carbon content, CrNiMo is the chemical symbol of the main alloying elements, and 17-13-3 refers to the nominal % of the main alloying elements.

Table 2.5. The chemical composition of various stainless-steel grades (Markeset et al., 2006)

American (AISI)	European (EN 10088-1)		Chemical composition (%)									
	Grade	Name	Grade	C	Si	Mn	P	S	Cr	Ni	Mo	N
				Ma x	Ma x	Ma x	Max	Max	Max	Max	Ma x	Max
2205	X5CrNi 18-10	1.430 1	0.3	1.0	2.0	0.35	0.01	5	21.0 / 23.0	4.5/ 6.5	2.5 / 3.5	0.10/ 0.22
2304	X5CrNiM 17-12-2	1.440 1	0.3	1.0	2.0	0.35	0.01	5	22.0 / 24.0	3.5/ 5.5	0.1 / 0.6	0.05/ 0.20
LDX 2191	X2CrNiM 17-13-3	1.442 9	0.3	0.4	5.0	-	-	-	21.5	1.5	0.3	max 0.22
316LN	X3CrNiM 22-2-0	1.416 2	0.3	1.0	2.0	0.04	0.01	5	16.5 / 18.5	11.0 / 14.0	2.5 / 3.0	0.12/ 0.22
316	X3CrNiM 23-4	1.436 2	0.7	1.0	2.0	0.04	0.3	5	16.5 / 18.5	10.0 / 13.0	2.0 / 2.5	max 0.11
304	X2CrNiM 22-5-3	1.446 2	0.7	1.0	2.0	0.04	0.3	5	17.5 / 19.5	8.0/ 10.5	-	max 0.11

2.8 Material properties

Stainless steels are known for their superior corrosion resistance, weldability, toughness, and strength. However, their material properties can vary depending on several factors, such as the direction of rolling, the level of cold working, the material thickness, and the chemical composition. Compared to carbon steels, duplex, and austenitic stainless steels exhibit significantly higher strength and strain-hardening properties. These grades are also characterized by high ductility, which can exceed 40%. Conversely, martensitic, or ferritic stainless steels have lower strength and strain hardening. Precipitation-hardened stainless steels offer exceptionally high strength, often exceeding 1500 N/mm², but limited ductility, depending on the heat treatment condition (British Stainless-Steel Association, 2000).

The elasticity modulus of various stainless-steel categories is generally the same as that of carbon steel. According to the European standard (EN 10088-2, 2014), an elasticity modulus value of 200,000 N/mm² can be used for all stainless-steel grades. Table 7.2 provides information on the mechanical properties of some typical grades of stainless steel.

Table 2.6.

Stainless steel type	Grade	Minimum 0.2% proof strength N/mm^2	Ultimate tensile strength N/mm^2	Modulus of elasticity, E kN/mm^2	Minimum elongation after fracture (%)
Ferritic	1.400 (410S)	220	400-600	200	19
	1.4512 (409)	210	380-560	200	21
Duplex	1.4362 (SAF2304)	400	600-850	200	20
	1.4462 (2205)	400	640-840	200	20
Austenitic	1.4301 (304)	210	520-720	200	45
	1.4307 (302L)	200	500-650	200	45
	1.4401 (316)	220	520-670	200	40
	1.4404 (316L)	220	520-670	200	40

Mechanical properties of stainless steels grades (EN 10088-2, 2014)

2.8.1 Recycle

The construction industry generates a significant amount of waste material, and there is a need to use more environmentally friendly materials to reduce waste. Stainless steels are durable materials that contain high residual values of essential elements such as molybdenum, chromium, and nickel (British Stainless-Steel Association, 2000). Research shows that around 80% of new stainless steel manufactured in Europe comes from recycled waste stainless steel (Aalco, 2013), which makes stainless steel a more sustainable and economically beneficial option.

2.8.2 Cost

Stainless steels are generally more expensive than carbon steels in structural applications (Eladly, 2020; Sharif et al., 2019), which has limited their widespread use. However, the initial material cost does not reflect the overall cost of construction during its lifetime. Factors such as inspection and maintenance costs, as well as the immediate cost associated with fire and corrosion protection, must be taken into account when making an informed decision. When all of these aspects are considered simultaneously, stainless steel is a superior option to carbon steel, especially for buildings that are exposed to extreme environments.

2.9 Stainless steel reinforcing bars in concrete structures

Reinforced concrete is one of the most popular structural solutions used in building construction due to its efficiency, cost-effectiveness, versatility, and well-established design guidelines. Recently, stainless steel has emerged as a promising material for reinforced concrete structures due to its excellent durability, corrosion resistance, long life cycle, and great ductility.

One of the most commonly used structural solutions in building construction is reinforced concrete. It is popular because it is an efficient, cost-effective, and versatile solution with plenty of performance criteria and design guidelines. Owing to their great ductility, significant strain hardening, excellent durability, exceptional corrosion resistance and long-life cycle, stainless steel has recently been used in reinforced concrete structures.

Reinforced concrete constructions are widely used for various applications, such as bridges, multi-storey buildings, and tunnels, due to the effective use of readily available constituent materials.

However, the constitutive behavior of stainless steel differs significantly from that of carbon steel. Stainless steel exhibits a rounded behavior from the start, with high ductility and significant strain hardening, without a clearly defined yield point, as shown in Figure 2.14. In contrast, carbon steel has a more linear relationship in the elastic stage, with a moderate degree of strain hardening and a well-defined yield point. When there is no observable yield point, the 0.2% proof stress is typically used in the design.

To represent the behavior of stainless steel, the modified-Osgood stainless steel material model is often used, which is an improvement of the original version presented in Ramberg and Osgood (1943).

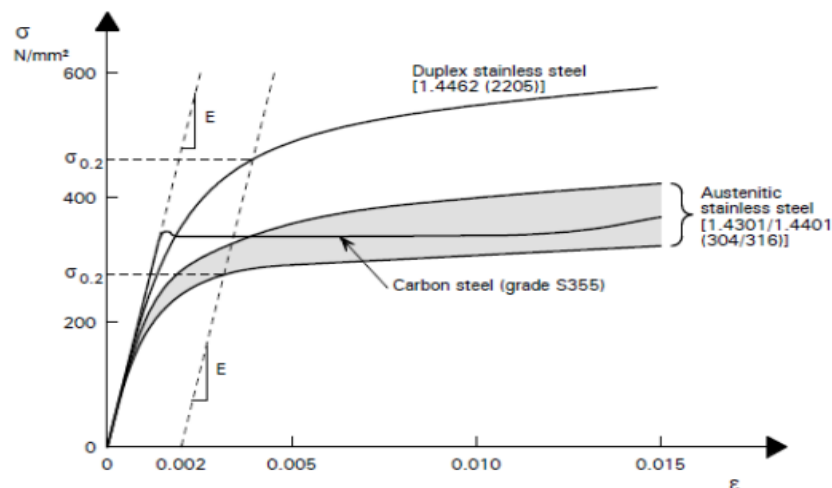


Figure 2.14. Stress-strain curves for stainless steel and carbon steel (Baddoo and Burgan, 2012).

2.9.1 Life cycle cost

Stainless steel reinforcing bars have a higher initial cost than ordinary carbon steel reinforcing bars, ranging from three to eight times more depending on the grade (Metals4U, 2021; Nationwide Stainless, 2021). Due to this high initial cost, stainless steel reinforcement is sometimes limited to the outer layer, which is more vulnerable to chloride-ingress.

However, stainless steel reinforcement has been proven to save total maintenance costs by

up to 50% throughout the life of a structure, particularly marine and bridge structures (Cramer et al., 2002). A study conducted by the Arup Research and Development team, overseen by the UK Highways Agency, revealed that incorporating stainless steel reinforcement can significantly enhance the lifetime of buildings while lowering maintenance costs (Gedge, 2003). This quality is crucial for infrastructure and highways to minimize rerouting and road closures, as well as carbon emissions and delays that come with them. Moreover, employing corrosion-resistant reinforcing bars like stainless steel can save a lot of money by relaxing some durability criteria, such as the need for reinforcement coating, design crack width, and depth of concrete cover. Incorporating these adjustments into the design of reinforced concrete buildings can save a lot of money, especially on big projects.

The Oland Bridge in Sweden, which employed both carbon and stainless-steel reinforcing bars, is presented in Figure 2.15 as an instance of real-life cycle costs. The data in the figure demonstrated that the cost of a bridge with stainless steel stays unchanged during its lifetime, suggesting no extra expenses, but the cost of a carbon steel-reinforced concrete solution increases drastically after around 20 years. Another study on the Schaffhausen bridge in Switzerland found that the use of stainless steel resulted in a 14% lower life cycle cost than carbon steel rebar (McGurn, 1998). This provides compelling evidence of stainless steel reinforcement's long-term cost-effectiveness in infrastructure projects.

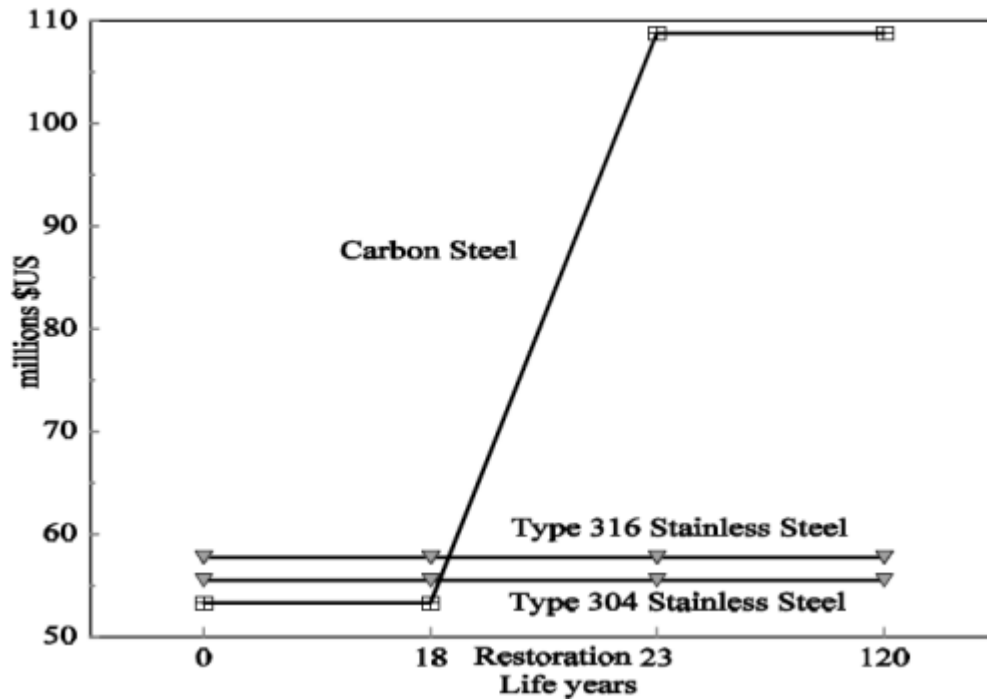


Figure 2.15. Life cycle analysis for Sweden's Oland bridge (McGurn, 1998)

2.9.2 Durability

There is a growing need to increase the life cycle cost and durability of reinforced concrete buildings due to the high maintenance costs associated with carbonation and steel reinforcement corrosion of the concrete. This is especially true for buildings in harsh environments such as those found in industrial, coastal, and marine settings. Corrosion is difficult to avoid in buildings with carbon steel that are exposed to harsh environments. While changing design parameters such as controlling the alkalinity of the concrete mix or the thickness of the concrete cover is a common approach to increasing the durability of reinforced concrete structures (British Highways Authority, 2003), these precautions may not be sufficient to prevent the intolerable level of corrosion from forming in harsh environments.

Using stainless steel reinforcement in exposed structures like tunnels, bridges, and retaining walls can be an effective way to combat corrosion and deterioration and may even eliminate the need for future rehabilitation work and expensive inspections. Additionally, existing concrete structures can be rehabilitated and restored using stainless steel reinforcement (Pérez-Quiroz et al., 2008).

2.9.3 Mechanical behaviour

When compared to traditional carbon steel, stainless steel reinforcement exhibits superior mechanical behavior. In recent years, a limited number of experiments have been conducted on the mechanical behavior of stainless steel reinforcement. Stainless steel reinforcement grades demonstrate greater hardness and strength properties compared to carbon steel reinforcement (Castro et al., 2003).

Medina et al. (2015) studied the mechanical and ductility properties of stainless steel reinforcement grades 1.4482, 1.4301, and 1.4362, with reference to carbon steel grade B500SD. The study found that stainless steels exhibit three times the ductility of carbon steel. However, these stainless steels had a 15% lower elasticity modulus than carbon steels, which is attributed to their nonlinear behavior from the beginning, making the modulus of elasticity difficult to measure.

Table 2.7 provides an overview of some of the mechanical parameters of several grades of stainless steel reinforcement. The stainless steels exhibit excellent ductility, significant strain hardening, and outstanding tensile strength. These characteristics are crucial in design to minimize unexpected collapse.

Overall, stainless steel reinforcement has shown to have superior mechanical properties compared to traditional carbon steel reinforcement, making it an ideal choice for structures that require high strength and durability.

Table 2.7. Mechanical properties of stainless-steel reinforcement (Mcgee, 2017).

Product form	Grade	Bar diameter (mm)	Yield strength $\sigma_{0.2}$ N/mm^2	Tensile strength N/mm^2	Modulus E (kN/mm ²)	Elongation ϵ_u
Ribbed bars	1.4311	12	480	764	202.6	48.3
	1.4311	16	528	717	199.9	47.9
	1.4162	12	682	874	199.1	32.4
	1.4162	16	646	844	195.2	32.9
	1.4362	16	608	834	171.4	35.1
Plain Round bars	1.4307	12	562	796	210.2	39.9
	1.4307	16	537	751	211.1	42.4
	1.4162	12	805	964	308.7	18.8
	1.4162	16	760	860	197.5	22.0

2.9.4 Use of stainless-steel reinforcement

It is widely recognized that carbon steel reinforcement used in reinforced concrete structures may not be as durable as previously thought in all conditions (British Stainless Steel Association, 2003). Corrosion of carbon steel reinforcement in harsh environments such as coastal and marine regions can lead to inconvenient and very expensive rehabilitation work. Stainless steel reinforcement is an effective and long-lasting option in such situations. The Gatwick Bridge in Australia, depicted in Figure 2.16, was the first of its kind built in 1986 using grade stainless steel and is one of the earliest examples of the use of stainless steel reinforcement. The bridge has been in service for more than 70 years without requiring any significant maintenance or major repair work.

Other projects that have utilized stainless steel reinforcement include the Saint George Bridge in Genova and the Aillt Chonoglias Bridge in Scotland, depicted in Figures 2.17 and 2.18, respectively. Both of these bridges are made of stainless steel. Stainless steel reinforcement has been employed for both restoration and renovation as well as new construction.



Figure 2.16 Gatwick bridge in Austria (Stainlessrebar, 2021)



Figure 2.17. Stonecutters Bridge (Mark, 2021)



Figure 2.18. Allt Chonoglias Bridge in Scotland (Stainlessrebar, 2021)

2.9.5 Fire behaviour

One of the most crucial factors for creating fire-resistant buildings is the material's ability to maintain strength and stiffness at high temperatures. Due to its chemical composition, stainless steel has exceptional strength and stiffness retention at extreme temperatures (Baddoo, 2008). Although there have been numerous studies on stainless steel's fire performance (e.g., Huang and Young, 2014; Lopes et al., 2012; Fan et al., 2016), very few

research studies have examined the performance of stainless steel at high temperatures (e.g., Gardner et al., 2016).

Figures 2.19 and 2.20 compare the stiffness and strength retention factors between carbon steel and stainless steel at 0.2% proof stress. Stainless steel has a distinct advantage over carbon steel in terms of stiffness and strength at high temperatures. These distinguishing characteristics are immensely useful in the event of a fire, giving the structure the resistance needed for a longer duration of time.

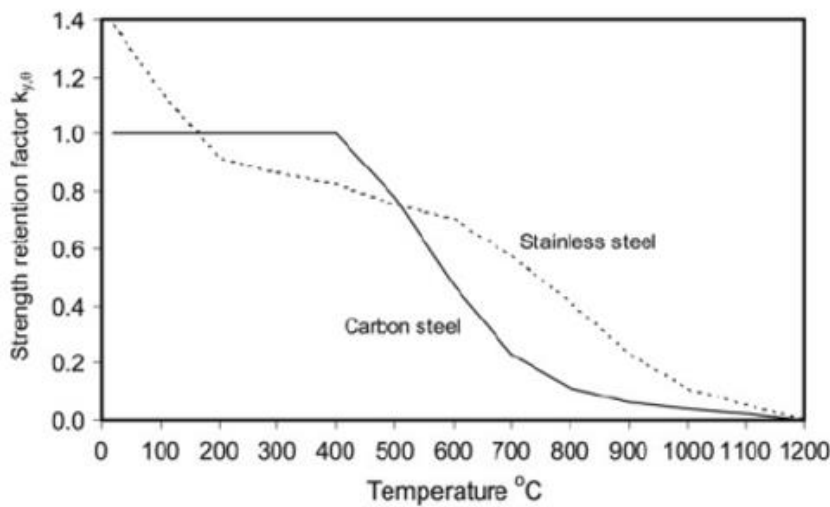


Figure 2.19. Comparison of carbon steel and stainless-steel strength retention factor (Badoo, 2008)

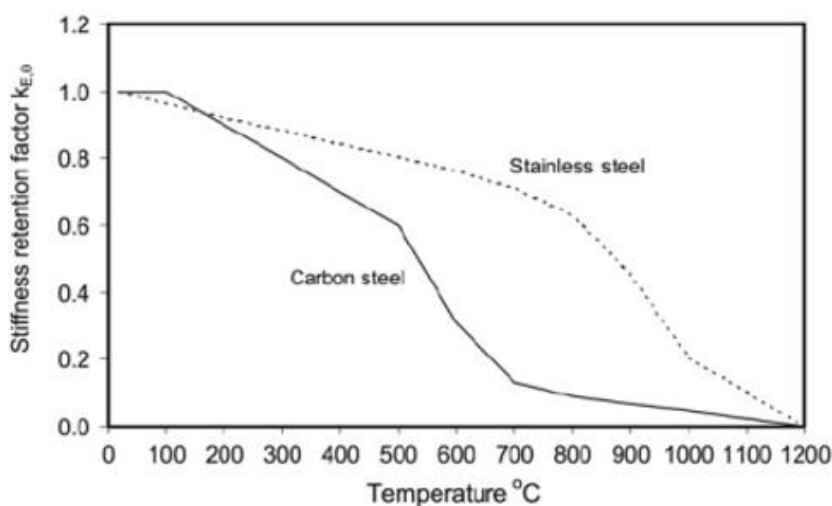


Figure 2.20. Comparison of carbon steel and stainless-steel stiffness retention factor (Badoo, 2008)

2.9.6 Corrosion behaviour

Corrosion of reinforcement is now recognized as one of the most significant issues facing reinforced concrete structures, particularly those in harsh environments (Helland, 2013). Corrosion weakens the bond strength between the surrounding concrete and the reinforcement, and reduces the nominal reinforcement area, which compromises the integrity and safety of concrete structures. Corrosion can occur due to carbonation and chloride penetration of concrete. Carbonation is caused by carbon dioxide in the surrounding air attacking the calcium in the concrete, while chloride ingress from marine environments or de-icing salts in frosty weather causes the latter.

The corrosion protection of reinforcement in a typical reinforced concrete design is mainly dependent on the durability of the steel passivation layer and the concrete cover. However, this passivation layer on typical carbon steels can quickly break down, allowing corrosion to form, particularly in harsh or contaminated environments. The usual methods of decreasing the potential corrosion risk include controlling the concrete alkalinity, using reinforcement coating materials or cement inhibitors, or increasing the depth of concrete cover (British Steel Association, 2003). While these precautions may be effective to some extent, they may not be sufficient to prevent corrosion to undesirable levels.

In this situation, stainless steel reinforcement is an excellent alternative for dealing with inherent corrosion issues. Due to its high chromium content (i.e., a minimum of 10.5%), stainless steel offers excellent corrosion resistance, even in harsh environments. In the presence of oxygen, chromium produces a thin, self-regenerating chromium oxide coating on the material's surface, forming a strong passive protective layer (Medina et al., 2015; Evans, 2002).

Stainless steel reinforcement is known to be ten times more resistant to corrosion than carbon steel reinforcement (García-Alonso et al., 2007; Nurnberger, 1996). Moreover, duplex reinforcement, which has a combination of austenitic and ferritic structures, has corrosion resistance that is equal or even superior to that of austenitic reinforcement (Serdar and Bjegović, 2013; Bautista et al., 2007; Nurnberger, 1996). Figure 2.21 compares the corrosion performance of various stainless steel grades and carbon steel with respect to concrete pH and chloride concentration. It is evident that carbon steel has poor corrosion resistance even at very low chloride concentrations and is highly sensitive to concrete pH. In

contrast, stainless steel reinforcement exhibits excellent corrosion resistance, even at low pH values and high chloride concentrations.

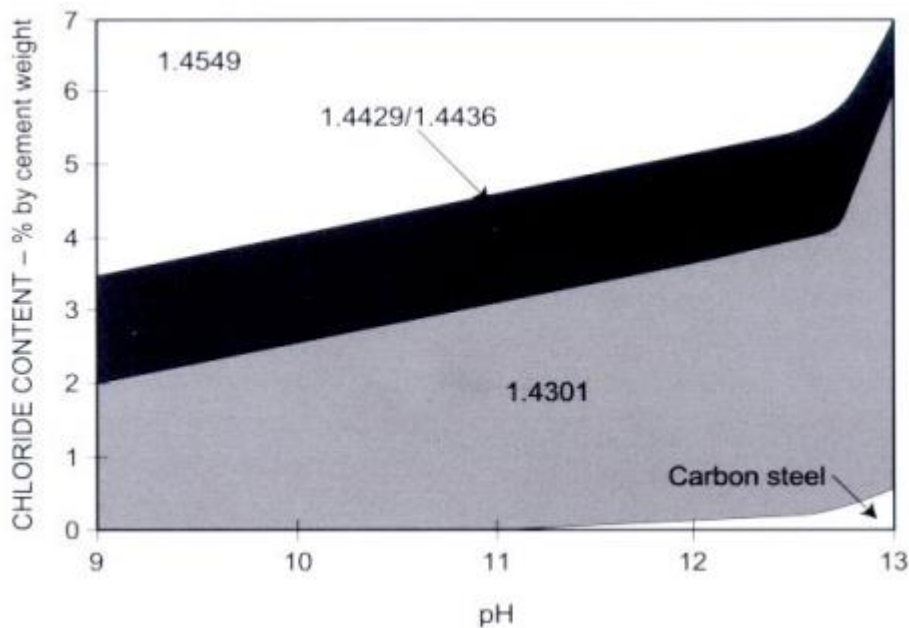


Figure 2.21. Corrosion performance of various stainless steel compared to carbon steel.

2.9.7 Bond behaviour

In the design of reinforced concrete structures, achieving a strong bond between the concrete and steel reinforcement is essential to efficiently transfer loads. Insufficient bond can cause various problems, including excessive rotation or deflection, inadequate anchorage, and cracking. The bond is influenced by several interconnected factors, such as the surface geometry of the reinforcement and the quality of the concrete, as well as bar size, cover distance, casting direction, spacing, and layering of the reinforcement.

While the bond performance of carbon steel reinforcement in concrete is well researched, there has been relatively little investigation into the bond behavior of stainless steel reinforcement, particularly in corrosive environments. Some studies suggest that the bond developed by some types of duplex and austenitic stainless steel bars is relatively low compared to similar carbon steel bars, even under normal conditions. Therefore, more research is needed to better understand the bonding properties of stainless steel reinforcement in concrete.

It is worth noting that many international design guidelines, such as MC2010 and Eurocode 2, do not have specific bond design rules for stainless steel-reinforced concrete structures. As a result, designers often use the same guidelines established for conventional carbon steel reinforcement. However, this approach may not always be safe, as stainless steel may have a lower bond strength than carbon steel. Therefore, designers should use specific test data when designing reinforced concrete structures with stainless steel reinforcement.

2.10 Analysis and summary

The semi-empirical expression used to estimate the bond resistance of ribbed reinforcing bars was calibrated from statistical experimental data to provide a margin of safety. However, the experimental samples used to calibrate the different coefficients are typically designed to investigate particular aspects of bond behaviour and may not necessarily represent normal construction practices. The following are the main distinctions between the tests and the actual practice:

- Lapped/spliced joints are typically placed in the most heavily stressed region of an experimental sample, whereas designers prefer to place them in regions where stress in reinforcement is low in actual practice.
- In experiments, lap joints/splices are usually placed in the constant moment region of a beam where shear force is zero, even though they are usually placed where it is present.
- All bars are lapped/spliced at the section in all but a handful of investigations of lapped joints, even though many design standards impose a penalty on lap length to discourage this.
- In the vast majority of experiments, both lapped bars are of the same diameter, although their diameter may differ in many situations.

These differences have implications for the development of design guidelines concerning bond resistance. The passage also highlights several aspects considered in the analysis of design and detailing, including Lapped Bars of Different Diameter, Interaction between Shear and bond requirements, location of Lapped Joints, continuity of reinforcement in lap Joints, and minimum confining reinforcement. These aspects affect the circumstances in

which reinforcement is required to transmit stress to concrete through bond and the available resistance, both directly and indirectly.

2.10.1 Lapped bars of different diameter

When lapped bars have different diameters, the lap length is determined based on the diameter of the smaller bar. According to ACI Committee 408 (2003), if the bars have different diameters, the lap length or splice should exceed either the anchorage length of the larger bar or the diameter of the smaller bar. However, the reason behind this requirement is unclear. While it is reasonable to ensure that both bars can generate the necessary force, the significance of the anchorage length of the larger bar is unknown. If the assumption is that anchorage bond strengths are inherently higher than lap bond strengths, it contradicts the findings of semi-empirical bond analyses in Fib Model Code (2010) and other design standards.

2.10.2 Interaction between shear and bond requirement

When shear occurs within a lap, the stress and moment distribution across the lap length are not constant, leading to certain areas of the lap being underutilised. While most experiments in the lap database focus on spliced laps in the constant moment region, in reality, laps can be positioned where shear forces are present. The presence of shear can affect the bond conditions in several ways:

- a) The difference in moment leads to varying forces at opposite ends of the lap, resulting in lower force transmission through bond in one bar compared to the other.
- b) Regions with higher bond stress coincide with areas where denser stirrups or links are present for shear reinforcement, thereby enhancing bond strength to some extent.
- c) Shear stress affects the links, and it has been suggested that shear-induced stress in links may enhance active confinement in laps similarly to transverse compression from reactions and loads.
- d) The presence of shear influences the variation of bond stress along the bar.
- e) Due to the aforementioned factors, the spliced bars may have different sizes.

The study conducted by Reynolds and Beeby (1982) compared the strength of shear span laps with equivalent laps in the constant moment region. They concluded that shear span laps were stronger and observed increased strength when shear forces were resisted by transverse reinforcement within the shear span. They attributed this enhanced strength to the increased stress developed in the transverse reinforcements. However, the dependency of this enhancement on diagonal shear cracking limits its applicability in design provisions, despite its value in understanding bond behavior.

The development length experiments carried out in the United States in the 1960s and 1970s provide an opportunity to evaluate the bond model in the zone of varying moments. The experimental setup is depicted schematically in Figure 2.22. However, due to the challenges in evaluating bond strength because splice length is not well-defined as a result of the ambiguity in the inclination of the diagonal cracking, this type of test has fallen out of favor. Jirsa et al. (1995) recognized the difficulty in carrying out bond experiments when shear is present; however, they observed no difference in bond strength due to shear acting simultaneously with the moment in the single test that failed in bond. Jirsa's findings are similar to Vollum and Micallef's (2017), in which they discovered that shear does not affect the bond strength of tested laps. Although no firm evidence is available, it has been hypothesized that the variation of force at the lap ends may lead to an increase in mean bond strength in the lap. The variation in stress between the ends will be small in most cases, so further design complications are unnecessary. As a result, it is not desirable to investigate this further.

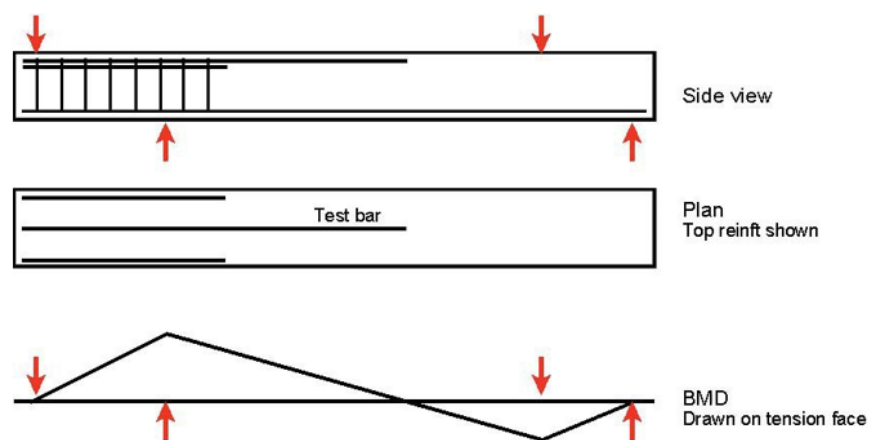


Figure 2.22. Development length type test sample (Jirsa et al., 1995).

2.10.3 Location of lapped joints

Most lap splicing experiments position the lap joint in the constant moment region of a simply supported beam, where shear is minimal and stress in reinforcement is highest. However, in construction, it is preferable to place lap joints where stress in reinforcement is low. Under normal service conditions, a bar lap spliced at the point of contraflexure needs to develop stresses near the design strength of the reinforcing bar, which is much lower than the full yield strength.

In the event of an internal column loss, the beam would need to span two ways, resulting in significant deflections. The load-carrying mechanism would shift from flexural to catenary action. To prevent full collapse in such situations, the lap joint may need to develop strains beyond the yield point. It is also important to ensure that links used to withstand excessive collapse can yield instead of experiencing brittle failure in bond.

Eurocode 2 and Model Code 90 allow for a reduction in lap length when an excess of reinforcement is provided beyond what is required by calculations, subject to specific minimum requirements. Figure 2.23 illustrates the relationship between the proportion of bars lapped at a section and the reduced lap length allowed by Model Code 90, considering the ratio of reinforcement area required by calculations. The graph is based on a basic lap length of 25ϕ and a bar diameter of 20 mm. Although the values presented are influenced by these parameters, the overall trends would generally apply in different cases. Similar patterns for AC1318 and Eurocode 2 are shown in Figures 2.23 and 2.24, respectively.

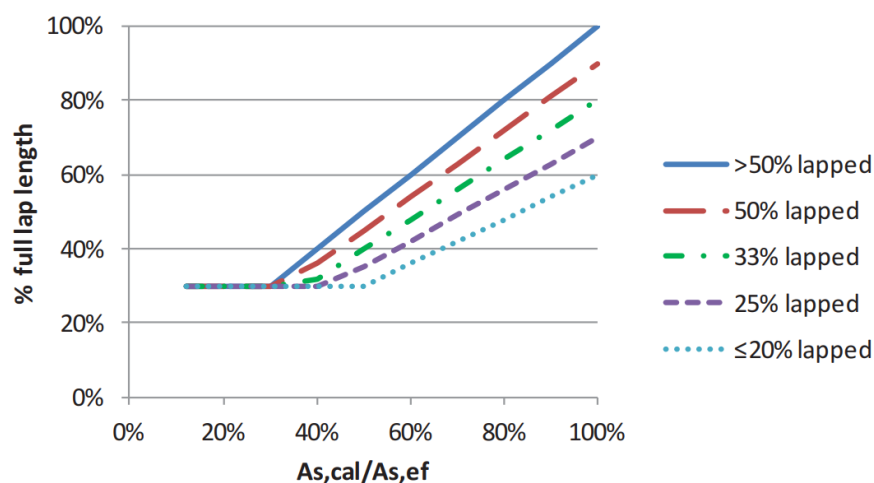


Figure 2.23. Reduction in lap length permitted for excess reinforcement (Model Code, 1990).

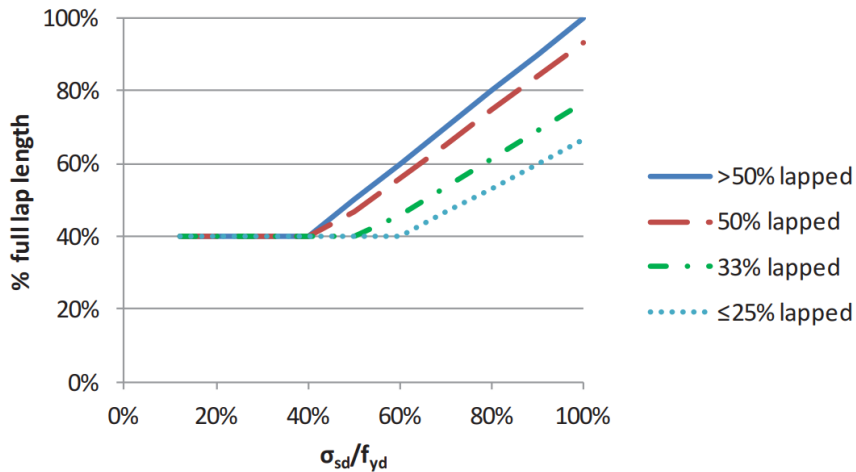


Figure 2.24. Reduction in lap length permitted for excess reinforcement, EC2(Metelli, Cairns and Plizzari, 2015).

Figure 2.15 demonstrates that Model Code 90 allows for significantly reduced lap lengths compared to those needed to achieve the design strength of a bar, based on the ratio of provided reinforcement area to the required area. Even if all bars were spliced at the same section, the code permits a lap length of only 30% if the reinforcement area provided is three times that required. Similarly, if the provided area is twice the required amount and only 20% of bars are spliced at a location, a lap length of 30% of the total design length is allowed. Such lap splices near a point of contraflexure could result in brittle failure if they were to fail.

While a lap joint may only need to exhibit ductile behavior in cases of overstress or accidental damage, the appropriate partial safety factor for these situations would be applied. However, even if the partial safety factor for resistance is smaller for accidental loads than for permanent and variable loads, the reduction in lap length allowed for extra reinforcement area would not be sufficient to allow the reinforcement to reach its yield point. Therefore, while Eurocode 2 and Model Code 90 guidelines ensure force capacity by adjusting the ratios of $(A_{s,cal} / A_{s,ef})$ in strength calculations, the strain capacity of a member may be significantly reduced if the lap length is inadequate for the bar to yield.

In current construction practice, regardless of the ratio $A_{s,cal} / A_{s,ef}$, detailers commonly use a "standard" lap length. As a result, when a lap occurs within the span of a beam, designers often employ a "full-strength" lap, which is overly conservative. Under normal conditions, a

partial safety factor of 1.5 is typically used to design bond resistance. For accidental loading, the partial safety factor on material strength decreases to 1.2. Lap lengths in low-stress regions can be reduced by 33% by considering the nonlinear relationship between lap length and lap strength. This reduction accounts for a factor of $(1.2/1.5)^{1.82}$, while still providing sufficient robustness margin in the event of accidental loading. ACI 318 (2011) guidelines align with this limit (Figure 2.25), but the rules in Eurocode 2 and Model Code 90 do not. Staggered laps, despite minimizing brittleness, do not provide ductility, and it seems that the standards in Model Code 90 do not offer adequate robustness.

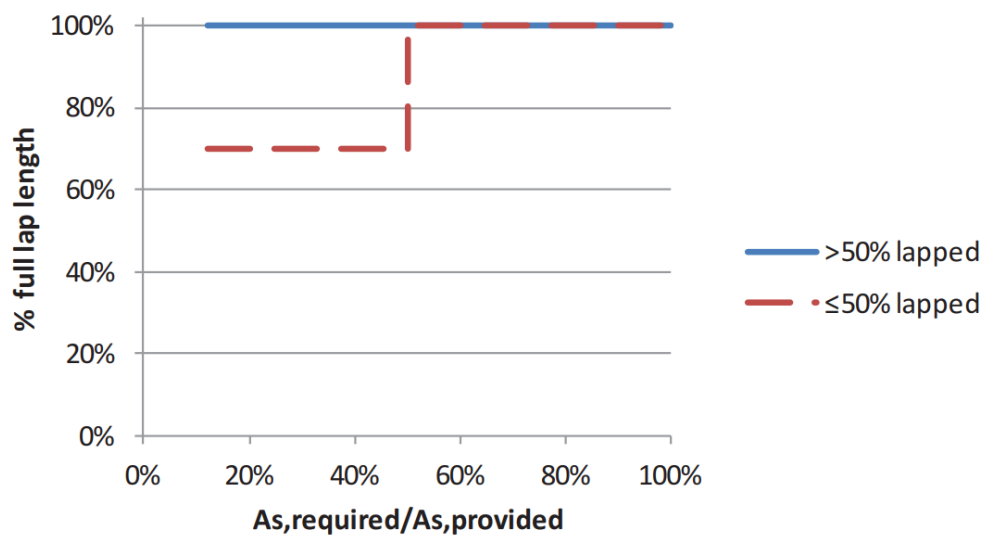


Figure 2.25. Reduction in lap length permitted for excess reinforcement (ACI 318, 2011).

It is recommended that for structural members of significant importance, lap lengths should not be reduced to less than 70% of what is allowed to achieve the design yield strength, even if there is excess reinforcement provided beyond the calculated requirement. This precaution is advised until a better understanding of the impact of staggered laps on ductility can be gained.

2.10.4 Continuity of reinforcement in lap joints

In many studies, the main reinforcement in a section is typically lap spliced at the same location within the span, despite codes discouraging this practice and imposing penalties on lap length. The proportion of lapped reinforcement has not received much attention, despite its significant impact on bond length. Experimental tests have shown that increasing the proportion of continuous reinforcement leads to significant enhancements in flexural

strength. Longer lap lengths have also been investigated, with some experiments showing that beams with 50% of the bars continuous through the lap region were slightly stronger on average, but the difference becomes negligible when considering the greater spacing between laps. Other experiments have shown that doubling the beam width or increasing the cover can increase the spliced strength, and tying a splice with stirrups can further enhance its strength. The size of the reinforcement bars also affects bond strength, even when other factors such as beam width, splice length, and cover are the same.

Rezansoff et al. (1992) conducted experiments on forty beams in the constant moment region to study tension lap splices under static loading. They found that specimens with larger concrete covers had slightly lower splice strengths compared to those with smaller covers. They also observed that beams with heavily reinforced lap splices performed as well as beams with lightly confined splices. The confinement provided by concrete was slightly less effective than stirrups in enhancing splice strength.

Jukka et al. (2023) investigated lap splices in confined concrete. They tested 119 samples subjected to axial tension following ACI standards, considering variables such as lap length, splicing detail, number of spirals, bar size, and concrete strength. They observed a significant scatter in results at low confinement levels, but reasonable predictions with high confinement. They concluded that confinement could significantly reduce the required lap length.

Chinn et al. (1955) and Vollum and Micallef (2017) conducted experiments on wide beam lapping using continuous edge bars in some samples and spliced bars in others. Both studies reached similar conclusions. Vollum and Micallef's study involved 18 beam specimens, and they examined the influence of different lap lengths and staggering arrangements. They found that shear had no significant influence on the strength of the lap length tested. Increasing lap lengths beyond what is required for reinforcement yield did not provide additional ductility. Staggering laps between bars did not show benefits in terms of bonding. The stiffness difference between lapped bars and continuous bars was responsible for the observed behavior. These findings cast doubt on the advantages of staggering laps.

Continuity of reinforcement through a lap zone may not always guarantee sustained bar force due to several factors. Firstly, in actual construction, all reinforcing bars can be spliced

with staggered laps, unlike in research studies where some bars were continuous. Bond failure with limited ductility in splitting modes is a concern, as the failure of one spliced lap can transmit additional stress to adjacent lap regions and continuous bars passing through the lap.

Secondly, a lapped pair of bars has different stiffness compared to a single continuous bar, and the stiffness of the lap region is influenced by the proportion of lapped bars. The overall elongation of a pair of spliced bars over the lap length depends on two components: the slip of the loaded end of a spliced bar and the elongation of the bar along the lap length. The difference in stiffness between continuous and spliced bars affects the balance of forces transferred by each. The continuous bar, being less stiff, experiences lower stress outside the lap, while the spliced bars endure greater stress. The slip of lapped bars further reduces lap stiffness and increases the overall elongation of the lapped pair, partly compensating for the stress difference caused by bar elongation.

Figure 2.26 presents the strain distribution across spliced laps for sections with different proportions of bars spliced, as determined by Cairns (2014) through numerical analysis. The graphs in Figure 2.26 illustrate the change in bar force as a percentage of the overall force for all bars at a specific location. The percentage of bars lapped at a location has a significant impact on the distribution of bar force and, consequently, the elongation of bars along the lap length, influencing the lap stiffness.

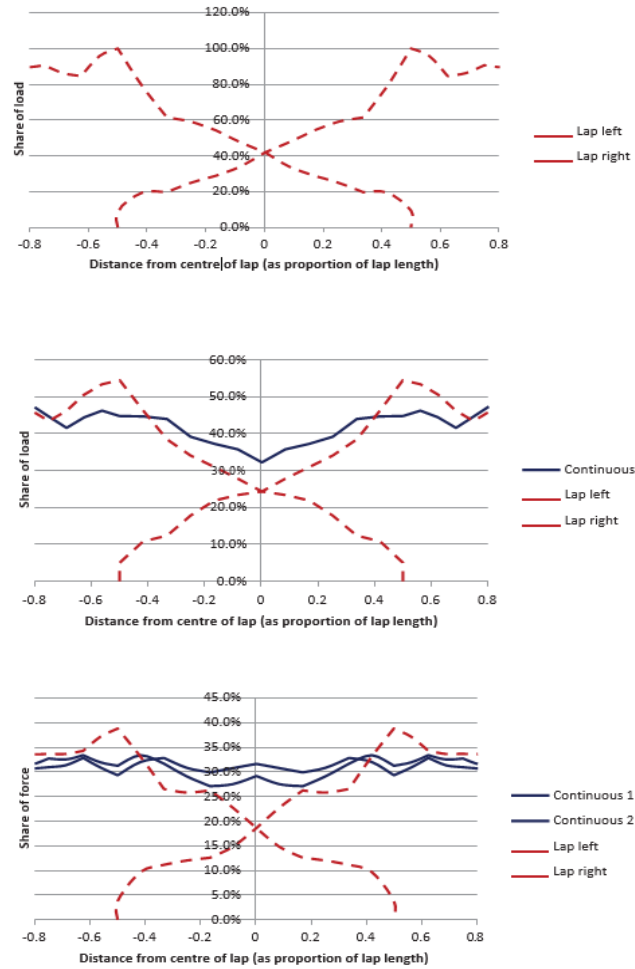


Figure 2.26. Change in bar stress along lap (a) 100% lapped (b) 50% lapped (c) 33% lapped (Cairns, 2014).

However, it should be noted that the trend predicted by Equation 2.45, which is used to plot the change in stress within the mid-length of the lap against the proportion of spliced bars, overestimates the differences observed in Figure 2.26. Equation 2.45 simplifies various factors such as bar slip, tension stiffening, and load sharing. Nevertheless, the figure demonstrates that when only some of the reinforcing bars are spliced, the percentage of bar force transmitted during the end half of the tension length increases. This can lead to a higher maximum bond stress near the end of a long lap, potentially resulting in splitting bond failure. The ratio of the maximum bond stress to the average stress over the entire lap length increases as the proportion of force to be developed over the end half of the lap length increases. Consequently, under equal conditions, the average bond strength at failure throughout the entire lap length decreases as the proportion of lapped bars increases.

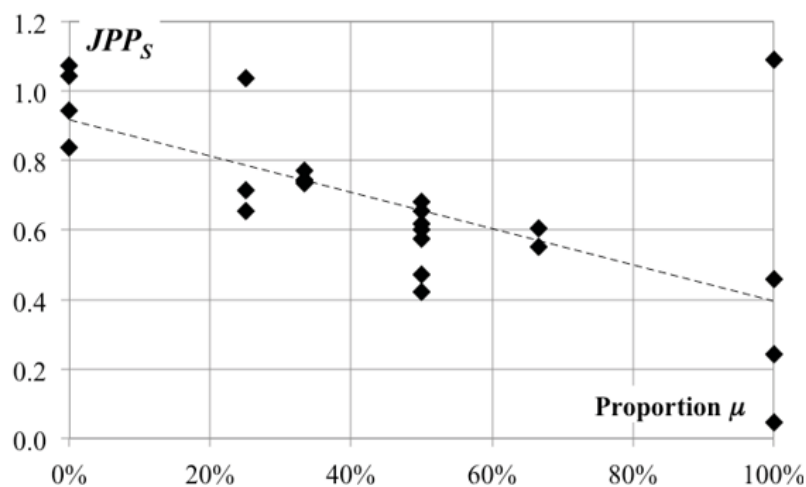
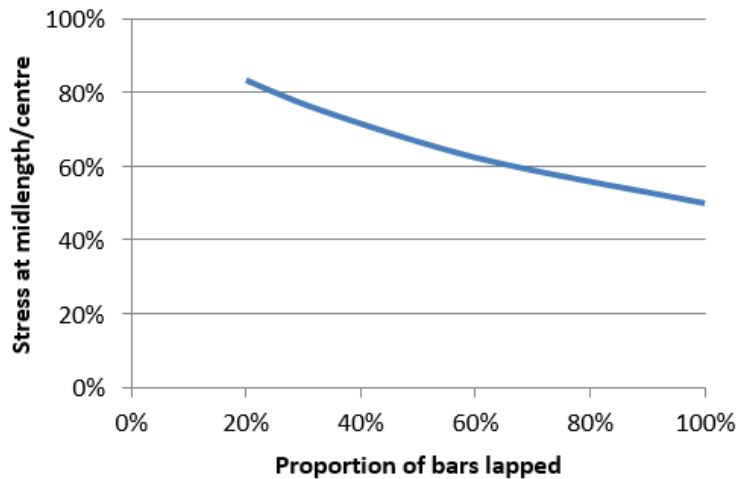


Figure 2.27. Influence of proportion of bars lapped at the section on stress at mid-length of lap and Influence of percentage (μ) of lapped bars on joint post-peak strength (JPP_s), (Metelli et al., 2016).

Figure 2.27 demonstrates that spliced bars experience higher stress at the ends of the lap compared to continuous bars. Therefore, when analysing experimental results, assuming that all bars are stressed evenly at failure can lead to the misconception that lap strength is reduced when only a portion of bars are spliced at a location, even though the bond resistance of the spliced bars remains constant.

In a tension lap where all reinforcing bars are spliced at the same location, the bars in the center of the lap tend to be stressed at approximately half the level of those on the outside. If we consider a lap that is at the maximum region area, stressed in the elastic range, and long enough to ensure that all reinforcing bars in the cross-section are under the same strain at mid-length, then when only some of the bars in the section are lapped, the overall

cross-sectional area of reinforcement within the lap length is less than double that outside. This implies that the stress at the mid-length must exceed half of that outside (according to Equation 2.45). However, if all reinforcing bars are spliced at the same section, the overall cross-sectional area of reinforcement inside the lap length is twice that outside the lap. Consequently, the bar strain and stress at the mid-length of the lap approach half of that outside the lap.

$$f_{ml} = f_c \cdot \frac{EA^0}{EA_{ml}} = f_0 \frac{1}{1 + P_{lap}} \quad (2.46)$$

Where: P_{lap} is the proportion of reinforcement lapped at the section

f_o and f_{ml} are the bar stress at mid-length and outside of the lap, respectively.

ΣA_{ml} and ΣA_0 are the reinforcement within and outside of the lap, respectively.

f_c is the strut force (compression force)

E is the modulus of elasticity

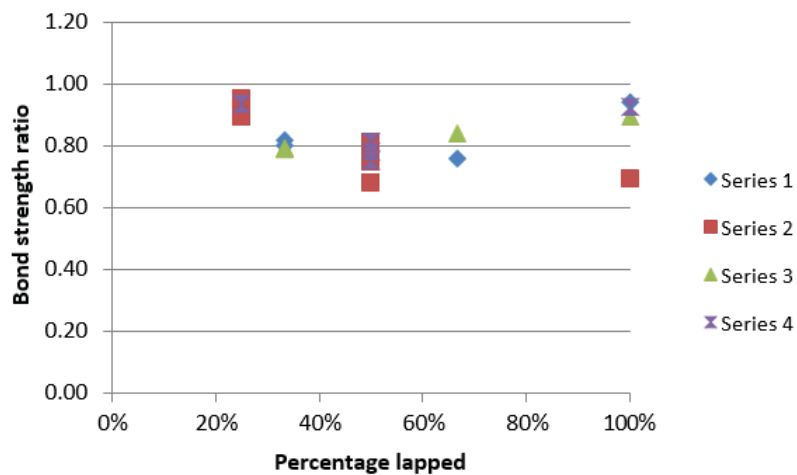


Figure 2.21. Influence of proportion lapped on lap strength (Metelli et al., 2010).

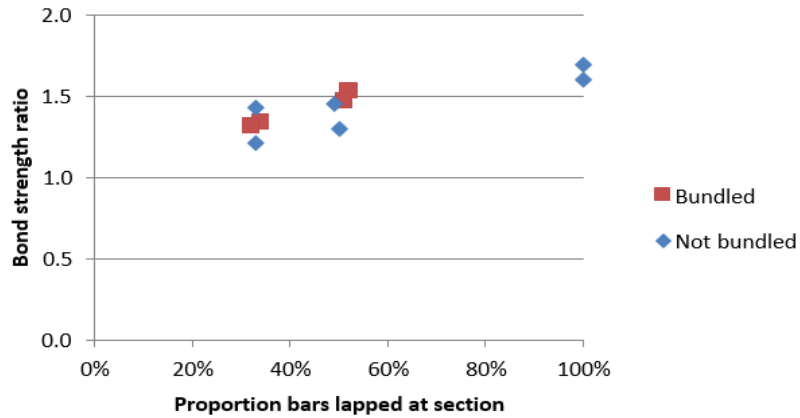


Figure 2.28. Influence of proportion lapped on lap strength (Cains and Jones, 2012).

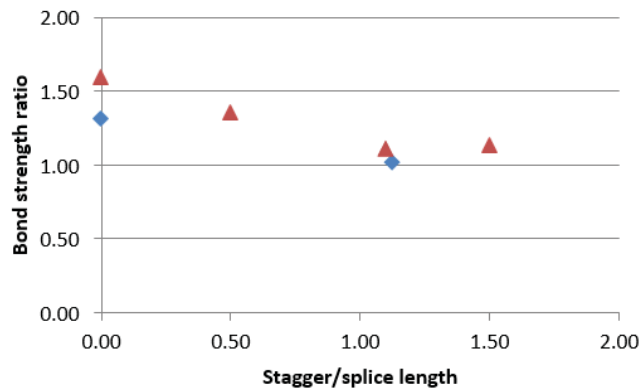


Figure 2.29 Influence of staggering laps on lap strength, (Cairns, 2011)

2.10.5 Minimum confining reinforcement

Minimum reinforcement in the form of shear links is necessary for most beams to enhance their shear capacity and prevent compression bars from buckling in RC columns. Confining reinforcements are used in lap joints to mitigate the brittleness of splitting failure by providing tensile resistance over splitting cracks. In practical terms, confining reinforcement is required in all lap regions except where transverse compression from high concrete cover or beam ends can provide sufficient confinement against bond-bursting stresses. Minimum requirements for confining reinforcement apply in other areas that don't meet these conditions. These guidelines are in addition to any other minimum reinforcement requirements. While confining reinforcement for shear links contributes to anchorage and bond, its primary role is to reduce the brittleness of splitting failure. The minimum quantity

of confining reinforcement can be estimated by analysing the bursting forces generated by bond action.

In ultimate strength models, it is commonly assumed that bond generates radial bursting forces of the same magnitude as the bond stress, with uniform distribution around the bar circumference. Equation 2.46 provides the bursting stress perpendicular to a crack on the plane through the bar axis, as depicted in Figure 2.30.

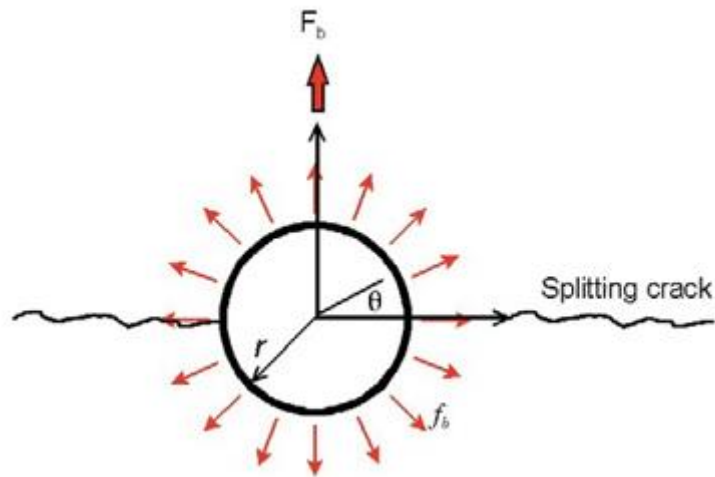


Figure 2.30. Bursting stress around the bar (Cairns and Jones, 2012).

$$F_{sp} = l_b \int_c^n f_b r \cos\theta d\theta = f_b \rho l_b \quad (2.46)$$

Where

F_{sp} is the bursting force perpendicular to crack plane

r is the radius

f_b is the bond force transmitted along the transmission length

l_b is the bond length

Equation (2.43) gives the total bursting force by substituting for bond stress f_b to anchor the yield strength of the bar from equation (2.45) into equation (2.46).

$$f_s A_s = f_b m \rho l_b \quad (2.47)$$

Where

A_s is the cross-sectional area

m is the bending moment

ρ is the reinforcement ratio

f_s is the fracture stress

$$F_{sp} = f_s A_s / m \quad (2.48)$$

As a result, the bursting force is 0.32 multiplied by the developed force in the bar by the bond. Equation (2.45), which gives a similar result, is used by (Canbay and Frosch, 2005) to estimate the bursting force.

$$F_{sp} = F_l \tan 20^\circ \quad (2.49)$$

In which F_l the longitudinal force transmitted by bond

Equations (2.47) and (2.48) indicate that the bursting forces resulting from bond action are approximately one-third of the force transmitted by bond. Since bond stress is not uniformly distributed along the spliced length or around the bar circumference, it is prudent to set a slightly higher requirement for confining reinforcement. This entails providing reinforcement to resist half of the total force transferred by bond, allowing for a more uniform distribution of secondary reinforcement along the bond length.

Direct strain measurements, such as those shown by Chinn et al. (1955) in Figure 2.25, have established a correlation between bond and transverse pressure. Studies by Canbay and Frosch (2005) and Cairns and Jones (1997) have found that stress in transverse reinforcement confining laps generally reaches around 80 MPa at maximum load. However, transverse reinforcement strains continue to increase as bond-slip progresses due to reduced confinement from crack widening. Cairns and Plizzari (2003) have deduced that yielding of transverse reinforcement occurs at an earlier stage in pull-out tests. The full yield strength of transverse reinforcement may eventually be mobilised, but only after achieving maximum bond strength. Therefore, if the full yield strength of a bar is to be utilised for anchorage, and the transverse reinforcement is of the same grade as the longitudinal bars (main bars), then an area of secondary reinforcement equal to or less than half of the total cross-sectional area of the bonded bars must be provided within the lap length.

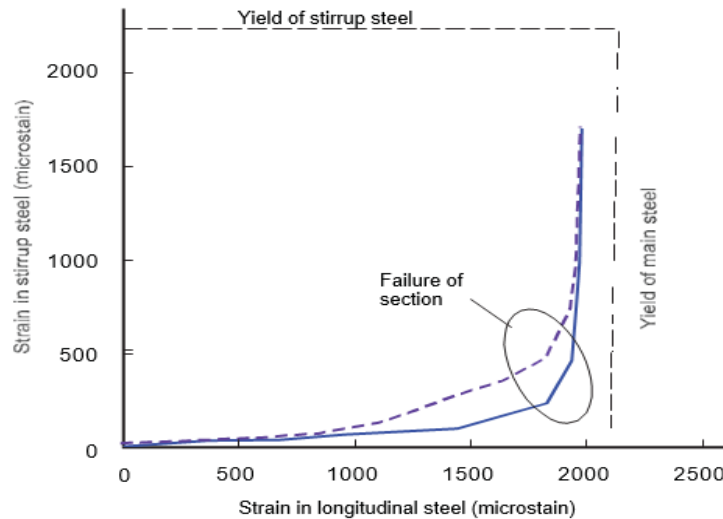


Figure 2.31. Direct strain measurements (Chinn James Phil M., Ferguson Phil M., and Thompson J Neils., 1955)

When splicing larger diameter bars, the bond behavior tends to be more brittle, likely due to the higher concentration of force and bursting forces at the ends of these bars. Although there is limited evidence to establish specific design rules, it is recommended that bars with a diameter of 50 or more require double the minimum confining reinforcement. This means providing an area of secondary reinforcement equivalent to the overall cross-sectional area of the bonded bars. The Fib Model Code (2013) allows for a linear increase in confining reinforcement from 25 to 50 diameters.

Experimental findings demonstrate that even when this additional reinforcement is provided and transverse reinforcement crosses the splitting crack, achieving a ductile mode of bond failure is challenging, as depicted in Figure 2.31. While the transverse reinforcement balances the bursting forces on the underside of the bars, bond exerts an upward bursting force on the concrete cover above the bar. The concrete cover can fail in various ways, such as shear and flexural failure between adjacent transverse reinforcements. However, the anchorage of transverse reinforcement in the concrete cover is typically weak due to its shallow embedment, as shown in Figure 2.26. The reaction from the transverse reinforcement is mainly confined to a short length of the main bars in close proximity, resulting in limited resistance to upward bursting forces on the underside of the concrete cover. By the time the transverse reinforcement reaches yield, only the underside of the bar is fully engaged, leading to a reduction in residual bond strength of approximately 50%.

Consequently, achieving ductile bond failure becomes challenging regardless of the amount of confining reinforcement provided

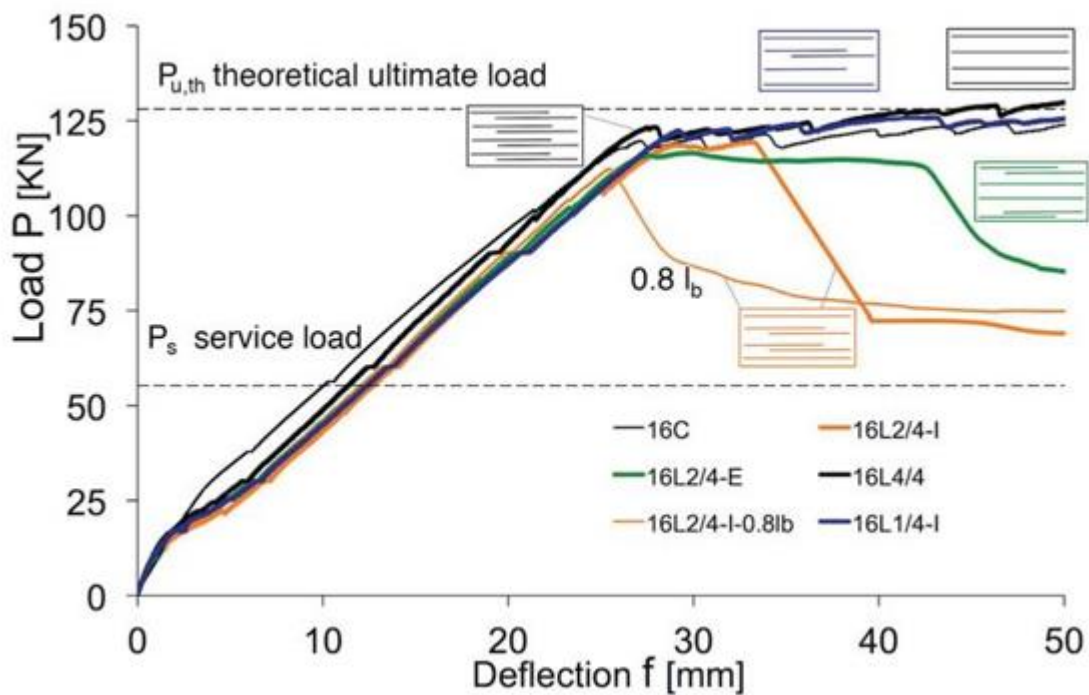


Figure 2.32. Typical load-deformation plot of lap confined by links, $K_{tr}=2.3\%-3.9\%$ (Metelli et al., 2010)

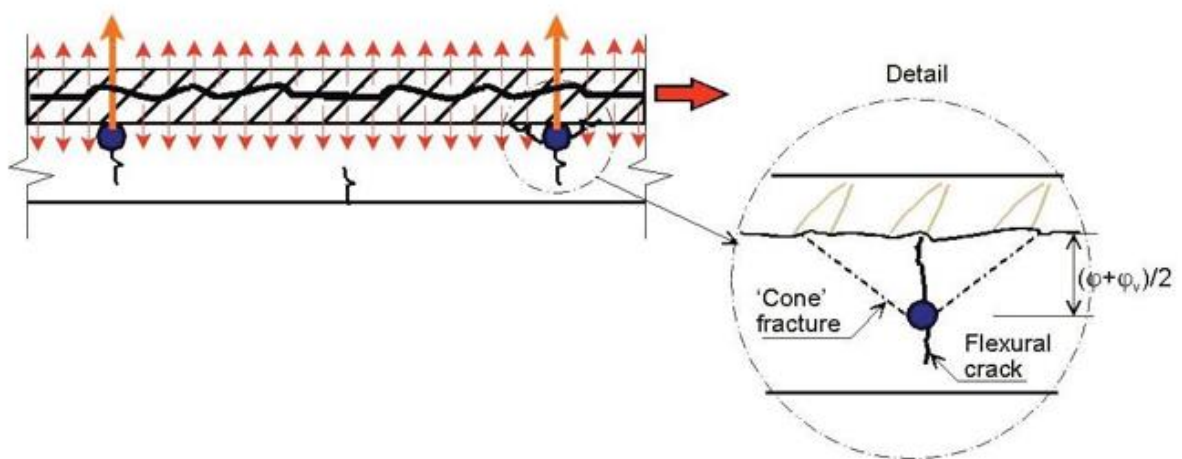


Figure 2.33. Weakness of cover concrete after splitting crack formation (Fib Bulletin, 2014)

There is advanced experimental evidence that supports the notion that conventional transverse reinforcement can provide satisfactory bond ductility. Some of these findings include:

- Cairns and Jones (1997) conducted a lap joint test and observed excellent ductility. They achieved this by anchoring transverse reinforcements above and below the lapped bars deep into the large concrete covers, as shown in Figure 2.28.
- Jirsa et al. (1995) observed that the bond resistance of the inner layer of bonded bars increased after failure, while the resistance of the outer layer decreased significantly. This was attributed to the transverse reinforcement passing around the outer longitudinal bars, effectively confining the cover of the inner layer.
- Magnusson (2000) found that the amount of transverse reinforcement is nearly as crucial as its size in determining bond resistance. Increasing the number of transverse reinforcements, regardless of their size, reduces the span of the concrete cover between them and improves the anchorage of the concrete cover in members.

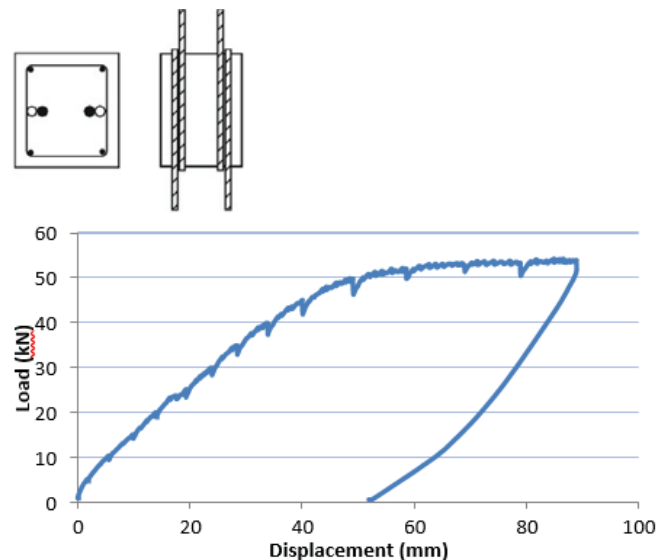


Figure 2.34. Bond ductility with transverse reinforcement well confined into cover (Cairns and Jones, 1996).

Conventional lap spliced joints with transverse reinforcement in contact with bonded bars may not exhibit fully ductile failure in a splitting mode. To ensure ductility, two options are available: (1) maintain continuous reinforcement through the joint, or (2) ensure sufficient bonded length for the bar to reach yield.

2.10.6 Comment and summary

Although there is a general understanding of the factors that affect bond behavior and bond strength, quantifying that influence is subject to a wide variety of expressions and approaches. This section summarises the main areas of consensus and major trends.

Methods used for the strength of laps are mainly derived from the weaker splitting mode of failure. The bursting forces produced by the bond action are associated with the splitting resistance provided by the cross-section of the member as a limiting condition. Most models are primarily concerned with equilibrium conditions on a plane at a right angle to the bonded reinforcement's axis. Therefore, these methods do not directly address the bond/slip.

However, some options leverage kinematic relations between the radial displacement of the inner radius of the concrete layer around the bar and the longitudinal bar displacement (slip). This approach allows equilibrium conditions and compatibility to be considered simultaneously. In general, the resulting expressions use the least bond conditions as a benchmark, which is in line with other detailing criteria.

Bond strength enhancements correspond to scenarios that are above the benchmark.

Earlier researchers, such as Ferguson and Briceno (1969) and Tepfers (1973), used theoretical techniques to derive expressions unique to individual splitting sub-modes, in which the effect imparted by varying factors was based on the sub-mode, as depicted in Figure 2.35.

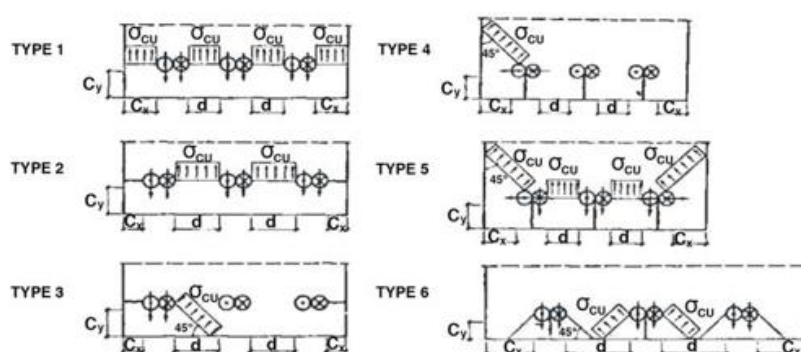


Figure 2.35. Splitting failure modes (Tepfers, 1973).

The current method of analysing bond-slip behavior and strength involves considering various potential splitting modes, choosing the weakest mode as the dangerous case, and

requiring high computational power. However, recent methods rely on a single, less mode-specific physical model that is validated against an experimental results database, resulting in a semi-empirical approach.

Analytical modelling of local bond-slip behavior commonly uses the pull-out failure mode, where concrete is sheared on the surface defined by the profile of the bar ribs and focuses primarily on behavior parallel to the bonded reinforcement's axis. Early advancements, such as those by Eligehausen et al. (1983), were based on a high confinement experimental reference condition. Subsequent advancements by Giuriani et al. (2000), Eligehausen et al. (1983), and Fib (2000) considered reducing the pull-out bond strength to achieve the lower splitting bond strength of the failure mode. However, these lessening factors, which describe the effect of smaller confinement constraints, are often less thorough than those established for lap strength, and they are not well standardized for splitting failure types. Additionally, the appropriateness of the coefficients for 'other' casting positions is also questionable, given that the experiments from which these models are created tend to be shorter and smaller in length, utilizing conditions where the casting position is considered 'good.'

Both the aforementioned methods are fundamentally one-dimensional and two-dimensional. Recently, advances in processing capabilities have allowed for comprehensive three-dimensional simulations of the region of bond action encompassing concrete, primary and secondary reinforcements (Lundgren and Gylltoft, 2000). However, these models require an enormous amount of testing and calibration to correlate with measured results in a wide range of situations. As such, their use is limited to the research community and possibly those undertaking forensic investigations of failures, as they are too complex for routine design. While progress is being made, more work is necessary before these models can be used to formulate design procedures.

Some of the features recognised in the literature are as follows:

- Except for early analysis by Orangun et al. (1977), all samples incorporate a second concrete cover with lesser effect than the minimum concrete cover.

- Every researcher agrees that the bond strength rises with concrete strength, with confining reinforcement and with minimum cover, while the representation of that effect gain varies.
- All scholars agree that mean bond strength reduces with increasing the lap splice length, while the representation of that effect varies in the available models.
- All scholars agree that the strength of lap splices can be represented by the same expression. This is in direct contrast to a prior 'hydraulic pressure' physical model's prediction, which predicted that a pair of spliced bars would generate double the bursting force of single bar anchorages (all other factors being the same). Cairns and Jones (1997), Reynolds and Beeby (1982), and Tastani and Pantazopoulou (2002) are some of the researchers who have evaluated the hydraulic-pressure model's relevance in the case of lap splices. Fib Bulletin (2013) has different bond length requirements for anchorages and laps, and at first glance, it appears to contradict the findings from the semi-empirical test data analysis.

Unsurprisingly, there are many sets of discrepancies:

- Jirsa and Breen's formulation is the only one that includes transverse reinforcement yield strength. However, it is now broadly acknowledged that the stress in confined reinforcement does not approach yield in the region of low shear. The behavior in the high-shear zone is less certain (Reynolds and Beeby, 1982); however, there is no compelling data to justify the use of transverse reinforcement yield strength as a parameter.
- According to (Esfahani and Reza Kianoush, 2005), given the same lap length-to-bar diameter and cover-to-bar diameter ratios, the bond strength produced by a 12 mm diameter bar will be roughly 25% greater than that of a 40 mm diameter bar. Bamonte, Coronelli, and Gambarova (2002) showed a similar variation in their experiments with very short joint length.

3. Research Methodology

3.1 Research design

In this study, a combination of experimental work and simulation was conducted. Experimental work was performed in the concrete laboratory at the University of West London to investigate the ductility along the lap joints. The experiment aimed to investigate whether there is sufficient ductility at the lapped section for rotation to occur before the formation of a plastic hinge. The lab testing was carried out under four-point load bending (4PB) for a series of reinforced concrete beams with various lap lengths. The main variables for this study are lap length, transverse reinforcement, links, and loading arrangement. All laboratory experiments for this study were conducted to fit in with the time of the existing database for laps and anchorages, which continues to develop. The purpose is to develop the current database, which was compiled by the Concrete Centre and Fib Task Group 4.5. The database comprises the results of laboratory tests on laps and anchorages conducted by ACI (for casted beams at tension only), and some additional data from the Asian and European investigations. A total of 824 tests were collected and provided by the Concrete Centre for this research as part of ongoing collaboration.

3.2 Health and safety considerations

When conducting research in a concrete laboratory, it's important to consider potential hazards, such as dust inhalation and skin contact with cement. Therefore, health and safety precautions are of paramount importance during all aspects of the testing regime. Before conducting any work in the laboratory, the following measures were taken:

- A risk assessment was carried out.
- Proper personal protective equipment (PPE) was worn in the laboratory.
- Any faulty equipment in the lab was reported to the supervisor/technician.

3.3 Ethical Considerations

For the FE analysis in this study, a licensed software provided by the university was used. The research was conducted in compliance with the University of West London's ethics regulations concerning plagiarism. We ensured that there was no falsification or fabrication of results during the course of conducting this research. All data collected and used during

this research was protected in accordance with the Data Protection Act 2018. The UWL Research Ethics application form has been submitted (Reference ID: UWL/REC/SCT-00441).

3.4 Laboratory Experiments

3.4.1 Details of the reinforcing bars

The mild reinforcing bars used in the test programme were 8 mm and 12 mm diameter rib bars according to BS EN 1992-1-1 (2004) and were obtained from a local supplier (Metal4U). The bars were supplied in 6 m lengths and cut into various lengths in the laboratory, with consideration given to exclude any damaged bars from within the lapped section of the beam specimens. The steel for experiments was used in its as-delivered state without any surface preparation or special cleaning taking place. The link cages were made from 8 mm diameter reinforcing bar taken from the laboratory stocks.

3.4.2 Casting procedure

All the beams were cast using the same mix design. The concrete was mixed in an ELE Concrete Mixer 34-3540 for 5 minutes. After the concrete mix was completed, a slump test was conducted according to British Standards using the 'ELE International Slump' testing kit, as shown in Figure 3.1.

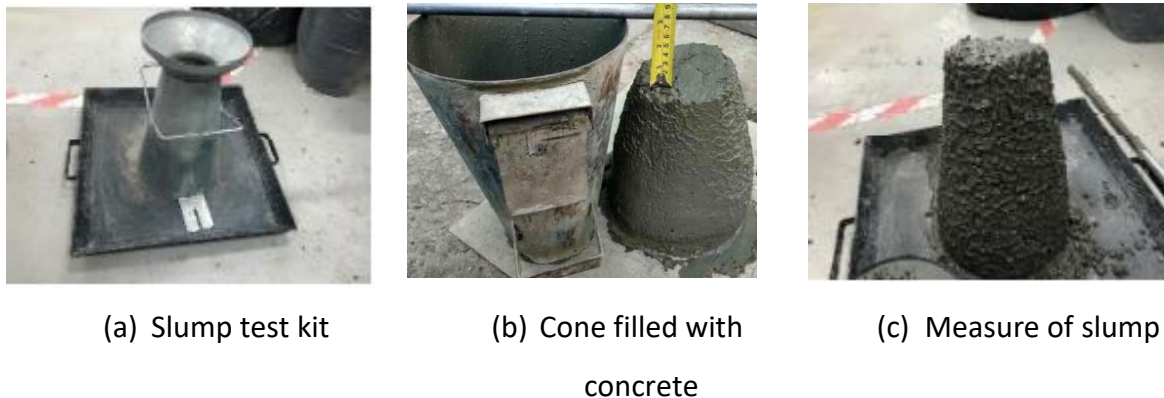


Figure 3.1. Slump test.

After the completion of the slump test, separate beams were cast using marine plywood as formwork (Figure 3.2(a)). The beams were cast with the tension rebars placed horizontally. The reinforcement cage was positioned within the mould and held in place during casting by a 15mm concrete cover connected to the sides and bottom of the cage. In the lap test specimens, the lapped longitudinal reinforcement was placed at the bottom of the formwork to ensure good bond properties. The concrete was cast in two layers, each being

compacted using a mechanical vibrator poker. A stainless-steel float was used to smooth off the top surface of the beams, leaving a smooth finish (Figure 3.2 (i)).



(a) Mould



(b) Reinforcement cage for mild steel reinforcing bar



(c) Reinforcement cage with lap bars



(d) Bending of shear links



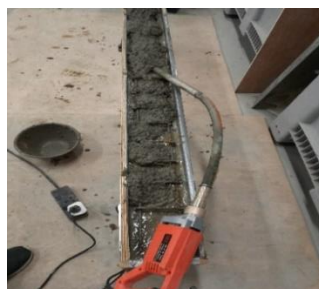
(e) Reinforcement cage for stainless steel reinforcing bar



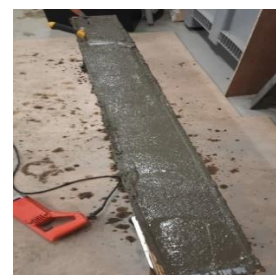
(f) Reinforcement cage for control stainless steel beam



(g) Vibrating poker



(h) Compacted concrete



(i) Cast beam

Figure 3.2. Sample casting

Three-cylinder samples (150 × 300 mm) and three small beam samples (150 × 150 × 750 mm) were cast simultaneously with the main beams using the same fresh concrete. The concrete was poured into the cylinders in three layers and compacted 25 times in each layer using the stroke rod, while the beam samples were compacted using a vibrating poker. After compaction, a shaking table was used to vibrate the concrete within the cylinders to remove

any trapped air, as shown in Figure 3.3. The beam and cylinder samples were then used to determine the compressive and tensile strength of the concrete. The entire casting process took about an hour, and all the beams and cylinders were left in their moulds for 24 hours after casting. After the formwork was removed from the beams and cylinders, the samples were stored in a curing tank at (20 ± 2) °C until testing, which took place after 28 days.

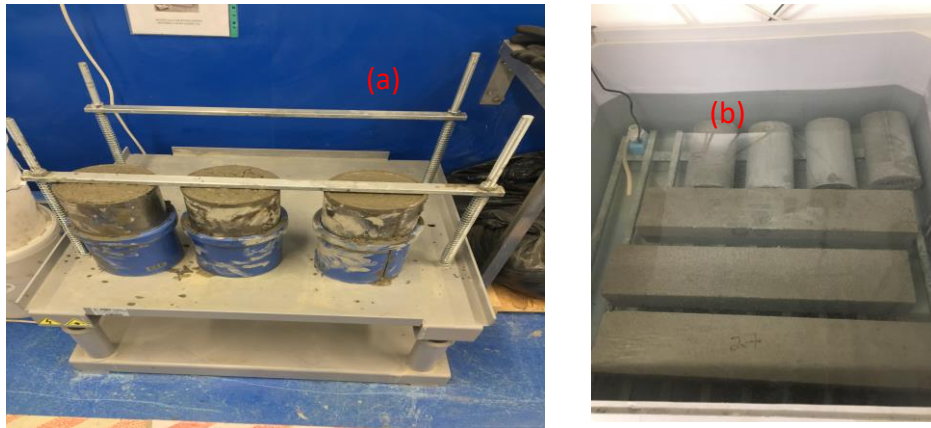


Figure 3.3. Vibrating cylinder samples with shake table, (b) cylinders samples in curing tank.

3.4.3 Testing procedure

3.4.3.1 Compressive strength

The concrete cylinder specimens were removed from the curing tank after 28 days. The density of three-cylinder specimens was determined by weighing them in air and water using a gravity apparatus (BS:1881-114) to calculate the compressive strength of the concrete. The compressive strength of the specimens was assessed using the ELE ADR-Auto V2.0 200 standards. The specimens were crushed at a speed of 10.6m/s using a compression machine (see Figure 3.4). The average compressive strength of the cylinders is presented in Table 3.1.

Table 3.1. Average compressive strength of the cylinders

ID	Compressive strength MPa	Average compressive strength (MPa)
Sample 1	32.61	
Sample 2	32.67	
Sample 3	32.87	32.72

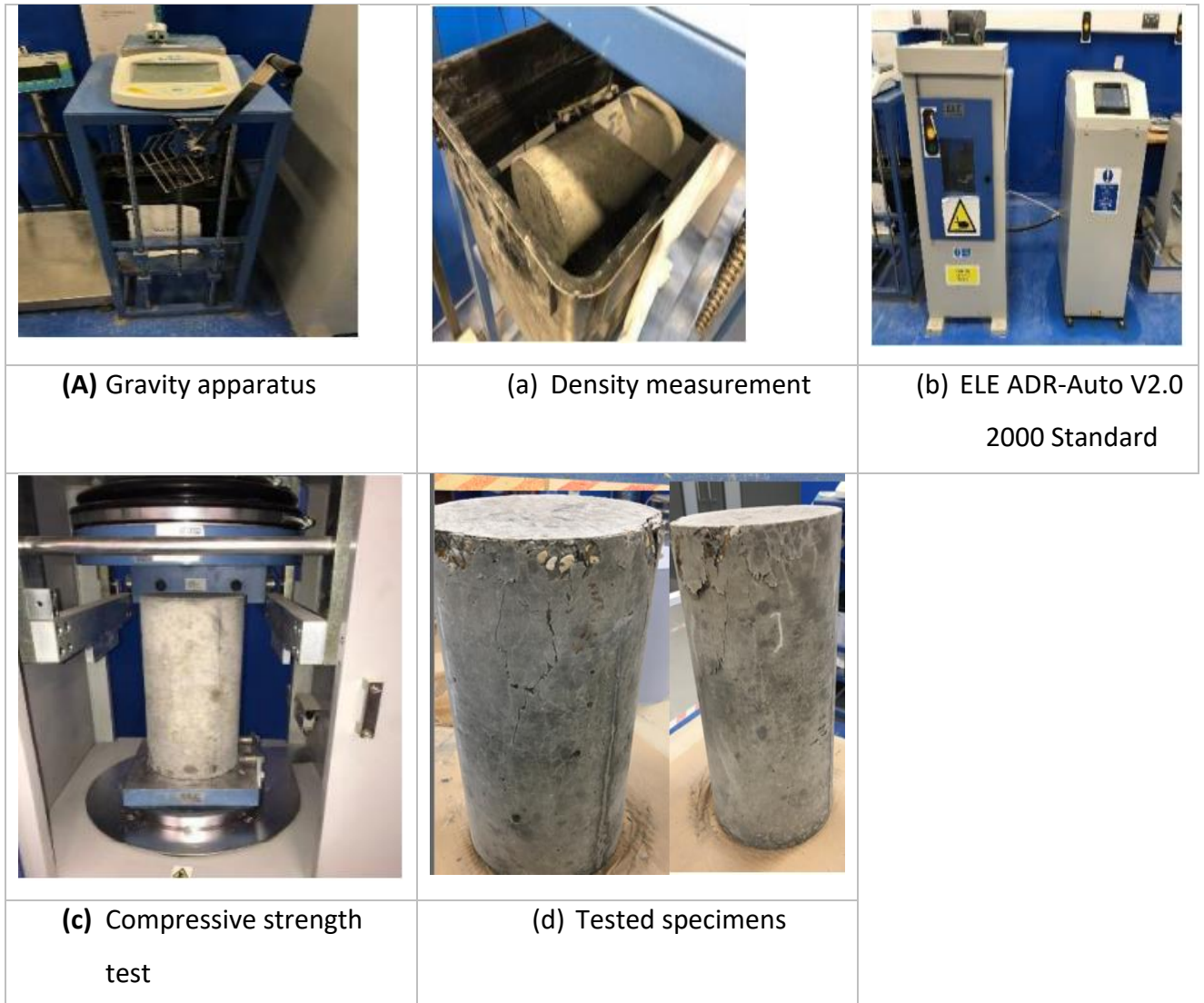


Figure 3.4. Compressive strength apparatus and tested samples

3.4.3.2 Flexural test (beams without reinforcement)

Prior to conducting the experiments, the bearing surfaces of the testing machine were carefully wiped to remove any loose grit or other extraneous materials from the surface of the specimen that would be in contact with the rollers.

For the beam specimens, excess moisture was wiped off the surfaces of the specimens after they were removed from the curing tank, before placing them in the testing machine. The specimens were then positioned at the center of the machine with the longitudinal axis of the specimens perpendicular to the longitudinal axis of the upper and lower rollers, as shown in Figure 43. The test specimens were cast in 150 mm × 150 mm × 750 mm beam Molds that conform to BS EN 12390-5:2020, as depicted in Figure 3.5 and equation 3.1.

The three-beam specimens were then crushed at a pacing rate of 0.45KN/s using the compression machine.

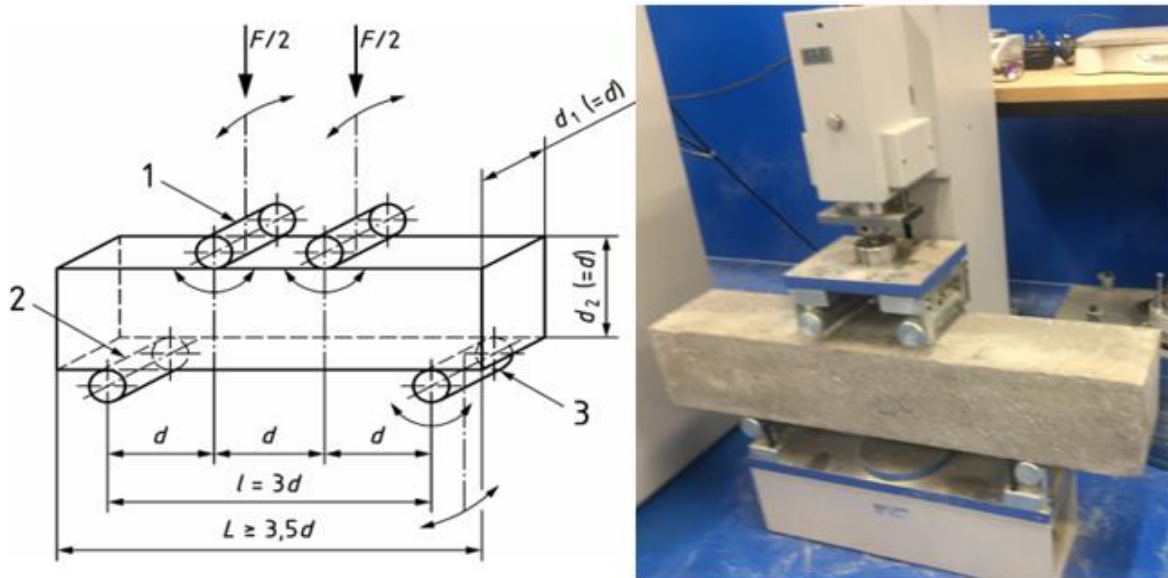


Figure 3.5. Arrangement of loading test specimen (four-point loading).

Stress calculations

The beam's stress is calculated using the following formula: -

$$f_{ct,fl} = \frac{L \times P}{d_1 \times d_2^2} \quad (3.1)$$

Where,

$f_{ct,fl}$ is the flexural strength, in N/mm²

L= is the distance between the lower rollers, in mm

P= is the peak load, in KN

d_1 and d_2 are the lateral dimensions of the specimen, in mm (see Figure 3.11).

3.4.3.3 Flexural test (reinforced concrete beam)

For the main reinforced concrete beams, the specimens were positioned in the middle of the hydraulic actuator, and a vertical load was applied at the top-middle surface of the beam (see Figure 3.6). Four-point bending was performed on beams with a span of 700 mm and a shear span of 400 mm. The laps were positioned in the constant moment zone between the two loading points.

During the test setup, the terminating criteria chosen for the hydraulic actuator was deflection control. The limit was based on the deflection throughout the testing, as it was easier to manage and to avoid damaging the variable displacement transducer that was placed at the bottom of the beam. As a result, the actuator machine was programmed to terminate the experiments when the midspan beam deflection reached 100 mm or the failure of splices, whichever comes first, by applying the displacement with a hydraulic actuator with a stroke of 350 mm and maximum load capacity of 500 KN.

The average rate of displacement was 0.20 mm/min. The machine ramp was used to apply the load, and a rigid steel beam (150 mm × 150 mm × 750 mm) was placed in the middle of the RC beam specimen to distribute the load between the two point loads (P1 and P2) at 0.7 m apart on the beam. As shown in Figure 3.6, the hydraulic actuator can apply the required ramp load and measure the corresponding deflection at the midspan of the beam using a built-in AEP TC4 transducer, while storing the results in a LabVIEW-based software attached to the actuator.

In addition to the in-built displacement transducer, one variable displacement transducer was placed at the centre of the bottom face of the beam.



Figure 3.6. Experimental set-up with linear variable displacement in position.

3.4.3.4 Tensile test (rebar)

The machine used to test the tensile strength of the reinforcing bars was an Instron 5584 150kN electromagnetic frame unit equipped with an Instron 2640 50 mm gauge length

extensometer. The results of the experimental tests for 8 mm and 12 mm reinforcing bars are presented in Tables 3.4 to 3.7 and Figures 3.13 to 3.16, respectively.

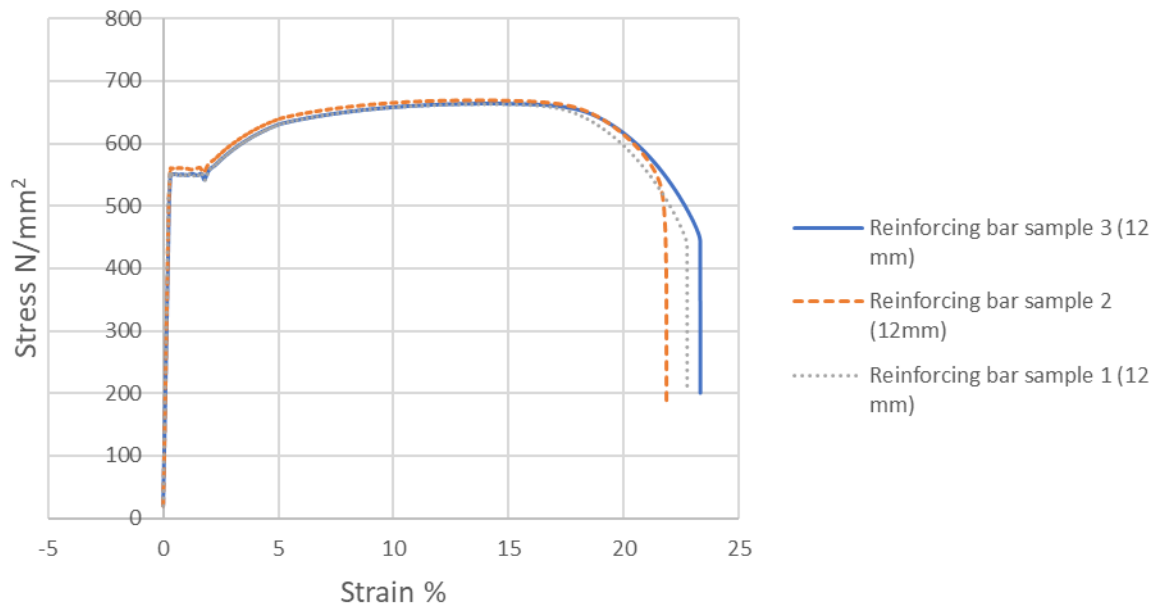


Figure 3.7. Stress- strain graphs for 12 mm mild steel reinforcement

Table 3.2. Average results for mild steel reinforcing bar (12 mm).

	Modulus (E) (GPa)	0.2% Offset Yield (Rp0.2) (MPa)	Strain Rate at 0.2% Offset Yield (Rp0.2) (mm/mm/s)
1		554.14	0
2	0.5% Offset Yield (Rp0.5) (MPa)	Plastic Stain at Tensile Strength (Ag) (%)	Plastic Strain at Break (A) (%)
	553.43	13.30	22.47
3	Total Strain at Break (At) (%)	Tensile Strength (Rm) (MPa)	Maximum Force (Fm) (KN)
	22.6	665.45	75.277

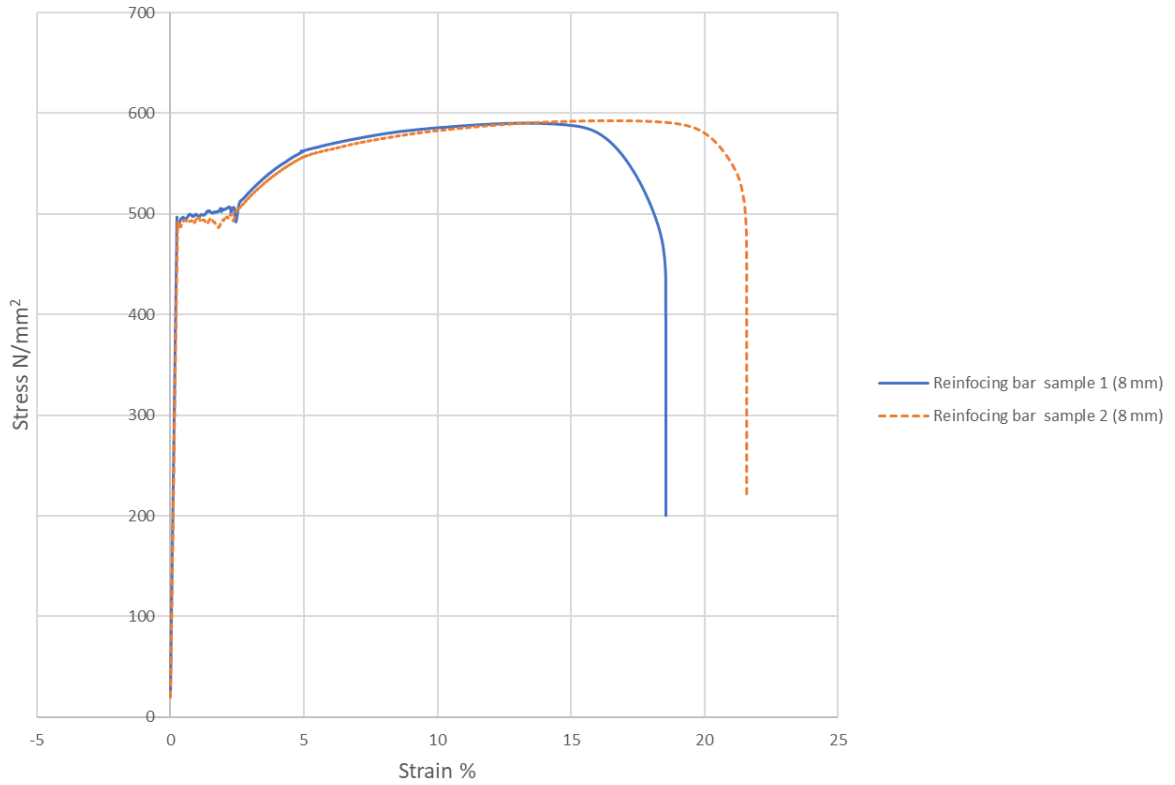


Figure 3.8. Stress-strain graphs for 8 mm mild steel reinforcement.

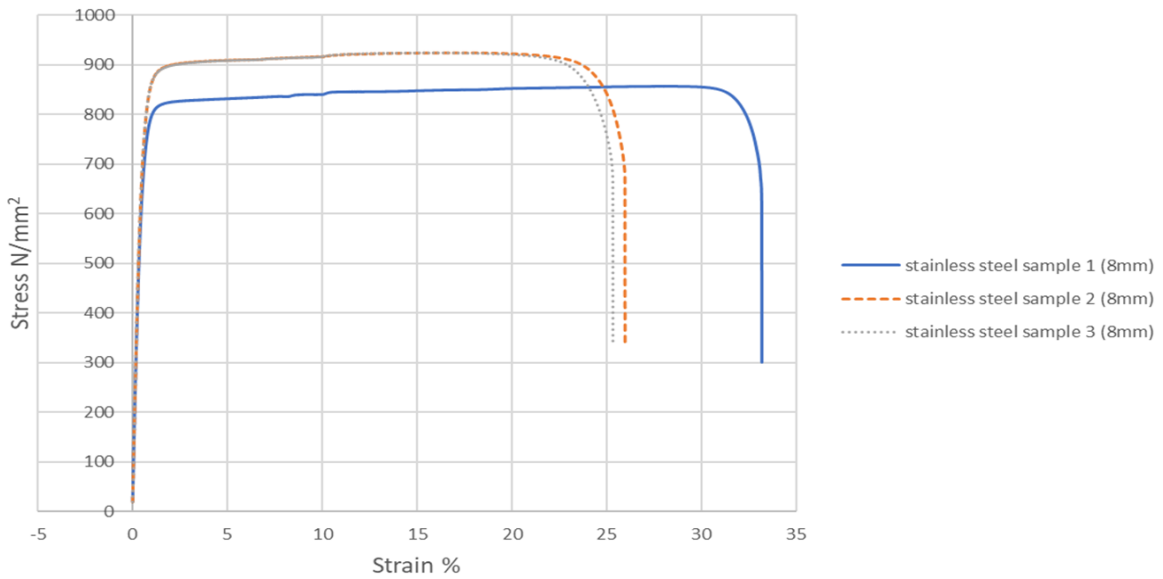


Figure 3.9. Stress-strain graphs for 8 mm stainless steel reinforcement.

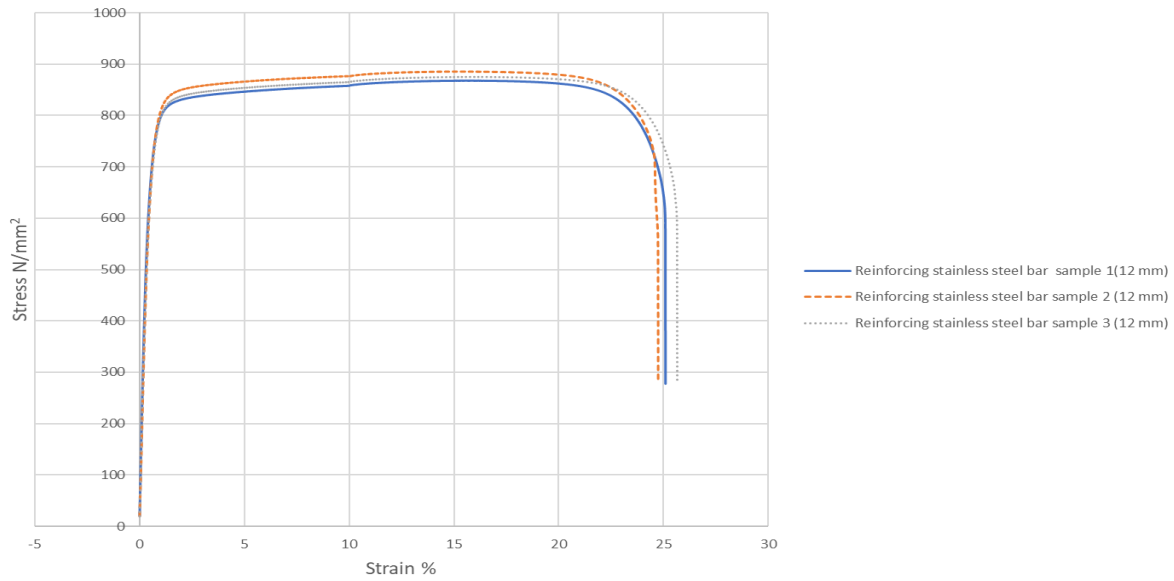


Figure 3.10. Stress-strain graphs for 12 mm stainless steel reinforcement.

Table 3.3. Average results for mild steel reinforcing bar (8 mm).

	Modulus (E) (GPa)	0.2% Offset Yield (Rp0.2) (MPa)	Strain Rate at 0.2% Offset Yield (Rp0.2) (mm/mm/s)
1		504.60	0
2	0.5% Offset Yield (Rp0.5) (MPa)	Plastic Strain at Tensile Strength (Ag) (%)	Plastic Strain at Break (A) (%)
	505.51	14.26	20.03
3	Total Strain at Break (At) (%)	Tensile Strength (Rm) (MPa)	Maximum Force (Fm) (KN)
	20.27	605.95	30.473

Table 3.4. Average results for stainless steel reinforcing bar (8 mm).

	Modulus (E) (GPa)	0.2% Offset Yield (Rp0.2) (MPa)	Strain Rate at 0.2% Offset Yield (Rp0.2) (mm/mm/s)
1	178.14	733.43	0
	0.5% Offset Yield (Rp0.5) (MPa)	Plastic Stain at Tensile Strength (Ag) (%)	Plastic Strain at Break (A) (%)
	836.66	19.19	27.8
	Total Strain at Break (At) (%)	Tensile Strength (Rm) (MPa)	Maximum Force (Fm) (KN)
	28.17	901.57	45.33

Table 3.5. Average results for stainless steel reinforcing bar (12 mm).

	Modulus (E) (GPa)	0.2% Offset Yield (Rp0.2) (MPa)	Strain Rate at 0.2% Offset Yield (Rp0.2) (mm/mm/s)
1	174.97	694.32	0
	0.5% Offset Yield (Rp0.5) (MPa)	Plastic Stain at Tensile Strength (Ag) (%)	Plastic Strain at Break (A) (%)
2	793.37	14.86	24.83
	Total Strain at Break (At) (%)	Tensile Strength (Rm) (MPa)	Maximum Force (Fm) (KN)
3	25.13	876.12	99

3.5 Finite element simulations with LUSAS, (2021)

The London University Structural Analysis finite element software (LUSAS) was utilised for verification. LUSAS is a widely used large-scale multi-purpose FE programme that can solve a wide range of engineering problems. The LUSAS model is a graphical representation consisting of lines, volumes, surfaces, and points. LUSAS features are organized in a hierarchy where volumes are composed of surfaces, which are defined by lines that are in turn defined by points. Attributes are assigned to material properties, mesh size, loading and support conditions. Increasing the discretization of the features improves the accuracy of the solution, but at the cost of more disk space and longer solution times. All analyses presented in this thesis were conducted using LUSAS. Chapter 4 provides a detailed description of the material model and elements used, as well as the verification of experimental findings. Figure 3.11 illustrates the entire design process for the finite element simulations.

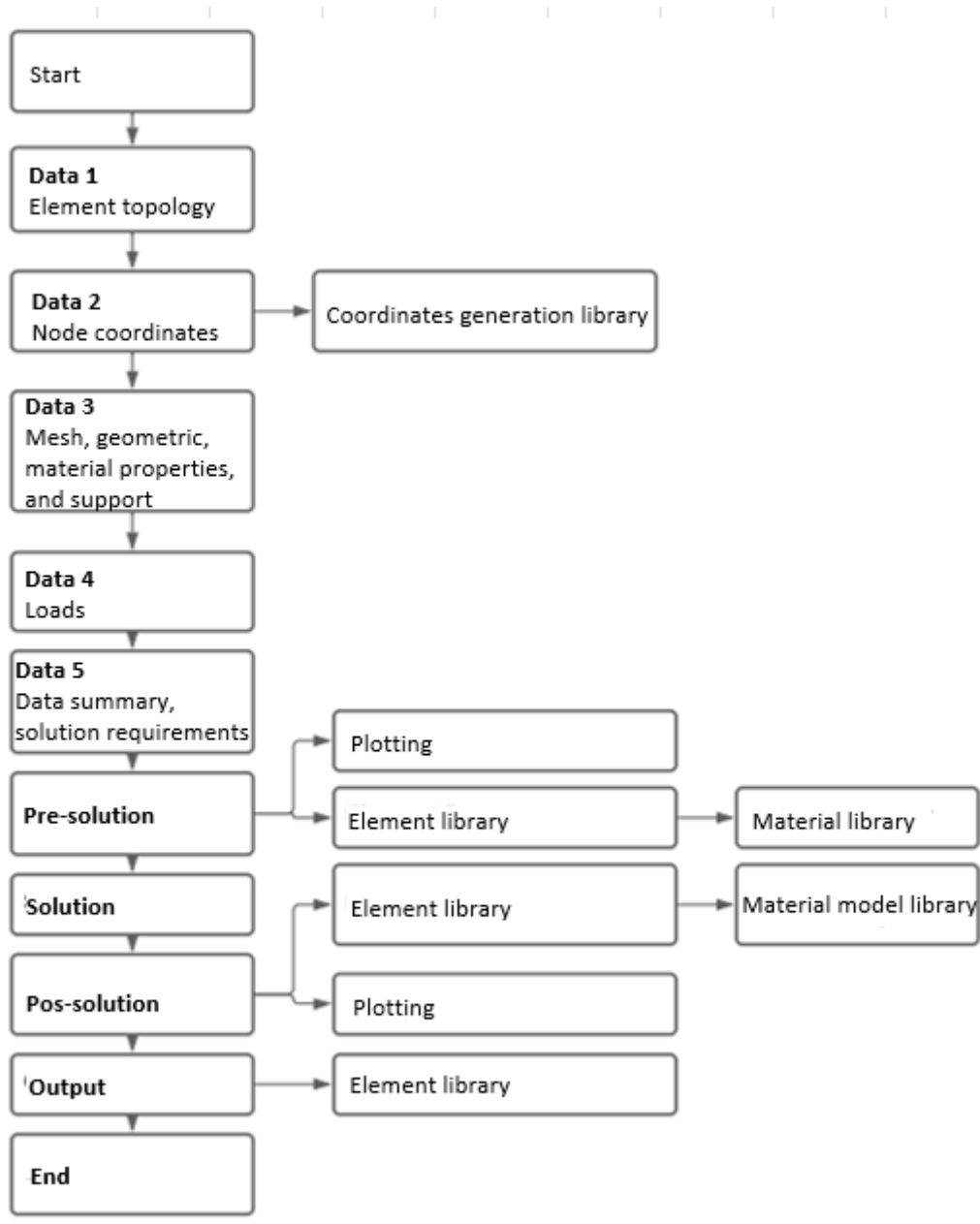


Figure 3.11. A flowchart depicting the steps required in developing the numerical model.

Reinforced concrete structures require appropriate finite element models. In this section, we provide an overview of the typical methods and their applicability. The constitutive law for concrete and embedded steel can be considered as a continuum at the micro-level, or by superimposing material models for constituent parts (i.e., reinforcing steel and concrete). Models of the first type are more popular due to their greater range of applicability. Superimposition of material models for constituent sections of a composite material is ideally suited for the finite element approach. This type of material model can be used for almost any form of a reinforced concrete structure. Depending on the type of problem to be

addressed, concrete can be represented using beam elements, plate, shell, and solid elements.

Reinforcement can be simulated either by a distribution of reinforcement to thin layers of an equivalent thickness (distribution representation), by separate elements of the same type as the concrete elements that are superimposed on the latter (embedded representation), or by separate beam or truss elements (discrete representation). To account for bond action at the concrete-steel interface, constitutive models must be superimposed on reinforcing steel and concrete to simulate reinforced concrete. The use of bond elements is not allowed in the embedded and distribution representation of reinforcement because the displacements of the reinforcing steel and concrete are assumed to be the same at the interface. As a result, bond-slip can only be implicitly compensated for by changing the constitutive relation for steel and concrete. Discrete representation of reinforcement, however, allows the modelling of the bond using special elements connecting adjacent nodes of reinforcing steel and concrete.

The material behaviour of reinforced concrete at the macro-level is characterised as if the composite material were a single material, when reinforced concrete is modelled by a constitutive law for the embedded steel and composite concrete viewed as a continuum. This type of constitutive model is based on the results of experiments on RC panels (Maekawa and Okamura, 2003; Vitanov and Collins, 1982; Selby et al., 1996). Because RC is regarded as a single material, there is no need to represent the concrete-steel interaction or the reinforcement individually.

Three types of nonlinear analysis can be modelled using LUSAS: boundary nonlinearity, material nonlinearity, and geometrical nonlinearity. Geometrical, as well as material nonlinearities, have been used in the current study. To ensure the model's integrity, an initial linear elastic analysis is performed to verify the model's correctness and determine the peak stress induced by a unit intensity load. This information is used to design the incrementation strategy for the initial coarse nonlinear analysis.

3.5.1 Element type

The potential of finite element analysis in investigating reinforced concrete beams with mild and stainless-steel bars has been explored using beam elements. This section provides an

overview of the elements used and how they were employed. Beam elements have been employed because the detailed distribution of strains and stresses inside the beam is of interest. Beam elements are also useful because they allow for the efficient application of refined constitutive laws for concrete due to their better depiction of multi-axial stress states. This proved to be highly beneficial for both an accurate evaluation of the bar rotation and strains and for a good prediction of the overall behavior of the structural elements, which are critical in beam failure. A material model featuring the fracture energy based smeared crack concept has been used. The constitutive law for reinforcing bar is according to the common practice of linear perfectly plastic. Three- and two-dimensional versions of the complete models have been set up. Details of each analysis can be found in the sections related to that particular analysis.

3.5.1.1 Two-dimensional analysis (2D)

For the 2D analysis of reinforced concrete beams, QPM8 isoperimetric continuum elements with 8 nodes and 2 degrees of freedom (U and V) per node are used to model the concrete.

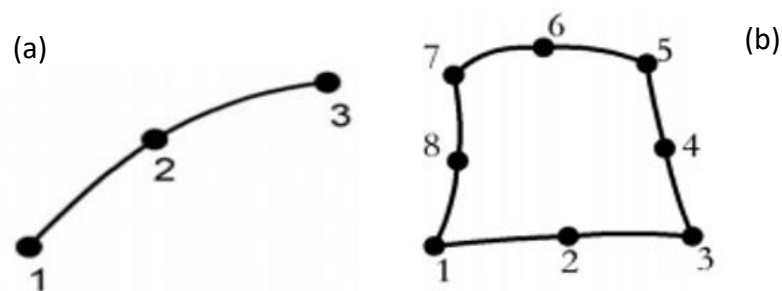


Figure 3.12. Details of bar element BAR (a) and (b) Plane stress element QPM8 (LUSAS, 2018).

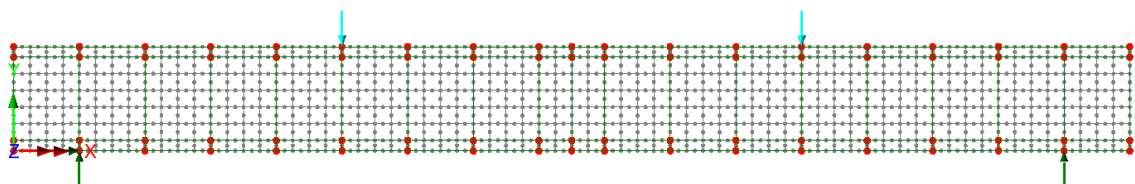


Figure 3.13. Side view of 2D model

This element has the following specifications: quadratic interpolation order; quadrilateral element shape; and plane stress structural element type. The element formulations are based on the standard isoperimetric approach, and for lower-order elements (corner nodes

only), the variation of stresses within an element can be regarded as constant, while for higher-order elements (mid-side nodes), it is linear. The reinforcement was modelled using a quadratic 2D bar element (BAR3) with two nodes, which only transmits longitudinal forces, has no bending stiffness, and transfers axial stress only. The variables are the displacement U and V at each node (see Figure 3.13).

3.5.1.2 Three-dimensional analysis (3D)

For the three-dimensional analysis, the concrete elements were modelled using 3D isoperimetric solid continuum elements with a 20-noded element, with three degrees of freedom for each node represented by a displacement U , V , and W in all three directions. Full numerical integration was conducted for all 3D elements, i.e., 3×3 Gaussian for quadrilateral elements. The reinforcement was modelled using a quadratic 3D bar element (BRS3) with three nodes, which only transmits longitudinal forces, has no bending stiffness, and transfers axial stress only. The variables are the displacement U , V , and W at each node, and the cross-sectional area coincides with the reinforcement steel area. The superposition of the nodal degrees of freedom at the concrete-reinforcing bar interface assumes a perfect bond between the two components. Figure 3.14(a) and (b) show the finite elements used in the model (BRS3 and HX20).

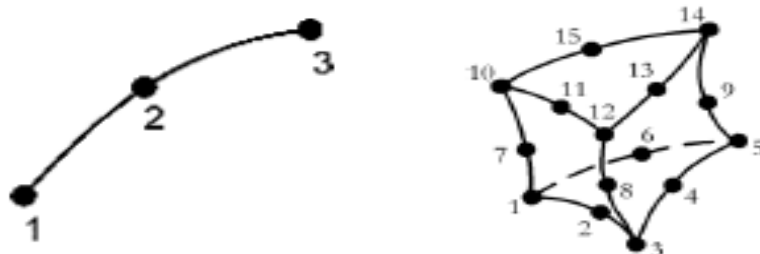


Figure 3.14. Details of bar element BRS3 (a) and (b) Plane stress element HX20 (LUSAS, 2018).

3.5.1.3 Loading and boundary condition

Figure 3.15 shows that the beam model is designed to replicate the four-point bending arrangement used in the experiments, with concentrated point loads assigned to 2D models and distributed line loads to 3D models. Pinned and roller support conditions were used in both the 2D and 3D simulations. Pinned support was assigned to support 1, which had no movement in the x , y , and z directions, while roller support was used for support 2, allowing free movement in the x direction and restricting movement in the other directions (y , z).

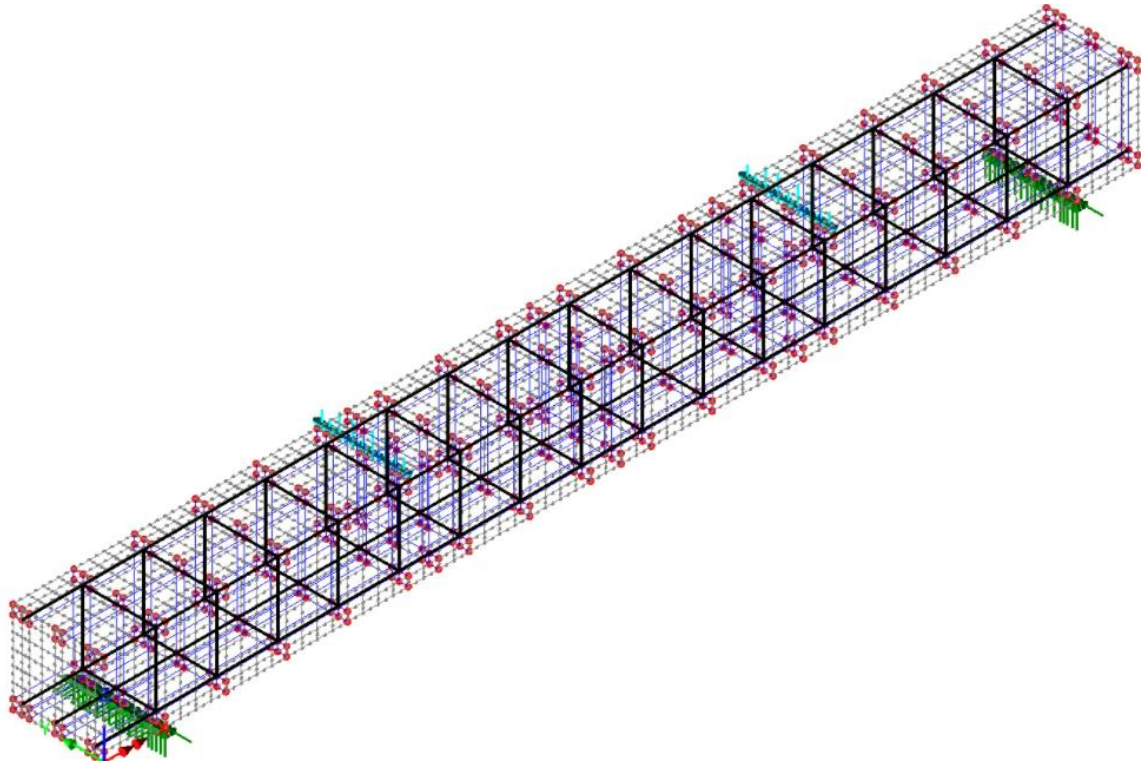


Figure 3.15. *Loading and boundary condition of the 3D model.*

3.5.2 Material Model

3.5.2.1 Concrete

Different types of finite elements can be employed for modelling concrete, depending on the application. These can be either structural elements (beams, shells) or continuum elements (solids). The elements mentioned above are often the same as those used for other materials. Multi-layered shells or fibre beams, which subdivide an element into fibres or layers to deal with nonlinear behavior of the main material, deserve special mention. However, this study does not explore fibre and multi-layered elements, even though they offer another way to represent reinforcement.

Several concrete material models are available in LUSAS, including the linear with creep/shrinkage concrete model (Model 86) and the smoothed multi-crack model (Model 109). The former is based on a simplified linear approach with creep and assumes that the service stress in the concrete is not exceeded. In contrast, the latter considers the nonlinear behavior in compression and tension, including cracking and crushing. Model 109 allows the nonlinear stress-strain behavior of structural concrete to be simulated up to failure and enables the simulation of multiple non-orthogonal cracks with a basic softening curve. This can be achieved through a fracture energy-controlled softening curve or by a strain at the

end of the softening curves in compression and tension, as shown in Figure 3.16. However, LUSAS (2016) recommends using a strain at the end of the softening curve in RC models, and thus, this method was employed in this study.

Model 109 was selected in this study for simulating the concrete behavior as it is more suitable in RC applications and is the latest evolution of LUSAS concrete models, offering greater accuracy and faster analysis time. In this model, the concrete elements are modelled using an isoperimetric continuum element with eight nodes, two degrees of freedom for each node, represented by a displacement U and V in both directions.

Model 109 is based on continuum damage mechanics and considers two failure modes, crushing in compression and cracking in tension. The material behaviours are described in terms of elastic, plastic, tensile, and compressive properties. In tension, the strain-stress behavior for concrete is simulated as a nonlinear relationship up to the ultimate tensile strength, followed by a gradually unloading branch, which includes the tension stiffening effect (Figure 3.16). The effect of the bond between the concrete and the reinforcing bars is estimated in the tension stiffening branch. The term "tension stiffening" refers to a phenomenon in which concrete can continue to withstand certain tensile loads despite the formation of cracks, while the tensile strength decreases slowly with an increase in tensile strain. This is depicted in the unloading branch of the stress-strain model, which can be explained using a nonlinear, linear, or bilinear relationship in LUSAS. In this study, the stress-strain proposed by LUSAS (2016) is used for the unloading failure branch, as presented in equation (3.2), and described in Figure 3.18. This nonlinear equation is established to provide reliable predictions of the experimental response and has been employed by many researchers in previous studies (e.g., Bencardino and Condello, 2014; Yuan et al., 2016; Guizani et al., 2017; Fib Model Code, 2010; do Carmo & Lopes, 2005; LUSAS, 2015).

The function illustrated in Figure 5.1, in terms of fracture stress (f_s) and the strain parameter ζ), has control parameters: the associated strain (ε_{ti}), the stress at first damage (f_{ti}), the strain at the effective end of the curve (ε_0), the uniaxial strain (f_t), and the strain at peak stress (ε_k). The basic function for the damage plane is as follows:

$$f_s = f_{ti} \cdot f_{uc}(\zeta) = (1 - \omega(\zeta)) E \zeta$$

(3.2)

With

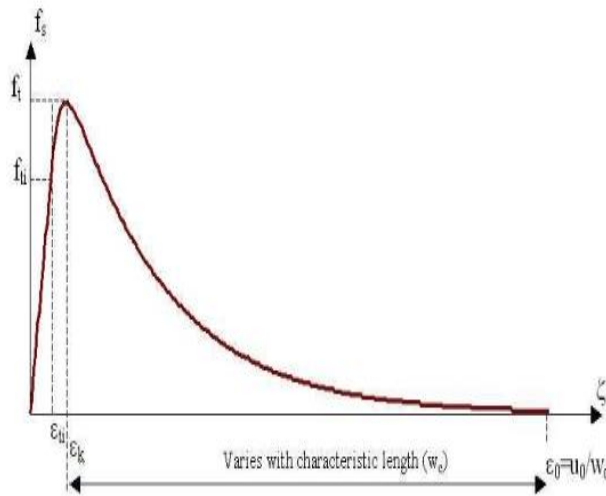


Figure 3.16. Damage evaluation function (softening curve) (LUSAS, 2016).

$$\omega = 1 - \frac{\varepsilon_{ti}}{\zeta} e^{-c_1 \eta} (a - b e^{-c_1 m \eta} - c e^{-c_1 m p \eta}) \quad (3.3)$$

The form used to derive the contact is the direct relationship between f_s and ζ :

$$f_s = f_{ti} e^{-c_1 \eta} (a - b e^{-c_1 m \eta} - c e^{-c_1 m p \eta}) \quad (3.4)$$

In which $\eta = \frac{\zeta - \varepsilon_{ti}}{\varepsilon_0 - \varepsilon_{ti}}$

C and p are both assumed to be fixed at 5. The constants a, b, c, and m are determined from the following four conditions.

$$f_s = f_{ti} \quad \text{at } \eta = 0 \quad (3.5)$$

$$\frac{\partial f_s}{\partial \zeta} = E \quad \text{at } \eta = 0 \quad (3.6)$$

$$f_s = f_t \quad \text{at } \eta = \eta_k \quad (3.7)$$

$$\frac{\partial f_s}{\partial \zeta} = 0 \quad \text{at } \eta = \eta_k \quad (3.8)$$

The mean uniaxial tensile strength (f_{ctm}) can be calculated as follows (BS EN 1992-1-1, 2004):

$$f_{ctm} = 0.3(f_{ck})^{\frac{2}{3}} \quad (3.9)$$

Where f_{ck} = is the cylinder characteristics strength

To estimate the (f_{ctm}) from the mean flexural strength $f_{ctm,fl}$, the following expression is adopted:

$$f_{ctm} = \alpha_{fl} \times f_{ctm,fl} \quad (3.10)$$

Where:

$$\alpha_{fl} = \frac{0.06 \times h_b^{0.7}}{1 + 0.06 \times h_b^{0.7}} \quad (3.11)$$

h_b is the beam depth (mm).

For the compression behaviour, Model 109 requires the peak compressive stress (ε_c) to be estimated as follows:

$$\varepsilon_c = 0.002 + 0.001 \frac{(f_{cu}-15)}{45} \quad 0.002 \leq \varepsilon_c = 0.003$$

$$\text{Where } f_{cu} = 1.25f_c \quad (3.12)$$

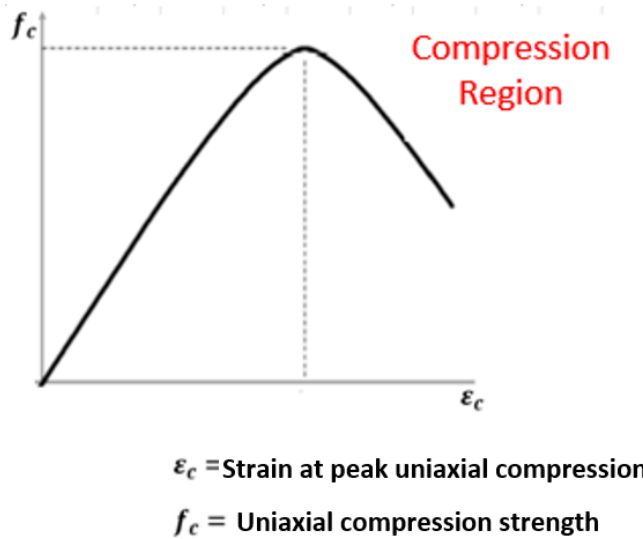


Figure 3.17. Post-failure stress-strain relationship (LUSAS, 2016).

Similarly, for the compression behaviour, the model given in Eurocode 2 (BS EN 1992-1-1, 2004) and the Fib Model Code for Concrete Structures (2010) are adopted, given by following expressions:

$$\sigma_c = \left(\frac{\kappa\eta - \eta^2}{1 + (\kappa - 2)\eta} \right) f_{cm} \quad \text{this equation is valid for } 0 < |\epsilon_c| < |\epsilon_{cu1}| \quad (3.13)$$

Where:

ϵ_{cu1} is the nominal ultimate strain.

ϵ_{c1} is the strain at peak stress.

ϵ_c is the compressive strain in the concrete.

f_{cm} is the ultimate compressive strength of the concrete, given as:

$$f_{cm} = f_{ck} + 8 \text{ (MPa)} \quad (3.14)$$

While the parameters η and k are calculated from equations (3.15) and (3.10), respectively:

$$K = 1.05 E_{cm} \frac{|\epsilon_{c1}|}{f_{cm}} \quad (3.15)$$

$$\eta = \frac{\varepsilon_c}{\varepsilon_{c1}} \quad (\varepsilon_c < 0) \quad (3.16)$$

In which E_{cm} is the elastic modulus of the concrete and ε_{c1} is the strain at the peak stress and E_{cm} calculated from equations (3.17) and (3.18), respectively:

$$E_{cm} = 22 \left[\frac{f_{cm}}{10} \right]^{0.3} s \quad (3.17)$$

$$\varepsilon_{c1}(0/00) = 0.7(f_{cm})^{0.31} \leq 2.8 \quad (3.18)$$

The normal ultimate strain (ε_{cu1}) expressed as a percentage:

$$\varepsilon_{c1} (0/00) = 2.8 + 27 \left[\frac{(98 - f_{cm})}{100} \right]^4 \quad (3.19)$$

Model 109 requires assigning the compressive damage parameter at each inelastic strain increment, starting from 0 for uncracked material and progressing to 1 when the concrete completely loses its load-bearing capacity. As illustrated in Figure 60, this parameter is determined by analysing the stress-strain diagram of concrete in compression, as shown below.

The effective end of the softening curve parameter (ε_o), if set, is calculated as:

$$\varepsilon_c = 0 \quad \text{for} \quad \varepsilon_o \approx 5G_f / W_c f_t \quad (3.20)$$

Where W_c is a characteristic length for the element.

The fracture energy (G_f) can be determined using the following equation:

$$G_f = k_b^2 \times c_f \times f_{ct} \quad (3.21)$$

In which k_b accounts for the reinforcement size related to the beam size, while the parameter c_f considers all the secondary effects. The parameter k_b is determined using the following relationship:

$$k_b = \sqrt{\frac{k \cdot \left(2 - \frac{b}{B}\right)}{1 + \frac{b}{B_{10}}}} \quad (3.22)$$

Model 109 considers the nonlinear behavior of concrete in compression, which is characterized by several parameters. These include the uniaxial tensile strength, the biaxial to uniaxial stress ratio (1.15), the strain at peak uniaxial compression (2.2E-3), the dilatancy factor ($\psi=-0.1$), the initial relative position of the yield surface (0.6), the contact multiplier on ϵ_0 for the first opening stage (0.5), the constant in the interlock state function (0.3), the angular limit between crack planes (1.0 rad), and the final contact multiplier on ϵ_0 (5.0). Additionally, the slope of the friction asymptote for damage ($\mu=0.8$) is considered to define the surface of local damage, and the shear intercept to tensile strength ($r\sigma=1.25$) is also taken into account. These values were adopted based on the recommendations in the LUSAS manual.

For the plastic phase, the ability of cracked concrete to transmit tensile stresses (strain softening) and transfer shear is considered. The softening behavior follows an exponential descending law based on two parameters: the slope at the end of the softening curve (3.5E-3) and the uniaxial tensile strength of concrete (2.9 MPa), whose value is linked to the behavior of the ductile element. In the elastic phase, Poisson's ratio (0.2) and Young's modulus (31000 MPa), which are calculated based on Eurocode 2 (2004), are the input parameters.

3.5.2.2 Reinforcement

Different elements are available in LUSAS for modelling reinforcing bar, but bar element was adopted for one major reason: which, is due to the element, only transmits longitudinal forces, has no bending stiffness, and only transfers axial stress. In the model, the reinforcement was modelled using a beam element for the analysis. The variables are the displacement U and V, at each node. The cross-sectional area coincides with the reinforcement steel area. The superposition of the nodal degrees of freedom at the concrete-reinforcing bar interface assumes that a perfect bond exists between the two components.

The behaviour reinforcing bar in linear elastic range is defined by Poisson's ratio ($\nu_s = 0.3$) and young's modulus ($E_s = 20000 \text{ MPa}$), while in plastic range has been simulated in accordance with the von Mises yield criterion with isotropic hardening. The strain hardening was defined through hardening yield stress (s_y), the ultimate plastic strain ($u_s = 0.2$) and the slope of strain hardening. The von Mises yield criterion was preferred over the Tresca criterion for two reasons. The first reason is that the von Mises criterion predicts a greater pure shear yield stress than the Tresca criterion, which indicates that the Tresca criterion is on the conservative side and hence is not preferred (Boresi and Schmidt, 2003). The second reason is that yield surfaces drawn based on the von Mises yield criterion are continuous and convex, whereas yield surfaces developed based on the Tresca criterion are not continuous.

For the plastic phase, the ability of cracked concrete to transmit tensile stresses (strain softening) and transfer shear is considered. The softening behavior follows an exponential descending law based on two parameters: the slope at the end of the softening curve ($3.5E-3$) and the uniaxial tensile strength of concrete (2.9 MPa), whose value is linked to the behavior of the ductile element. In the elastic phase, Poisson's ratio (0.2) and Young's modulus (31000 MPa), which are calculated based on Eurocode 2 (2004), are the input parameters.

3.5.3 Material nonlinearity

In material nonlinearity, the change in stress is disproportionate to the change in strain. This phenomenon occurs during the collapse of beam structures due to the effects of material yield. When irrecoverable stresses are present on unloading, this material yield is referred to as plasticity in metals. Plasticity can be best handled when analysing beam issues using an appropriate associated flow theory and yield criterion.

3.5.4 The von Mises yield criterion

The von Mises yield criterion is an appropriate yield criterion to determine the stress level at which plastic deformations begin. For an isotropic material, this can be determined based on the magnitude of the three principal stresses, not their orientation (Carlos, 2016).

Therefore, the function can be expressed as:

$$f(J_1, J_2, J_3) = 0 \tag{3.23}$$

Where

J_1 is the first deviatoric stress variant

J_2 is the second deviatoric stress variant

J_3 is the third deviatoric stress variant

$$J_1 = \sigma_{ii} \quad (3.24)$$

$$J_2 = \frac{1}{2} \sigma_{ij} \sigma_{ij}$$

$$J_3 = \frac{1}{3} \sigma_{ij} \sigma_{ik} \sigma_{ki}$$

Experiments have demonstrated that yielding in metal is primarily independent of tension or hydrostatic pressure, whether superimposed on the state of combined stress or applied alone. Any yield criteria for metals may therefore be reduced to the deviatoric stress invariants and expressed as:

$$f(J_1, J_3) = k(\mathcal{K}) \quad (3.25)$$

Almost all of the proposed yield criteria for metals are now of historical relevance due to their contradiction with experimental findings. The two simplest yield criteria proposed by von Mises and Tresca do not have this flaw. Experiments comparing the two have found that the von Mises hypothesis is more realistic. Therefore, the von Mises criterion has been adopted in this research, and the choice is justified in the reinforcement modelling section.

According to von Mises, yielding takes place when the deviatoric stress invariant J_2 reaches a critical value. His criterion can also be written as:

$$\begin{aligned} J_2 &= \frac{1}{2} \sigma_{ij} \sigma_{ij} = k^2 \quad (3.26) \\ &= \frac{1}{6} (\sigma_1 - \sigma_2)^2 + \frac{1}{6} (\sigma_2 - \sigma_3)^2 + \frac{1}{6} (\sigma_3 - \sigma_1)^2 = k^2 \\ &= \frac{1}{6} (\sigma_x - \sigma_y)^2 + \frac{1}{6} (\sigma_y - \sigma_z)^2 + \frac{1}{6} (\sigma_z - \sigma_x)^2 + \sigma_{yz}^2 + \sigma_{zx}^2 + \sigma_{xy}^2 = k^2 \end{aligned}$$

In which k is dependent on the strain hardening expressed as:

$$k = \sigma^- / \sqrt{3} \quad (3.27)$$

In which σ^- is the von Mises stress. The material is at point of yield when the von Mises equivalent stress is equal to the uniaxial yield stress ($\sigma^- = \sigma_y$). Any increase in strain

beyond this point will produce plastic deformation. The material is assumed to be elastic if the von Mises stress is less than the uniaxial yield stress ($\sigma^- < \sigma_y$).

3.5.5 The Prandtl-Reuss flow rule

It is considered that the stresses inside a continuum may be computed by dividing the continuum vector strain increments into plastic and elastic components during the elastoplastic deformation.

$$\delta\varepsilon = \delta\varepsilon_e + \delta\varepsilon_p \quad (3.28)$$

Where

$\delta\varepsilon$ is the iterative strain, $\delta\varepsilon_p$ is the iterative plastic strain and $\delta\varepsilon_e$ is the elastic strain.

By decomposing the stress terms into their hydrostatic and deviatoric components, the elastic strain increments $\delta\varepsilon_e$ may be related to the stress increments such that

$$\delta\varepsilon_e = \frac{\delta\sigma}{2G} + (1 - 2\nu)\delta\frac{\partial\sigma}{E} \quad (3.29)$$

Where ν is the poisson's ratio, G is the modulus of shear, $\partial\sigma$ is the iterative stress and E the young's modulus.

The normality condition may be used to describe a relationship between the corresponding stress increment and plastic strain increment in metals. This may be expressed for a material whose plastic potential coincides with the yield surface (associate flow) as:

$$\delta\varepsilon_p = \delta\lambda \frac{\partial F}{\partial\sigma} \quad (3.30)$$

Where $\delta\lambda$ is a proportionality constant termed the plastic strain rate multiplier and $\frac{\partial F}{\partial\sigma}$ is a flow vector directed normal to the yield surface. Equation (3.8) is unknown as the Prandtl-Reuss equation when the von Mises yield criterion is used.

3.5.6 Isotropic Strain Hardening

The stress level at which additional plastic deformation occurs after initial yielding may be affected by the existing degree of plastic straining, also known as strain hardening or work. Isotropic and kinematic hardening are the two most commonly used mathematical methods to account for strain hardening. In this research, the isotropic hardening procedure is used, which assumes that the yield surface expands uniformly during plastic deformation while

maintaining the same orientation, origin, and shape. On the other hand, the kinematic hardening procedure assumes that the yield surface maintains its shape and size during plastic deformation but is translated as a rigid body. The yield surface for an isotropic hardening material can be expressed as follows:

$$F(\sigma, k) = f(\sigma) - k(k) = 0 \quad (3.31)$$

Where k is the strain hardening parameter and σ is the current stress level.

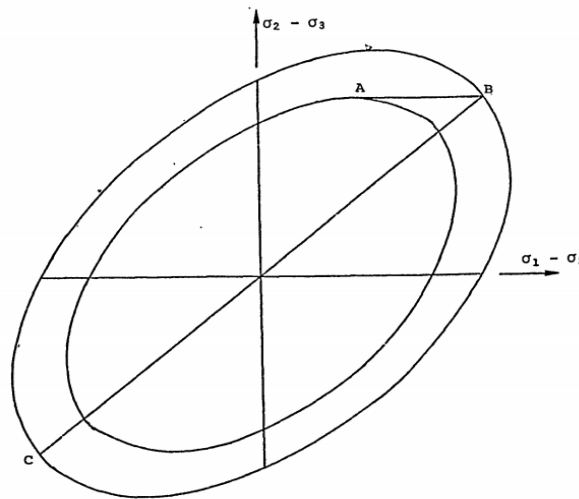


Figure 3.18. Isotropic hardening model used in the nonlinear material model (Version, 2014)

When the stress level moves from point A to point B, the effect on the yield surface is illustrated in Figure 3.18. At point C, yielding will occur if the body is unloaded and reloaded in the opposite direction. Therefore, the von Mises yield criterion does not account for the Bauschinger effect. Nevertheless, it is widely used because it produces reliable results when the loading direction remains constant.

In the current study, it is assumed that the progressive development of the yield surface depends solely on the total plastic strain. This can be expressed in terms of the work hardening parameter k as follows:

$$\delta k = \sigma^T \delta \varepsilon_p \quad (3.32)$$

Where

k represents the amount of work done during plastic deformation

$\delta \varepsilon_p$ represent iterative local plastic strain

δk represent iterative hardening parameter.

3.5.7 Geometric Nonlinearity

The assumption of small displacements in linear elastic analysis is not valid in many problems, and to achieve valid results, the impact of geometric variation of the structure during deformation (geometric nonlinearity) must be considered. There are five methods for accounting for geometric nonlinearities in LUSAS software: Updated and Total Lagrangian, Eulerian, co-rotational, and P-Delta. The Updated Lagrangian formulation is continually updated with structure geometry and has its reference at the end of the last converged increment. The Total Lagrangian formulation relates the displacement of the structure to the initial geometric configuration throughout the solution. The Eulerian formulation has its reference as the current configuration. The co-rotational formulation relates large displacement effects to the set axes that follow and rotate with the elements. P-Delta takes into account the interaction between the vertical and horizontal sway loading.

The Total Lagrangian technique has been used throughout the current work. This has the advantage of requiring the element shape functions to be formulated only once (at the beginning of analysis), making the method more computationally efficient.

3.6 Modelling of steel rebar

This section describes in detail the three methods for modelling reinforcing bars mentioned above.

3.6.1 Embedded modelling

Embedded modelling uses different elements for steel and concrete. However, the reinforcement and concrete are represented using the same type of elements with the same degree of freedom, shape function, and number of nodes. Thus, the embedded method is defined by the incorporation of a one-dimensional bar into two- or three-dimensional elements (see Figure 3.6). They are computed by integrating along the curves that represent the reinforcing bar segments within each element. After that, the embedded reinforcing bar elements are superimposed on the concrete elements in question. The reinforcement bars do not need to match the concrete elements' boundaries. Instead, the reinforcement bar passes through the concrete element in an arbitrary manner. A perfect bond between the steel and the concrete is achieved because the concrete and the

reinforcing bar elements must be assigned the same degrees of freedom. Therefore, bond-slip may only be simulated implicitly by changing steel or concrete constitutive relations. One drawback of this method is that it requires the use of specific reinforcing bar elements. Furthermore, like the discrete technique, each reinforcing bar must be taken into account while generating the analytical input. It is worth noting that, as we will see later, this method (embedded representation) is the only way to appropriately simulate lap joints or lap/splice length using LUSAS to address the goals of this research.

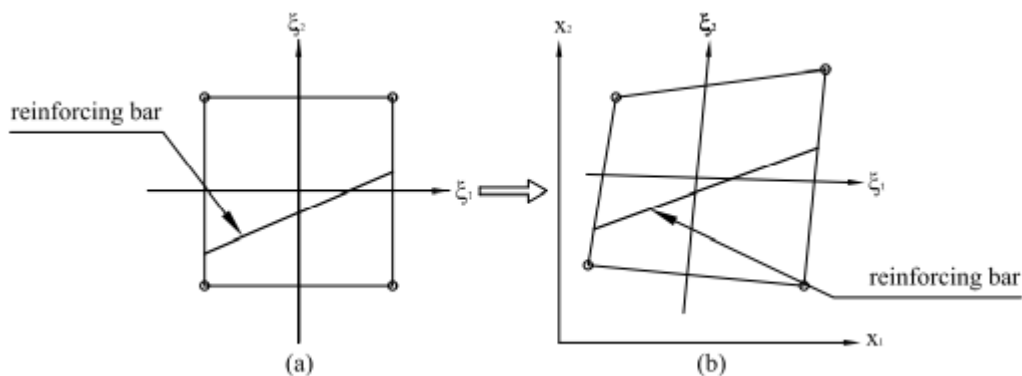


Figure 3.19. Embedded reinforcing bar element: in the local and global coordinate system (a) and (b) (LUSAS, 2014).

3.6.2 Distribution modelling

Distributed reinforcement modelling refers to the technique of smearing reinforcing bars across an element that is overlaid on the primary concrete element. This approach can be used, for instance, by overlaying membrane elements with eccentricities onto shell elements to simulate the reinforcement layer. By assigning an equivalent thickness to the elements, the appropriate area of reinforcement along a unit length section of the structure can be determined.

In the constitutive equation for an element with a unidirectional layer of smeared reinforcement, the local directions of the elements that are normal and parallel to the reinforcing bars are typically taken into account.

The tangent material modulus of the steel bar, E_T^S , is used to convert the tangent material stiffness matrix to the global system by applying the appropriate transformation for the element under consideration. This results in obtaining the contribution of the tangent

stiffness matrix to the steel layer of the composite material. However, before computing the stresses in the reinforcing bars, the actual strains must be transformed to the direction parallel to the reinforcement steel (i.e., the local direction 1).

To achieve a combination of the embedded and distributed representation of the reinforcement, the reinforcement is smeared into thin layers, embedded into the element of a similar type as the concrete element, and then superimposed on the concrete elements. It is important to assume a perfect bond between steel and concrete layers when combining them within an element. Thus, bond-slip can only be represented implicitly by changing the steel and concrete constitutive relations. This method is only suitable for reinforcing bars that are uniformly distributed.

3.6.3 Discrete modelling

For discrete modelling, the reinforcing bars are represented as a separate element, commonly using cable or truss elements. Two-dimensional or even three-dimensional elements are occasionally used to investigate structural details. Cable and truss elements convey axial forces only and have no rotating degrees of freedom. A one-dimensional constitutive relation is used to describe the material behaviours of cable and truss elements. To ensure the compatibility of reinforcement and concrete displacement, the boundary of the concrete elements must correspond with the cable and truss elements, and both types of elements' node points must be the same. Therefore, the cable or truss elements' shape functions and the concrete elements' shape functions must be in the same sequence.

For concrete modelling, two-dimensional isoperimetric quadratic 8-node elements and three-dimensional isoperimetric quadratic 20-node elements are compatible, as are quadratic 3-node elements for steel bars. The reinforcement element's location is determined by the reinforcement layout. Hence, the concrete element boundaries must match the steel bars, and the reinforcing bar layout significantly affects the finite element mesh of a concrete structure.

Coinciding nodes of steel and concrete elements are assigned the same degrees of freedom when investigating overall structural behaviours. By changing the constitutive relations of steel or concrete, bond-slip is either considered or disregarded implicitly. However, to simulate bond-slip more accurately, particularly when investigating the behaviours of

structural details, varying degrees of freedom are provided to the converging nodes of steel and concrete elements. Interface elements, such as contact or bond elements, connect the distinct degrees of freedom of coincident concrete and nodes elements. Simple interface elements, also known as joint elements, link a single steel element to a single node of a concrete element. Nonlinear springs are one example of such elements.

3.7 Model Interface Behaviour

The explicit representation of bond-slip behaviours has a significant disadvantage as it cannot be properly coupled with an embedded method in the context of the current study; therefore, it is not employed in the application. As the embedded representation is used to simulate the reinforcement due to the size of the model and complexity of the geometry, the implicit approach is the only possibility to model the interface behaviours. Bond-slip causes interface behaviours at steel to concrete interfaces, which is implicitly modelled by relating the tension stiffening effect to either steel or concrete. As a result, either the steel constitutive law or the concrete constitutive law is changed accordingly.

Models that incorporate tension stiffening in concrete are more popular than models that consider tension stiffening in steel. Tension stiffening is accounted for in concrete-related models by substituting the average stress-average strain diagram for the concrete component of reinforced concrete for the softening branch of the tensile stress-strain diagram for plain concrete. The magnitude of the ultimate strain is what distinguishes plain concrete from reinforced concrete. However, the ultimate strain of reinforced concrete can be assumed to be one order of magnitude more than the ultimate strain of plain concrete, as a rule of thumb.

3.8 Nonlinear solution procedure

Solving nonlinear finite element problems is a challenging and time-consuming process. The aim is to create a solution approach that is accurate, inexpensive, and reliable, which is very tough to accomplish in reality. Difficulties vary depending on the issue; thus, solution strategies that work for one type of issue may not work for another. The engineer must utilize his knowledge and judgment to choose the best solution approach for each problem. In the current study, a combination of iterative and incremental techniques was used to obtain the equilibrium equations.

The incremental methods separate the solution into several linear steps and combine the displacement and loads obtained at each iteration. The incremental displacement ($\Delta\delta_n$) is calculated using a tangential estimation related to the current displacement (δ_n) when each load increment (Δp_n) is applied, as follows:

$$\Delta p_n + p_n = \left(\frac{\partial p}{\partial \delta} \right)_n \Delta \delta_n \quad (3.33)$$

Where:

$$\Delta \delta_n = k_T^{-1} \Delta p_n \quad (3.34)$$

In which $\Delta\delta_n$ is the applied stress increment and K_T is the tangent matrix of stiffness computed at the beginning of each step. After each load step, the loads and displacements are added as:

$$\begin{aligned} p_{n+1} &= p_n + \Delta p_n \\ \delta_{n+1} &= \delta_n + \Delta \delta_n \end{aligned} \quad (3.35)$$

And the loading of the next increment is applied.

The equilibrium equations are not fulfilled after each iteration when using solely incremental techniques, and the solution diverges from the actual solution path. Returning to the equilibrium path by applying residual correctness after each step is an improvement in this approach.

$$g_n = p_n - \int_v B^t \sigma_n \delta v \quad (3.36)$$

Where

g_n is the residual correctness

p_n is the load

Δp_n is the displacement load

The residual correction is applied with the next load increment. If small enough steps are taken, incremental techniques can provide reliable results. However, because equilibrium is

not satisfied at the end of each increment, the results are never guaranteed to be on the solution path. Due to the number of steps required to obtain an accurate solution, incremental techniques alone are too costly. By utilizing a combination of iterative and incremental approaches, it is possible to enhance the accuracy of the solution for greater load increments. Before proceeding to the next step, these approaches usually reduce the out-of-balance forces to a small value.

The Newton-Raphson approach involves continually increasing the displacement or load and updating the stiffness matrix to obtain a better approximation solution until convergence is achieved. If an appropriate solution $\delta = \delta_1$ is attained using g_1 as the out-of-balance force, a better approximation can be obtained by utilizing Taylor's series as follows:

$$g_{1+1} = g_1 + \left(\frac{dg}{d\delta} \right)_i \Delta\delta_i = 0 \quad (3.37)$$

As a result, the new displacement increments may be derived from

$$\Delta\delta_i = -k_T^{-1} g_i \quad (3.38)$$

and a new solution approximation may be expressed as

$$g_{1+1} = \delta_1 + \Delta\delta_i \quad (3.39)$$

To obtain a new approximation solution until convergence is achieved, the displacements obtained in each iteration can be used. However, updating the stiffness matrix after each iteration can be expensive. The Modified Newton Raphson (MNR) method addresses this by utilizing the stiffness matrix from the first approximation for all subsequent solutions, thus reducing computational costs. However, this approach can be unstable and slower to converge than the traditional Newton Raphson (NR) method, particularly for highly nonlinear problems.

To speed up convergence, various techniques have been proposed in recent years, such as those described in Cresfield (1997) and Fib Bulletin 45 (2008). These methods include Quasi-Newton, Conjugate Newton, Secant Newton, and Conjugate Gradient procedures, among others.

Quasi-Newton methods aim to update the stiffness matrix during the iteration process to improve convergence.

$$\alpha_{i-1}\Delta\delta_{i-1} = k_i^{-1}(g_i - g_{i-1}) \quad (3.40)$$

Which since

$$\Delta\delta_i = -k_i^{-1}g_i \quad (3.41)$$

It may be expressed as:

$$\Delta\delta_i^T(g_i - g_{i-1}) = -\alpha_{i-1}\Delta\delta_{i-1}^T g_1 \quad (3.42)$$

By multiplying both sides by g_i

Conjugate Newton techniques combine the Modified Newton Raphson with the Conjugate Gradient method to satisfy.

$$\Delta\delta_i = k_i^{-1}g_i + \beta_i\Delta\delta_{i-1} \quad (3.43)$$

Secant Newton method differs from the Conjugate Newton and Conjugate Gradient methods by satisfying equation (3.32) rather than Conjugate Gradient equation (3.34).

The Conjugate Gradient method repeatedly recalculates the residual forces, giving an iteration change in displacement vector, such that:

$$\Delta\delta_{i+1} = \delta_i + \alpha_i\Delta\delta_1 \quad (3.44)$$

Where

$$\Delta\delta_1 = -g_1 + \beta_i\Delta\delta_{i-1} \quad (3.45)$$

And β_i is chosen to minimise g_{i+1} , such that:

$$\Delta\delta_{i-1}^T = k_T\Delta\delta_1 \quad (3.46)$$

3.9 Convergence criteria

Realistic convergence criteria must be employed to terminate the iterative process in order for any iterative-based solution method to be effective. If these tolerances are too tight, the computational effort will be wasted, resulting in needless accuracy. Conversely, if the criteria are too loose, inaccurate results will be obtained. As the method computes

incremental displacements by removing out-of-balance forces after each iteration, it is reasonable to require that these factors be verified for convergence to zero. The Euclidean residual norm as a percentage of the total reactions, such that

$$Y_g = \frac{(\Sigma \Delta g_1^2)^{1/2}}{(\Sigma \Delta R_{1+1}^2)^{1/2}} \times 100 \quad (3.47)$$

And the Euclidean displacement norm as a percentage of the total displacement (Equation 3.38) are the two parameters utilised to control convergence in the current study

$$Y_\delta = \frac{(\Sigma \Delta \delta_1^2)^{1/2}}{(\Sigma \Delta \delta_{1+1}^2)^{1/2}} \times 100 \quad (3.48)$$

In order to determine when the required accuracy has been achieved, the computed values are compared to the input parameters. To avoid wasting computational resources searching for an unachievable solution, it is a good practice to verify the results after each increment for any signs of divergence. However, the divergence check, similar to the convergence criterion, should be realistic in order to avoid terminating the problem prematurely.

In LUSAS, after a certain number of iterations, the residual norm and Euclidean displacement percentages are checked. If the values are not excessively large (i.e., more than 100), the problem is continued because convergence can be reached in subsequent increments.

3.10 Solution approach

The nonlinear equations are solved in LUSAS using a Newton-Raphson-based iterative technique. There are two approaches available: (1) Modified Newton-Raphson, and (2) Full Newton-Raphson. The primary difference between the two techniques is that Modified Newton-Raphson reuses a previous stiffness, whereas the stiffness matrix is updated after each iteration in the Full Newton-Raphson technique. The Full Newton-Raphson method converges faster due to the stiffness matrix being updated after each iteration. However, with the Modified technique, the stiffness prediction is less accurate, leading to more equilibrium iterations and therefore a slower convergence rate. Nevertheless, it can be quite rapid for a realistic initial estimation, and with the use of acceleration methods such as line searches.

The incremental-iterative solution in LUSAS is based on the Newton-Raphson iteration,

where the load is slowly increased to attain equilibrium with each increment. The program controls three incremental procedures: displacement, arch-length controlled, and load methods. It is possible to combine the load and displacement methods with the arch-length method, which changes the iteration method at the given point. The incremental solution procedure can be stipulated in three ways: automatic, through predefined load curves, and manual. For conducting the actual analyses, the automatic procedure was employed since the program automatically reduces the step length by a predefined factor if convergence is not achieved within the increment after a specified number of iterations. This means that the increment size is automatically adjusted by LUSAS based on the convergence history. The maximum number of iterations permitted before automatic step reduction was set to 10. It is worth noting that LUSAS allows the user to control the incrementation by specifying the starting increment size and the maximum change in increment size.

Several convergence criteria are used in the program to monitor convergence, and the adoption of suitable convergence criteria is crucial. In this research, the following criteria were used as reference: Euclidian incremental displacement norm ($dtnrm=1.0$), Root mean square of residuals ($RMS=108$), Work norm ($wdnrm=108$), Maximum absolute residual ($MAR=108$), Euclidian displacement norm ($dpnorm=1.0$), and Euclidian residual norm ($rdnrm=0.1$). The program compares the values of these parameters to the input parameters to determine when the required accuracy is achieved. It is recommended to verify the results after each increment to avoid wasting computer time searching for an unachievable solution. This check, like the convergence criterion, should be realistic to avoid the problem being terminated prematurely. For each of the above parameters, the generic load increment convergence is satisfactory if a tolerance limit is imposed.

4. Comparative study of factors influencing tension lap joints.

4.1 Introduction

The practice of splicing reinforcing bars in reinforced concrete structures to manage insufficient bar length is common, mainly due to transportation limitations on bar length. Splicing reinforcing bars side by side offers a simple and economical solution to the problem of continuity. The bond between concrete and reinforcement requires sufficient anchorage of the reinforcing bar in concrete to ensure proper structural interaction. The required lap splices and anchorage length not only rely on the efficiency of the anchorage but also on the bar forces that may be transferred or developed, such as the bar yield strength and bar size.

The current Eurocode 2, Design of concrete structures - General rules and rules for buildings (BS EN 1992-1-1:2004), treats anchorage length and lap splice lengths as separate entities, although current research has shown that the two are similar and should be addressed with a single design equation (TG4.5, 2014). The Eurocode 2 requires a lap splice length calculated by multiplying the design anchorage length by a factor, the magnitude of which depends on the “class” to which the splice belongs. With larger confinement, bond failure occurs when the deformed reinforcing bars pull out of the concrete, crushing the concrete in front of the bar deformations (Bournas and Triantafillou, 2011). This represents an optimum bond resistance condition, while classes of concrete leading to confinement result in less likelihood of splitting failure before yielding.

This section of the study aims to examine the influence of concrete cover, lap splice length, shear links confinement, and concrete strength on the structural performance of lap splices. This examination is based on an extensive experimental database of laps and anchorage gathered by Task Group 2.5.

4.2 Database evaluation and design models

This section compares the equations for estimating mean tension bar stress with experimental results from a tension splice database. The objective is to evaluate the applicability of the design equations. The authors evaluate the Fib database of a large-scale experimental study for lap and anchorage, compiled by Fib Task Group 4.5 and the Concrete Centre. The database includes laboratory test results on laps and anchorages conducted by ACI (for casted beams at tension only), as well as additional data from Asian and European

investigations. The database studies a wide range of cross-sections, lap splice length, bar spacing, concrete cover, yield strength, bar diameter, confinement, and compressive strength, among other variables. Various researchers contributed to this database, including Darwin et al. (1995), Zuo and Darwin (1998), Azizinamini et al. (1993, 1995), Rezansoff et al. (1991, 1993), Hester et al. (1991, 1993), DeVries et al. (1991), Choi et al. (1990, 1991), Zekany et al. (1981), Thompson et al. (1975), Ferguson and Breen (1965), Ferguson and Thompson (1965), Mathey and Watstein (1961), Chamberlin (1956, 1958), Chinn et al. (1955), and Micallef and Vollum (2017, 2018). The number of spliced bars varies from 1 to 6, and the lap length ranges from 5ϕ to 80ϕ , while the concrete strengths and bar diameters fall within the range of 111 N/mm² to 14 N/mm² and 8 mm to 38.9 mm, respectively. The database comprises a total of 824 tests, including 397 lap and anchorage specimens in which the bars are not confined by shear links and 418 specimens in which the bars are confined by shear links. After filtering the database, 824 specimens remain (see Table 9 for the summary of data included in this study) based on the filtering limits proposed in accordance with Fib Bulletin 72 (TG4.5, 2014) recommendations for laps and anchorages.

Therefore, this study only includes test specimens where:

$$k_{tr} \leq 0.005;$$

$$15 \text{ MPA} \leq f_{cm} \leq 110 \text{ MPA}$$

$$0.5 \leq \frac{c_{min}}{\phi} \leq 3.5 \text{ and } \frac{c_{max}}{c_{min}} < 5$$

$$l_b \geq 17\phi;$$

The current study considers six experiments with shear links and sixteen experiments without them (as shown in Table 4.1).

Table 4.1. Summary of filtered specimens considered in this study.

Table 1				
	Total number of results	Test discarded	Test with links	Test without links
Overall number of tests	828	32	48	397
Filtered data	24	-	8	20

4.3 Results and Discussion

The test results are provided in A1-A5 in the appendix. The strength of the specimens is presented as the ratio of the stress measured in the test to that estimated by Fib bulletin 72 equation (4.10) for mean lap stress.

4.3.1 Effect of lap-length to bar-diameter ratio on lap strength

The experiment used splice lengths ranging from 570 mm to 950 mm (30 \emptyset to 50 \emptyset) to examine the impact of lap-length to bar-diameter ratio on the maximum measured bar stress. The lap stress measured in the experiment indicates the stress developed on the lap length. While the lap stress measured in the test decreases as the lap-length to bar-diameter ratio is increased, it does increase with an increase in the lap length to bar-diameter ratio.

Figure 4.5 illustrates the plot of the maximum bar stress measured in the test, σ_{max} , against the lap-length to bar diameter ratio. Increasing the lap-length to bar-diameter ratio by 33% from 30 \emptyset to 40 \emptyset (570 mm to 760 mm) resulted in a 22% increase in lap stress. A further 20% increase in lap-length to bar diameter ratio from 40 \emptyset to 50 \emptyset (760 to 950 mm) amplified the lap stress by 26%.

It is worth noting that the measured stress of 750 MPa in this experiment is very high. However, the reinforcement used in this experiment was Japanese steel, which has a yield

strength of 708 MPa, significantly higher than the mean strength of UK reinforcement at about 560 MPa.

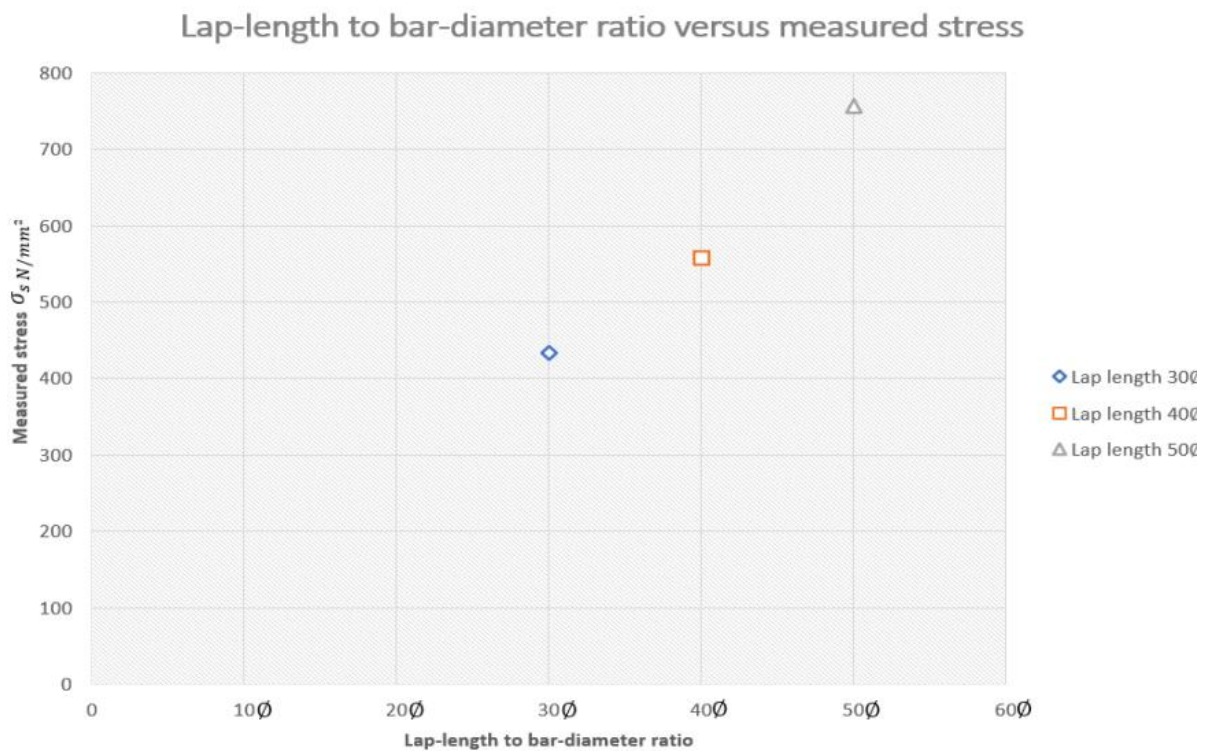
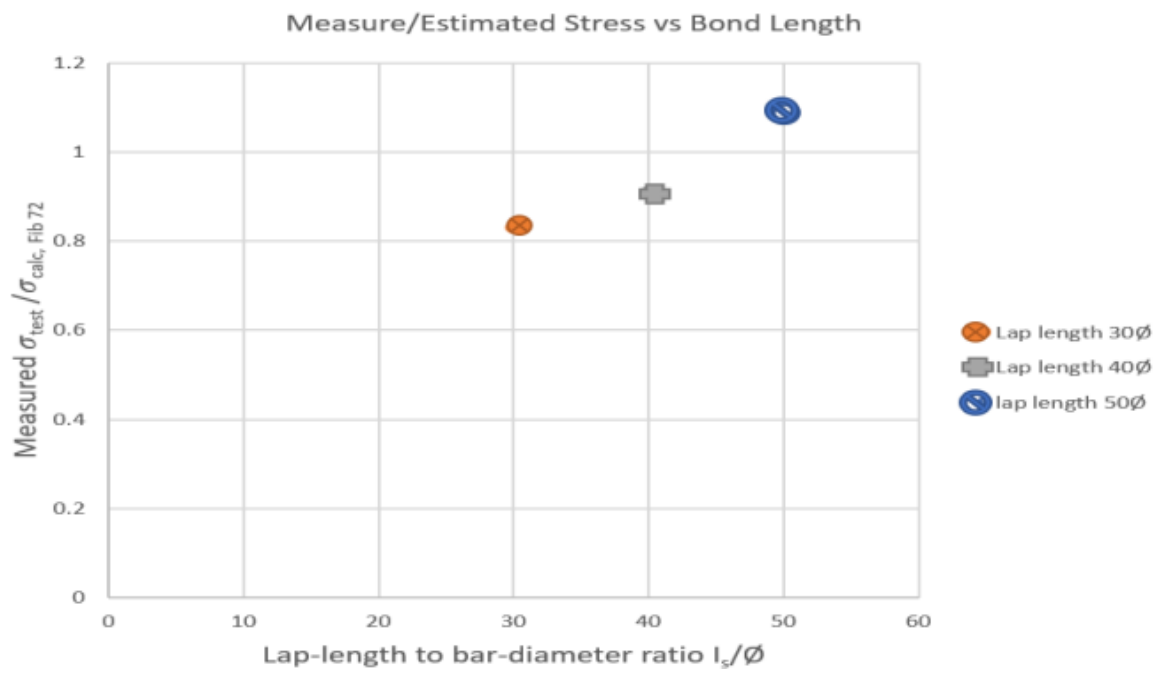


Figure 4.1. Influence of lap length to bar diameter ratio on maximum bar stress measured in the test.

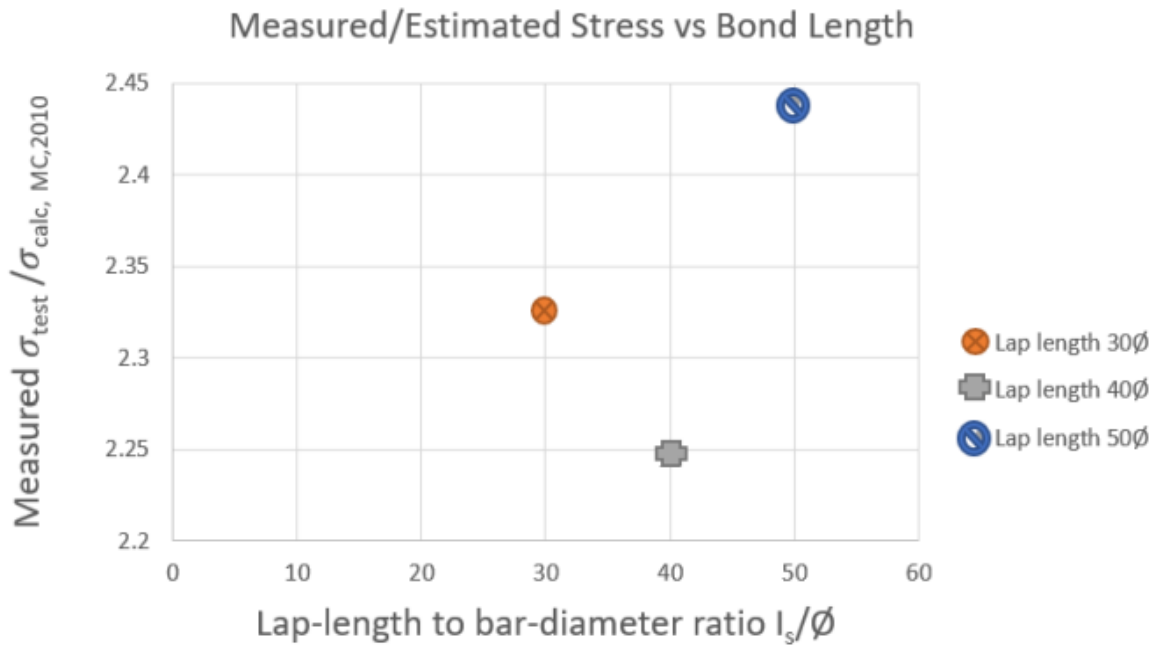
4.3.2 Influence of design models on estimating bar stress

Figure 4.6 illustrates the lap-length to bar-diameter ratio plotted against the ratio of maximum mean bar stress over the lap length measured in the test (σ_{test}) to the calculated average lap stress according to Fib bulletin 72 (Figure 4.6(a)) and Model Code (2010) (Figure 4.6(b)). As shown in Figure 4.6, the bar stress predicted by the Fib bulletin 72 (2014) equation increases at a rate that is less than proportional to lap-length to bar-diameter ratio. The comparison indicates that the design equation (4.10) for estimating the average bar stress in lapped bars according to Fib bulletin 72 (2014) overestimates the effect of lap length on the measured lap stress in the test (σ_{test}) in comparison to the Model Code's (2010) design equation (4.9) for mean bar stress. It is observed that the ratio of measured stress to estimated stress increases with lap length. Increasing the lap-length to bar-diameter ratio from 30∅ to 40∅ (570 mm to 760 mm) resulted in an 8% increase in the ratio of measured to estimated strength. However, a further increase in lap-length to bar diameter ratio from 40∅ to 50∅ increased the ratio of measured to estimated lap

strength by 17%. In comparison to the mean bar stress calculated according to the Model Code (2010), there is a reduction of 64%, 60%, and 55% for lap-length to bar-diameter of 30ϕ , 40ϕ , and 50ϕ , respectively. This means that the Fib bulletin equation (4.10) is less conservative than the recommended (Model Code, 2010) equation (4.9) for mean bar stress design.



(a) Fib Bulletin 72



(b) Model Code (2010)

Figure 4.2. Comparison of maximum bar stress in test to the calculated bar stress according to Fib bulletin 72 (a) and Model Code (2010) (b).

4.3.3 Effect of effective bond length on splice strength

Similarly, the effective bond length lb^* is plotted against the ratio of measured stress to estimated stress (σ_{test}/f_{stm}). As shown in Figure 4.7, it can be observed that, for lap lengths ranging from 30 ϕ to 50 ϕ , the effectiveness of increasing the lap length decreases as the splice length increases. Increasing the lap length by 25% from 30 ϕ to 40 ϕ (570 to 760 mm) resulted in a 14% decrease in effective bond length, whereas a similar increase in lap length by 20% from 40 ϕ to 50 ϕ (760 to 950 mm) reduced the effective bond length by around 18%. Overall, the relationship between the effective bond length and lap length did not seem to be linearly proportional.

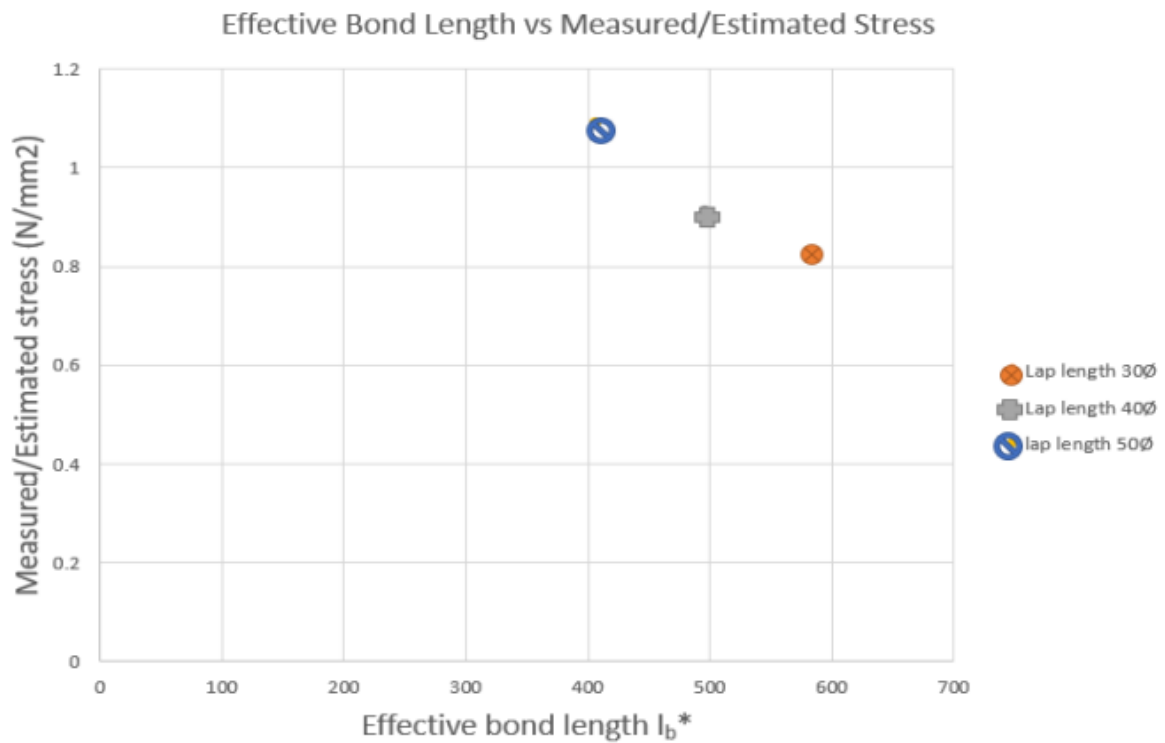


Figure 4.3. Effective bond length against splice strength.

4.3.4 Effect of bar spacing on splice strength

The dimensions of the concrete cover play a critical role in determining the failure mode of splitting. Small side covers C_x and small bar spacing (C_s) contribute to side-splitting, while small bottom cover C_y causes face splitting. As bar spacing affects load transfer between bars, it is accounted for by $C_s/2$. Thus, several design models (Fib bulletin 72, 2014; Model Code, 2010, and EN 1990, 2004) consider a minimum $C_{min} = \min \{c_y; c_x; c_s/2\}$. The concrete cover and the lap length to bar diameter are classified according to Table A6 in the appendix.

Figure 4.8 illustrates the impact of bar spacing on the maximum bar stress for the filtered database test with transverse reinforcement. Increasing the splice length from 210 mm to 570 mm resulted in a 24% decrease in lap stress. In addition, for the same 58Ø lap length, reducing the bar spacing from 29 mm to 14 mm resulted in a 10% decrease in lap stress. Similarly, for a lap length of 30Ø, increasing the bar spacing from 81.8 mm to 84 mm led to an 8% increase in lap stress.

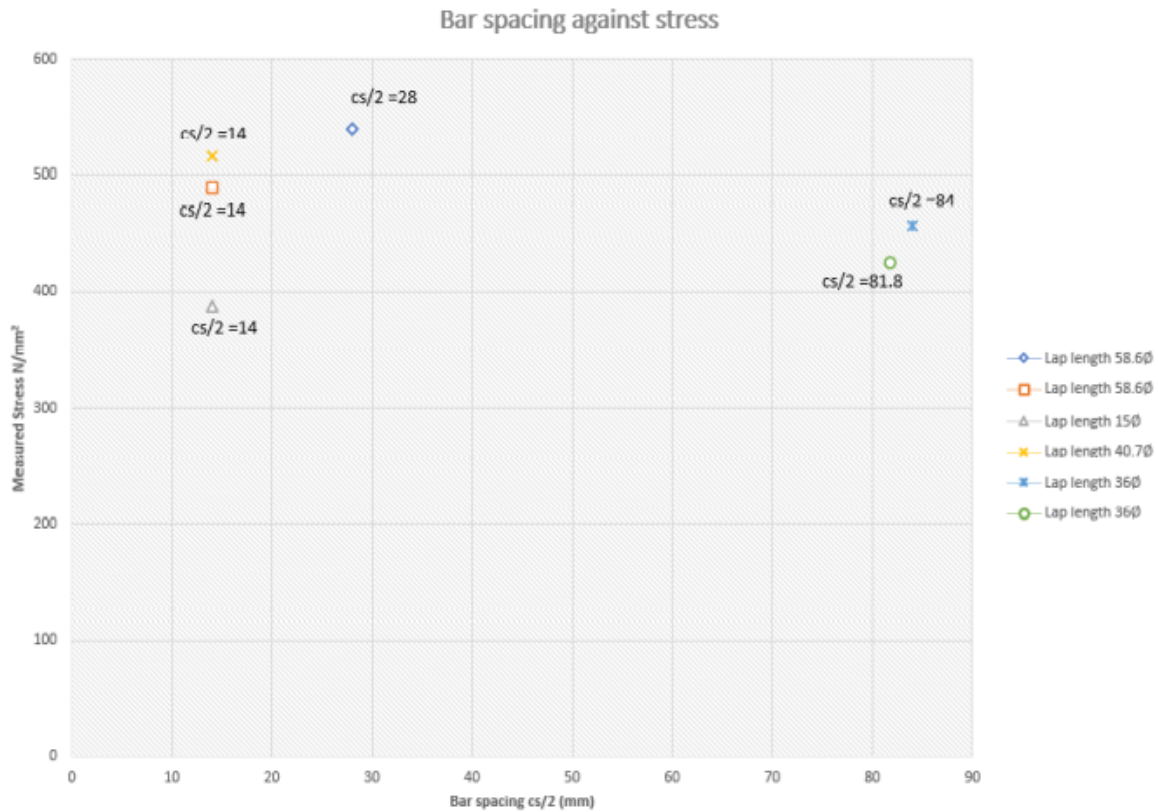
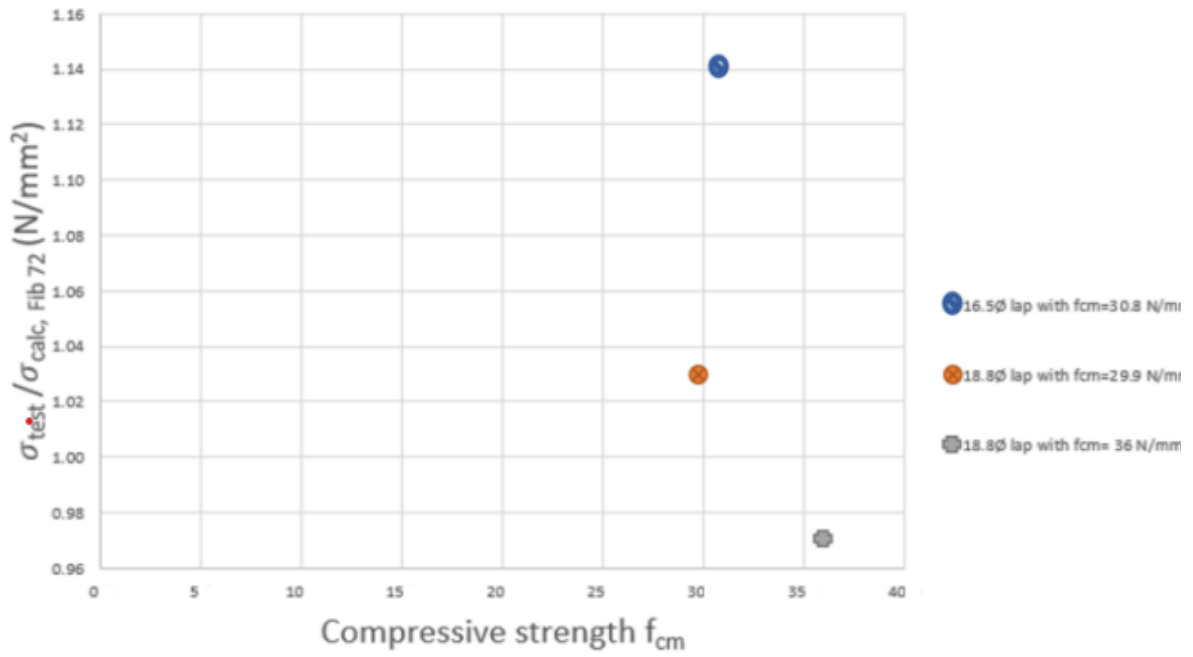


Figure 4.4. Effect bar spacing on the splice strength.

4.3.5 Effect of concrete strength on lap splice strength

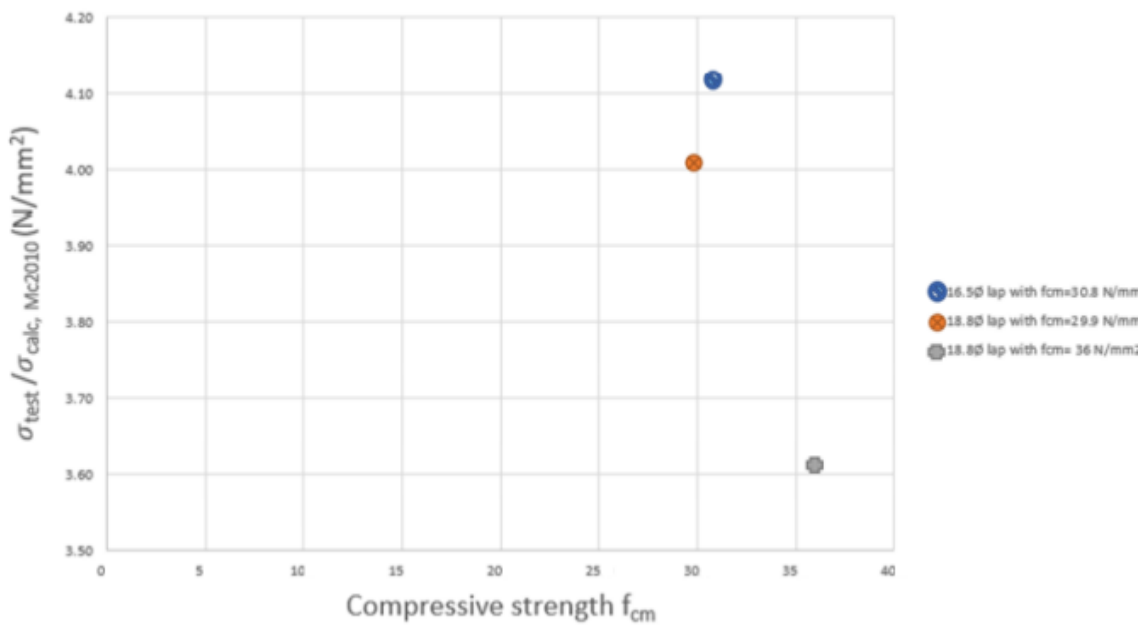
When examining the influence of concrete strength on lap strength, the ratio of lap length to bar diameter as well as the concrete cover must be considered as influential factors (Micallef and Vollum, 2018). Figure 4.9 shows a plot of compressive strength against the ratio of maximum mean bar stress over the lap length measured in the test (σ_{test}) to the estimated mean lap stress according to equation (4.10) of Fib bulletin 72 (2014) (Figure 4.9a) and equation (4.9) of Model Code (2010) (Figure 4.9b). The estimated bar stress calculated according to Fib bulletin 72 (2014) in the splice region with increasing concrete strength is much higher than the values estimated according to Model Code (2010). For the same concrete cover, confinement, and lap-length to bar-diameter ratio, better performance with a decrease in concrete strength is observed. It appears that a small reduction in the splice strength, relative to the predicted strength, occurs when the concrete strength is decreased from 36 to 29.9 N/mm² (Figure 4.9a). However, reducing the lap splice by 13% (from 18.8φ to 16.5φ) and decreasing the concrete strength from 36 to 30.8 N/mm² resulted in a 5% decrease in the measured lap stress.

Compressive strength vs measured/estimated strength



(a) Fib Bulletin 72

Compressive strength vs measured/estimated strength



(b) Model Code (2010)

Figure 4.5. Influence of compressive strength on the splice strength (a) Fib Bulletin 72 and (b) Model Code 2010.

4.3.6 Effect of stirrup confinement on lap splices strength

It is widely recognized that providing sufficient stirrups can not only modify the failure mode and bond-slip relationship but also delay the onset of splitting cracks (ACI Committee 408, 2003; Tepfers, 1973). In this section, we investigate the impact of stirrup confinement on lap splice strength by comparing three specimens with different levels of stirrup confinement. The direct comparison highlights the beneficial effect of stirrup confinement.

Figure 4.10 shows the ratio of measured to predicted strength plotted against the confining effect K_{tr} . As can be seen, an increase in the number of stirrups can significantly enhance lap splice strength. Specimens with more confinement in their lap splices outperformed those with less confinement. For a shorter lap length of 18.8ϕ , increasing the confinement level by 44% resulted in a 28% increase in splice stress length, compared to a longer lap length of 26.3ϕ . For the same splice length of 28.4ϕ , increasing the number of shear links from 5 to 8 resulted in a 4% increase in lap stress. Overall, the effectiveness of lap splices increases with the level of confinement. However, increasing the number of shear links to improve splice strength is not a sustainable and economical solution as it requires more steel.

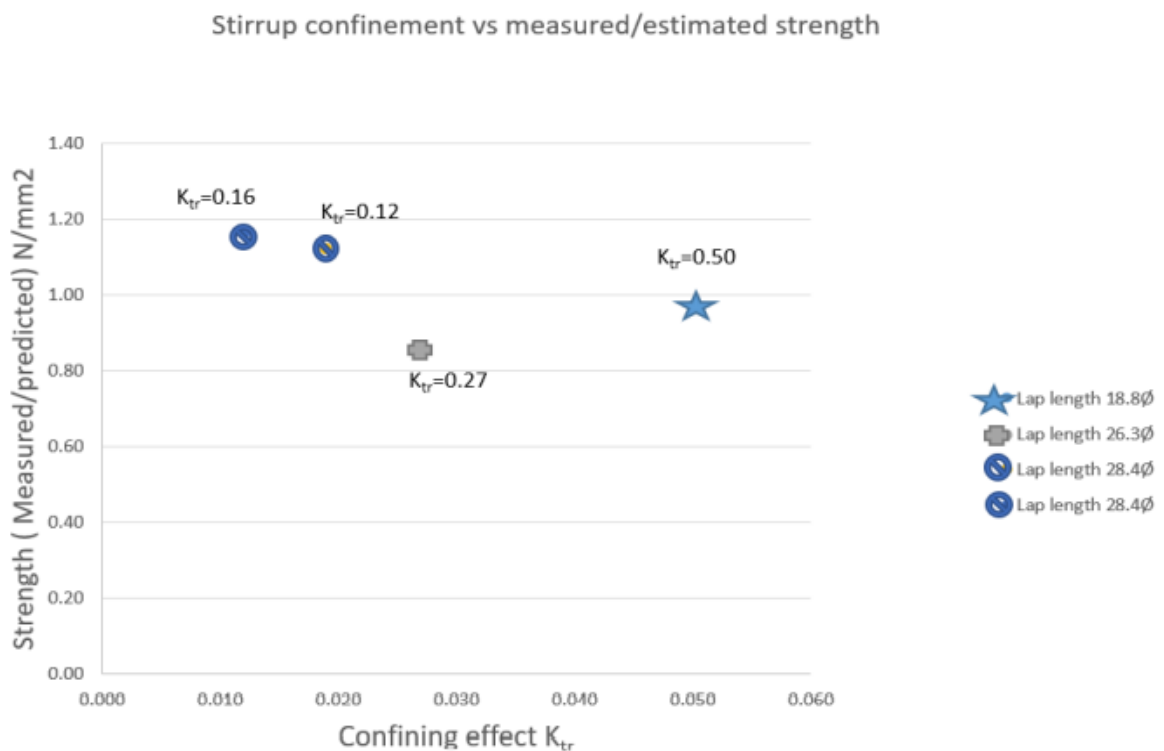


Figure 4.6. Influence stirrup confinement on the splice strength.

4.3.7 Effect of side cover on lap splice strength

Figure 4.11 shows the effect of side cover on the performance of lap splice in a reinforced concrete beam. Increasing the side cover from 1ϕ to 3ϕ (26 mm to 78 mm) for the same splice length of 60ϕ resulted in a 15% increase in lap stress. Similarly, for a splice length of 18ϕ , increasing the concrete cover from 2ϕ to 2.5ϕ led to a 13% increase in lap stress. Moreover, for a fixed side cover of 1ϕ , increasing the lap to bar diameter ratio from 60ϕ to 73.1ϕ resulted in a 3% increase in lap stress. However, when the splice length and concrete cover were increased by 20% and 44%, respectively, a 3% increase in lap stress was observed.

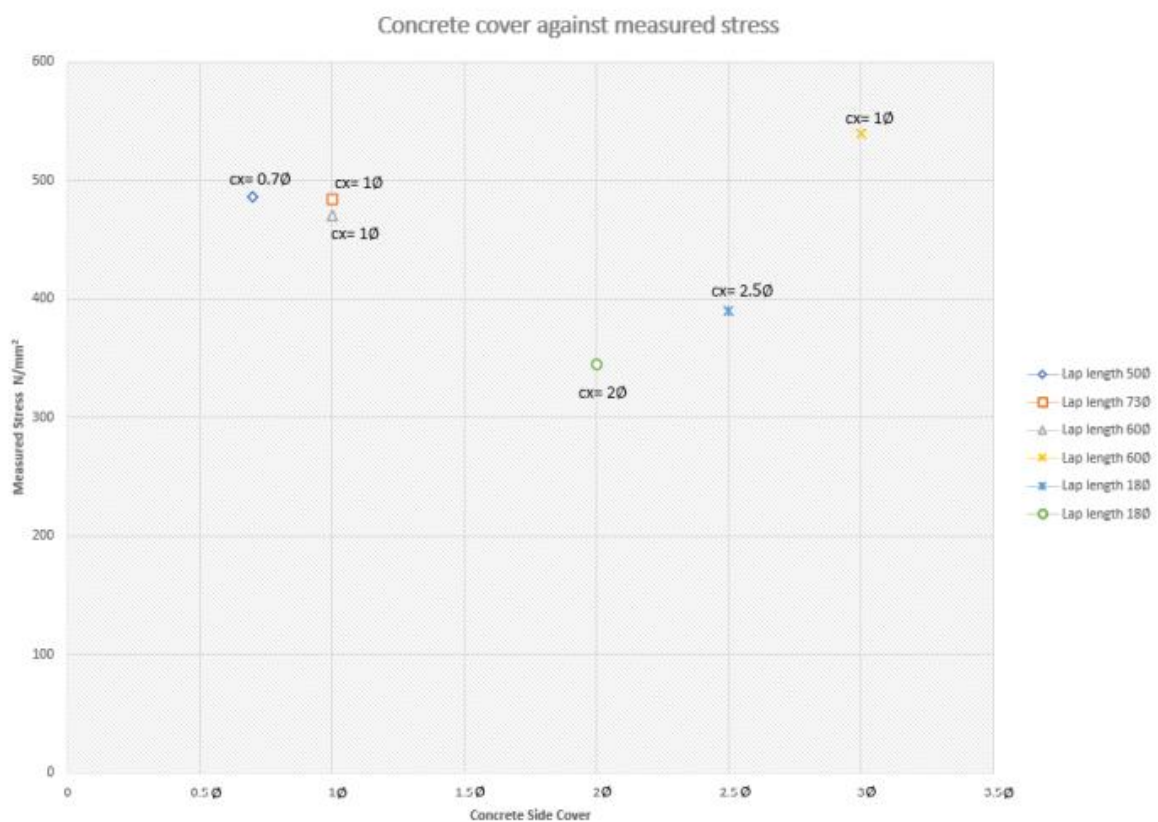


Figure 4.7. Effect of side cover on splice strength.

4.4 Concluding remark

This chapter investigates the performance of tension laps in concrete beams using a combination of experimental work and recommendations from the Model Code (2010) and Fib bulletin 72 for laps in reinforced concrete structures. The analysis examines the influence of different structural parameters such as concrete cover, lap splice length, shear

link confinement, and concrete strength on lap splices based on an extensive experimental database of laps and anchorage.

Based on the number of data analysed, the following conclusions can be drawn:

- The confinement provided by stirrups can significantly impact lap splice strength. Increasing the number of stirrups can improve splice performance, but careful consideration of the number and spacing of stirrups is necessary when designing lap splices to achieve optimal performance in a cost-effective and sustainable manner.
- The analysis shows that increasing lap splices beyond 50ϕ has no additional benefit for increasing strength. Results also indicate that specimens with larger concrete side covers show higher splice stress compared to those with smaller concrete covers relative to the measured stress.
- Beams containing lap splices with more confinement perform as well as beams in which the lap splices are lightly confined. Increasing confinement increases the effectiveness of the lap, but there is a trade-off between the steel used for longer laps and the steel used for increasing the number of shear links.
- Bond stress increases with an increase in concrete side cover and lap length-to-bar diameter ratio. For a similar lap length-to-bar diameter ratio, a 15% increase in lap stress was observed when the side cover was increased from 1ϕ to 3ϕ (26 mm to 78 mm). Similarly, at a constant side cover, increasing the lap length-to-bar diameter ratio from 60ϕ to 73.1ϕ resulted in a 3% increase in lap stress.
- The Fib bulletin equation (10) for estimating mean bar stress in laps is less conservative than the equation (9) recommended by Model Code (2010).

Overall, the analysis provides insight into the behavior of lap splices in reinforced concrete structures and highlights key factors that can influence lap splice performance. These findings can inform the design of lap splices for optimal performance while minimizing material usage and cost.

5. Development and validation of the finite element model

5.1 Introduction

In the field of engineering, the development and validation of numerical models play a crucial role in advancing and understanding of complex systems. The process of developing and validating a finite element model involves creating a virtual representation of the system under study, applying appropriate mathematical formulations, and verifying its accuracy against experimental data. This chapter aims to present the development and validation of a finite element model.

5.2 Validation of experimental results

Table 10 presents the validation of the 3D finite element model, which was carried out using three stainless steel beams and five reinforced concrete beams with mild steel reinforcing bars from experimental programs. All of the beams, except the control beams, were spliced at the maximum moment region. The spliced lengths considered for both the experiment and the FE model were 30ϕ , 40ϕ , 50ϕ , and 62ϕ lap. Figure 5.4 shows the details of the reinforcement and geometry of these beams.

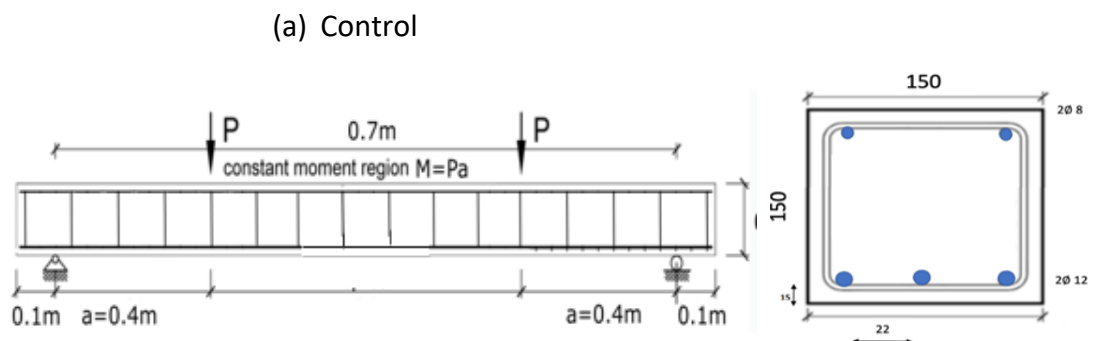


Figure 5.1. Details reinforcement and geometry used in validating the study.

All of the beams were subjected to monotonic loading in four-point bending using displacement control until failure. The reinforcement properties and material properties of concrete for each beam are presented in Table 5.1. The tensile strength and elastic modulus of the specimens were determined through tensile testing. The safety factor (α_6) for the percentage bar lapped was not considered for all samples, except for the beam with lap length, which was calculated based on the Eurocode 2 design guide for lap design.

Table 5.1. Material properties of reinforced concrete beams.

Beam	Concrete		Reinforcement				
	Young's modulus E (N/mm ²)	Compressive strength f_{ck} (N/mm ²)	Diameter (d) (mm)	Material	Yield stress s_y (N/mm ²)	Tensile strength (R_m) (N/mm ²)	Young's modulus
Control	200	32	12	Carbon Steel	559.91	664.05	21E3
30Ø lap	200	32	12	Carbon steel	559.91	664.05	21E3
40Ø lap	200	32	12	Carbon steel	559.91	664.05	21E3
50Ø lap	200	32	12	Carbon steel	559.91	664.05	21E3
EC2	200	32	12	Carbon steel	559.91	664.05	31E3
Control	177	32	12	Stainless steel	680.50	876.12	174970
30Ø lap	177	32	12	Stainless steel	680.50	876.12	174970

5.3 Mesh analysis

To obtain accurate results in numerical modelling, it is essential to use a fine mesh.

However, a fine mesh increases computational costs. Thus, it is important to choose a mesh size that provides accurate results while minimizing computational resources. Therefore, a sensitivity analysis of the mesh size was conducted by comparing the numerical model's load-displacement curves to the experimental results.

Figures 5.5 show the load-displacement curves computed numerically for EC2 lap (62Ø) beams using three different mesh sizes (30 mm, 35 mm, and 40 mm) in comparison to their corresponding experimental results. Overall, the load-displacement response produced with these various meshes agrees well with the experimental results. However, in the early stages, the coarse mesh produces a relatively stiffer response than the other two meshes (30- and 35-mm meshes). It has been observed that a mesh size of 35 mm provides accurate predictions that are comparable to those obtained using a 30-mm mesh, hence 35 mm elements were selected to minimize computational costs. There is no significant difference in terms of initial stiffness, ultimate load, and cracking load between the responses obtained using the three mesh sizes.

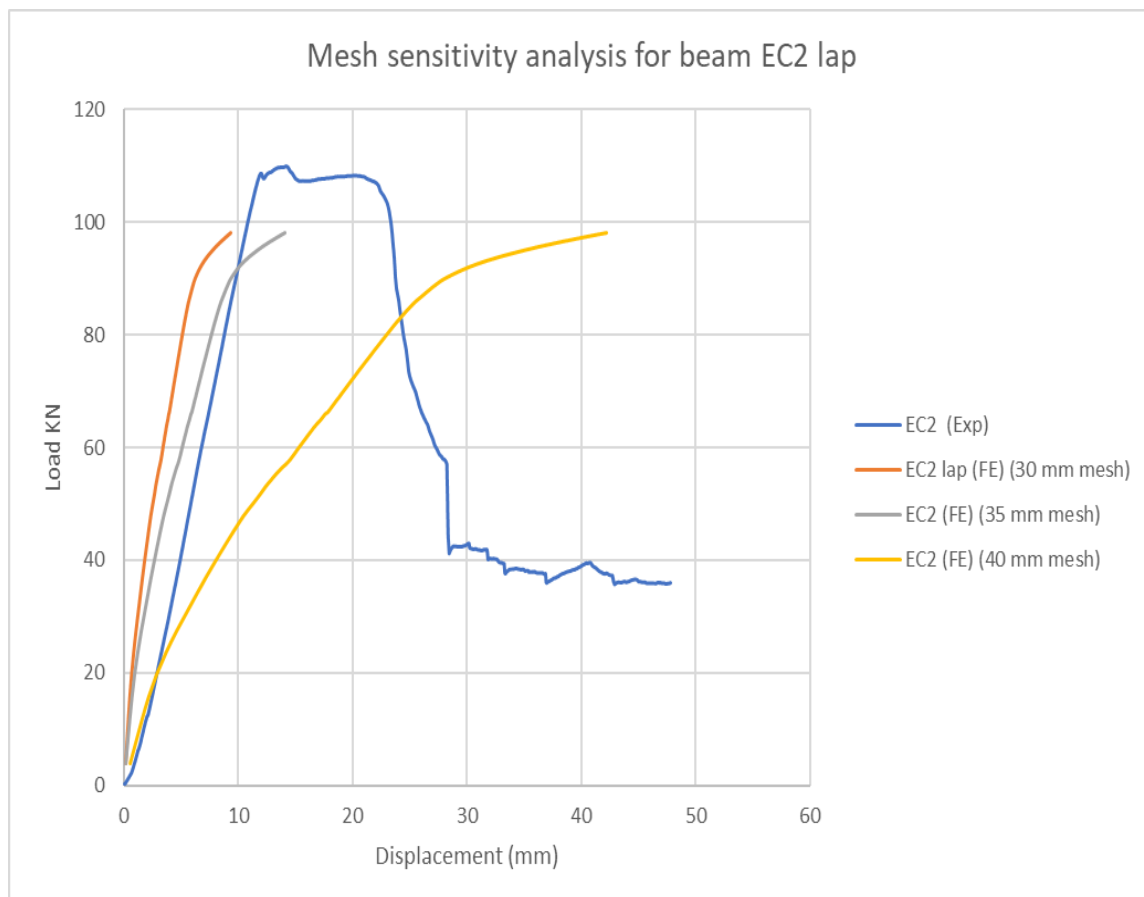


Figure 5.2. Mesh sensitivity analysis for EC2 beam with lap.

5.4 Beam failure

The ultimate failure of a conventionally reinforced concrete (RC) beam is typically considered to occur when the outer fibre of the concrete in compression exceeds the ultimate crushing strain, usually assumed to be 0.003 or 0.0035, in numerical analysis. Since

the strain in the concrete at the top surface is reached after the yielding of the reinforcement and the steel no longer contributes to the section's ultimate bearing capacity, this is more likely to happen when the reinforcement material has elastic-perfectly plastic stress-strain properties, as is the case for mild steel. However, due to the significant levels of ductility and strain hardening in stainless steel, as well as the absence of a well-defined yield point, the behavior is different when the reinforcement is made of stainless steel.

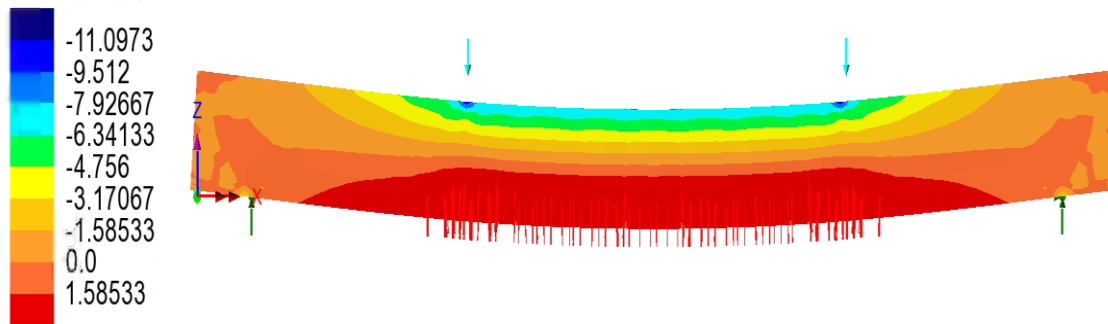
The reinforcement of stainless steel continues to contribute to the section's ultimate bearing capacity, even after the concrete reaches the crushing strain at the top surface. Moreover, it is challenging to precisely predict when the concrete will crush, so an assumption must be made about the point at which the concrete will fail. To avoid this uncertainty, the peak capacity of the section is taken at the ultimate load capacity of the section in this research, as is typically measured experimentally.

As shown in Figures 5.6 to 5.10, the experimental and analytical failures for all the beams were in good agreement. Failure for all the samples with lap splices occurred at the lap end. Although the finite element model slightly overestimates the beam's capacity, the comparison is still acceptable.



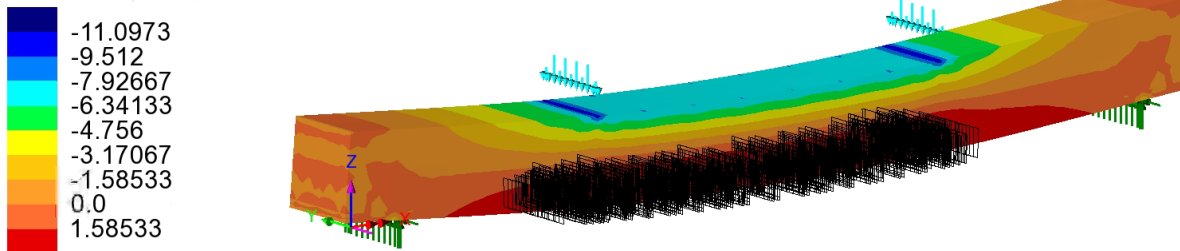
(a) Experimental mild steel sample control

Analysis: Analysis 1
 Loadcase: 1:Loadcase 1, 6:Increment 6 Load Factor = 0.240000
 Results file: CNT_2~Analysis 1.mys
 Entity: Stress - Solids
 Component: SX (Units: N/mm²)



Maximum 3.14856 at node 3078
 Minimum -11.1194 at node 7185

Analysis: Analysis 1
 Loadcase: 1:Loadcase 1, 6:Increment 6 Load Factor = 0.240000
 Results file: CNT_2~Analysis 1.mys
 Entity: Stress - Solids
 Component: SX (Units: N/mm²)



Maximum 3.14856 at node 3078
 Minimum -11.1194 at node 7185

(b) Finite element mild steel model control

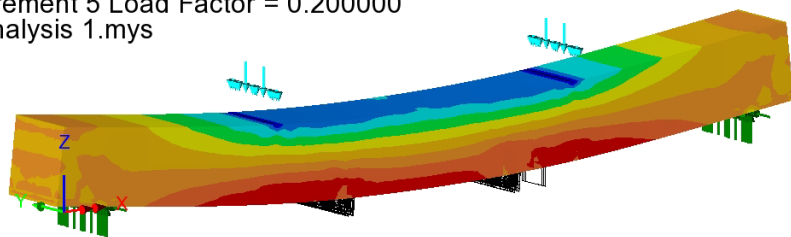
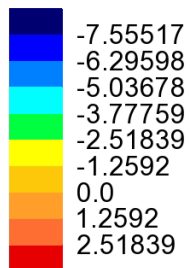
Figure 5.3. Experimental and analytical failure for control sample (a) and (b).



Lap ends

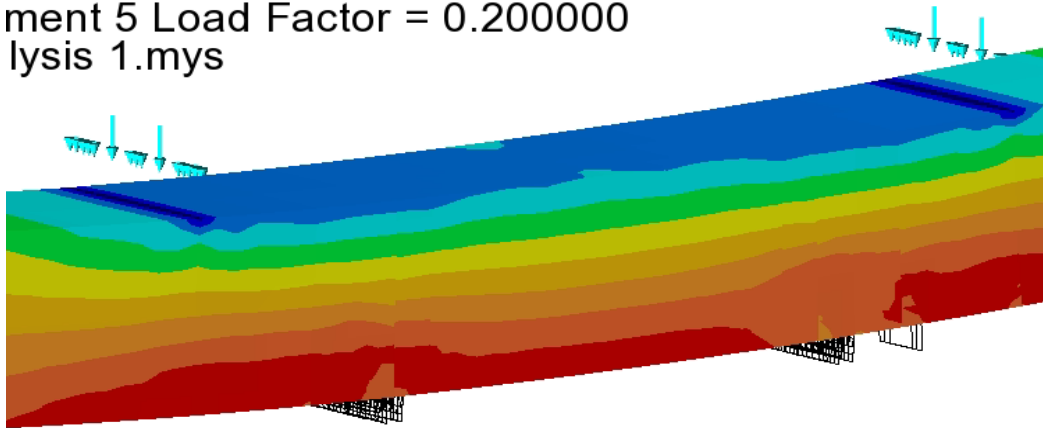
(a) Experimental mild steel sample 30Ø

Analysis: Analysis 1
 Loadcase: 1:Loadcase 1, 5:Increment 5 Load Factor = 0.200000
 Results file: 30_diameter_lap~Analysis 1.mys
 Entity: Stress - Solids
 Component: SX (Units: N/mm²)



Maximum 3.03959 at node 2548
 Minimum -8.29316 at node 8352

ment 5 Load Factor = 0.200000
lysis 1.mys



(b) Finite element mild steel model 30Ø

Figure 5.4. Experimental and analytical failure for 30Ø lap sample (a) and (b).





Lap ends

(a) Experimental mild steel sample 40Ø

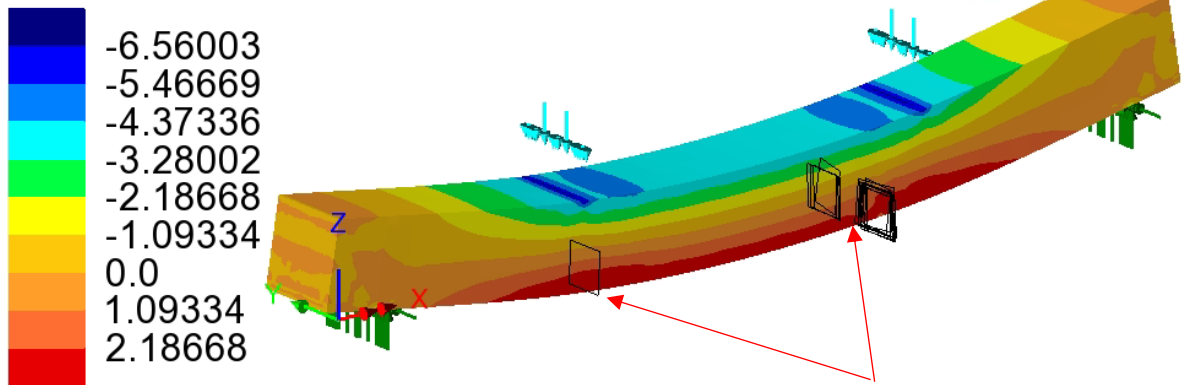
Analysis: Analysis 1

Loadcase: 1:Loadcase 1, 4:Increment 4 Load Factor = 0.160000

Results file: 40_dia_lap~Analysis 1.mys

Entity: Stress - Solids

Component: SX (Units: N/mm²)



Lap end cracks

Maximum 3.07249 at node 2180

Minimum -6.76756 at node 8680

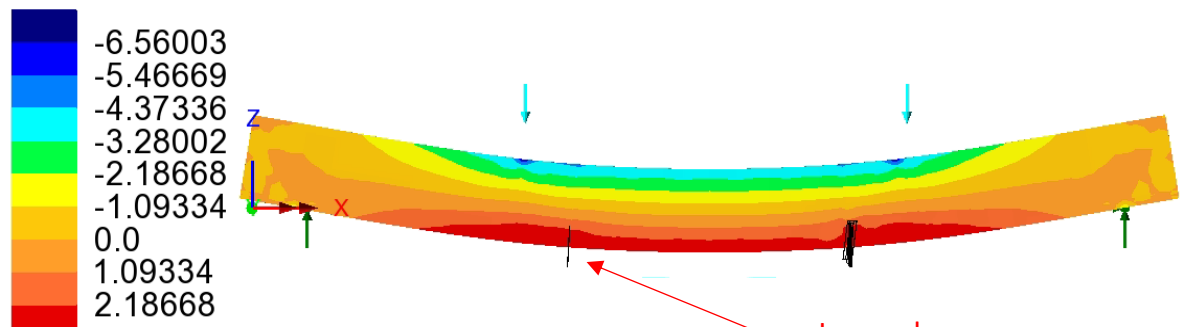
Analysis: Analysis 1

Loadcase: 1:Loadcase 1, 4:Increment 4 Load Factor = 0.160000

Results file: 40_dia_lap~Analysis 1.mys

Entity: Stress - Solids

Component: SX (Units: N/mm²)



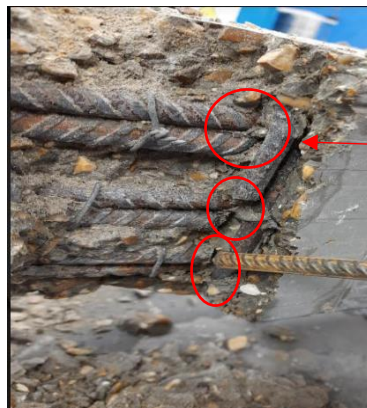
Lap end

Maximum 3.07249 at node 2180

Minimum -6.76756 at node 8680

(b) Finite element mild steel model 40Ø

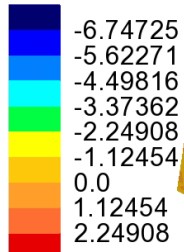
Figure 5.5. Experimental and analytical failure for 40Ø lap sample (a) and (b).



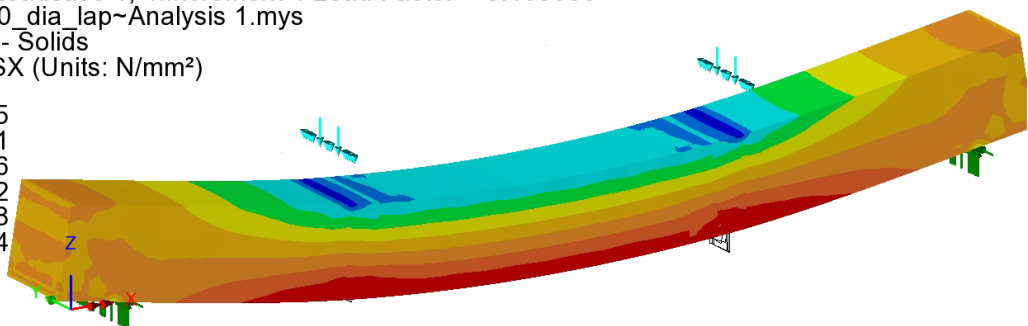
Lap ends

(a) Experimental mild steel sample 50Ø

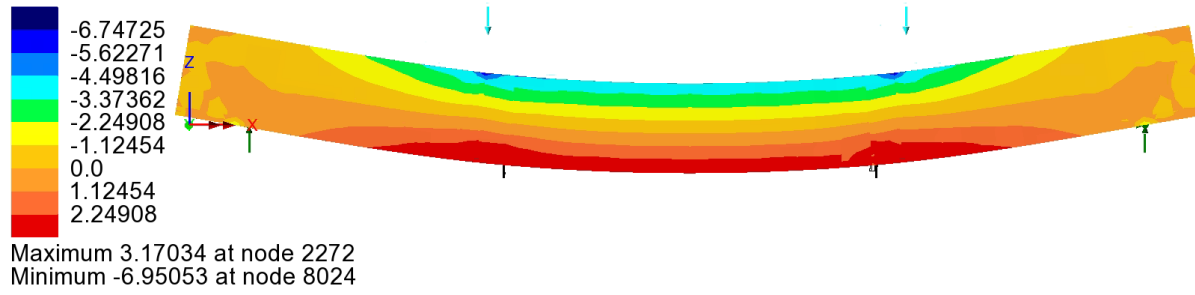
Analysis: Analysis 1
Loadcase: 1:Loadcase 1, 4:Increment 4 Load Factor = 0.160000
Results file: 50_dia_lap~Analysis 1.mys
Entity: Stress - Solids
Component: SX (Units: N/mm²)



Maximum 3.17034 at node 2272
Minimum -6.95053 at node 8024



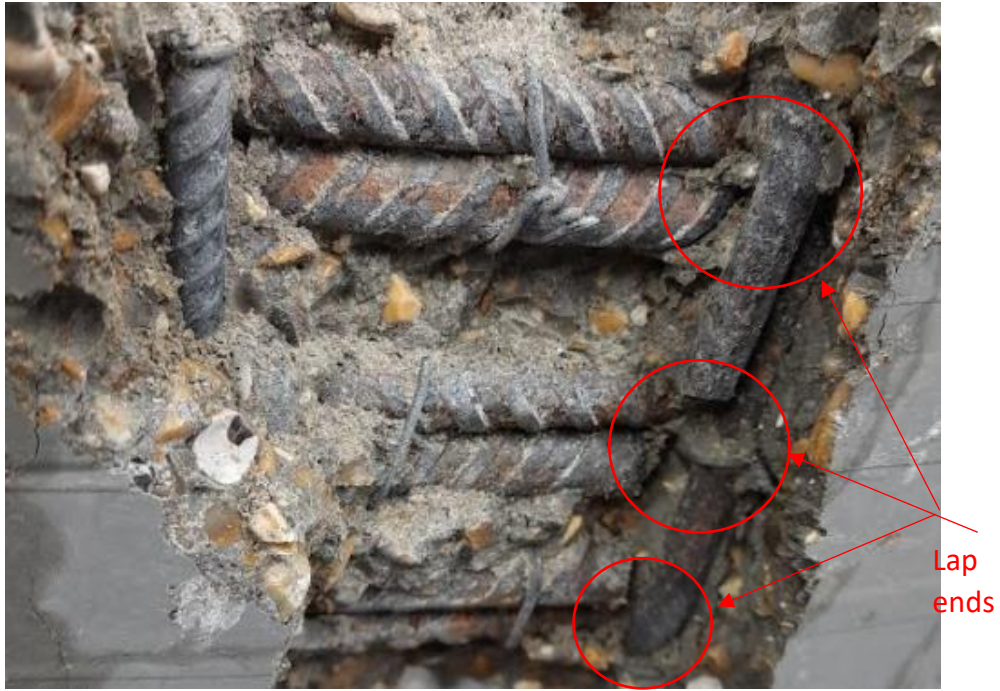
Analysis: Analysis 1
Loadcase: 1:Loadcase 1, 4:Increment 4 Load Factor = 0.160000
Results file: 50_dia_lap~Analysis 1.mys
Entity: Stress - Solids
Component: SX (Units: N/mm²)



(b) Finite element mild steel model 50Ø

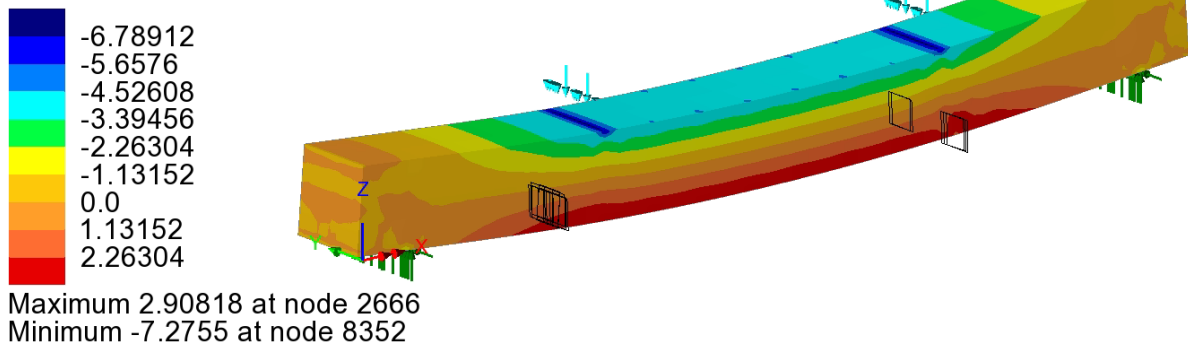
Figure 5.6. Experimental and analytical failure for 50Ø lap sample (a) and (b).



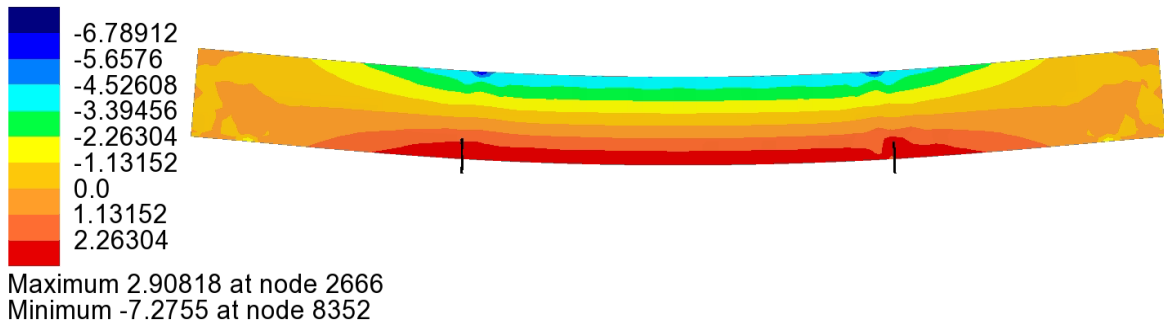


(a) Experimental sample EC2

Analysis: Analysis 1
 Loadcase: 1:Loadcase 1, 4:Increment 4 Load Factor = 0.160000
 Results file: EC2_lap~Analysis 1.mys
 Entity: Stress - Solids
 Component: SX (Units: N/mm²)



Analysis: Analysis 1
 Loadcase: 1:Loadcase 1, 4:Increment 4 Load Factor = 0.160000
 Results file: EC2_lap~Analysis 1.mys
 Entity: Stress - Solids
 Component: SX (Units: N/mm²)



(b) Finite element model EC2

Figure 5.7. Experimental and analytical failure for EC2 calculated lap (62 Φ) sample (a) and (b).

5.5 Finite element model validation

It was necessary to conduct a comparative study using numerical results and experimental data to validate the finite element package and establish that the selected mesh configurations would converge to an acceptable solution. While previous researchers have shown the validity of the finite element package for nonlinear analysis, it is preferable to validate any complex analytical model for nonlinear problems using experimental results to ensure its validity and accuracy. In this section, reinforced concrete beams with mild steel and stainless-steel reinforcements were compared with the corresponding experimental results. The beams were tested in the concrete lab at the University of West London for this study, providing full confidence in using the package and model for parametric studies in subsequent chapters.

5.5.1 Load displacement

In the load displacement analysis, the load-deflection curves (Figure 70) describe the global response of the tested beams, taking into account the effect of the steel beam (0.98KN) placed on the specimen and the equivalent bending moment due to the self-weight of the tested reinforced concrete beam. During the transition from the uncracked to the cracked stage, gradual nonlinear behaviour was observed. Several vertical cracks developed within the constant moment zone, followed by shear cracks near the support (as shown in Figures 5.6 to 5.10). Figures 5.11 and 5.12 compare the load-deflection curves for beams from the series with different lap-splice configurations (but the same materials and rebar diameter). Beams with lapped bars exhibited varying degrees of ductility with the development of longitudinal splitting cracks along the lap splices, whereas the control beams with all continuous bars failed in a ductile manner with vertical flexural cracking due to rebar yielding. Two types of splice splitting failures were observed: face splitting failure with cracks developing vertically below the lapped bars and side-splitting failure with cracks developing on the beam sides of the bars.

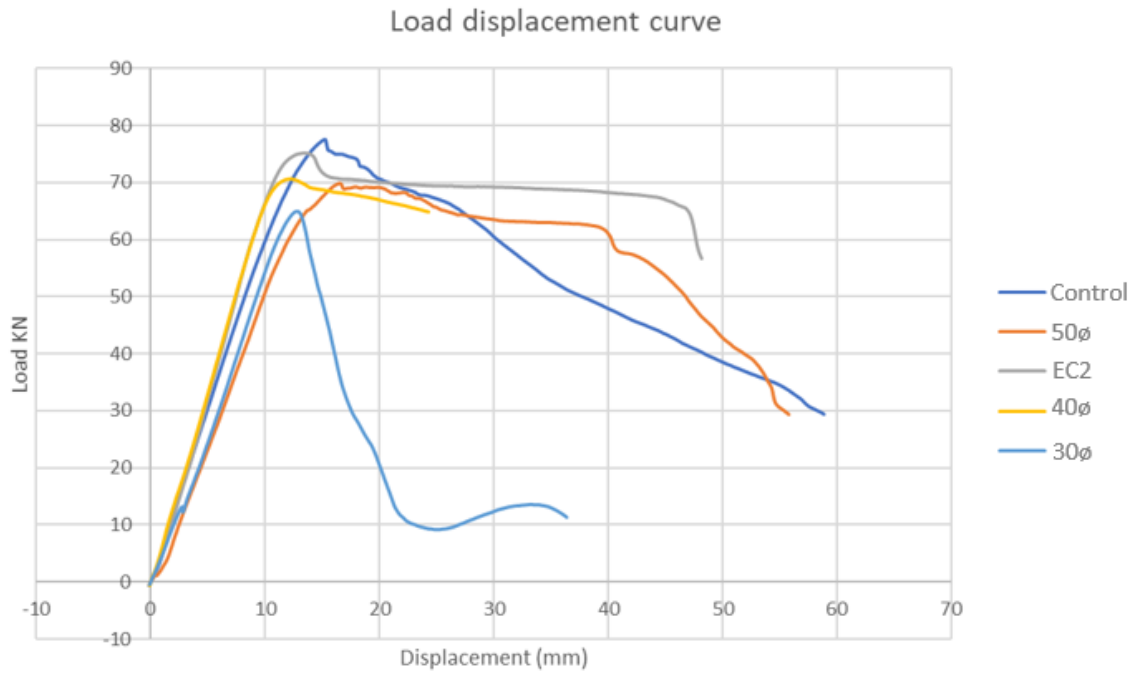


Figure 5.8. Load displacement graphs for experimental beams

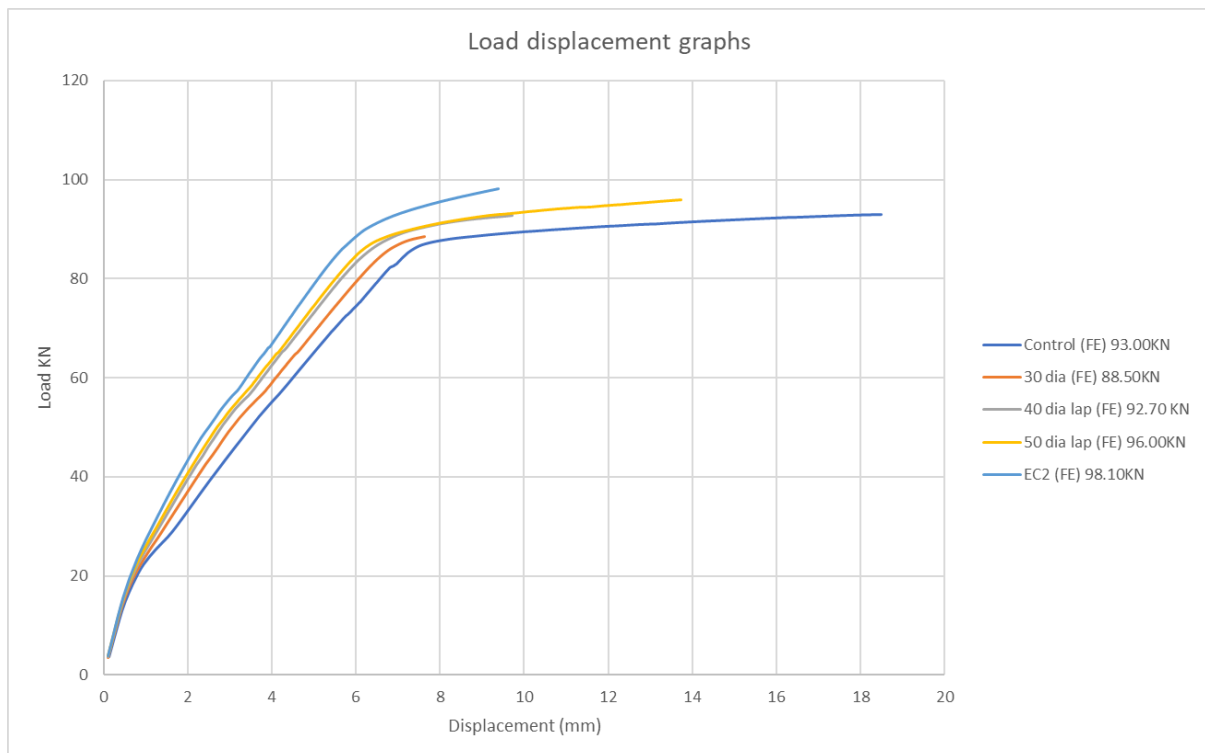


Figure 5.9. Load displacement graphs FE.

5.5.2 Crack formation

During the experiments, crack propagation in the tension face of the beams was visually observed (see Figure 5.6 to Figure 5.10). The initial cracks initiated at roughly half of the failure load. Transverse flexural cracks first formed at the applied load locations in all the control samples. The first cracks developed at the end of the lapped bars, and then transverse cracking was followed by the formation of a longitudinal crack along the lap edge. As the load was increased to failure, the cracks spread along the laps in short, irregular lengths. However, it is worth highlighting that, in the case of beam samples with longer lap lengths ($50\emptyset$ and $EC2\ 62\emptyset$), shear cracks spread toward the beam support after the lap cracks as the load is increased to failure. The existing longitudinal cracks broadened and spread over the lap length when the bond failed. It is also worth mentioning that the experimental beam failures are identical to the analytical beams that were simulated using LUSAS software. The failure mechanism in all samples with lap splice was bond failure. However, the beam with $30\emptyset$ lap failed before the yielding of steel in a brittle manner due to insufficient lap length.

5.6 Concluding remarks

Analysing a reinforced concrete beam is a challenging task. The nonlinear effects of lap splice length and bar slip at the interface must be appropriately accounted for using a correct method of analysis. The finite element model presented incorporates these effects as well as material properties. The experimental and analytical values of loads, cracks, deflection, and failure mode compared well. The model reliability gains a lot of confidence as a result of these findings. The mechanical properties of the concrete and reinforcing bar have to be experimentally determined and employed in the analysis to achieve the high correlation between the experimental and analytical results.

The models can be considered appropriate for evaluating the influence of the lap joint on the ductility of reinforced concrete beams based on the results obtained, assuming that the load is applied monotonically. Thus, the models may be confidently used to conduct research to analyse the influence of various parameters on the behavior of reinforced concrete beams.

6. A numerical and experimental study into the tension lap joints.

6.1 Introduction

In recent years, the length of reinforcement laps required by building codes has increased significantly from previous design recommendations, such as the superseded UK code BS 8110-1. This paper is motivated by the current revision of Eurocode 2, which is due to be published in 2023. The draft revision of Eurocode 2 for laps and anchorage is heavily influenced by the recommendations of Fib model code 2010 and Fib bulletin 72.

For context, the Fib model code 2010 requires a considerably longer lap length than Eurocode 2, which many UK practitioners find excessive compared to previous UK practice. Any increase in lap length is an issue for UK designers who already find that the current Eurocode 2 reinforcement detailing requirements are complicated and make the design costly and unsustainable (Micallef and Vollum, 2017). The flexural capacity of a reinforced concrete (RC) beam, with respect to the bond between reinforcement and concrete, that has been lap spliced in tension under ultimate load is a crucial issue for the safety and strength of the RC beam (Cairns, 2016). In this regard, most design codes, such as the American Concrete Institute and Eurocode 2, specify different requirements for the design of minimum required lap splice for a certain bar diameter.

In this study, the impact of lap joint length variation on the structural performance of RC beams under ultimate load is investigated using LUSAS finite element software to simulate a four-point loading test under monotonic loading until failure (see Figure 6.1). The computational study considers reinforcement bar diameter (d_b), concrete design tensile strength (f_{ctd}), concrete cover (c_d), and yield strength of the steel (f_y) as variables, conforming to Eurocode 2.

6.2 Range of parameters

To prevent shear failure in the beam, all members in this study were assumed to be simply supported beams under four-point bending (4PB), with a span of 700 mm and a shear span of 400 mm. A 3D finite element model was developed to investigate the effects of lap length, concrete grade, depth, and link spacing on the structural performance under ultimate load. The parameters considered in this study are summarized in Table 6.1, and the compressive strengths were chosen according to EN1992-1-1:2004 (2014) concrete grades.

The shear link spacing was set to the recommended value of $0.75d$ in Eurocode 2. The uniaxial tensile strength was determined as a function of the uniaxial compressive strength using the model given by Eurocode 2 (2004): $E_c = 22(0.1f_{cm})^{0.3}$. Each analysis was conducted using this approach.

Table 6.1. Parameters studies.

Parameter	Ranged studied
Lap length	30Ø, 40Ø, and 50Ø, EC2 (62Ø)
Span/depth ratio	6.8 mm and 11.3 mm
Distance between points loads	500 mm and 700 mm
Concrete grade	C30, C45, and C60
Shear link spacing	50 mm and 100 mm

6.3 Methodology

Table 12 presents the details of the five series of beams (A, B, C, D, and E) analysed under four-point bending with laps located in the maximum moment zone, as shown in Figure 72. All RC beams had a length of 1,700 mm, a height of 150 mm, and a width of 150 mm, with a span to depth ratio of 11.3, except for series E & E, which had a zero-shear span distance of 500 mm and 300 mm, respectively, with the same span to depth ratio. As depicted in Figure 6.3(a), (b), and (c), the tension face of each sample was reinforced with three 12 mm diameter bars, lapped with bars of the same diameter. All laps were located in the same section, as permitted by MC2010 and (BS EN 1992-1-1, 2004), but not staggered as recommended by Eurocode 2. Three different concrete grades (C30, C45, and C60) were used for all series. Nominal 8 mm diameter shear links were provided at 100 mm spacing for all series except D, where 50 mm link spacing was used. The transverse requirements of Eurocode 2 were met for all series. The distance between the two-point loads was fixed at 700 mm for all series, except for series E, where it was reduced to 500 mm to accommodate the laps within the loading points.

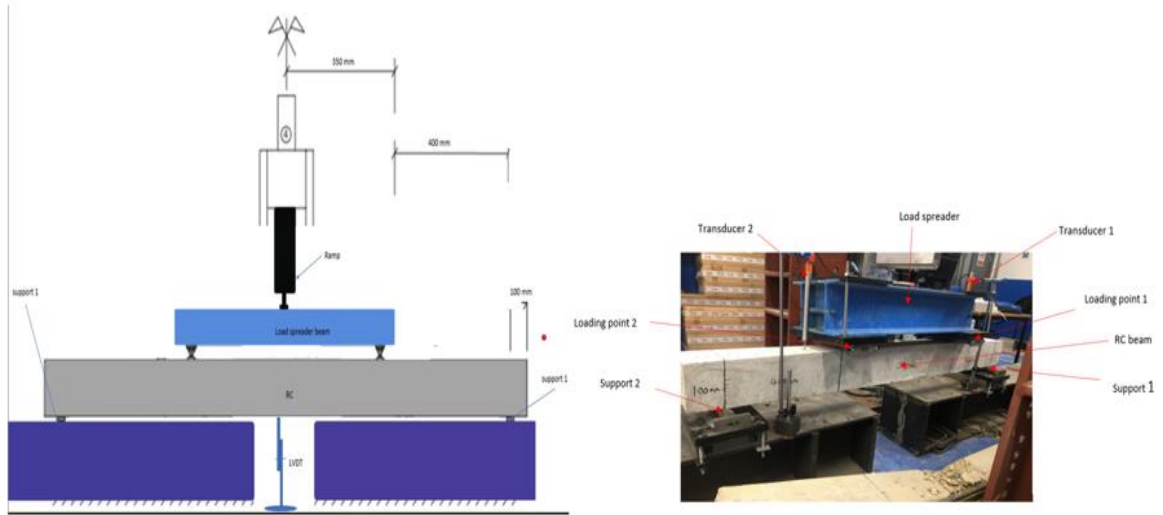


Figure 6.1. Typical laboratory four-point loading arrangement.

Table 6.2. Samples specifications

Series	Test ID	Bar diameter (mm)	Lap length (mm)	Concrete grade	Link spacing (mm)	Depth (mm)	Distance between point loads (mm)	Span/depth ratio
A	4P-Control	12	n/a	C30	100	150	700	11.3
	4P- 30Ø	12	360	C30	100	150	700	11.3
	4P- 40Ø	12	480	C30	100	150	700	11.3
	4P- 50Ø	12	600	C30	100	150	700	11.3
	4P-EC2 (62Ø)	12	744	C30	100	150	700	11.3
B	4P- 30Ø	12	360	C45	100	150	700	11.3
	4P- 40Ø	12	480	C45	100	150	700	11.3
	4P- 50Ø	12	600	C45	100	150	700	11.3
	4P-EC2 (62Ø)	12	744	C45	100	150	700	11.3
C	4P- 30Ø	12	360	C60	100	150	700	11.3
	4P- 40Ø	12	480	C60	100	150	700	11.3
	4P- 50Ø	12	600	C60	100	150	700	11.3
D	4P- 30Ø	12	360	C30	50	150	700	11.3
	4P- 40Ø	12	480	C30	50	150	700	11.3
	4P- 50Ø	12	600	C30	50	150	700	11.3
	4P-EC2 (62Ø)	12	744	C30	50	150	700	11.3
E	4P- 30Ø	12	600	C30	100	150	500	11.3
	4P-40Ø	12	480	C30	100	150	500	11.3
	4P-50Ø	12	600	C30	100	150	500	11.3
	4P-EC2 (62Ø)	12	600	C30	100	150	500	11.3
F	4P- 30Ø	12	300	C30	100	150	900	11.3
	4P- 40Ø	12	480	C30	100	150	900	11.3
	4P- 50Ø	12	600	C30	100	150	900	11.3
	4P-EC2 (62Ø)	12	744	C30	100	150	900	11.3

6.4 Experimental Program

The effect of rebar laps on the ductility of the lapped section was investigated through eighteen four-point bending tests with lapped bars. The reinforcing bars were lapped in the constant bending moment region of four-point flexural testing to study lapped splices, and deformations were measured using linear variable displacement transducers for all specimens.

The experimental beam specimens in this study were simply supported and subjected to four-point loading, with a beam shear span of 700 mm and a span of 1,500 mm centre-to-centre of support. The beams were incrementally loaded until failure was attained and were designed in accordance with Eurocode 2. The compression reinforcement comprised of 2 ϕ 8 mm bars, and the tension reinforcement consisted of 3 ϕ 12mm bars. The beams had a shear link of 8 @100 mm.

All the test specimens were made of concrete mixed in the University of West London's concrete laboratory, using the same concrete mix design for all samples (Figure 6.2). The concrete mix had a target mean compressive strength of 30 Nmm^2 and consisted of coarse aggregate (10 mm gravel), fine aggregate (sharp sand), and cement (blue circle general purpose) in the proportions of aggregate/cement ratio 4.2, coarse/fine sand ratio 1, and water/cement ratio 0.45, as shown in Table 6.3. The lapped longitudinal reinforcement was positioned at the bottom of the formwork in the lap test specimens to ensure good bond properties.

Overall, the study findings will provide valuable insights into the behavior of rebar laps in RC beams and contribute to enhancing the design of structures.



(a) Mixer

(b) Dry mix

Fresh concrete

Figure 6.2. Details of concrete materials and casting.

Table 6.3. Concrete Mixture.

Water/ cement ratio (W/C)	Total Aggregates (Kg)	Water % of Mix	Water quantity (L)	Cement % of Mix	Cement quantity (Kg)	Coarse aggregates % of Mix	Coarse aggregates (Kg)	Fine aggregates % of Mix	Fine aggregate (Kg)
0.4	106.9	7.85	8.40	19.64	21.00	49.11	52.50	27.23	23.39

6.5 Finite Element Model

The beam model was created to simulate a four-point bending test configuration in which the loads were applied through a two-point load in displacement control, as shown in Figures 6.3. The beams being analysed were modelled using finite element software (LUSAS version, 2018). The 3D modelling was conducted without utilizing the symmetric requirement of the constraint and the load, which may simplify the problem. This approach was chosen since the current study mainly focuses on the maximum moment region of the

beams where the reinforcing bars are lapped. Applying a symmetric boundary condition to the modelled half of the beam would deviate from the scope of this study.

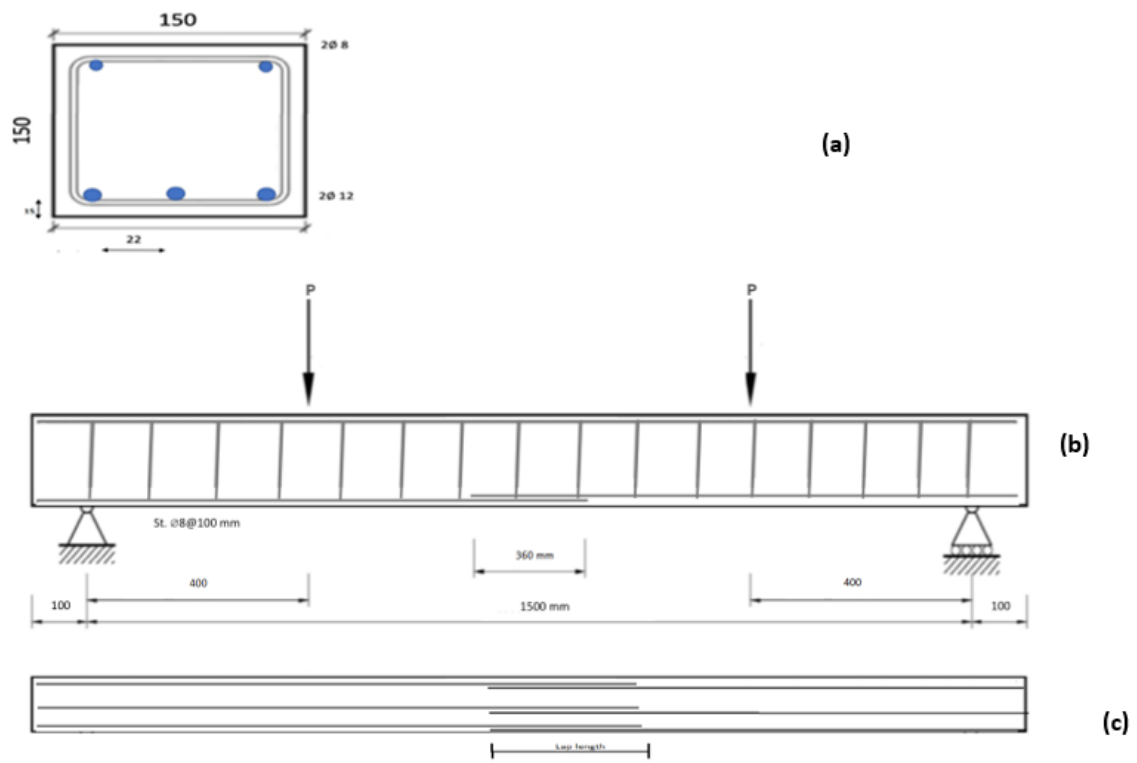


Figure 6.3. Details of beam end elevation (a), side elevation (b), and (c) reinforcement layout.

6.6 Results and Discussions

The load-deflection curves (Figure 6.4) describe the global response of the tested beams, with the load including the effect of the steel beam (0.98KN) placed on the specimen and the equivalent bending moment owing to the self-weight of the tested reinforced concrete beam. As the beams transitioned from the uncracked to the cracked stage, a gradual non-linear behavior was observed. Within the constant moment zone, several vertical cracks developed first followed by shear cracks near the support.

Figure 6.4 compares the numerical and experimental results in terms of load-midspan deflection curves of the beams. The experimental investigation showed that the control beam failed at the ultimate load of 65.1 KN, in a flexural mode with yielding of tension reinforcement, followed by crushing of concrete in the compression zone. For the finite

element model, the analysis of the control beam was stopped because the limit displacement of the control point was reached.

The proposed finite element model reproduced the experimental outcomes satisfactorily with an acceptable tolerance for the current work (3% for the ultimate load values). Usually, the numerical values of the loads at the critical stages are slightly lower than the same loads detected experimentally. This proves the reliability of the 3D model.

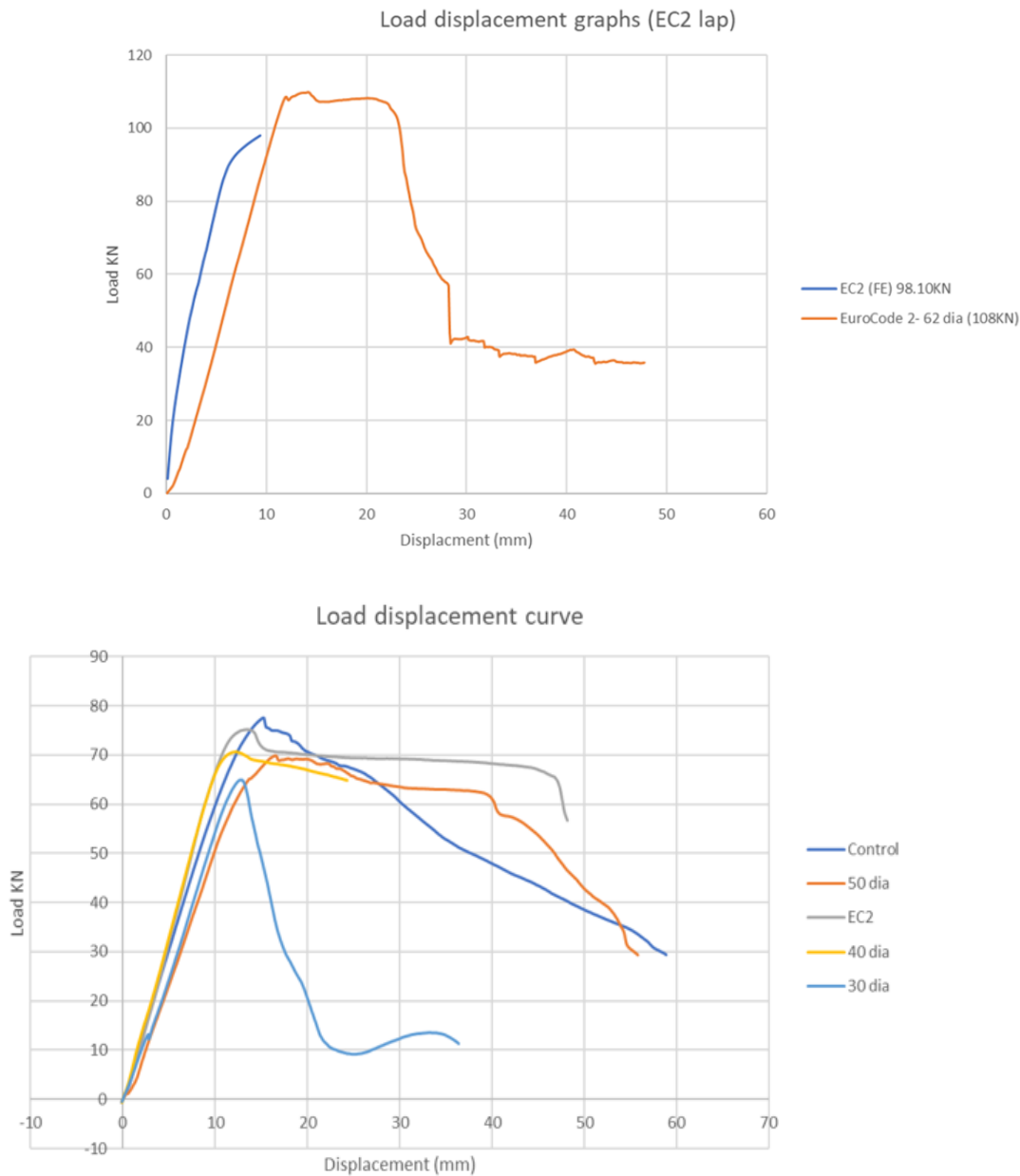


Figure 6.4. Load versus displacement response of the control beams.

6.7 Impact of lap length on bar stress

It is generally assumed that the bar stress is constant along the splice length at failure, and thus, the force is uniformly distributed along the spliced bars (BS EN 1992-1-1, 2004). Figure 6.5(a) depicts the relationship between bar stress and the lap splice length by plotting bar stress against the lap-length-to-bar diameter ratio. As shown in the figure, bar stress increases as the lap-length-to-bar diameter ratio increases, which corresponds well with other experimental studies (Anwar and Khandaker, 2008; Kim and Eom, 2019; Kim et al., 2013; Yang and Wang, 2012). This can be attributed to the fact that the bar stress is uniformly distributed over the reinforcing bar length when the lap length is longer. A 107% increase in the lap-length-to-bar diameter ratio leads to a 2% increase in bar stress.

Opposite results were found for specimens with a different concrete grade. Figure 6.5(b) shows that, when the concrete grade increased from C30 to C60, the bar stress decreased by about 0.6% for the 360 mm lap length specimens. Whereas for beams with the 480 mm lap length, the reduction in bar stress was 0.2% when the concrete grade increased from C30 to C45, and a 1.2% reduction in bar stress when the concrete grade was further increased from C30 to C60. This is because the bar stress distribution along the lap length is influenced by concrete strength, partly due to the slip of reinforcement and weaker concrete adjusting to a differential strain (CIBFIP, 1991; Lundgren, 2005).

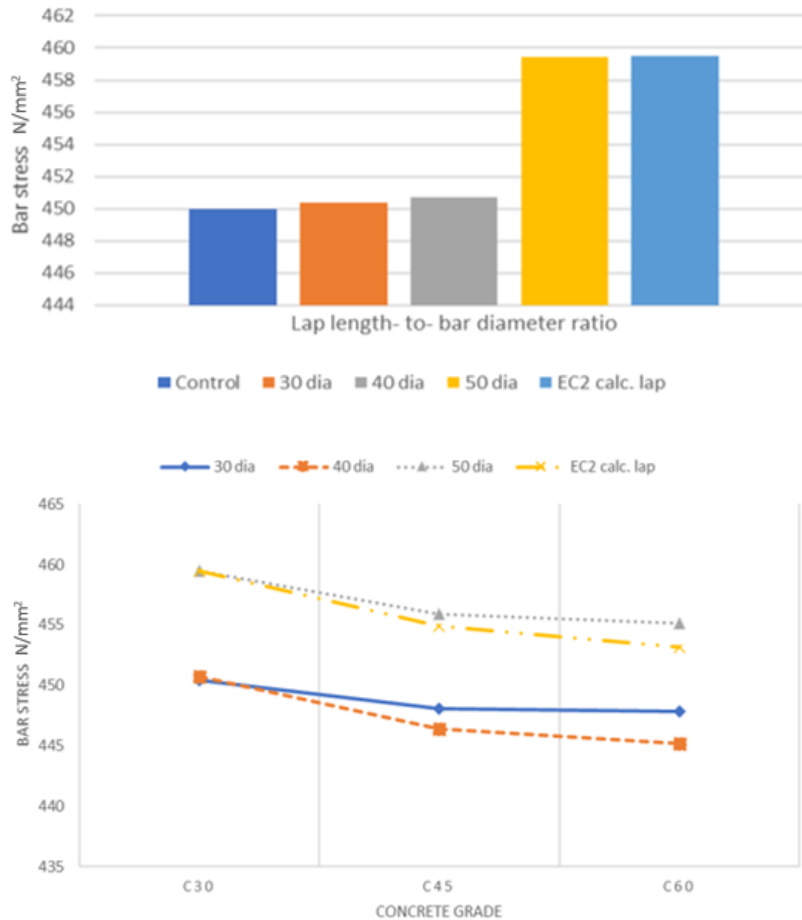
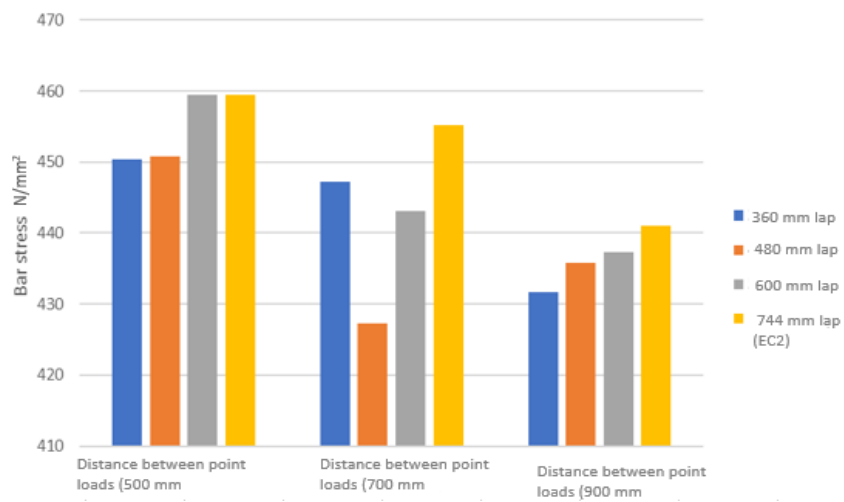


Figure 6.5. Influence of lap length-to-bar diameter ratio and concrete grade on lapped bar stress (a) and (b).

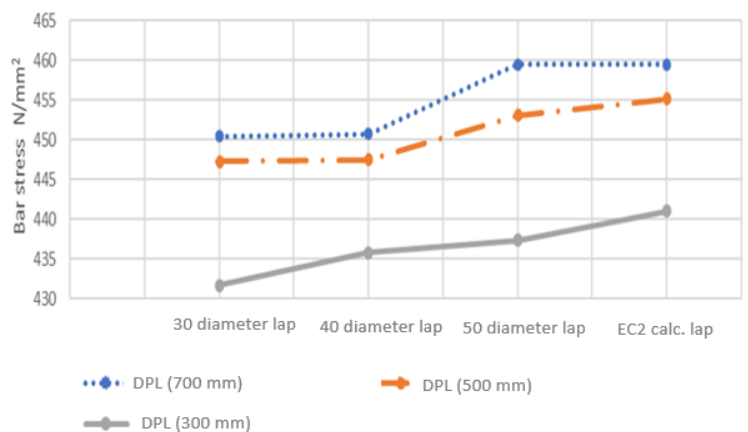
Figure 78 illustrates the impact of the zero shear span distance (the distance between two-point loads) on both the concrete grade (Figure 6.6[a]) and the lapped bar stress (Figure 6.6[b]). In particular, the figure shows that for a lap length of 360 mm, increasing the zero-shear span distance by 40% results in a 0.7% reduction in bar stress for beams made of C30 grade concrete, as demonstrated in Figure 12(a). This finding indicates an inverse relationship between the zero shear span distance and the concrete grade.

A similar trend was observed when comparing the lapped bar stress of beams with zero shear span distances of 360 mm, 480 mm, 600 mm, and 744 mm to those of beams with a zero shear span distance of 700 mm (Figure 6.6[b]). However, this trend changes when the zero shear span distance is increased to 900 mm, as shown in Figure 6.6(b). The figure illustrates that the larger the zero-shear span distance, the lower the lapped bar stress.

Overall, it is noteworthy that the bond stress of lap splices decreases with increasing zero shear distance, regardless of the concrete grade and lap length.



(a). Effect zero shear span distance on concrete grade.



(b). Effect zero shear span distance on lapped bar stress.

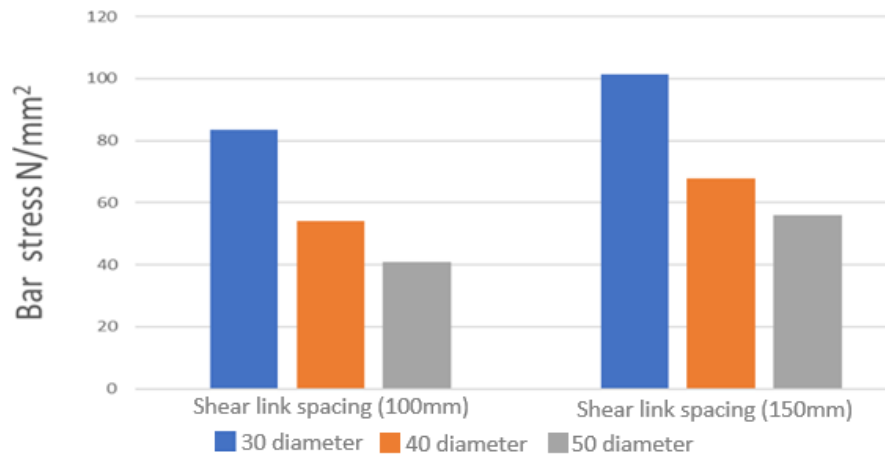
Figure 6.6. Effect of zero shear span distance on concrete and bar stress.

6.8 Influence of shear links spacing

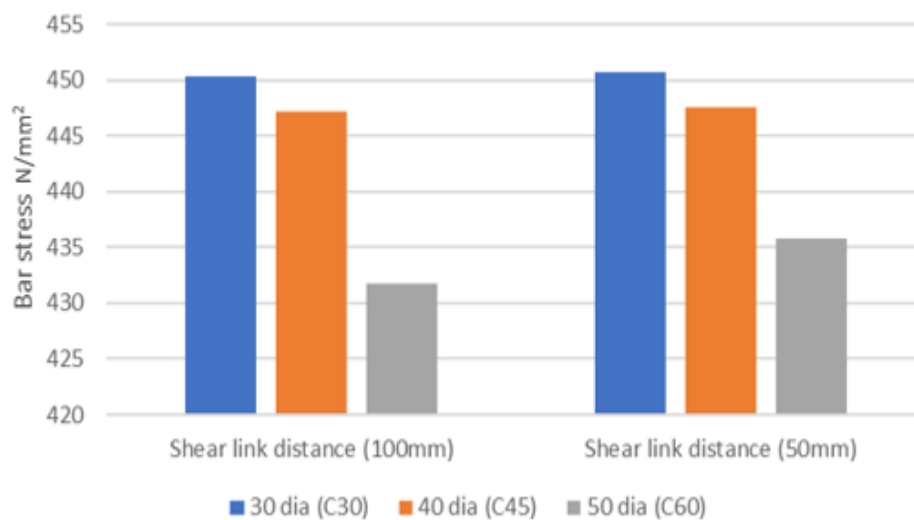
The results of the analysis indicated that beams with smaller shear link spacing exhibited greater lapped bar stress compared to those with larger link spacing. Figures 6.7(a) and 6.7(b) present the bond stress and ductility analysis of three similar specimens (30Ø, 40Ø, and 50Ø) with the same cover but different shear link spacing (50 mm and 100 mm), in accordance with Eurocode 2 recommendations. The figure clearly shows that as the shear link spacing decreases, the lapped bar stress, and the load capacity of the beams increase, as captured by the simulations.

Figure 6.7(a) depicts the graph of lapped bar stress against the shear link spacing. For the same lap-length to bar diameter ratio of 30ϕ , increasing the shear link spacing by 100% from 50 mm to 100 mm resulted in a 22% increase in lap stress. This increase was also observed for specimens with different concrete grades.

Furthermore, Figure 6.7(b) demonstrates a 28% decrease in lapped bar stress for the 30ϕ specimens when the concrete grade increased from C30 to C45.



(a). Effect of shear link spacing on bar stress.



(b). Effect shear link spacing on concrete grade.

Figure 6.7. Effect of shear link spacing on bar stress and concrete grade.

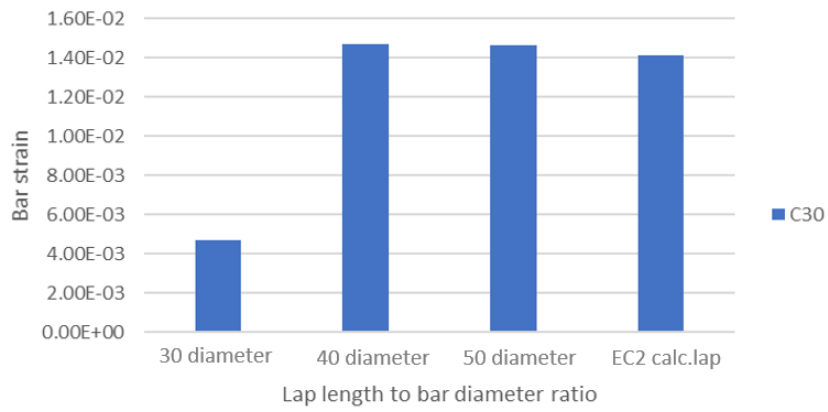
6.9 Bar forces versus strain

Figure 6.8(a) shows a nonlinear relationship between the strain and the lap length-to-bar diameter ratio. This suggests that increasing the lap length-to-bar diameter ratio leads to a corresponding increase in the obtained strain for a reinforced concrete (RC) beam.

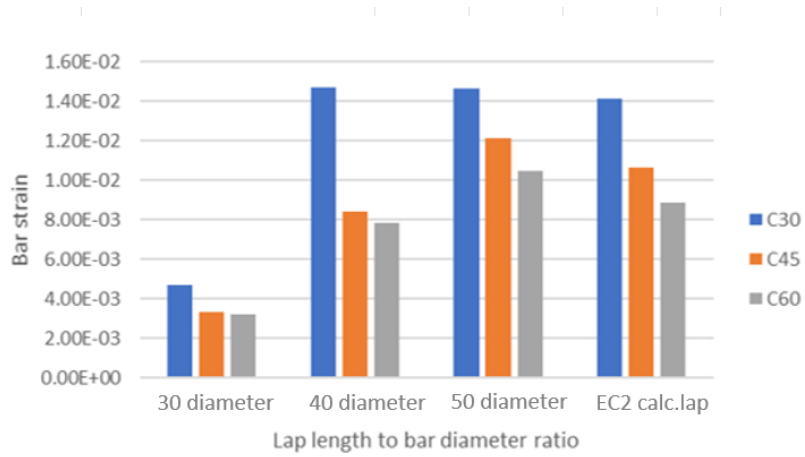
Therefore, it can be inferred that the lap length-to-bar diameter ratio plays a significant role in determining the overall strain of an RC beam, as evidenced by the data trend in Figure 6.8(a). For instance, increasing the lap length-to-bar diameter ratio from $30\emptyset$ to $40\emptyset$ resulted in a 215% increase in lapped bar strain. However, a further 25% increase in lap length-to-bar diameter ratio from $40\emptyset$ to $50\emptyset$ only reduced the lapped bar strain by 0.6%.

Figure 6.8(b) demonstrates the effect of concrete grade on the strain in an RC beam. It appears that there is an inverse relationship between the lapped bar strain and the concrete grade, as increasing the concrete grade leads to a decrease in lapped bar strain. For example, for the same lap length-to-bar diameter ratio of $30\emptyset$, increasing the concrete grade from C30 to C45 resulted in a 29% reduction in lapped bar strain, as depicted in Figure 6.8(b). This pattern is also observed when the concrete grade is increased from C45 to C60, as shown in the same figure.

Furthermore, Figure 6.8(a) illustrates the effect of force on bar strain. Similar to the lapped bar stress, there is a nonlinear relationship between bar force and lap length. The maximum force in pairs of lapped bars decreases as the lap length increases, which is typical for the analysed splices and consistent with the splice being in a constant moment zone.



(a) Effect of lap length to bar diameter ratio on strain.



(b). Effect of concrete grade on force.

Figure 6.8. Effect of lap length to bar diameter ratio on bar force and strain.

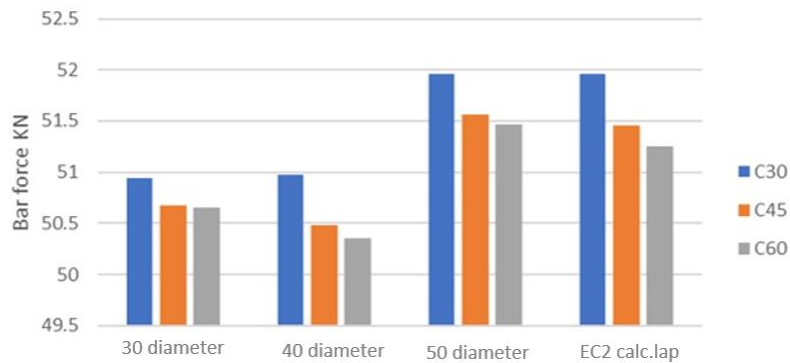


Figure 6.9. Effect of concrete grade on bar force.

In Figure 6.9, the influence of concrete on lapped bar force is presented. The graph clearly illustrates an inverse relationship between the concrete grades and lapped bar force, which means that as the concrete grade increases, the lapped bar force decreases. Moreover, the effect of zero shear distance on lapped bar force is also demonstrated in this figure, as increasing the zero shear distance leads to a decrease in lapped bar force.

6.10 Concluding remarks

The objective of this chapter was to investigate the impact of concrete grade, link spacing, load location, and lap length on the behaviour of reinforced concrete (RC) beams through experimental testing and nonlinear finite element analyses. The finite element model was able to accurately simulate the experimental behaviour of RC beams with and without lap splice under four-point bending, yielding good agreement between the two in terms of ultimate load and deflection curve. Based on the behaviour model and simulation results, the following conclusions were drawn:

- Decreasing the shear link spacing effectively delayed the formation of cracks, resulting in increased load-carrying capacity of the beams. Smaller shear link spacing was found to be more effective than larger spacing.
- Bar stress decreases as the concrete grade is increased from C30 to C60, with reductions of 49% and 46% observed for samples with lap lengths-to-bar diameter ratios of 40ϕ and 50ϕ , respectively.
- Zero shear span distance is inversely proportional to bond stress and bond force. Increasing the zero-shear distance by about 44% led to a decrease in bar stress of approximately 191% for beams with C30 grade concrete.
- Lap lengths beyond 50 diameter laps are not recommended as they may hinder effective pouring of concrete and vibrating, resulting in air bubbles that could affect construction quality and performance. Furthermore, increasing the lapping length of the reinforcing bars can cause rebar congestion and raise construction costs.

Overall, this study provides valuable insights into the influence of various factors on the performance of RC beams, which can aid in designing and constructing more efficient and durable structures.

7. Tension lap joints in reinforced concrete beams

7.1 Introduction

Reinforced concrete is one of the most commonly used structural materials in construction due to its versatility, efficiency, and economy, as well as performance criteria and ample guidance for designers. Recently, stainless steel has been used in reinforced concrete buildings due to its long life cycle, excellent durability, exceptional corrosion resistance, great ductility, and significant strain hardening. Reinforced structures are widely used for various applications, including bridges, tunnels, and multi-storey buildings, thanks to the effective utilisation of readily available constituent materials.

The bond property plays a critical role in the design of reinforced concrete structures. It is essential for achieving composite action between the two material constituents, allowing loads to be efficiently transmitted. Insufficient concrete-steel bond can lead to excessive slippage of reinforcement, causing ineffective anchorage of reinforcement bars, excessive rotation or deflection, and serious cracking of the concrete. The development of a bond is a complicated phenomenon, with many interrelated parameters affecting it. The surface geometry of the reinforcing bar and the quality of the concrete are the most crucial factors to consider.

One major advantage of stainless steel over mild steel is its higher strain hardening and ductility capacity. Due to the strain-hardening characteristics and ductility of stainless steel, a large number of international design codes, such as Eurocode 2, do not provide a separate design model for concrete structures with stainless reinforcing bars. However, using a mild steel reinforcing bar and a stainless reinforcing bar with a lap splice in a reinforced concrete section produces erroneous results, despite the technical capability of the Eurocode 2 design model to account for different reinforcement types. While there have been many studies on the behavior of plain stainless-steel members in recent years, little research has been done on reinforced concrete or stainless-steel reinforced concrete with lap splices. Therefore, the purpose of this chapter is to evaluate and compare the behavior of stainless and mild steel reinforced concrete with and without lap splices. The chapter also describes and analyses the stress and strain distribution of tension lap joints.

7.1.1 Material characteristics

7.1.1.1 Concrete

To achieve a target concrete compressive strength of C30, a mix proportion of 0.45 water to cement ratio, 21kg cement, 52.50 kg and 23.39kg coarse aggregate and fine sand, respectively, was used. The maximum aggregate size used was 10 mm. Three beam specimens without reinforcement (150 mm ×150 mm ×750 mm) were cast from the same batch to allow for the flexural test to be performed on the day of beam testing, following the guidelines provided by BS EN 12390-5:2020. Additionally, three concrete cylinder samples were cast from the same concrete mix to perform the compressive strength test according to EN12390-3,2009. After casting, the cylinders and beams were placed in a curing tank the following day. Table 7.1 below shows the mean concrete compressive strength for the cylinders and the average maximum load of beams without reinforcement.

Table 7.1. Mean compressive of the cylinders.

ID	Compressive strength MPa	Average compressive strength
Cylinder 1	32.61	32.72
Cylinder 2	32.67	
Cylinder 3	32.87	

7.1.1.2 Stainless steel rebar

EN 1.4301 grade 304 stainless steel is widely used due to its corrosion resistance, composition, and mechanical properties (Metals4u, 2021). In this study, grade 304 was used as it is easily available from local suppliers and is commonly used in all fields. Two different diameters of stainless-steel reinforcing bars, 8 mm, and 12 mm, were used. Both the stainless-steel and mild steel reinforcing bars had two transverse and longitudinal ribs at each cross-section. The mild steel and stainless-steel reinforcement met the criteria of BS4449+A3, 2005 and BS 6744, 2016, respectively. The stainless-steel chemical composition based on the product information provided by the local supplier is shown in Table 7.2.

Tensile tests were conducted to determine the stress-strain constitutive response and mechanical characteristics of the stainless steel in conformity with EN 6892-1, 2016. Figure

Table 7.3 show the outcomes of the experiments. Three repeat experiments were conducted for each rebar, and the mean response was used in the finite element simulations. Table 7.6 shows the average results for the two types of reinforcement tested. In this table, P_m is the maximum load capacity corresponding to the mid-span deformation (δ_m), ϵ_u is the elongation at failure of the reinforcement, σ_m is the maximum strength of the reinforcement, l_b is the lap splice length, and σ_y is the yield strength of the rebar (which is taken as the 0.2% proof strength $\sigma_{0.2}$ for stainless steel). The lap splice length for each beam is described in Table 7.6 by the lap length-to-bar diameter ratio (e.g., $30\emptyset$ refers to 30 multiplied by the tension bar diameter of 12 mm). The stainless-steel specimens demonstrated nonlinear behavior from the onset, followed by a rounded response with considerable ductility.

Table 7.2. Beam test results and material properties.

	C	Mn	Si	P	S	Cr	Ni	N
Min						18.0	8.0	
Max	0.08	2.0	0.75	0.045	0.030	20.0	10.5	0.10

Table 7.3. Beam test results and material properties.

Beam	f_{ck} (N/mm ²)	l_b (mm)	σ_y (N/mm ²)	σ_m (N/mm ²)	ϵ_u %	P_m (KN)	δ_m (mm)	Failure mode
MS-00	32.72	N/A	554.14	665.45	22.47	77.63	15.18	[Y,c]
MS-30Ø	32.72	30Ø	554.14	665.45	22.47	64.99	12.72	[B]
MS-40Ø	32.72	40Ø	554.14	665.45	22.47	70.72	12.24	[Y,b]
MS-50Ø	32.72	50Ø	554.14	665.45	22.47	77.44	14.58	[y,b]
MS-62 Ø[Eurocode 2]	32.72	62Ø	554.14	665.45	22.47	88.44	12.34	[Y,b]
SS-00	32.72	N/A	694.32	876.12	24.83	105.12	16.23	[c]
SS-30Ø	32.72	30Ø	694.32	876.12	24.83	77.29	12.57	[B,c]

Failure modes:

[b]-bond failure

[c]-crushing

[y]-yielding

δ_m - maximum deflection

σ_m - maximum stress

σ_y - yield stress

l_b - lap length

P_m - maximum loading

Loading set-up

A total of seven RC beam experiments were performed, as listed in Table 7.1. Five of the beams were reinforced with mild steel and two with stainless steel, for comparison. One

beam was reinforced with stainless steel and lap-spliced in the middle (SS-30 \emptyset), and four contained mild steel with lap splices at the centre (MS-30 \emptyset , MS-40 \emptyset , MS-50 \emptyset , and MS-62 \emptyset). The final two beams had no lap splices and were reinforced with stainless steel and mild steel (SS-00 and MS-00). Each specimen is identified by a reference system, where the first two terms denote the rebar type (e.g., SS for stainless steel and MS for mild steel), and the second term indicates the lap splice length or lap length (30 \emptyset , 40 \emptyset , 50 \emptyset , and 62 \emptyset , corresponding to splice lengths of 360 mm, 480 mm, 600 mm, and 744 mm, respectively). The configuration of the beams, including geometrical and reinforcement details, is shown schematically in Figure 7.1(a), and a photograph of the formwork used to place the reinforcement before and after casting the concrete is presented in Figure 7.1(b).

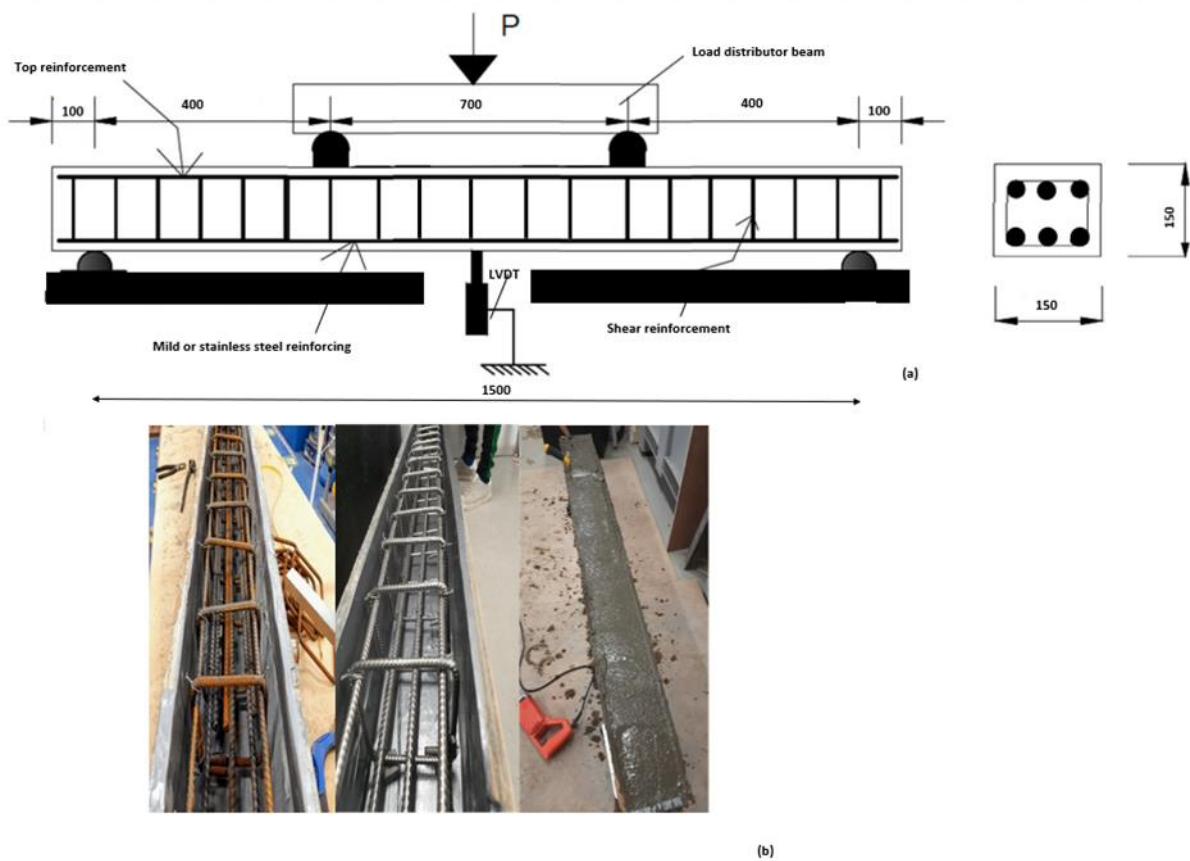


Figure 7.1. Beam samples configuration including (a) the geometrical and reinforcement details and (b) reinforcement arrangement and formwork.

All of the beams had an overall length of 1700 mm, a width of 150 mm, and a height of 150 mm. They were tested under a four-point loading configuration across a 1600 mm clear span. The thickness of the clear cover concrete was 23 mm on the side, top, and bottom of the beam, measured from the outer surface of the concrete to the surface of the

longitudinal reinforcement. The length of the constant moment zone in the centre of the beam was 700 mm. The shear stirrups and top reinforcement in the compression zone had a diameter of 8 mm and were made of either mild or stainless steel, while the tension reinforcement on the bottom face of the beam was also made of either mild or stainless steel and had a bar diameter of 12 mm. Shear links were placed in all beams at 100 mm spacing. In order to provide a more comprehensive evaluation of the behavior, the current study also examined the finite element results of mild and stainless steel.

Experimental procedure

Five reinforced concrete beams made with mild steel were tested and fabricated at the University of West London's concrete laboratory. In addition, two beams reinforced with stainless steel were investigated for comparison. The investigation aimed to examine the load-carrying capacity and flexural behavior of these members. Four different lap splice lengths (30 \emptyset , 40 \emptyset , 50 \emptyset , and 62 \emptyset [according to EN 1992]) and two different types of reinforcing bars (stainless and mild steel rebars) were examined. Similarly, two RC beams (one with mild steel rebars and one with stainless steel rebars) with continuous rebars were used as reference samples (control). The material properties of the concrete were obtained using a standard compression testing machine based on BS EN 12390-5:2020, while the mechanical characteristics of the rebars were determined by employing standard tension experiments for reinforcements (EN6892-1, 2016).

A hydraulic actuator with a 500 KN capacity was used to apply a load monotonically through a machine ramp on a load spreader beam, resulting in two equivalent point loads on the top surface of the beam. A rate of load application of 0.20 mm/min was used in displacement control for all experiments. The vertical displacement at the centre of the beam span was measured using a built-in TC4 transducer and a linear variable displacement transducer. LabVIEW-based software linked to a computer was used for storing the results during the experiments. Before testing, the surfaces of all samples were dried out to easily identify crack patterns and formation.

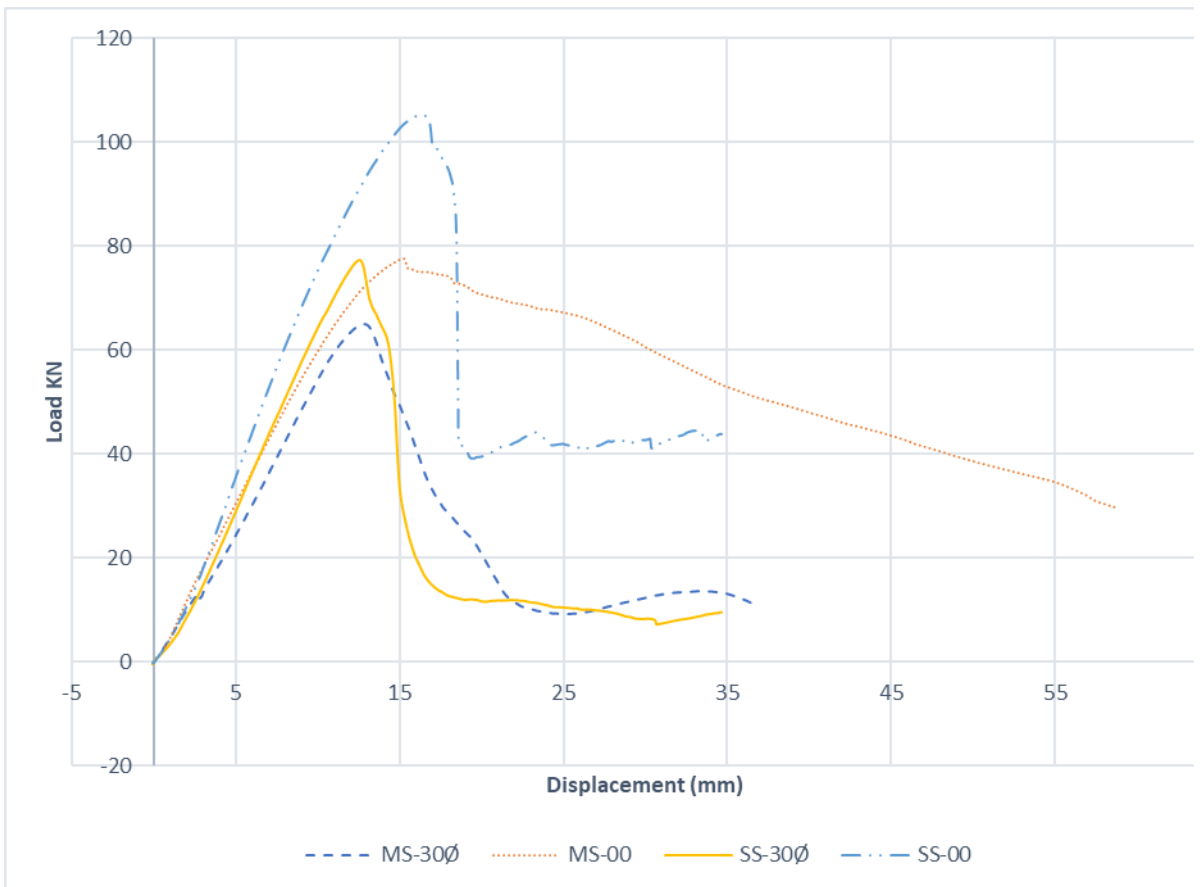
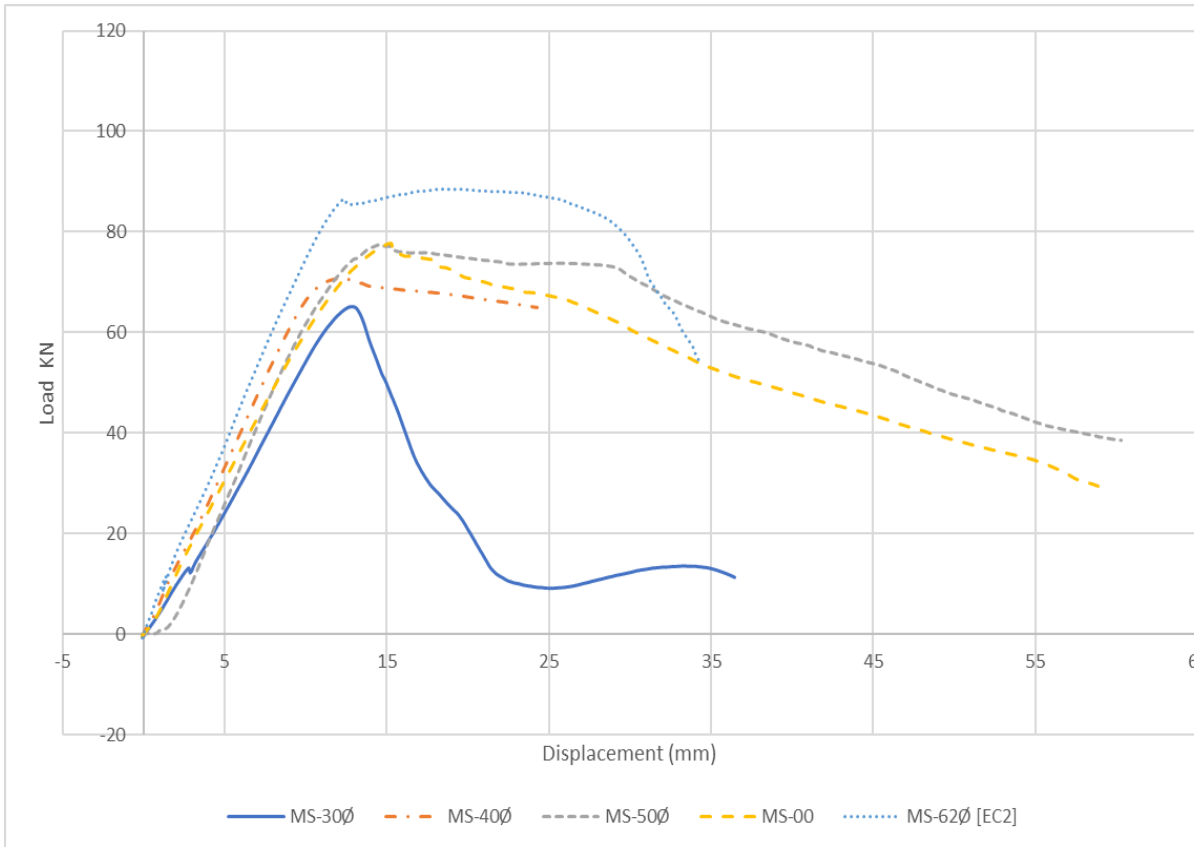


Figure 7.2. Load displacement graphs for mild steel and stainless steel

7.2 Results and discussion

The observations and key findings from the experiment are analysed and discussed in this section. The main performance measures for RC beams, including crack patterns, cracking moments, load-deflection response, maximum moment capacities, and stress and strain distribution across the lap splice length, are evaluated.

7.2.1 Load displacement behaviour

Figure 7.10 shows the load-displacement behavior for the seven tested beams. Additionally, Table 4 presents the displacement and corresponding maximum load. Overall, all beam samples performed well during the experiment, showing sufficient warning of failure and good ductility, except for samples with the shortest lap splice length (SS-30 \emptyset and MS-30 \emptyset) with $l_b/\emptyset=30\emptyset$, which failed abruptly in the bond after the reinforcement yield. All the beams with lap splice lengths behaved similarly at low load levels with regard to the first cracking point and initial stiffness. However, after the cracking moment was reached, the stainless steel reinforced concrete beams exhibited a more rounded and nonlinear behavior compared to the mild steel samples (MS-30 \emptyset , MS-40 \emptyset , MS-50 \emptyset , and MS-62 \emptyset). Table 7.6 and Figure 7.10 show some key and more detailed observations from the load-displacement response.

- The load-displacement behavior (shown in Figure 7.10(a) of MS-62 \emptyset (EC2)) was comparable to that of MS-00 with continuous reinforcing bars; however, the initial stiffness of MS-62 \emptyset (EC2) was higher due to the introduction of lap length.
- Regarding the failure mode, mild steel reinforced beams (MS-40 \emptyset , MS-50 \emptyset , and MS-62 \emptyset) failed by bond after the reinforcement yield, while stainless steel RC beams specimen SS-00 failed by crushing of the concrete. This is due to the high ductility of stainless steel. When compared to mild steel reinforcement, stainless steel reinforced concrete beams provided adequate warning before failure, including attaining substantial degrees of deformation followed by severe cracking, as demonstrated in Figure 7.10(b).
- Peak loads were greater in the beams with a higher lap length-to-bar diameter ratio, as expected. However, it is worth noting that the ductility at maximum load was larger in the case of beams with higher lap length. This is probably because as the lap splice length is increased, the rates of strain and stress in the reinforcing bars

decrease, causing the behaviour to become less ductile, and strain hardening in the stainless-steel reinforcing bars to be underutilised.

- Compared to the other beams, the beams with higher lap length-to-bar diameter ratios (MS-62Ø [EC2] and SS-62Ø [EC2]) achieved higher maximum load and displacement before failure. After reaching the maximum load, the capacity of the RC beams steadily decreased until collapse due to bond and concrete crushing.
- Samples MS-30Ø and SS-30Ø had similar concrete strength, geometry, reinforcement ratio, and lap splice length, but had a different type of reinforcing steel. Compared to the stainless reinforced concrete beam (SS-30Ø), the MS-30Ø beam showed a stiffer initial response but yielded sooner. However, as given in Table 4, the displacement at the maximum load was higher for the MS-30Ø RC beam than for SS-30Ø. There are likely various contributing factors to this, such as the weaker bond that exists between the concrete and stainless steel rebars when compared to the surrounding concrete and mild steel reinforcement. This results in more cracking throughout the member and greater strain distribution in the rebar, leading to greater deformation and ductility. Moreover, the maximum load was about 19% higher for reinforced concrete beams made of stainless steel. The reasons for this, as previously mentioned, are the two materials' different constitutive relationships. Stainless steel exhibits a more nonlinear stress-strain response, excellent ductility, and no clearly defined yield point. On the other hand, the stress-strain response of mild steel is linear elastic up to the point of yielding, after which there is a yield plateau followed by limited strain hardening up to failure.

7.2.2 Deformation

Maintaining a building's suitability for occupancy requires designers to consider the amount of deformation that occurs in building elements under service loading. As previously mentioned, the mild steel reinforced concrete beam (MS-30Ø) analysed in this study showed slightly higher deformation levels at failure than the stainless-steel RC beam (SS-30Ø). However, the opposite was observed in the case of the RC beam with continuous rebars; the stainless RC beam (SS-00) showed a noticeably higher degree of deformation at failure than the mild steel RC (MS-00). This is because of the ductile properties of stainless-

steel rebar, which enable the section's ductility to be mobilised as strain concentrations distribute and more cracks form.

The next section of this study evaluates the design technique for quantifying and estimating satisfactory deflection levels. The deformation level that is considered satisfactory depends on various factors, such as the type of load applied, the structure being considered, and the importance of a particular structural member (Shamass and Cashell, 2020). Most design guidelines, such as ACI 318-11 (2011) and Eurocode 2, specify a permissible span-to-depth ratio for the concrete element. For mild steel reinforced concrete beams and slabs exposed to quasi-permanent loads, the limit is span/250. Otherwise, deformations may be calculated and compared to predetermined limitations by applying the analytical equations provided in the design guidelines.

In Eurocode 2, the deformation of a member is determined on the basis of the concept that the member contains uncracked and cracked sections. Members that are anticipated to crack but not completely cracked act as an intermediate between fully cracked and uncracked. Therefore, the ultimate deformation for reinforced concrete members subjected to flexure is calculated as follows:

$$\delta_{Eurocode\ 2} = \delta_1 + \zeta\delta_2(1 + \zeta) \quad (1)$$

Where

ζ is a distribution coefficient allowing for tension stiffening in the section and is determined as:

$$\zeta = \left(\frac{M_{cr}}{M_a}\right)^2 (1 - \beta) \quad (2)$$

Where,

β is a coefficient taking into account the influence of repeated loading or the duration of the loading on the mean strain, M_{cr} and M_a represent the bending moment values determined at the cracking and service loads, respectively. While δ_1 and δ_2 are the maximum deformation for the uncracked and cracked section and are determined as follows:

$$\delta_1 = (3L^2 - 4a^2) \frac{Pa}{24I_g E_c} \quad (3)$$

$$\delta_2 = (3L^2 - 4a^2) \frac{Pa}{24I_{cr} E_c} \quad (4)$$

Where

a is the distance between support and the nearest loading point, P is each individual applied point load, L is the clear span, and E_c is the modulus of elasticity of concrete calculated as:

$$E_c = 22000(0.1f_{ck})^{0.3} \quad (5)$$

I_{cr} and I_g are the cracked and gross second moment of areas of a section and are determined based on the principles of elastic analysis utilising provided equations (6) and (7), respectively:

$$I_{cr} = A_s \mu d^2 (1 - k)^2 + \frac{bd^3 k^3}{3} \quad (6)$$

$$I_g = \frac{bh^3}{12} \quad (7)$$

Where

$$k = \sqrt{(\mu\rho)^2 + 2\mu\rho} \quad (8)$$

In these equations, μ represents the modulus ratio between the concrete and the reinforcing bar ($\mu = \frac{E_s}{E_c}$), A_s and ρ are the reinforcement area and ratio.

ACI 318-11 (2011) adopted the same method for calculating the deformation of a member. Nonetheless, ACI necessitates determining the effective moment of area based on the second moment of area of the uncracked and cracked section as:

$$I_e = I_g \left(\frac{M_{cr}}{M_a} \right)^3 + I_{cr} \left[1 - \left(\frac{M_{cr}}{M_a} \right)^3 \right] \quad (9)$$

While I_{cr} and I_g are determined from expressions (6) and (7), and M_{cr} is the theoretical cracking moment calculated as:

$$M_{Cr} = I_g f_r / y_t \quad (11)$$

Where y_t is the vertical distance between the outer tension surface and the neutral axis of the beam, I_g is the second moment of area of the section, and f_r is the modulus of the rupture of the concrete. Expressions for f_r are given in equations (12) and (13), respectively, for ACI 318-11 (2011) and Eurocode 2 part 1-1 (EN 1992 1-1, 2004), which are used in conjunction with equation (11) to obtain $M_{cr,ACI}$ and $M_{cr,EC2}$ respectively; and the obtained values are shown in Table 5.

$$f_{r,ACI} = 0.62\sqrt{f_c} \quad (12)$$

$$f_{r,EC2} = 0.3(f_c)^{2/3} \quad (13)$$

The maximum mid-span deformation for beams subjected to four-point bending (4PB) configuration is calculated as follows:

$$\delta_{ACI} = \frac{Pa}{24I_e E_c} (3L^2 - 4a^2) \quad (14)$$

Based on ACI 318-11, the concrete modulus of elasticity E_c is determined as:

$$E_c = 4700\sqrt{f_c} \quad (15)$$

The current analysis evaluates the experimental deformation values ($\delta_{0.35}$ and $\delta_{0.62}$) that correspond to 35% and 62% of the maximum beam bending for two different service load levels. Table 7.7 summarizes the results and the corresponding design values. Based on the findings in Table 7.7, the experimental deformations at 35% and 62% of the ultimate bending moment M_m (i.e., $\delta_{0.35}$ and $\delta_{0.62}$, respectively) were significantly higher for beams reinforced with stainless-steel rebars (SS-00 and SS-30 \emptyset) than for beams with mild steel rebars (MS-00, MS-30 \emptyset , MS-40 \emptyset , MS-50 \emptyset , and MS-62 \emptyset [EN 1992]). For example, for the beams without lap splice length, $\delta_{0.35}$, and $\delta_{0.62}$ were 13% and 7% higher, respectively, for SS-00 than for MS-00. Similar trends were observed in the RC beam with 30 \emptyset lap splices. This is expected since the load-carrying capacity and strain levels in the reinforcing at service loading are greater for beams reinforced with stainless steel rebars than for mild steel rebars. However, the deformations that occur in reinforced concrete members before failure can be controlled in various ways depending on the application. Engineering

judgement can be used, for instance, to select and examine different geometry and deformation requirements for a specific purpose.

Table 7.4. Design deflection values

Samples	Experiment			Eurocode 2			ACI-308-11		
	δ_m (mm)	$\delta_{0.35}$ (mm)	$\delta_{0.62}$ (mm)	$\delta_{0.35,EC}$ (mm)	$\delta_{0.35,EC2}$ $/\delta_{0.35}$	$\delta_{0.62,EC}$ (mm)	$\delta_{0.35,A}$ (mm)	$\delta_{0.35,ACI}$ $/\delta_{0.35}$	$\delta_{0.62,ACI}$ (mm)
MS-00 8	15.1	4.48	7.96	5.47	1.22	7.20	4.86	1.08	7.49
MS-30 \emptyset 2	12.7	4.64	7.68	5.20	1.14	6.85	5.04	1.10	7.13
MS-40 \emptyset 4	12.2	3.77	6.52	4.67	1.24	5.82	4.02	1.06	6.20
MS-50 \emptyset 8	14.5	5.18	7.98	5.29	1.02	6.02	4.30	0.83	6.62
MS-62 \emptyset (EC2) 8	12.3	4.12	7.21	5.06	1.23	6.76	4.56	1.11	6.99
SS-00 3	16.2	5.10	8.58	5.48	1.06	7.28	4.72	0.93	7.62
SS-30 \emptyset 7	12.5	4.79	7.68	5.80	1.21	6.78	5.12	1.07	7.22

Furthermore, it is observed that both ACI 318-11 and Eurocode 2 typically provide deformation values that are lower than the experimental deformation values. The deformation limits specified in both design codes, ($\delta_{0.62,EC2}$ and $\delta_{0.62,ACI}$), were found to be lower than the deformation values determined from the experiments at higher load levels (62% of the maximum beam bending). This unconservatism was particularly apparent at

higher load levels $0.62M_m$). Additionally, the deformation predictions from Eurocode 2 ($\delta_{0.35,EC2}$) were generally higher than the experimental deformations ($\delta_{0.35,ACI}$) at very low load levels (35% of the maximum beam bending), which are likely to be less than service loading. On the other hand, ACI 318-11 provides deformation values ($\delta_{0.35,ACI}$) that are lower than the test values.

The values of $\delta_{0.35,ACI}/\delta_{0.35}$ and $\delta_{0.35,EC2}/\delta_{0.35}$ from the experiments with continuously reinforced mild steel bars were 1.08 and 1.22, respectively, while the corresponding values at $0.62M_m$ were 7.49 and 7.20, respectively. For the equivalent stainless steel reinforced concrete beam, the values were 4.72 and 1.06 at $0.35M_m$ and 7.62 and 7.28 at $0.62M_m$. This indicates that both codes generally provide deformation limits that are slightly lower than the deflection observed in the test at $0.62M_m$ and higher than that which occurred in the test at $0.35M_m$ for the stainless steel RC member (SS-00). Similar conclusions were drawn for RC beams with lap splice length (MS-30 \emptyset). Compared to the corresponding stainless-steel beam (SS-30 \emptyset), these members had estimated-to-experimental values that were approximately 15% higher.

7.2.3 Crack development

The propagation and formation of cracks in reinforced concrete (RC) beams have a significant impact on failure, stress formation, ductility, and structural performance. Several interrelated factors influence cracks, including reinforcement type, bond, concrete strength, and lap splice length. Because of this, observing crack patterns and formation received a lot of attention throughout the experimental programme. The bending moment ($M_{cr,test}$) related to the initial cracks was determined, and the outcomes are provided in Table 7.8, where they are compared with finite element cracking moments.

The test cracking moments for samples MS-30 \emptyset and SS-30 \emptyset were very different, as expected given that the two samples have different types of reinforcing (mild and stainless steel). Based on the results in Table 7.8, both ACI and Eurocode 2 design guidelines estimate the initial cracking moment conservatively, with the American standard (ACI) being comparatively less conservative. For the stainless steel reinforced concrete samples in this study, the mean ratio of the design cracking moment to experimentally obtained value was 0.72 for the American standard and 0.64 for Eurocode 2. For mild steel beams, the

equivalent values were 0.0 and 0.67, respectively. Similar deductions were made when evaluating the results from the finite element analysis with the design guideline forecasts, as depicted in Table 7.8, where the estimated test cracking moments from American and Eurocode 2 standards were 0.7 and 0.6 for the mild steel RC sample and 0.76 and 0.66 for the stainless-steel reinforced concrete sample, respectively.

Transverse flexural cracks initially appeared close to the load application locations in all specimens. The initial cracks within the lap developed at the lapped bar end and spread upward to the compression region. Some additional cracks developed in the shear zone (that is, the zone between the point load locations and support) as the load was applied. Due to the mixture of shear and flexural stress in this region, these cracks spread diagonally to the position of the applied load.

The mode of failure is another crucial observation from the experiment. As previously mentioned, the samples reinforced with mild steel rebars failed by bond after the yielding of reinforcement, with the exception of the MS-30Ø. Meanwhile, the stainless-steel reinforced samples failed by concrete crushing, except for SS-30Ø, which failed in bond before the yielding of reinforcement. This is mostly owing to the greater ductility levels in the stainless-steel rebar compared to mild steel reinforcement. This ductility, along with strain redistribution in the reinforcing bar at greater deformation levels, allowed a ductile failure behaviour characterized by a progressive decrease in the sample load-bearing capacity after the maximum load, as depicted in Figure 7.8.

7.2.4 Maximum bending capacity

Table 7.9 presents the maximum bending moment values obtained from the experimental testing ($M_{m,Test}$) for each of the samples, as well as the corresponding values predicted by Eurocode 2 ($M_{m,EC2}$) and finite element analysis ($M_{m,FE}$). The table also includes the ratio of the design values to the test values for comparison.

The results indicate that the maximum moment capacity of the stainless steel beams with lap splices was 5% higher than that of the mild steel beams with lap splices. Additionally, the maximum bending moment capacity of SS-00 was 25% greater than that of MS-00. This is attributed to the higher ductility and significant strain hardening of the stainless-steel rebar,

which allowed the SS-00 and SS-30Ø samples to achieve higher moment capacities after reaching the value of their proof strength.

The ultimate moment capacity of a singly reinforced concrete member under ACI 318-11 ($M_{m,ACI}$) and Eurocode 2 ($M_{m,EC2}$) is determined by applying equilibrium of the internal forces and adopting an equivalent rectangular stress distribution through the section, together with an elastic-perfectly plastic constitutive material model of the reinforcement. Therefore, $M_{m,ACI}$ and $M_{m,EC2}$ are calculated using equations (16) and (17), respectively.

$$M_{m,ACI} = \rho f_y b d^2 \left(1 - 0.59 \frac{\rho f_y}{f_c} \right) \quad (16)$$

$$M_{m,EC2} = f_y A_s \left(d - \frac{\lambda x}{2} \right) \quad (17)$$

In which b is the width of the cross-section, f_c is the compressive strength of the concrete, ρ is the tensile reinforcement ratio, d is the effective depth from the top of a reinforced concrete beam, f_y is the yield strength and A_s is the cross-section area of the steel reinforcement. λx is obtained as follows:

$$\lambda x = A_s f_y / \eta \alpha_{cc} f_c b \quad (18)$$

The value of α_{cc} recommended by Eurocode 2, 0.85, was used in the analysis. For $f_c \leq 50\text{MPa}$, η was taken as 1, in accordance with Eurocode 2. Since ACI 318-11 and Eurocode 2 use equivalent reinforcement material models and are based on the same bending theory, both codes provide similar estimates of the maximum moment capacities ($M_{m,ACI} = M_{m,EC2} = M_{m,des}$) in the current samples. According to Table 7.9, the design guidelines give a conservative prediction of the maximum moment capacity for all the investigated beams, with the mean ratio of design-to-test maximum moments being 0.62 for mild steel RC beams and 0.73 for stainless steel reinforced concrete beams. In comparison to mild steel RC, the flexural capacity estimations for stainless steel reinforced concrete beams are somewhat less conservative.

Additionally, the results show that there is a strong agreement between the simulation values obtained from the finite element model and the experimental results. The mean ratio

of the predicted capacity to the test values for all beams was 0.71 and 0.73, indicating a high level of accuracy and reliability of the finite element simulation in estimating the maximum bending moment capacity. Compared to the design codes, the finite element analysis provides more realistic and accurate estimations, which are reliably conservative.

7.3 Tension lap joints

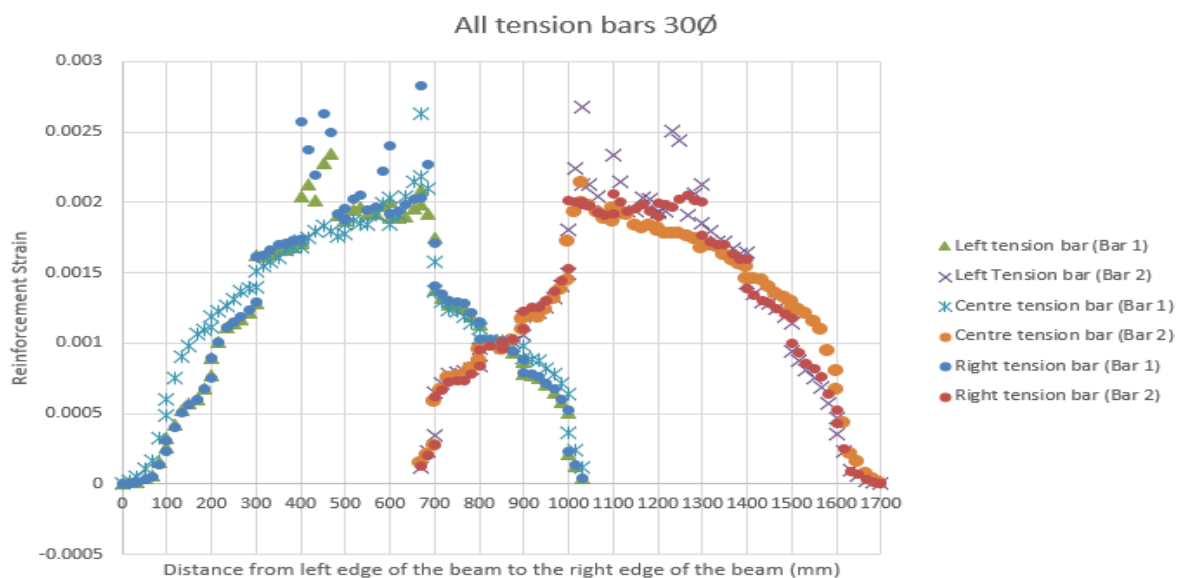
This section provides detailed information on the distribution of bond stress and strain along the tension lap joints and compares the performance of beams with different lap lengths. The following sections explain the results of the strain and stress analysis.

7.3.1 Strain distribution in longitudinal bars

Detailed information on the bond stress and strain distribution along the tension lap joints is presented in this section, along with a comparison of the performance of beams with different lap lengths. The results show visible strain distributions along the spliced steel rebars, indicating significant bending in the sample. Strains at one end of the lap were somewhat larger than those at the other end, but this did not affect the distribution of strain, especially in the stiffer lap section. Figure 7.11 illustrates the strain distribution in the reinforcing bar for each of the four samples (30Ø, 40Ø, 50Ø, and 62Ø [EC2] laps) after beam failure. The figures show that strains increased at the crack, where the reinforcing bar took the full load, and the maximum reinforcement strain at a crack varied in magnitude depending on the lap length. The maximum strains at the crack outside the joints were equal in size, as all specimens were reinforced with bars of the same diameter, resulting in nearly symmetrical strain distribution in the middle of the sample. However, reinforcing bar strains were lower at the lap ends on either side of the lap length, particularly at the maximum load phases. Moreover, it was observed that as the lap length to bar diameter ratio increased, the strain distributions became less symmetrical. This trend was particularly noticeable when comparing the 50Ø lap sample with that of the 62Ø [EC2 recommendation] (see Figure 7.11).

In a tension lap splice, the free end of the rebar experiences very little strain, as confirmed by our results. The strain distribution tends to zero at this point, resulting in high strain gradients at the lap end, especially if a crack develops within the lap zone, as shown in samples 40Ø, 50Ø, and 62Ø bar 1. The nature of the strain distribution at the end of the lap

is heavily influenced by the value of the reinforcing bar strain at the crack. Transverse and longitudinal crack formation in the beam significantly alters the distribution of strain, which remains constant across all samples irrespective of the lap length. Failure in the steel-concrete bond was only found at the lap ends of the splice, with a discontinuity in reinforcing bar stiffness leading to a greater level of strain outside of the lap splice length. As a result, the initial crack in each beam developed at the lap end, with the offset of the spliced rebars becoming more obvious. The cracks widening at the end of laps were one failure characteristic and resulted in a sample hinge at these positions. This is in line with the findings of Tepfers (1980), Judges et al. (1990), and Michellef (2017), who performed experiments on RC samples under four-point bending. At greater load levels, all of the samples exhibited longitudinal cracks, which were related to the significant bond stresses and their appearance was a good indication of bond distress. The cracks were observed at peak in the bond stress distribution at the lap end, with several of the cracks forming at the lap joint's ends. These were more likely caused by the offset in the spliced rebars and the bending forces created in the sample. The value of the strain upon crack development varied between the lap splice lengths, with the 50 \emptyset and 62 \emptyset [EC2 recommended lap design] samples differing slightly.



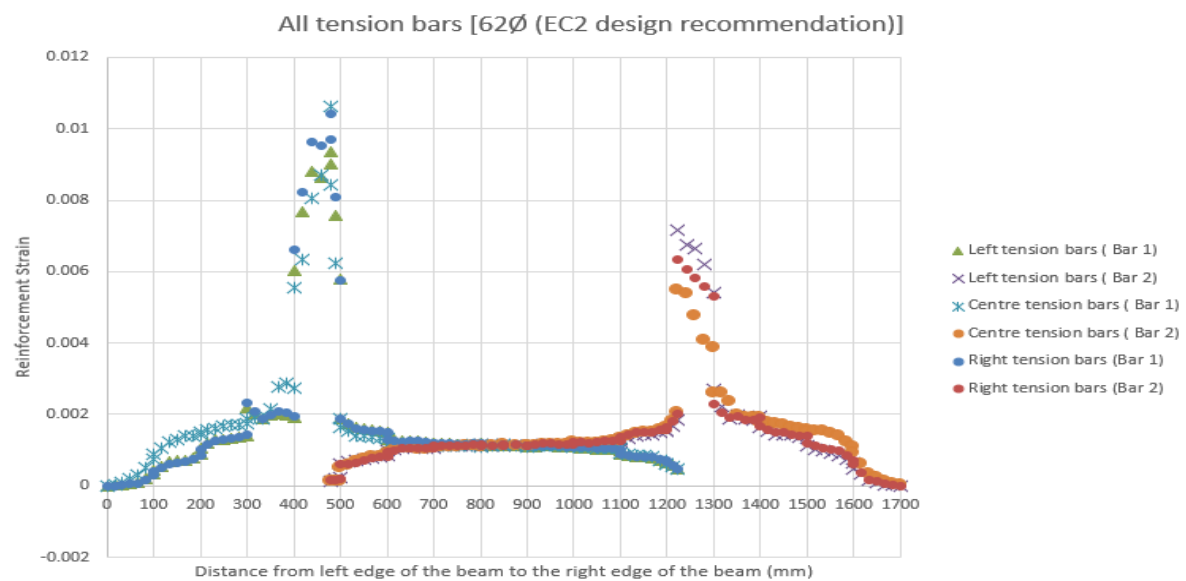
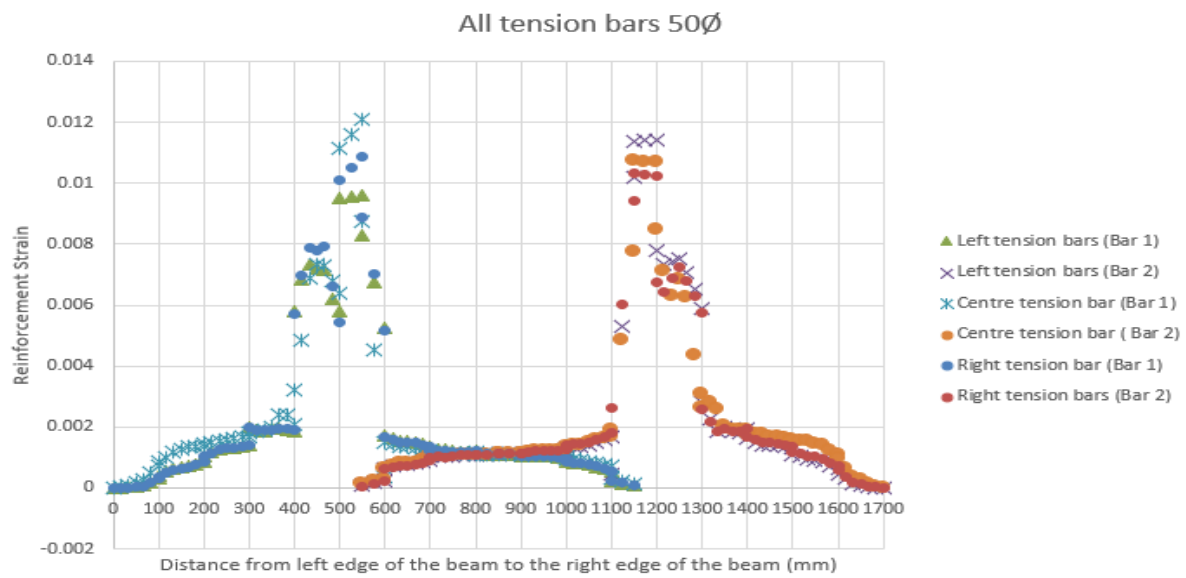
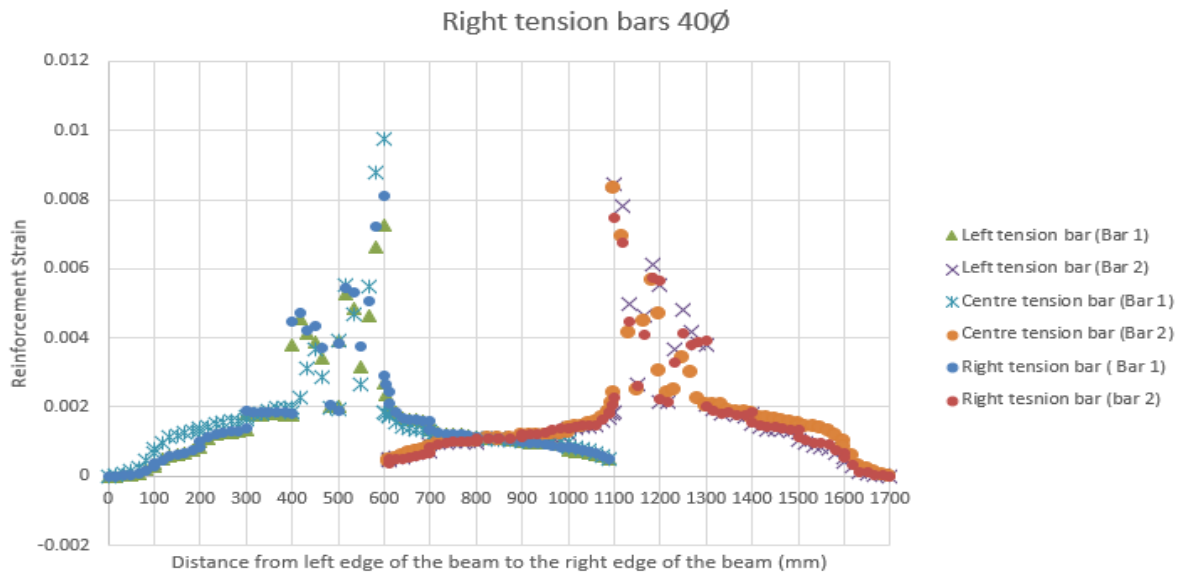


Figure 7.3. Reinforcement strain distribution sample 30Ø, 40Ø, 50Ø, and 62Ø [EC2] laps

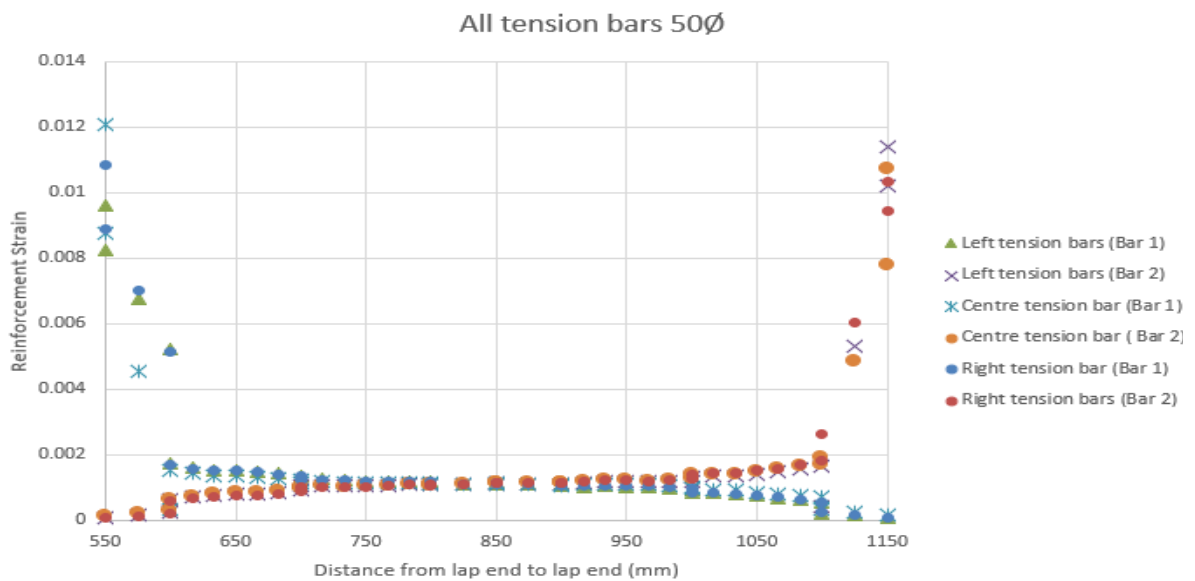
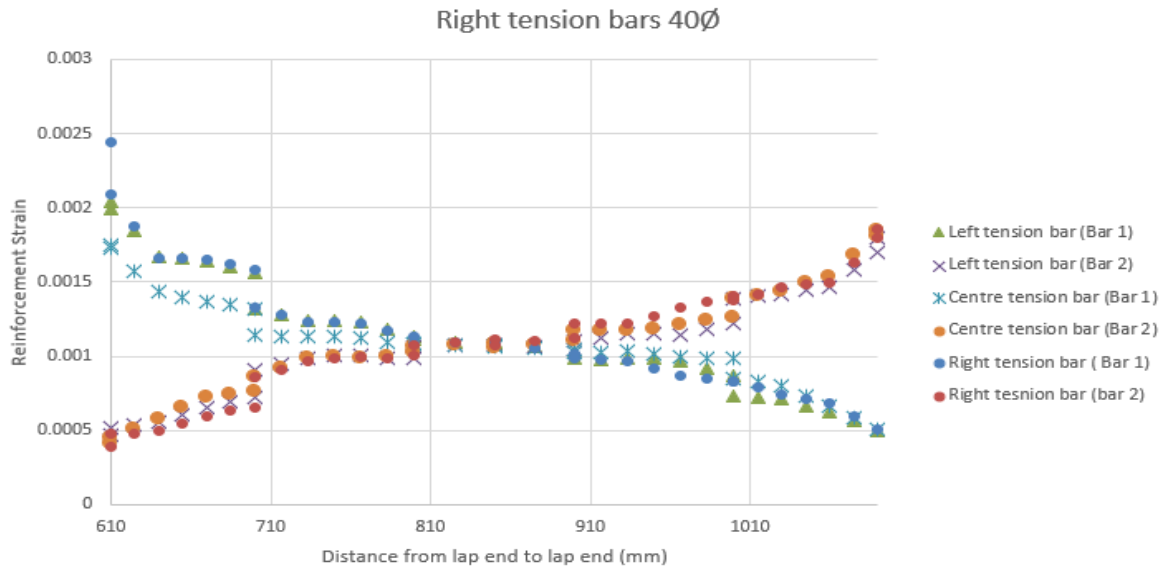
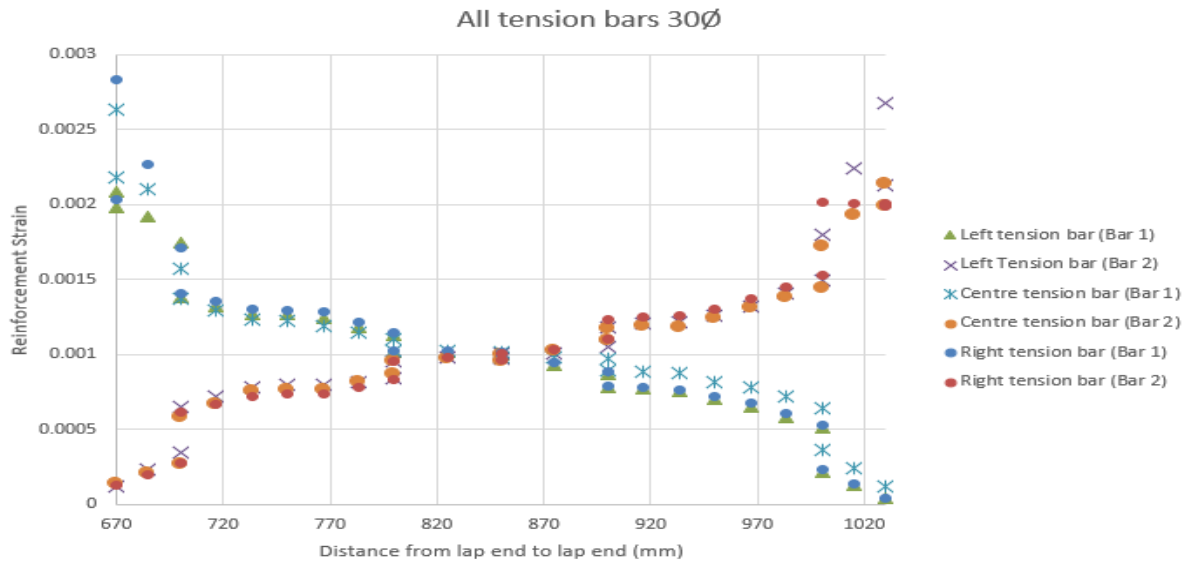
7.3.2 Transverse strain distribution

Before crack development, plateaus of uniform rebar strain were observed along the samples. The distribution of concrete stress followed the same pattern as the reinforcing strain, with constant stress zones on each side of the lap. Figure 7.12 depicts the distribution of reinforcing bar strain in terms of concrete stress. There was a small increase in the distribution at the lap ends where, despite the reduction in concrete area, the majority of the strain was supported by a single rebar.

The first cracks usually appeared outside the splice length, where both concrete and rebar strains were greater. In most cases, the cracks quickly spread over the concrete section, causing a sharp increase in strain levels at the crack location. The strains were highest at the cracks, where the reinforcing bars supported the majority of the load, and then dropped to each side of this location. As a result, the constant strain region reduced as cracks formed along the sample, and the distribution became a series of peaks (Figure 7.11).

Figure 7.12 shows the maximum distribution of strain along the lap length for samples 30 \emptyset , 40 \emptyset , 50 \emptyset , and 62 \emptyset laps. The formation of transverse cracks at the lap ends coincided with beam failure, and the maximum distribution of strain was observed. The strain result showed that as failure approached, the distribution across the lap splice length gradually became more linear. The dominating impact of the cracks at the ends of the lap partly contributed to this. The maximum distribution of strains gave the impression of linearity, which is in line with a previous study by Judges et al. (1990).

Increasing the lap-length to bar-diameter ratio from 30 \emptyset to 40 \emptyset (570 mm to 760 mm) resulted in an 8% increase in the ratio of measured to estimated strength. However, further increasing the lap-length to bar diameter ratio from 50 \emptyset to 62 \emptyset (EC2 design recommendation) resulted in a change in strain of about 18%. The difference in performance in terms of strength and ductility between 50 \emptyset and 62 \emptyset (EC2 design recommendation) is very negligible, considering that increasing lap length causes rebar congestion and makes the design costly and unsustainable.



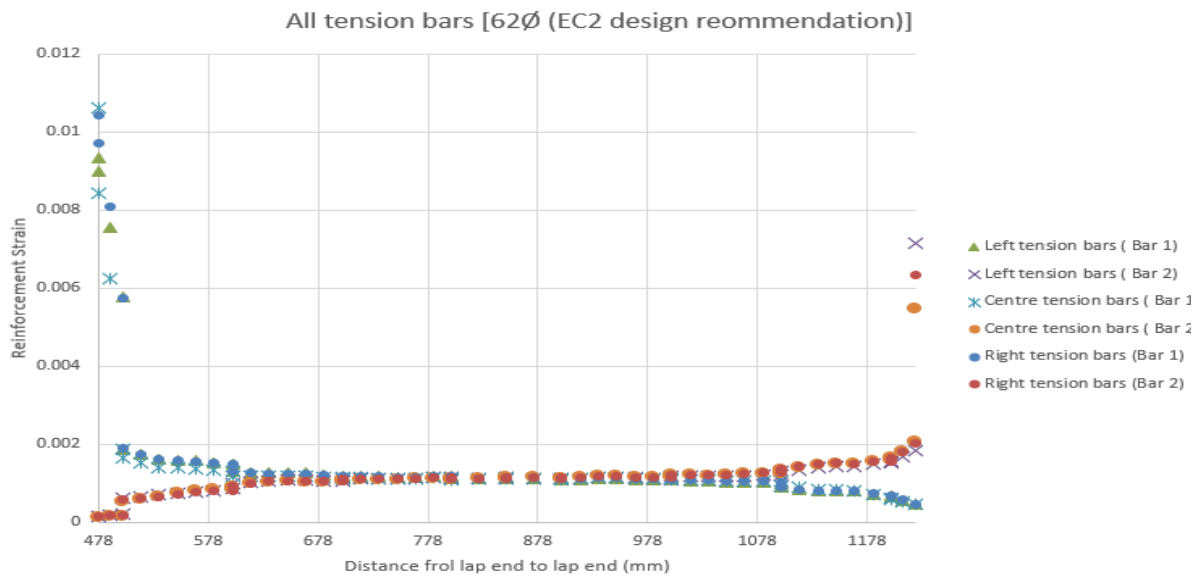


Figure 7.4. Rebar strain distributions along the lap splice 30Ø, 40Ø, 50Ø, and 62Ø [EC2]

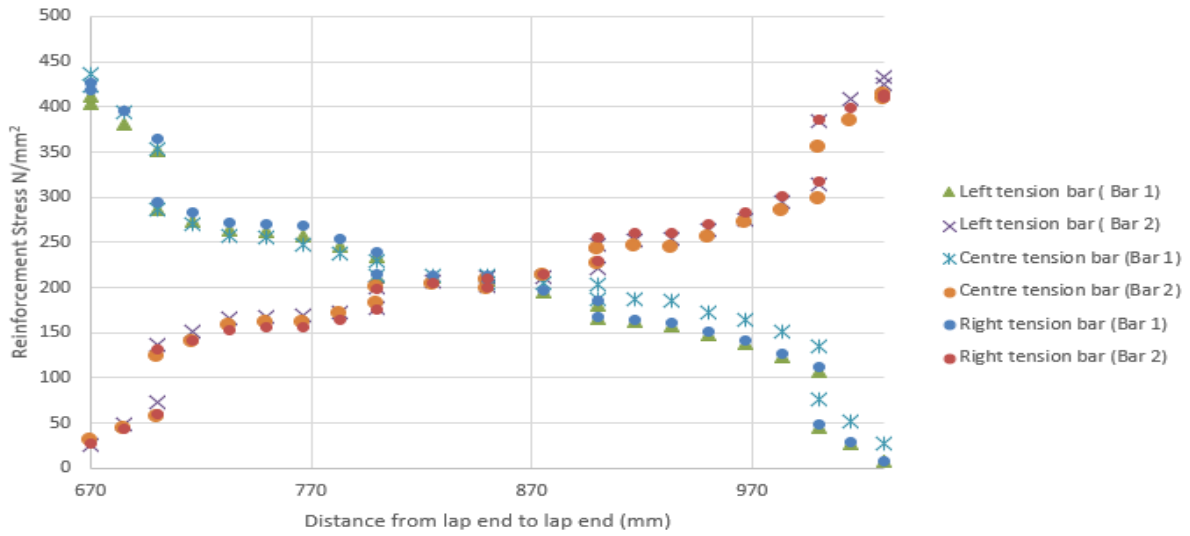
7.4 Lapped bar stress

7.4.1 Lapped bar stress distributions

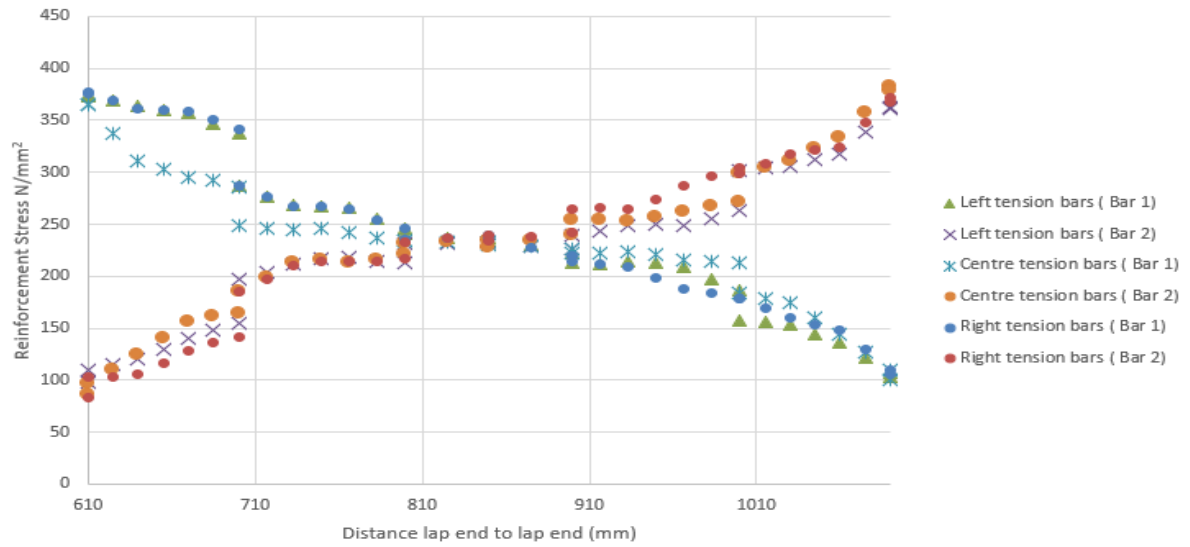
Due to the proportionality between the lapped bar at each location along a reinforcing bar and the rate of change in bar stress, the simulations allowed for a highly comprehensive assessment of lapped bar stresses. In the majority of the samples, strain gradients and lapped bar stress were insignificant before crack development. Bond stresses were present at the lap splice end, where the strains reduced abruptly to zero. The crack caused an abrupt drop in lapped bar stresses and greater strain linearity at the end of the lap. Following that, despite an increase in load, the lapped bar stress remained unchanged.

As each additional transverse crack appeared, the non-zero bond stress zone became larger until force transfer occurred across the entire length of the samples. The linear nature of the strain distributions showed that regions of constant bond stress existed along much of the samples at this point. Figure 7.13 depicts the lapped bar stress for all the samples in this study. The nonlinearity of the relationship showed a decrease in maximum bond stresses linked to an increase in lap splice length, presumably due to the formation of microcracks in the concrete. These findings were in line with those of Judges et al. (1990). Due to the stress redistribution caused by microcracking, maximum lapped stresses are carried over a longer splice length.

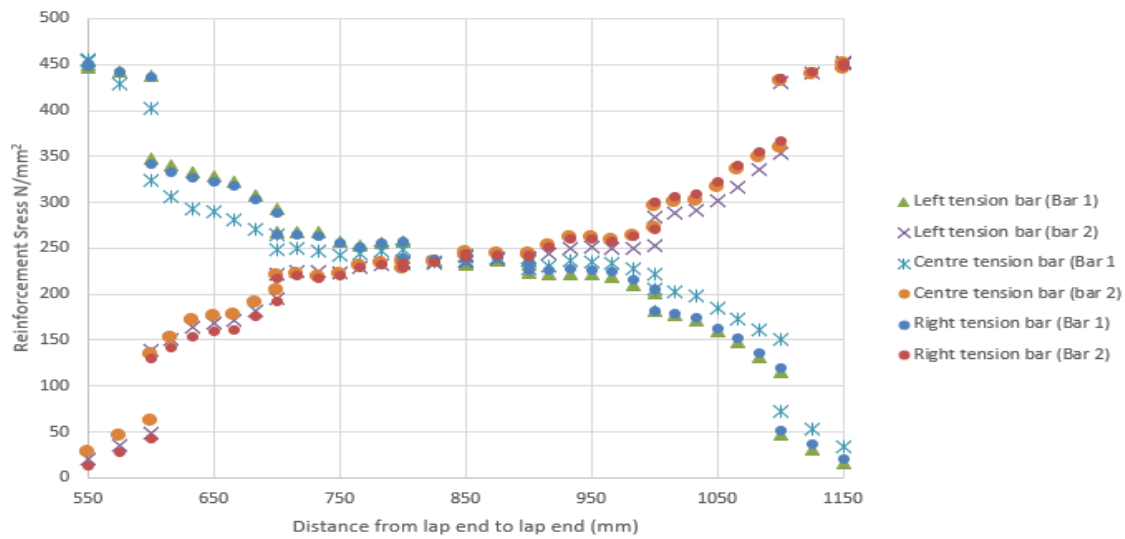
Right tension bars 30Ø



All tension bars 40Ø



All tension bars 50Ø



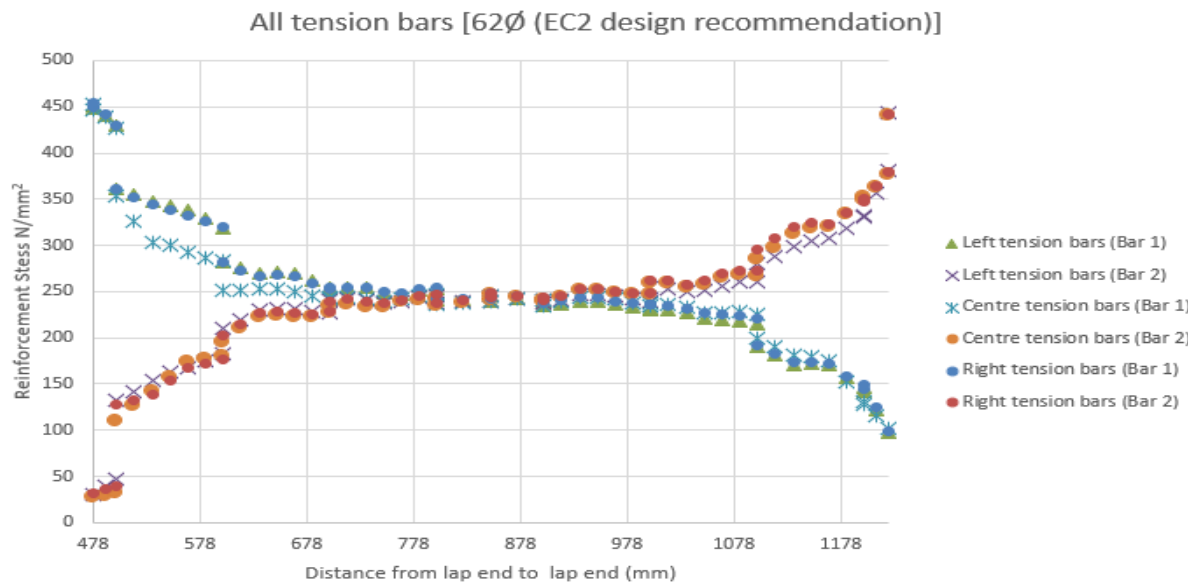
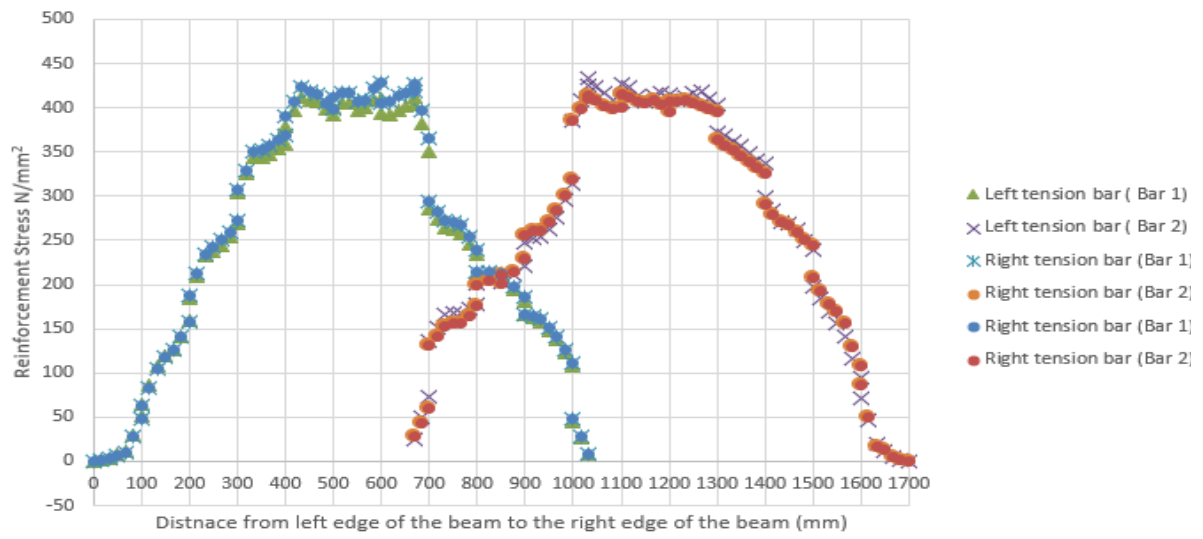


Figure 7.5. Rebar stress distributions along the lap splice 30Ø, 40Ø, 50Ø, and 62Ø [EC2]

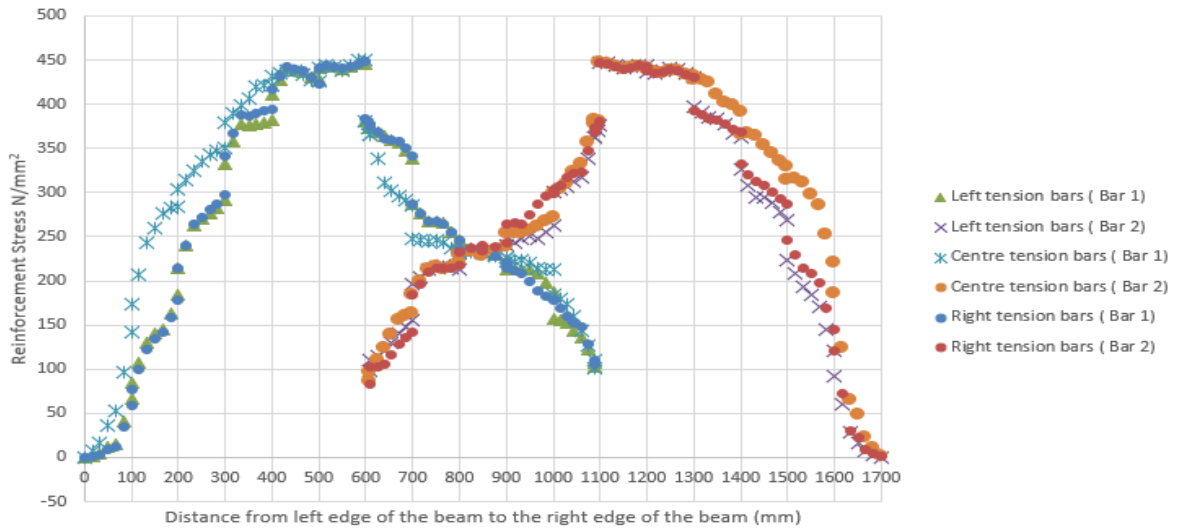
7.4.2 Ultimate lapped bar stresses

The ultimate lapped bar stress is believed to remain constant across the lap splice length, and the ultimate distribution of strain in the reinforcing is typically assumed to be linear. However, Figure 7.14 indicates that there were variations in lapped bar stress at collapse. Longitudinal cracking caused the strain of the reinforcing bar at the crack location to flatten, demonstrating that overall bond degeneration was greater near the transverse crack. Although the development of longitudinal cracks did not always lead to sample failure, failure was typically associated with the rapid spread of cracks along the lap splice length on the bottom and side faces of the concrete beam (see Figures 5.6 to 5.10). Despite the explosive nature of the collapse, significant chunks of concrete were prevented from flinging off the samples by shear links, which minimized spalling. The failure region was bounded at the lap ends by large transverse cracks, which spread simultaneously with the longitudinal cracks. Images of failed samples (Figures 5.6 to 5.10) demonstrate that the collapse was limited to a zone bordered by transverse cracks at the end of the laps.

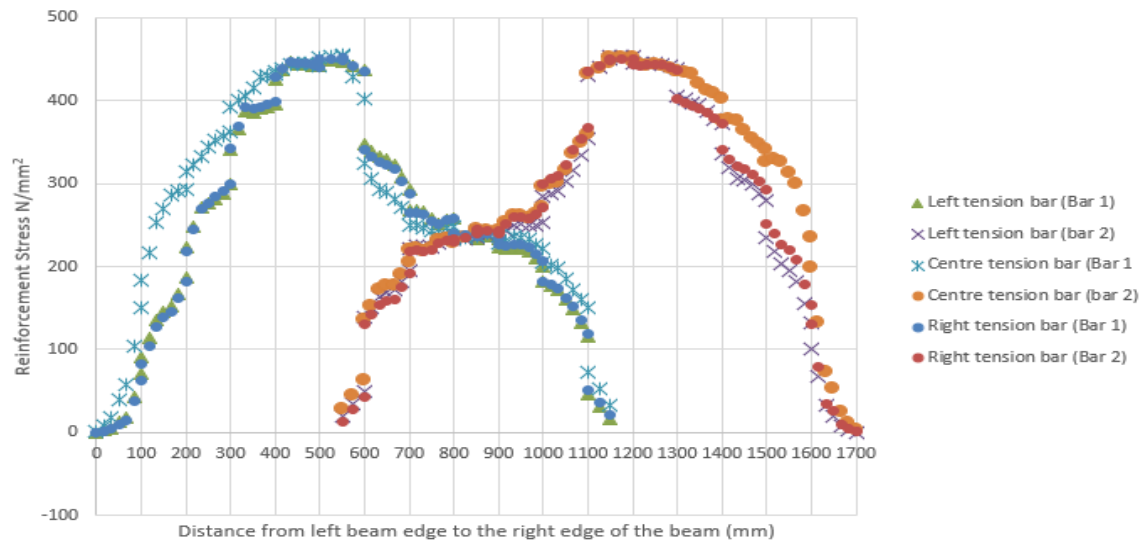
All tension bars 30Ø



All tension bars 40Ø



All tension bars 50Ø



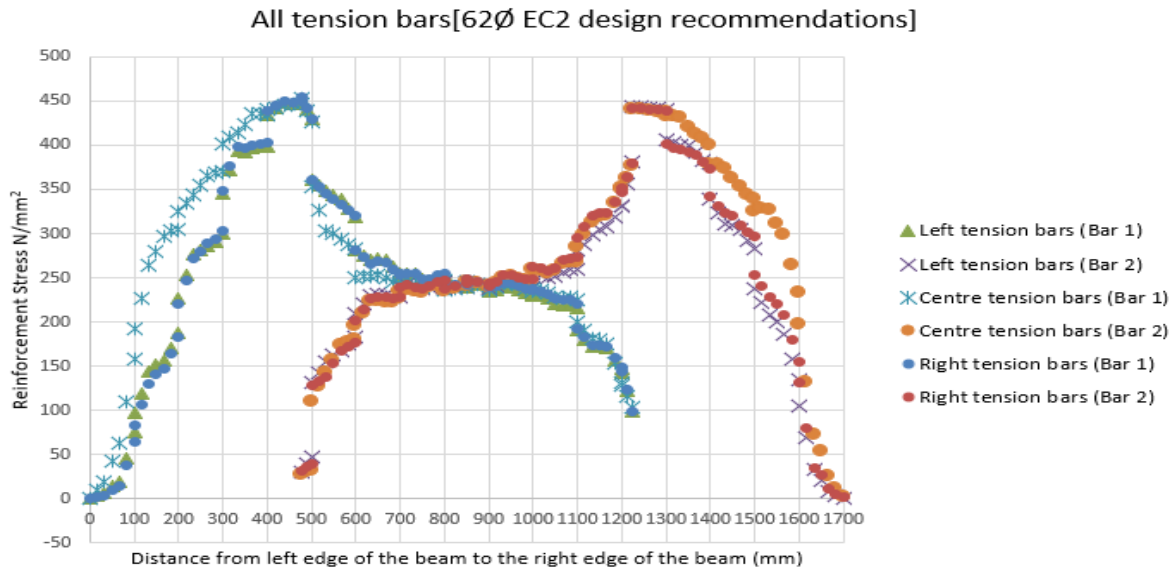


Figure 7.6. Reinforcement stress distribution sample 30Ø, 40Ø, 50Ø, and 62Ø [EC2] laps

7.5 Concluding remarks

This work presents comprehensive laboratory tests and examinations of the performance of both stainless and mild steel RC beams. Although there is limited performance information available in the current literature, the idea of substituting mild steel with stainless steel reinforcing bars to enhance robustness and durability is not new. The current design standard lacks a design guideline for tension members with lap splice, which prompted the present research to carry out laboratory tests to examine the major parameters. The study reports the findings of seven beam experiments, five of which employed mild steel rebars and two of which used stainless steel reinforcement. Among the seven beams, five had a lap splice in the middle while the remaining two contained continuous reinforcing bars for comparison purposes. The test results, along with Eurocode 2 capacity estimations, were compared to the finite element simulation results.

The study found that the deformations of stainless steel reinforced concrete beams coinciding with 35% and 62% of the maximum bending moment were higher than those of mild steel reinforced concrete beams, which was expected due to steel rebars' excellent ductility and the greater moments obtained from the stainless steel reinforced concrete beams. RC members with mild steel reinforcing bars are expected to deform less than those with stainless steel bars, since they endure less before the rebar ruptures.

8. Conclusions and Recommendations

8.1 Conclusion

In conclusion, this study successfully achieved its objectives, which were designed to address key aspects of lap joints in reinforced concrete beams. A critical review of existing literature provided a solid foundation of knowledge and identified gaps in the field, highlighting the need for further investigation. By developing a comprehensive methodology, various factors influencing lap joint performance were systematically considered, enabling a robust assessment of their effectiveness and reliability in practical applications.

The investigation into the impact of lap joint length on structural performance yielded valuable insights regarding ductility, load-carrying capacity, and failure modes. These findings contribute to the understanding of the relationship between lap joint length and optimal structural performance, thus offering recommendations for enhanced design practices.

Additionally, the investigation into the state of lap joint design in UK buildings, coupled with the potential implications of changes in design codes, provided valuable insights into prevailing approaches, challenges, and limitations faced by practitioners. This understanding is crucial for ensuring successful implementation of revised design codes and facilitating necessary adaptations in construction practices. The following are some of the key findings of Thesis.

- Three modes of failure were identified. “30 \emptyset ” laps, abruptly failed in bond before yielding of reinforcement. In “40 \emptyset ” laps, failed after the reinforcement yield and by bond in a brittle manner after considerable plastic deflection. Samples with “50 \emptyset and 62 \emptyset [EC2]” laps had a flexural failure. As a result, lengthening the lap from 50 \emptyset to 62 \emptyset (Eurocode 2 design lap length) results in increased ductility but not strength. The performance of 50 \emptyset laps was equivalent to that of the Eurocode 2 design lap length (62 \emptyset). Considering this in mind together with project cost, sustainability and reinforcement congestion associated with longer lap lengths, the current Eurocode 2 is not sustainable.

- The study's findings reveal that increasing lap splices beyond 50ϕ provides no additional benefit in terms of strength. Furthermore, specimens with larger concrete side covers exhibit higher splice stress compared to samples with smaller concrete covers, relative to the measured stress. The bond stress increases with an increase in concrete side cover and lap-length to bar-diameter ratio. For specimens with a similar lap-length to bar-diameter ratio, an increase in lap stress of 15% was observed when the side cover was increased from 1ϕ (26 mm) to 3ϕ (78 mm). Similarly, with a constant side cover, an increase in lap-length to bar diameter ratio from 60ϕ to 73.1ϕ resulted in a 3% increase in lap stress.
- The finding of the study demonstrates that the equation for estimating mean bar stress in laps as recommended by FIB Bulletin is less conservative than the equation recommended by Model Code 2020. Furthermore, reinforced concrete beams containing lap splices with higher levels of confinement exhibit comparable performance to those in which the lap splices were subjected to lighter confinement. Although increasing the confinement of the lap splice enhances its effectiveness, there exists a trade-off between using more steel to increase lap length and using steel to increase the number of shear links.
- The beams with a higher lap length-to-bar diameter ratio showed higher peak loads, as expected. However, an interesting observation was that the beams with a higher lap length also exhibited greater ductility at maximum load. This can be attributed to the decrease in the rates of strain and stress in the reinforcing bars as the lap splice length increases, resulting in a less ductile behaviour and underutilization of strain hardening in the stainless-steel reinforcing bars.
- The laboratory experiments showed that 30ϕ lap splices for both mild and stainless steel failed at lesser loads compared to samples with longer lap lengths, demonstrating that lap strength is directly proportional to its splice length. Three modes of failure were identified, with the 30ϕ laps abruptly failing in bond before yielding of reinforcement, the 40ϕ laps failing after the reinforcement yield and by bond in a brittle manner after considerable plastic deflection, and the 50ϕ and 62ϕ [EC2] laps having a flexural failure.

- Although increasing the lap-length to bar-diameter ratio leads to a decrease in the lap stress measured during the test, the measured lap stress shows an increase with an increase in the lap length to bar-diameter ratio.
- In general, higher levels of confinement lead to increased effectiveness of lap splices. However, increasing the strength of the splice by adding more shear links is not a sustainable or cost-effective solution since it requires the use of additional steel.
- The findings revealed that the maximum moment and bending capacity of stainless steel beams with lap splices was 5% and 25% higher than that of mild steel beams with lap splices. This can be attributed to the superior ductility and significant strain hardening of the stainless-steel rebar.
- Finite element is a reliable technique for determining the strain distribution in longitudinal bars. It provides accurate and detailed information of the lap joint behaviour.
- The 30Ø lap splices for both mild and stainless steel failed at lesser loads compared to samples with longer lap lengths. These experiments demonstrated that lap strength is directly proportional to its splice length.
- As the lap length to bar diameter ratio increased, the strain distributions became less symmetrical.
- The nature of the strain distribution at the end of the lap is heavily influenced by the value of the reinforcing bar strain at the crack.
- There is sufficient ductility at the ends of the lapped section (50Ø & 62Ø samples) for rotation to occur, thus, allowing the ultimate plastic hinges to occur at the lap ends.
- Transverse crack development in the concrete significantly altered the distribution of steel strains, with the highest observed at the crack locations.
- The distributions of strain in the lap region appeared to get increasingly linear as the failure load neared, however, the maximum bond stress distributions still exist at the lap ends.

- The strain in the reinforcement suggests that in “50 ϕ and 62 ϕ [EC2]” laps, the middle zone of the splice does not significantly contribute to transfers of force between the reinforcing bars. Based on the analysis conducted, it was observed that increasing the lap splices beyond 50 ϕ has no additional benefit for increasing its strength.
- Transverse cracks development in the concrete significantly altered the rebar strain distribution. The strains were observed to be maximum at the location of the crack.
- Lapped bar strain and force are directly proportional to the increase in lap length-to-bar diameter ratio. These trends were observed during the tests.
- Outside the lap joint, zones of constant rebar strain existed before the development of the crack. The rebar strain was identical when cracks formed outside the lap length.
- In most of the specimens, there were negligible strain gradients and stress in the lapped bars before the development of cracks. Bond stresses were present at the end of the lap splice, where the strains abruptly decreased to zero.
- The results of the analysis indicated that beams with smaller shear link spacing exhibited greater lapped bar stress compared to those with larger link spacing.
- It is not advisable to exceed a lap length of 50 times the diameter of the reinforcing bars because doing so may impede the pouring and vibrating of concrete, leading to the formation of air bubbles that could negatively impact the quality and performance of the construction. In addition, elongating the lapping length of the reinforcing bars can result in congestion of the bars and increased construction expenses.
- Failure in the steel-concrete bond was only found at the lap ends of the splice, with a discontinuity in reinforcing bar stiffness leading to a greater level of strain outside of the lap splice length.
- The ductility at maximum load was larger in the case of beams with higher lap length. This is because as the lap splice length is increased, the rates of strain and

stress in the reinforcing bars decrease, causing the behaviour to become less ductile, and strain hardening in the stainless-steel reinforcing bars to be underutilised.

8.2 Suggestions for future studies

This PhD study investigated the ductility of lap splices in reinforced concrete beams lapped at the same section, addressing issues identified in the construction industry related to the construction challenges like sustainability implications, cost, and congestion of reinforcement. The research contributed significantly by filling gaps in knowledge, such as the current state of lap design in the UK buildings, the impact of lap joints' length on structural performance under ultimate load, establishing recommendations on minimum lap length, exploring the impact of various factors on structural performance and the potential impact of existing regulations on lap joints' design. Other areas of reinforced concrete structures that need additional research and improvement, including the following criteria:

- The author's tests were conducted under monotonic loading. It has been discovered that the widths of cracks at the ends of overlaps, which are subjected to cyclic loads, are dependent on the length of the overlap, as the bond strength weakens under such load. Consequently, it is essential to examine the impact of fatigue loads on the necessary bond length. By conducting such an investigation, it would be possible to determine whether additional reinforcement or an increased overlap length, would be more effective in controlling cracks under cyclic loads.
- This thesis did not provide a discussion on the impact of weak bond conditions. To establish reduction factors for the strength of lapping in the next iteration of Eurocode 2, a more in-depth review of this effect is recommended.

9. References

- ACI committee 318 (2011) Building Code Requirements for Structural Concrete and Commentary (ACI 318M-11), American Concrete Institute, Farmington Hills, MI.
- ACI Committee 408 (2003) ACI 408R-03 Bond and Development of Straight Reinforcing Bars in Tension, American Concrete Institute.
- Ali, K. and Hamed, D. (2020) 'Cyclic performance of RC beam-column joints with mechanical or forging (GPW) splices; an experimental study', Science Direct, 28, pp. 2562-2571. doi: <https://doi.org/10.1016/j.istruc.2020.10.071>.
- Amin, R. (2009) 'End Anchorage at Simple Supports in Reinforced Concrete', London South Bank University.
- Anwar H. and Khandaker M. (2008) 'Bond characteristics of plain and deformed bars in lightweight pumice concrete', Construction and Building Materials, 22(7). doi: 10.1016/j.conbuildmat.2007.03.025.
- ASTM A944-10 (2015) 'Standard Test Method for Comparing Bond Strength of Steel Reinforcing Bars to Concrete Using Beam-end Specimens', ASTM International, i(Reapproved 2015).
- Azizinamini, A. et al. (1993) 'Bond Performance of Reinforcing Bars Embedded in High-Strength Concrete', ACI Structural Journal, 90(5), pp. 553-561.
- Azizinamini, A., Konkankar, U.S. and Fu, Y.C. (1995) 'Tension Development Length of Reinforcing Bars Embedded in High-Strength Concrete', Engineering Structures, 90(5), pp. 554-561.
- Bamonte, P., Coronelli, D. and Gambarova, P. (2002) 'Size effect in high bond bars', in International Conference on Bond in Concrete, Budapest.
- Bompa, D. and Elghazouli, A. (2018) 'Monotonic and cyclic performance of threaded reinforcement splices', Structures. Elsevier, 2018.

Bournas, D.A. and Triantafillou, T.C. (2011) "Bond strength of lap-spliced bars in concrete confined with composite Jackets," *Journal of Composites for Construction*, 15(2), pp. 156–167. doi:10.1061/(ASCE)CC.1943-5614.0000078.

BS EN 1992-1-1 (2004) "Eurocode 2: Design of concrete structures - Part 1-1 : General rules and rules for buildings," British Standards Institution, 1(2004), p. 230. doi:[Authority: The European Union Per Regulation 305/2011, Directive 98/34/EC, Directive 2004/18/EC].

BSI (2008) "Eurocode 2 : design of concrete structures : British standard," British Standards Institution [Preprint].

BURKHARDT, C.J. (2000) *Zum Tragverhalten von Übergreifungsstößen in hochfestem Beton*. Aachen University.

Cairns, J. (2013) "Lap splices of bars in bundles," *ACI Structural Journal*, 110(2), pp. 183–191. doi:10.14359/51684399.

Cairns, J. (2014) "Staggered lap joints for tension reinforcement," *Structural Concrete*, 15(1), pp. 45–54. doi:10.1002/suco.201300041.

Cairns, J. (2016) "An evaluation of EC2 rules for design of compression lap joints," *Structures*, 5, pp. 35–43. doi:10.1016/j.istruc.2015.07.004.

Cairns, J. and Abdullah, R. (1995) "An evaluation of bond pull-out tests and their relevance to structural performance," *Journal of The Institution of Structural Engineers*, 73(11), pp. 179–185.

Cairns, J. and Eligehausen, R. (2014) "An evaluation of EC2 rules for design of tension lap joints'," *The Institution of Structural Engineers*, p. 9.

Cairns, J. and Jones, K. (1996) "An Evaluation of The Bond Splitting Action of Ribbed Bars'," *American Concrete Institute Materials Journal.*, 93(1), pp. 10–19.

Cairns, J. and Jones, K. (1997) "Influence of rib geometry on strength of lapped joints: An experimental and analytical study," *Magazine of Concrete Research*, 49(180), pp. 259–262.

Cairns, J. and Jones, K. (2012) "The splitting forces generated by bond'," *Magazine of Concrete Research*, 47(171), pp. 153–165.

- Cairns, J. and Plizzari, G.A. (2003) "Towards a harmonised European bond test," *Materials and Structures/Materiaux et Constructions*, 36(262), pp. 498–506. doi:10.1617/13887.
- Canbay, E. and Frosch, R.J. (2005) 'Bond strength of lap-spliced bars,' *ACI Structural Journal*, 102(4), pp. 605–614. doi: 10.14359/14565.
- CEB. (1982) 'Bond Action and Bond Behaviour of Reinforcement. State of the Art Report,' in *Bulletin d'Information No. 151*. Paris.
- Chen, H. et al. (2019) 'Parametric study on the non-contact splices at drilled shaft to bridge column interface based on multiscale modeling approach,' *Engineering Structures*, 180, pp. 400–418.
- Chinn James Phil M., Ferguson Phil M., and Thompson J Neils. (1955) 'Lapped Splices in Reinforced Concrete Beams,' *ACI Journal Proceedings*, 52(10), pp. 201–213. doi: 10.14359/11597.
- Chu, S.H. and Kwan, A.K.H. (2018) 'A new method for pull out test of reinforcing bars in plain and fibre reinforced concrete,' *Engineering Structures*, 164(September 2017), pp. 82–91. doi: 10.1016/j.engstruct.2018.02.080.
- CIBFIP. (1991) *CEB-FIP model code 1990: design code*, *Bulletin d'Information*. London: Thomas Telford Services Ltd.
- Dahal P.K and Tazarv M. (2020) 'Mechanical bar splices for incorporation in plastic hinge regions of RC members,' *Construction and Building Materials*, 258, pp. 120–308.
- Darwin, D. et al. (1996) 'Development Length Criteria for Conventional and High Relative Rib Area Reinforcing Bars,' *ACI Structural Journal*, 93(3), pp. 512–516.
- Einea, A., Yehia, S. and Tadros, M.K. (1999) 'Lap splices in confined concrete,' *Structural Journal*, 86(6), pp. 947–955.
- ELIGEHAUSEN, R. (1979) 'Übergreifungsstöße zugbeanspruchter Rippenstäbe mit geraden Stabenden,' *Wilhelm Ernst & Sohn*. Berlin.
- Eligehausen, R., Popov, E. and Bertero, V. (1983) 'Local bond stress-slip relationship of deformed bars under generalized excitations,' *California*.

ELIGEHAUSEN, R., POPOV, E.P. and BERTERO, V. v. (1983) 'Local Bond Stress-Slip Relationships of Deformed Bars under Generalized Excitations,' California.

Esfahani, M. and Reza Kianoush, M. (2005) 'Development/Splice Length of Reinforcing Bars,' ACI Structural Journal, 102(1).

Feldman, L.R. and Cairns, J. (2017) 'Assessing historical provisions for bond of plain bars,' ACI Materials Journal, 114(2), pp. 463–473. doi: 10.14359/51689163.

Ferguson, P. and Breen, J. (1965) 'Lapped Splices for High Strength Reinforcing Bars,' ACI Journal Proceedings [Preprint]. doi: 10.14359/7738.

Ferguson, P.M. and Briceno, E.A. (1969) 'Tensile lap splices part 1: Retaining wall type varying moment zone', Centre for Highway Research, No. 113-2, Texas.

Fib Bulletin (2013) 'fib Model Code for Concrete Structures 2010', Wiley, doi: 10.1002/9783433604090.

Fib Bulletin 72 (2014) 'Bond and anchorage of embedded reinforcement: Background to the fib Model Code for Concrete Structures 2010', Lausanne, Switzerland.

Jukka, Haavisto, Hekki Alho and Anssi Laaksonen (2023). Behavior of lap splices in reinforced concrete beams after bar yielding. Structural concrete, <https://doi.org/10.1002/suco.202200501>

Goksu C. et al. (2014) 'The effect of lap splice length on the cyclic lateral load behaviour of RC members with low-strength concrete and plain bars', Advances in Structural Engineering, 16(5), pp. 639-658.

Hamad, B.S., Najjar, S.S. and Jumma G.K. (2003) 'Correlation between Roles of Transverse Reinforcement and Steel Fibres in Confining Tension Lap Splices in High-Strength Concrete', ACI Structural Journal, 100, pp. 19-24.

Hassan, M.N. and Feldman, L.R. (2012) 'Behaviours of Lap-Spliced plain steel bars', ACI Structural Journal, 109(2), pp. 235-244. doi:10.14359/51683634.

Hassan, T.K., Lucier, G.W. and Rizkalla, S.H. (2012) 'Splice strength of large diameter, high strength steel reinforcing bars', Construction and Building Materials, 26(1), pp. 216-225.

Hegger, J., Empelmann, M. and Schnell, J. (2015) 'Weiterentwicklung von Bemessungs- und Konstruktionsregeln bei großen Stabdurchmessern', Aachen.

Hwang, H.J., Park, H.G. and Yi, W.J. (2017) 'Nonuniform bond stress distribution model for evaluation of bar development length', *ACI Structural Journal*, 114(4), pp. 839-849. doi:10.14359/51689446.

Schoening, J.C. (2018) 'Anchorages and Laps in Reinforced Concrete Members under Monotonic Loading', Rheinisch-Westfälische Technische Hochschule Aachen.

Jiang, T., Xie, Y., Fang, X., Ma, C. and Zhang, J. (2020) 'Three-Dimensional Nonlinear Finite Element Modeling for Bond Performance of Ribbed Steel Bars in Concrete Under Lateral Tensions', *International Journal of Civil Engineering*, 18(5). doi:10.1007/s40999-019-00488-1.

Jirsa, J.O., Chen, W., Grant, D.B. and E. (1995) Development of bundled reinforcing steel. Austin Texas.

Karabinis, A.I. (2014) "Reinforced concrete beam-column joints with lap splices under cyclic loading," *Structural Engineering and Mechanics*, 14(6), pp. 649–660.

Kheyroddin, A., Ramezani-pour, A.A. and Sharbatdar, M.K. (2020) "Experimental investigation of using mechanical splices on the cyclic performance of RC columns," *Structures*, 24, pp. 717–727.

Kim, C.G., Park, H.G. and Eom, T.S. (2019) "Effects of type of bar lap splice on reinforced concrete columns subjected to cyclic loading," *ACI Structural Journal*, 116(2), pp. 183–194. doi:10.14359/51711142.

Kim, D.J., Lee, H.K. and Ryu, G.S. (2013) "Bond strength of steel deformed rebars embedded in artificial lightweight aggregate concrete," *Journal of Adhesion Science and Technology*, 27(5–6), pp. 495–506. doi:10.1080/01694243.2012.687552.

Kreller, H. (1989) On the nonlinear load bearing and deformation behaviour of reinforced concrete bar structures under the influence of load and force. University of Stuttgart.

- Lagier, F., Massicotte, B. and Charron, J.P. (2015) "Bond strength of tension lap splice specimens in UHPFRC," *Construction and Building Materials*, 93, pp. 660–668. doi:10.1016/j.conbuildmat.2015.05.009.
- Lee, C.S. and Han, S.W. (2019) "Cyclic behaviour of lightly-reinforced concrete columns with short lap splices subjected to unidirectional and bidirectional loadings," *Engineering Structures*, 189, pp. 373–384. doi:10.1016/j.engstruct.2019.03.022.
- LeRoy, A.L. and Gergely, G. (1967) "Mechanics of Bond and Slip of Deformed Bars in Concrete," *ACI Journal Proceedings*, 64(11), pp. 719–728. doi:10.14359/7600.
- Lundgren, K. (2005) "Bond between ribbed bars and concrete. Part 1: Modified model," *Magazine of Concrete Research*, 57(7), pp. 371–382. doi:10.1680/mac.2005.57.7.371.
- Lundgren, K. and Gylltoft, K. (2000) "A model for the bond between concrete and reinforcement," *Magazine of Concrete Research*, 52(1), pp. 53–63. doi:10.1680/mac.2000.52.1.53.
- Mabrouk, R.T.S. and Mounir, A. (2018) "Behavior of RC beams with tension lap splices confined with transverse reinforcement using different types of concrete under pure bending," *Alexandria Engineering Journal*, 57(3), pp. 1727–1740. doi:10.1016/j.aej.2017.05.001.
- Maekawa, K. and Okamura, H. (2003) *Non-Linear Mechanics of Reinforced Concrete*. Taylor & Francis.
- Magnusson, J. (2000) 'Bond and anchorage of ribbed bars in high-strength concrete', Chalmers University, Göteborg, Sweden.
- Masud, M. (2020) 'Performance of non-contact lap splices in geometrically dissimilar bridge column to drilled shaft connections', *Engineering Structures*, 209, pp. 110258. doi: 10.1016/j.engstruct.2020.110258.
- Metelli, G., Cairns, J. and Plizzari, G. (2015) 'The influence of percentage of bars lapped on performance of splices', *Materials and Structures/Materiaux et Constructions*, 48(9), pp. 2983-2996. doi: 10.1617/s11527-014-0371-y.

Metelli G, Marchina E, Plizzari GA (2022). Effects of the position of confining transverse links on lap strength. *Struct Concr.* **23**(5), pp. 2928– 41. <https://doi.org/10.1002/suco.202100642>

Micallef, M. and Vollum, R. (2017) 'The Effect of Shear and Lap Arrangement on Reinforcement Lap Strength', *Structures*, 12, pp. 253-264. doi: 10.1016/j.istruc.2017.09.004.

Micallef, M. and Vollum, R.L. (2018) 'The behaviour of long tension reinforcement laps', *Magazine of Concrete Research*, 70(14), pp. 739-755. doi: 10.1680/jmacr.17.00285.

Mousa, M.I. (2015) 'Flexural behaviour and ductility of high strength concrete (HSC) beams with tension lap splice', *Alexandria Engineering Journal*, 54(3), pp. 551-563.

Najafgholipour, M.A. et al. (2018) 'The performance of lap splices in RC beams under inelastic reversed cyclic loading', *Structures*, 15, pp. 167-181. doi: 10.1016/j.istruc.2018.07.011.

Nawaz, W. and Yehia, M. (2020) 'Lap splices in confined self-compacting lightweight concrete', *Construction and Building Materials*, 263, pp. 120580. doi: 10.1016/j.conbuildmat.2020.120580.

Orangun, C.O., Jirsa, J.O. and Breen, J.E. (1977) 'A Reevaluation of Test Data on Development Length and Splices', *ACI Journal Proceedings*, 74(3), pp. 114-122.

Plizzari G.A, Deldossi M.A and Massimo, S. (1998) 'Transverse reinforcement effects on anchored deformed bars', *Magazine of Concrete Research*, 50(2), pp. 161-177.

PT.SC2.T1 (2018) PTI working draft prEN 1992-1-1:2018. European Committee for Standardization. European Committee for Standardization; CEN, European Committee for Standardization.

Radovanović, M. (2019) 'Quality control of rebar couplers in splicing of reinforcement bars', in 13th IQC International Quality Conference, pp. 569-579.

REHM, G. and MARTIN, H. (1968) 'On the question of crack limitation in reinforced concrete construction', *Concrete and Reinforced Concrete Construction*, 63(8), pp. 175-182.

Reynolds, G. and Beeby, A.W. (1982) 'Bond in Concrete', in *Proceedings of the International Conference on Bond in Concrete*. London: Applied Science Publishers, pp. 434-445.

Rezaiee-Pajand, M., Karimipour, A. and Abad, J.M.N. (2021) 'Crack Spacing Prediction of Fibre-Reinforced Concrete Beams with Lap-Spliced Bars by Machine Learning Models', Iranian Journal of Science and Technology - Transactions of Civil Engineering, 45(2), doi: 10.1007/s40996-020-00441-6.

Rezansoff, T., Konkankar, U.S. and Fu, Y.C. (1992) 'Bond Performance of Reinforcing Bars Embedded in High-Strength Concrete', Canadian Journal of Civil Engineering, 19, pp. 447–453.

RILEM TC (1983) 'RC 6 Bond test for reinforcement steel', doi: 10.1617/2351580117.081.

Russo, G. and Pauletta, M. (2006) 'A simple method for evaluating the maximum slip of anchorages', Materials and Structures/Materiaux et Constructions, 39(289), pp. 533–546, doi: 10.1617/s11527-006-9092-1.

Sakurada T, Morohashi, N. and Tanaka, R. (1993) 'Effect of Transverse Reinforcement on Bond Splitting Strength of Lap Splices', Transactions of the Japan Concrete Institute, 15, pp. 573–580.

Schenkel, M. (1998) On the composite behaviour of reinforcement with small concrete cover.

ETH Zurich. Selby, R. G., Vecchio, F. and Collins, M. P. (1996) "Analysis of reinforced concrete elements subject to shear and axial compression," ACI Structural Journal, 96(3), pp. 572–582.

Skorobogatov, S. M. and Edwards, A. D. (1979) "INFLUENCE OF THE GEOMETRY OF DEFORMED STEEL BARS ON THEIR BOND STRENGTH IN CONCRETE," Proc Inst Civ Eng (London), 67(pt 2). doi:10.1680/iicep.1979.2460.

Sozen, M. A. and Moehle, J. P. (1990) Development and Lap-Splice Lengths for Deformed Reinforcing Bars in Concrete, The Portland Cement Association & The Concrete Reinforcing Steel Institute.

Steuck, K. P., Scott, B. D., and Veyera, G. E. (2007) Anchorage of large diameter reinforcing bars grouted into ducts. Washington.

Sturm, A. B. and Visintin, P. (2019) "Local bond slip behavior of steel reinforcing bars embedded in ultra-high performance fibre reinforced concrete," *Structural Concrete*, 20(1). doi:10.1002/suco.201700149.

Tarabia, A. M., Hassan, M. A., and Awad, M. A. (2016) "Performance of RC slabs with lap splices using headed bars," *Alexandria Engineering Journal*, 55(3), pp. 2729–2740.

Tarquini, D., de Almeida, J. P., and Beyer, K. (2019) "Experimental investigation on the deformation capacity of lap splices under cyclic loading," *Bulletin of Earthquake Engineering*, 17(12). doi:10.1007/s10518-019-00692-3.

Tastani, S. P. and Pantazopoulou, S. J. (2002) "Experimental Evaluation of The Direct Tension Pull-out Bond Test," in *Conference Bond in Concrete*. Budapest: Proc. Int.

Tastani, S. P. and Pantazopoulou, S. J. (2010) "Direct tension pull-out bond test: Experimental results," *Journal of Structural Engineering*, 136(6), pp. 731–743. doi:10.1061/(ASCE)ST.1943-541X.0000159.

Tazarv, M., & Saiidi, M.S. (2016). Seismic design of bridge columns incorporating mechanical bar splices in plastic hinge regions. *Engineering Structures*, 124, 507–520.

Tepfers, R. (1973). A theory of bond applied to overlapped tensile reinforcement splices for deformed bars (PhD Thesis). Chalmers University of Technology, Sweden.

Tepfers, R. (1980). Bond stress along lapped reinforcing bars. *Magazine of Concrete Research*, 32(112), 135–142. doi:10.1680/macr.1980.32.112.135.

Test Procedure to Determine Relative Bond Value of Reinforcing Bars (ACI 208-58). (1958). *ACI Journal Proceedings*, 55(7), 1523-1524. doi:10.14359/11256.

TG4.5, F. (2014). Bond and anchorage of embedded reinforcement: Background to the fib Model Code for Concrete Structures 2010.

Turk K, Bassurucu M. An investigation on the effect of hybrid fiber reinforced on the flexural behavior of RC beams having different lap-spliced lengths (2022). *Struct Concr.*; 1– 13. <https://doi.org/10.1002/suco.202200106>

Vecchio, F.J., & Collins, M.P. (1986). The modified compression field theory for reinforced concrete elements subjected to shear. *ACI Structural Journal*, 83(4), 219–231.

Version, L. (2014). Modeller Reference Manual. Lusas. (2).

Vitanov, V.I., & Collins, M.P. (1982). The response of reinforced concrete to in-plane shear and normal stresses (Report No. 82-03). University of Toronto, Department of Civil Engineering.

Viathanatepa, S., Popov, E.P., & Bertero, V.V. (1979). Effects of generalized loadings on bond of reinforcing bars embedded in confined concrete blocks. Earthquake Engineering Research Center, University of California, Berkeley.

WILDERMUTH, A. (2013) Investigations on the composite behaviour of reinforcing bars by means of simplified test specimens, DAfStb publication series. Berlin.

Yang, W., Yu, J. and Wang, Y. (2012) Study on the effect of bond-anchoring factor on bond behavior between deformed bar and shale ceramic concrete. In: Advanced Materials Research [online]. Available at: doi:10.4028/[www.scientific.net/AMR.403-408.444](https://doi.org/10.4028/www.scientific.net/AMR.403-408.444) [Accessed 19 March 2023].

Zuo, J. and Darwin, D. (2000) Splice strength of conventional and high relative rib area bars in normal and high-strength concrete. ACI Structural Journal, 97(4), pp. 630–641.

10. Appendix

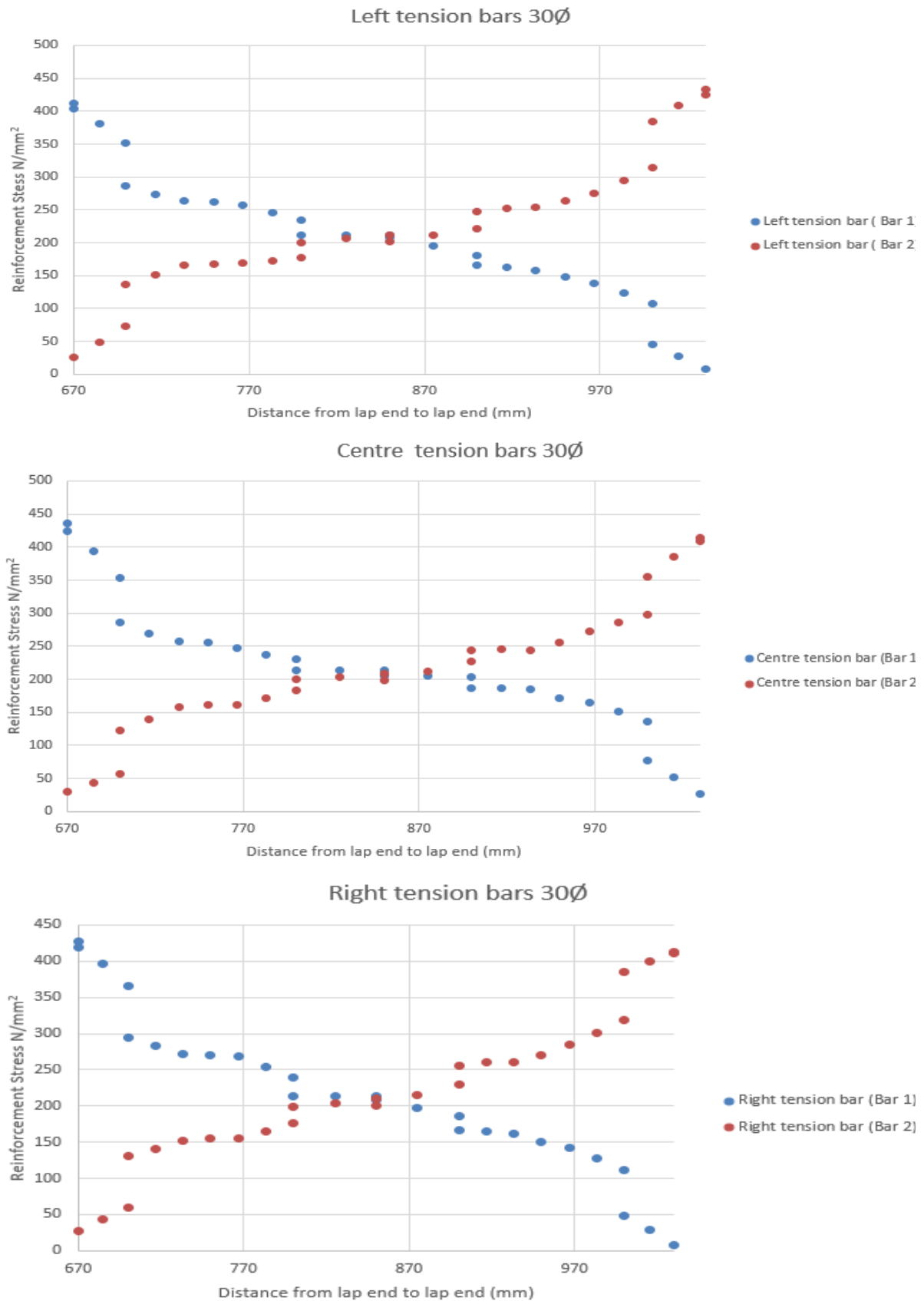


Figure 10.1. Rebar Strain Distribution Along Lap Specimen 40Ø

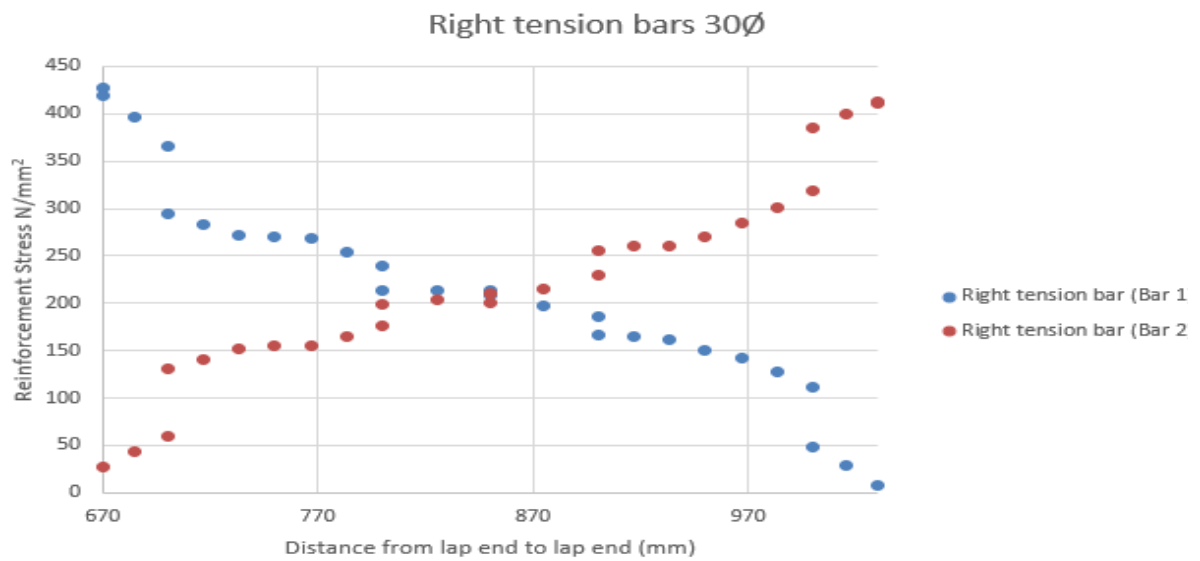
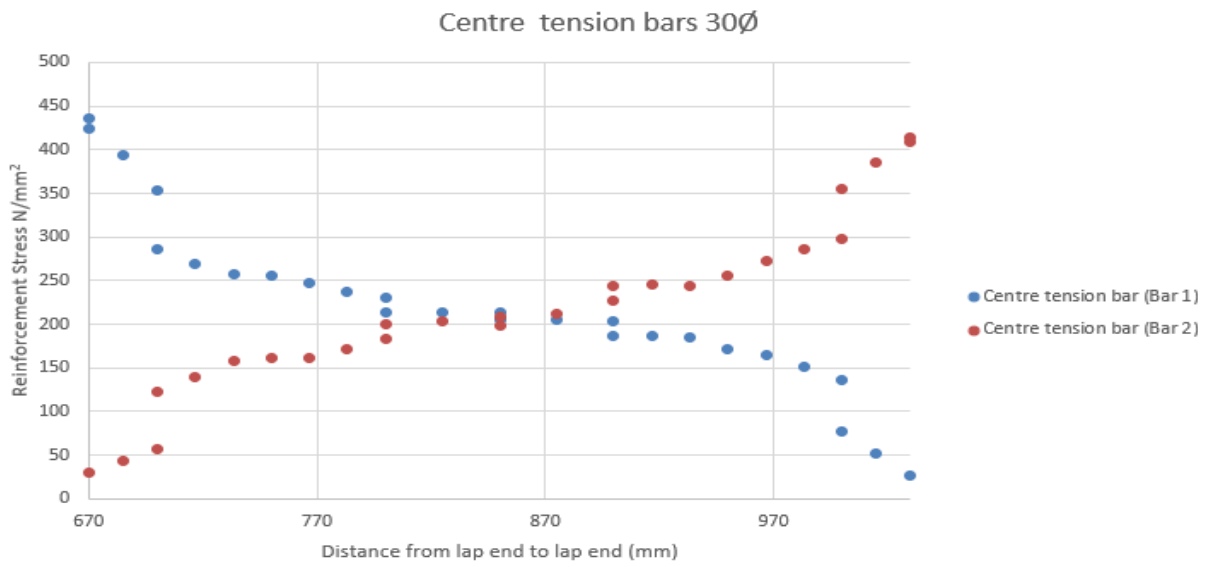
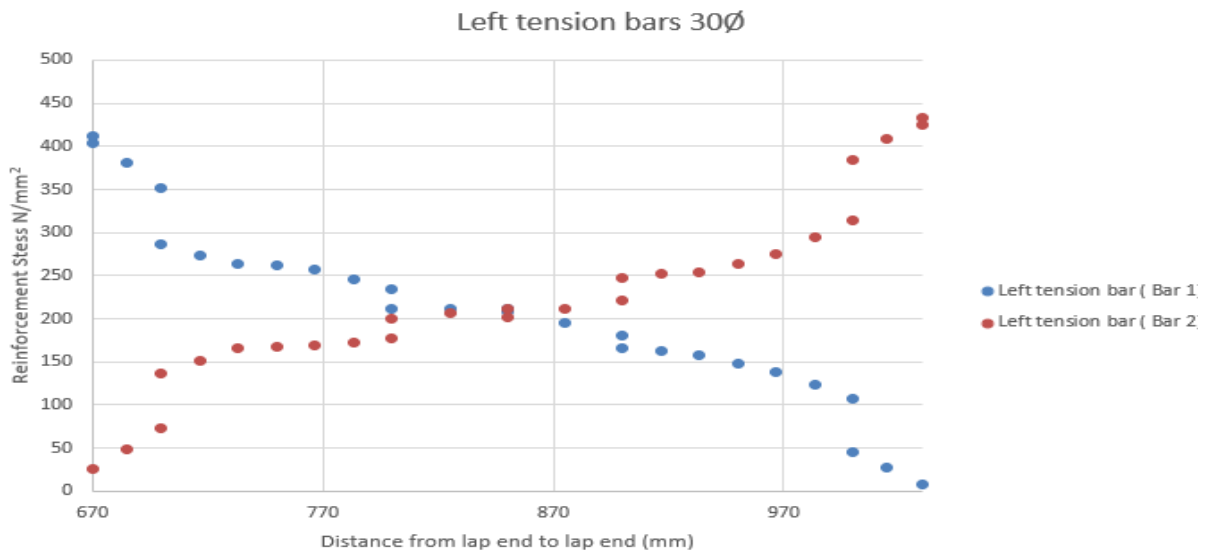


Figure 10.2. Rebar Stress Distribution Along Lap Specimen 30Ø

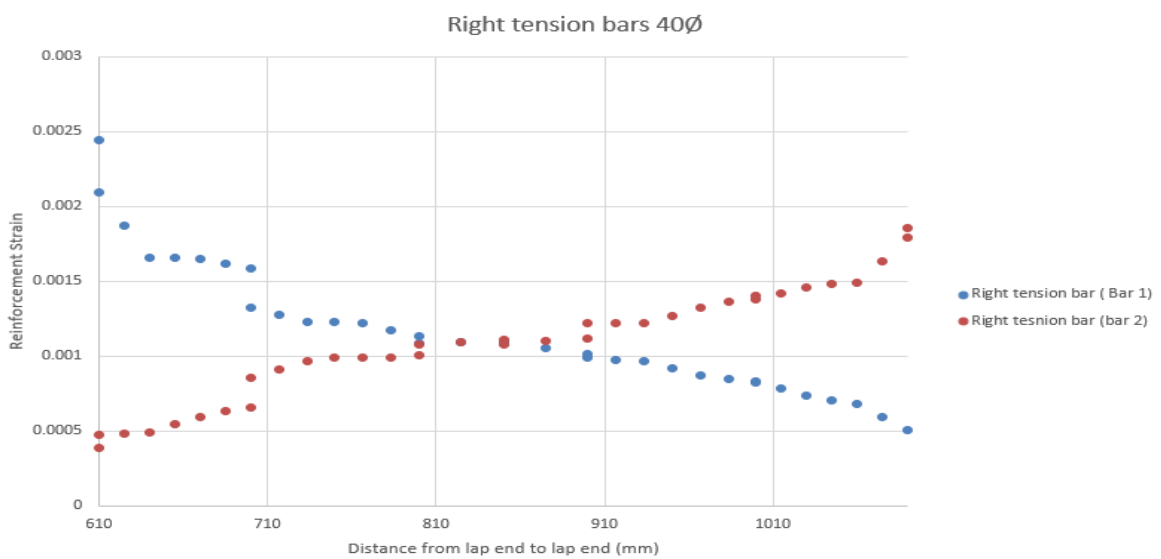
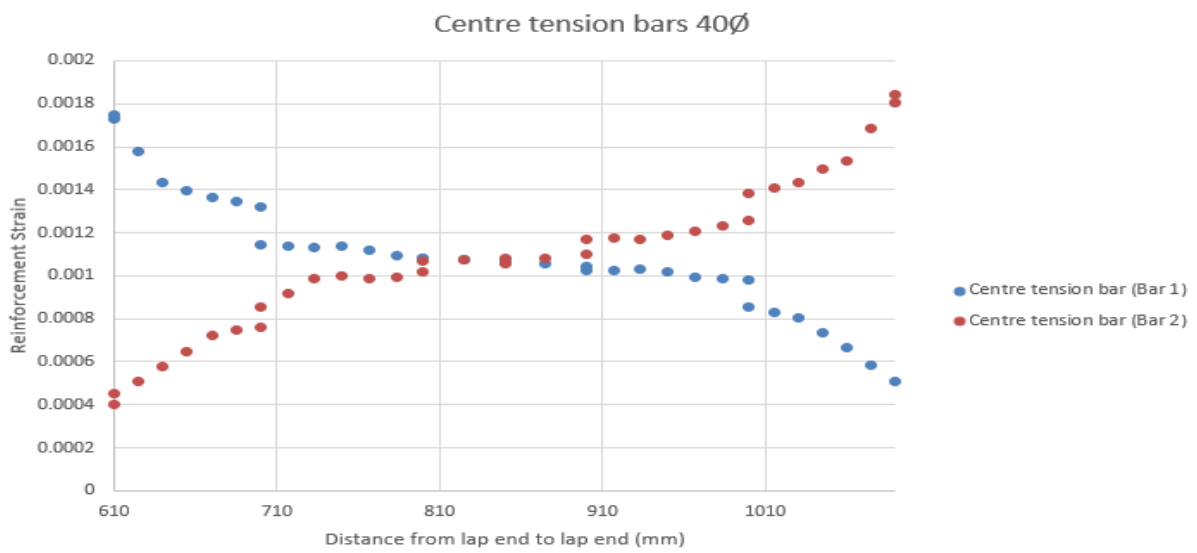
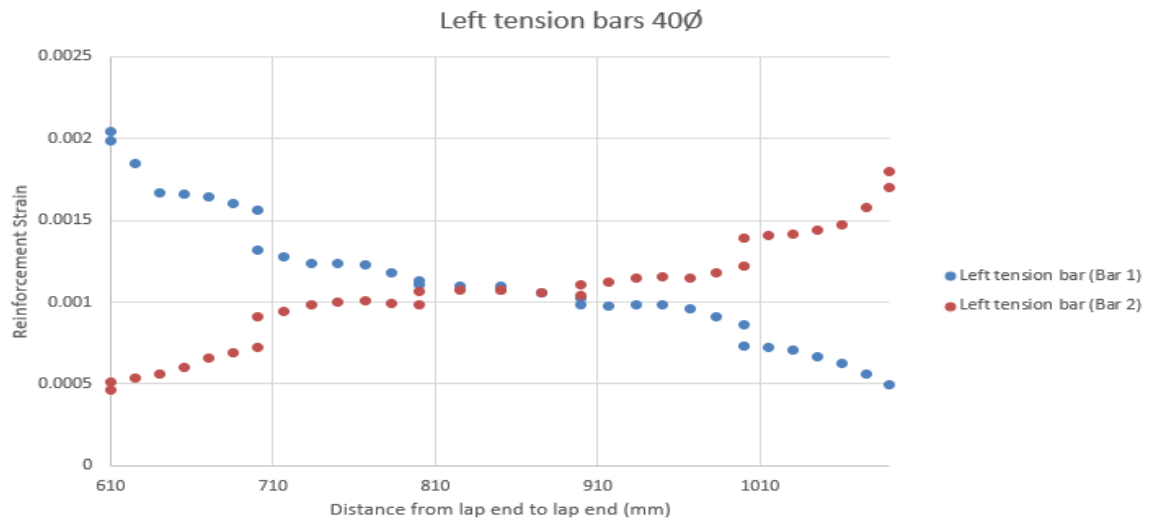
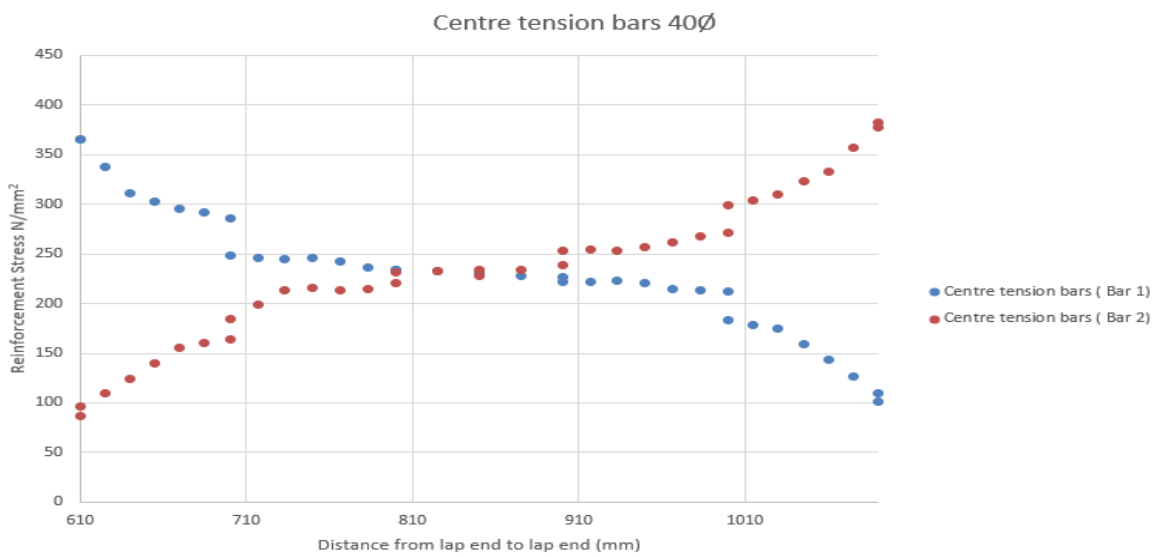
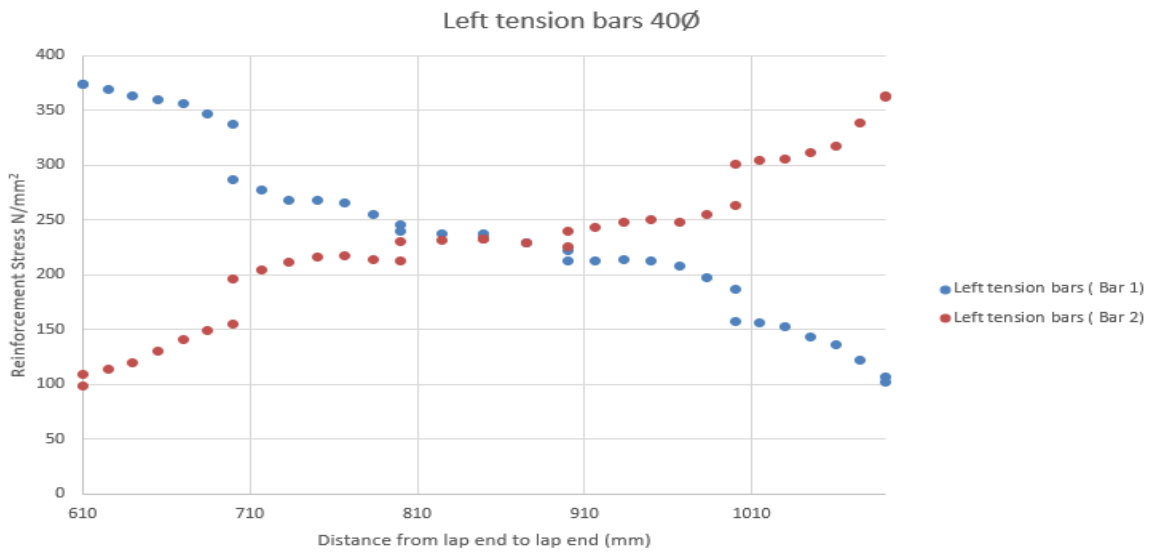


Figure 10.3. Rebar Strain Distribution Along Lap Specimen 40Ø



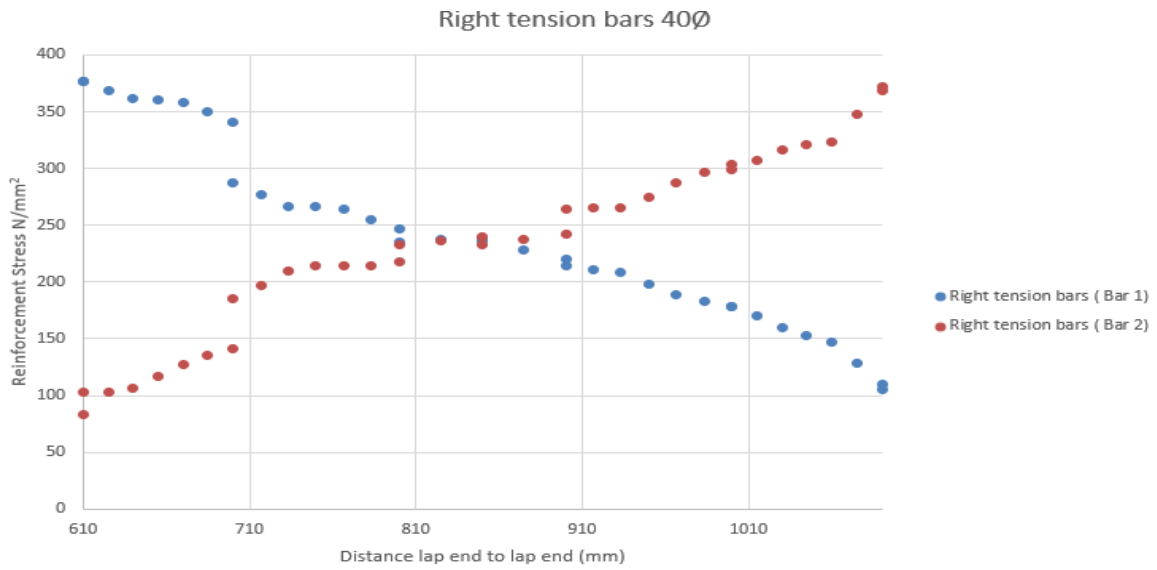
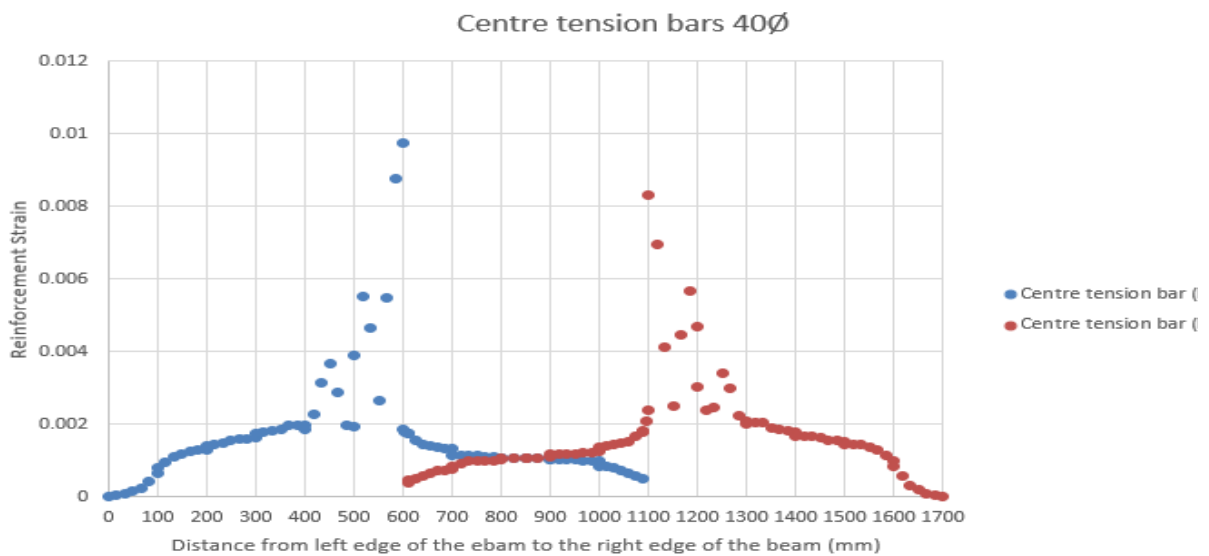
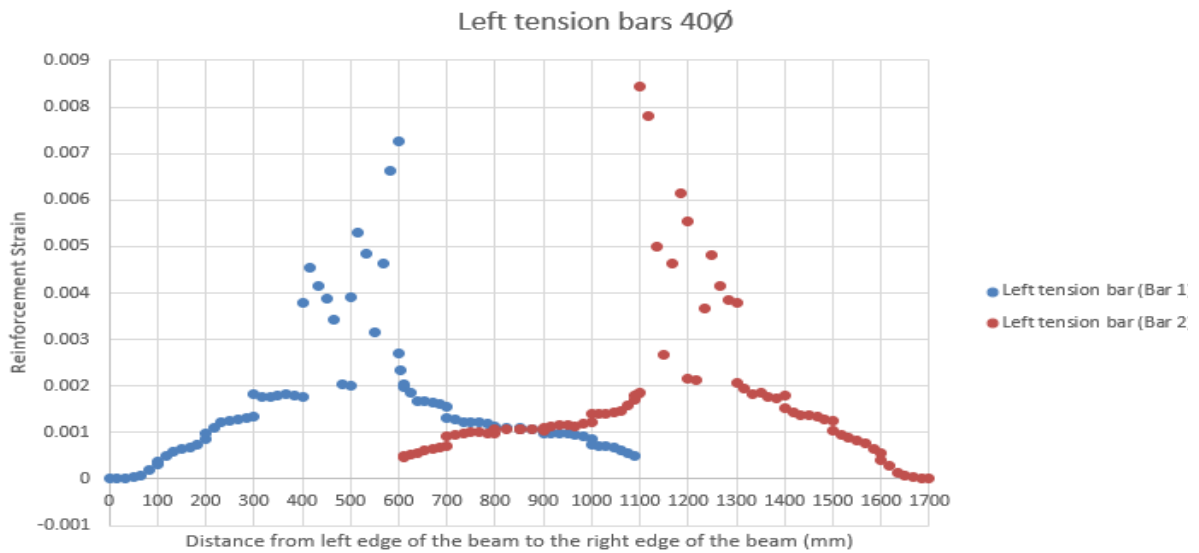


Figure 10.4. Rebar Stress Distribution Along Lap Specimen 40Ø



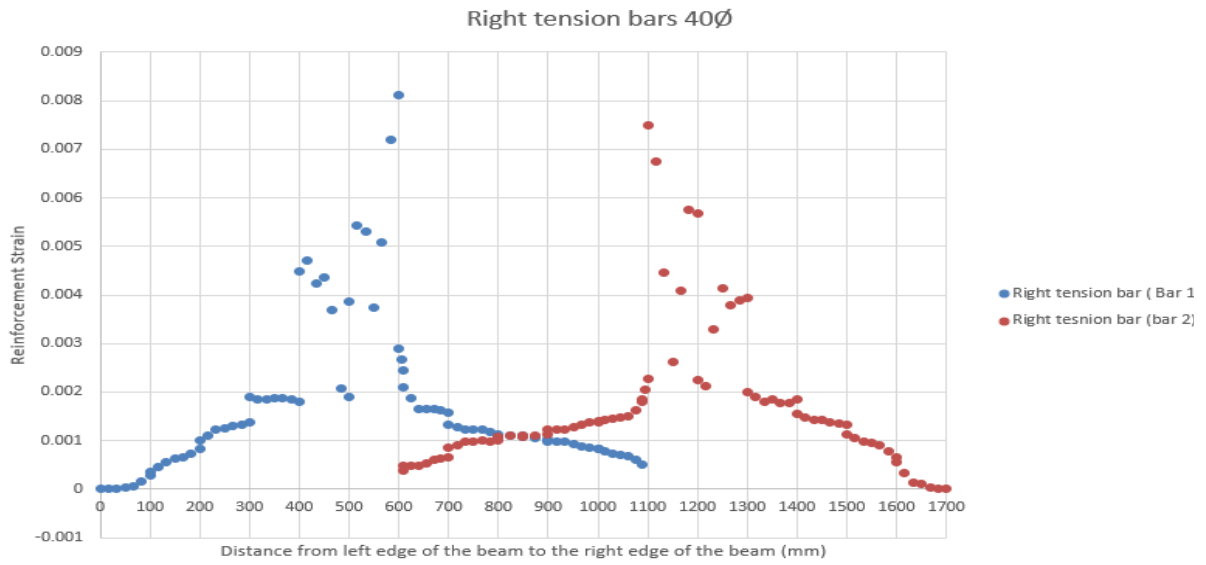
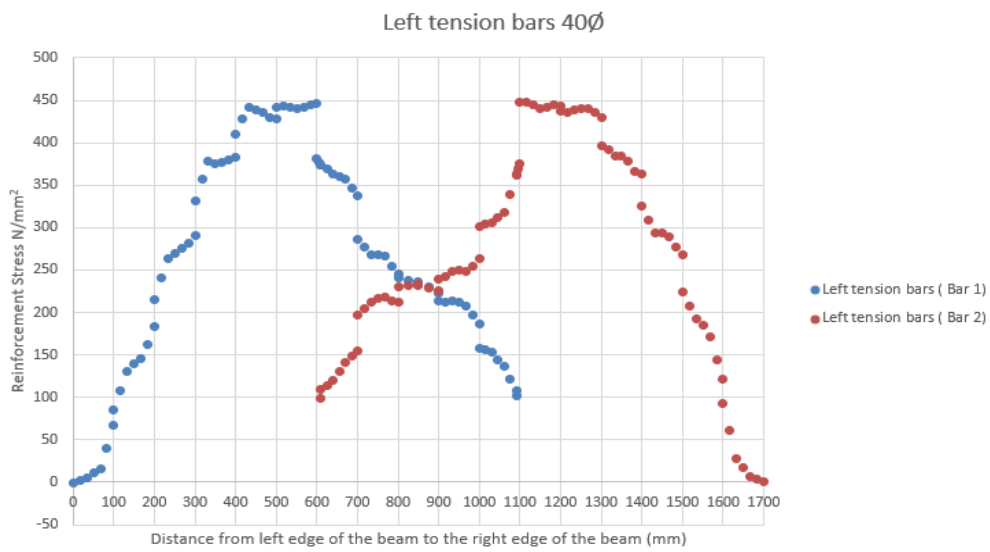


Figure 10.5. Reinforcement strain distribution sample 40Ø



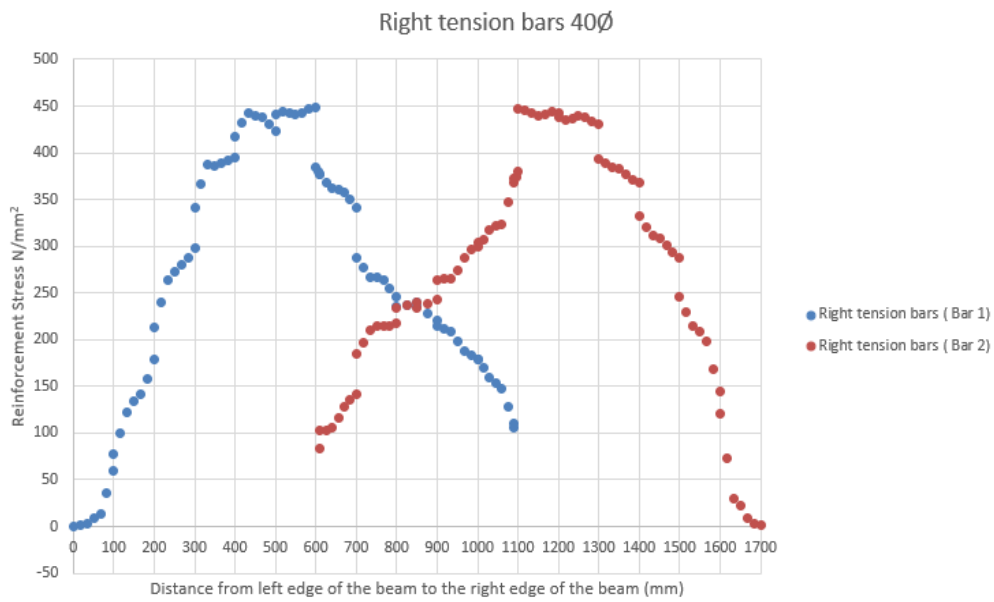
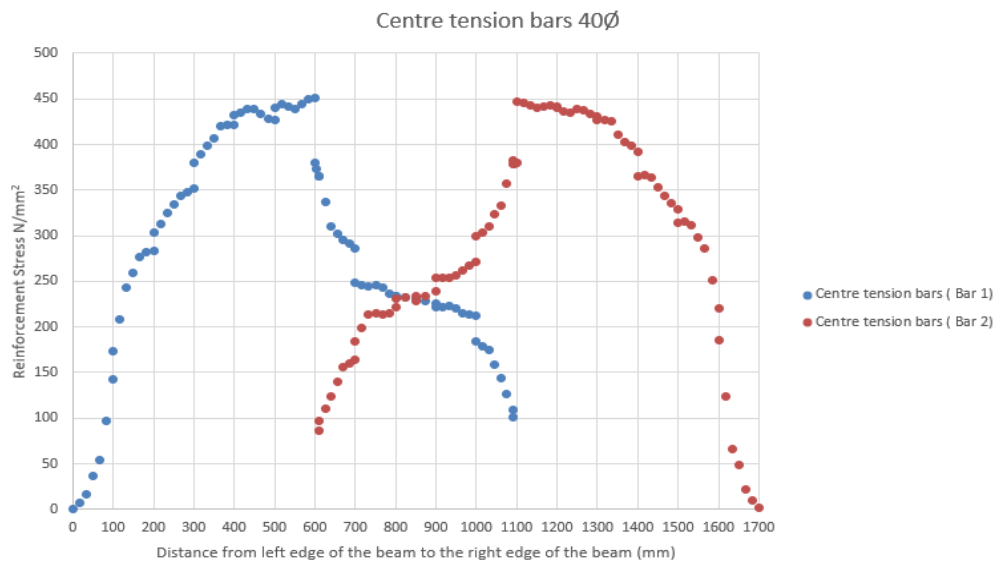


Figure 10.6. Reinforcement stress distribution sample 40Ø laps

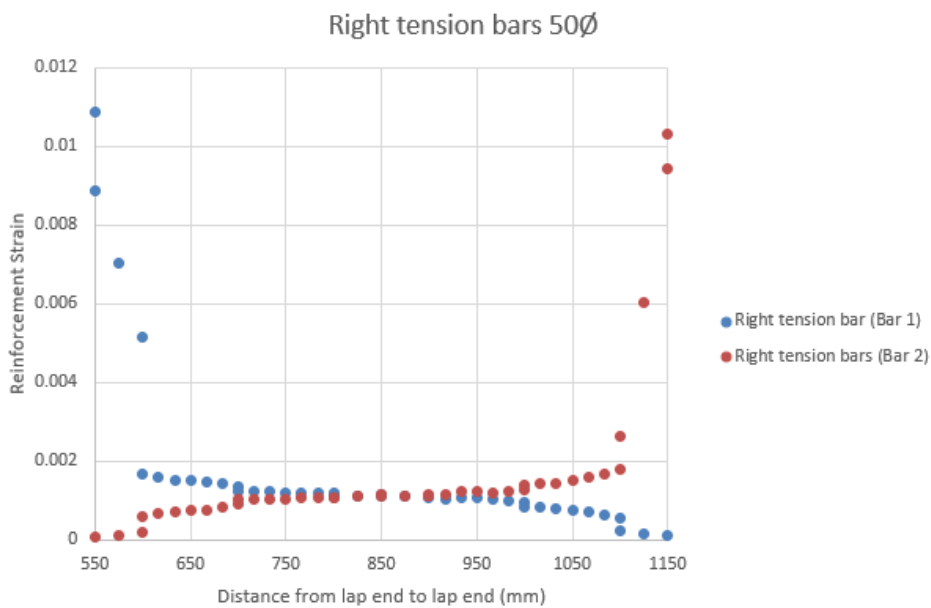
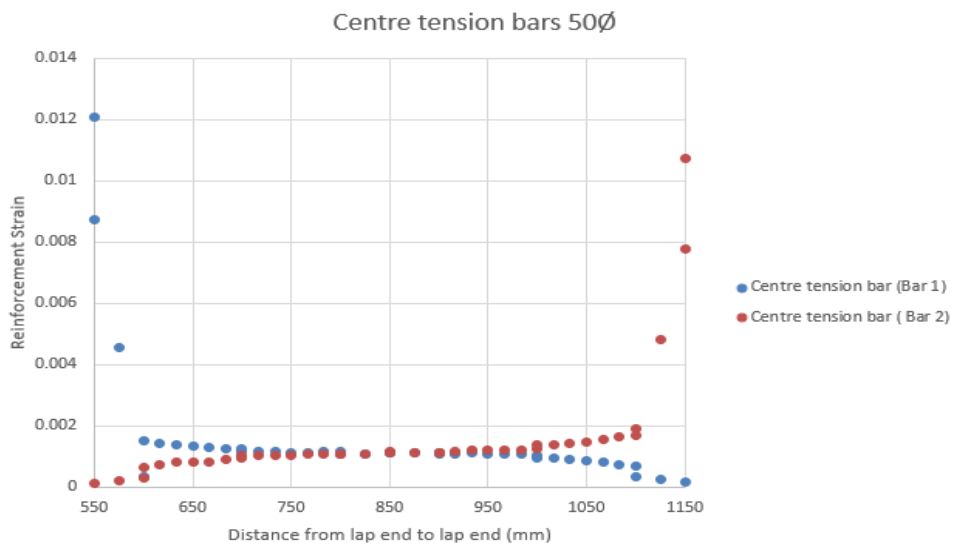
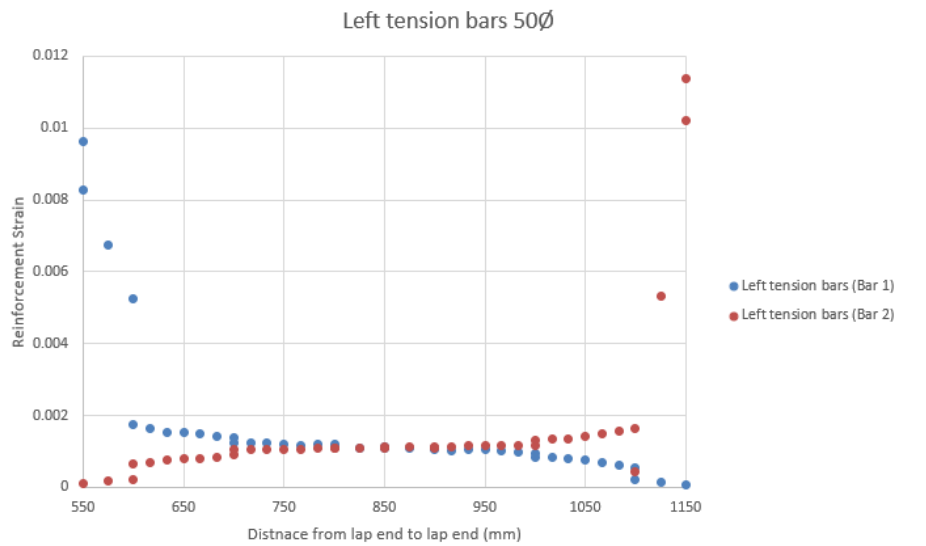


Figure 10.7. Rebar Strain Distribution Along Lap Specimen 50Ø

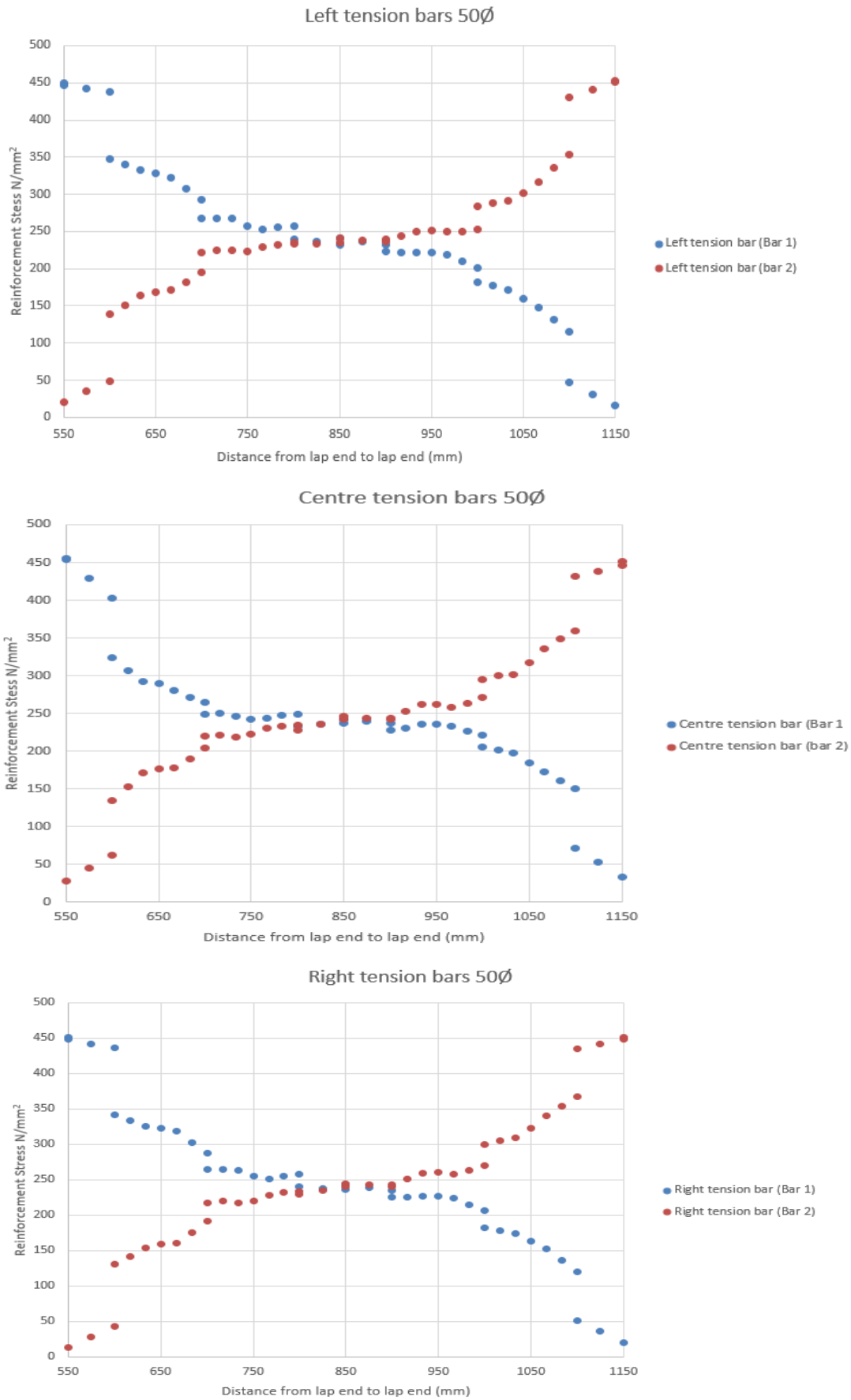


Figure 10.8. Rebar Stress Distribution Along Lap Specimen 50Ø

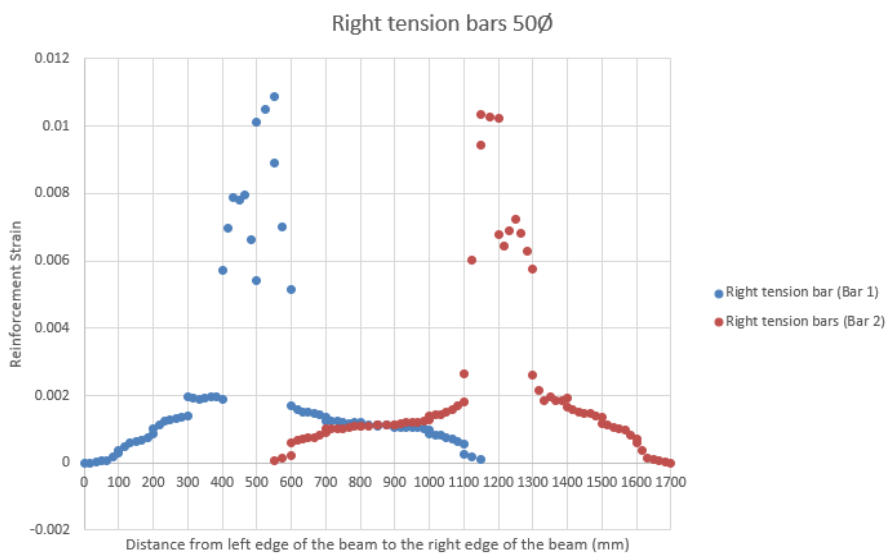
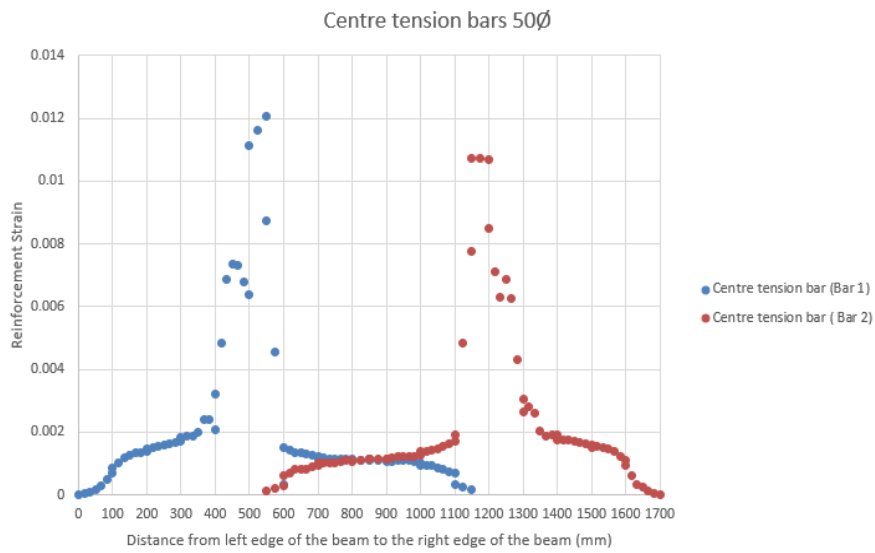
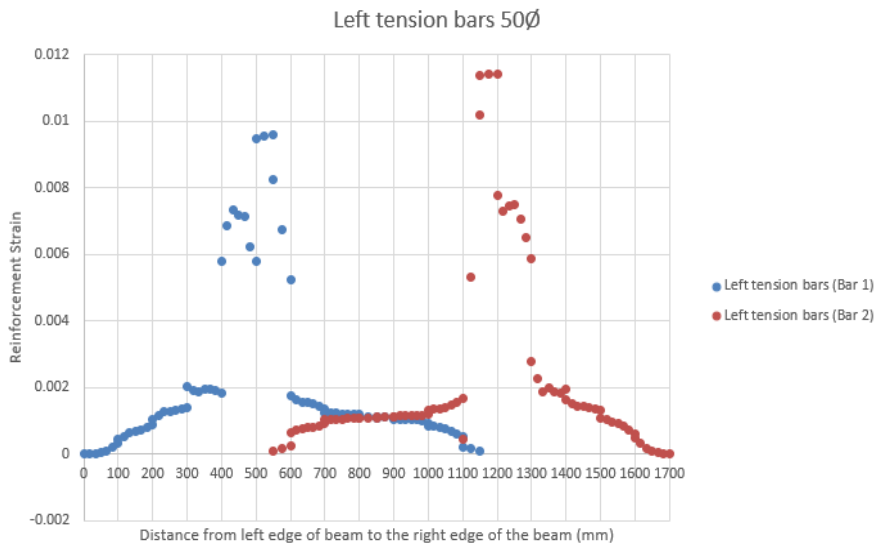
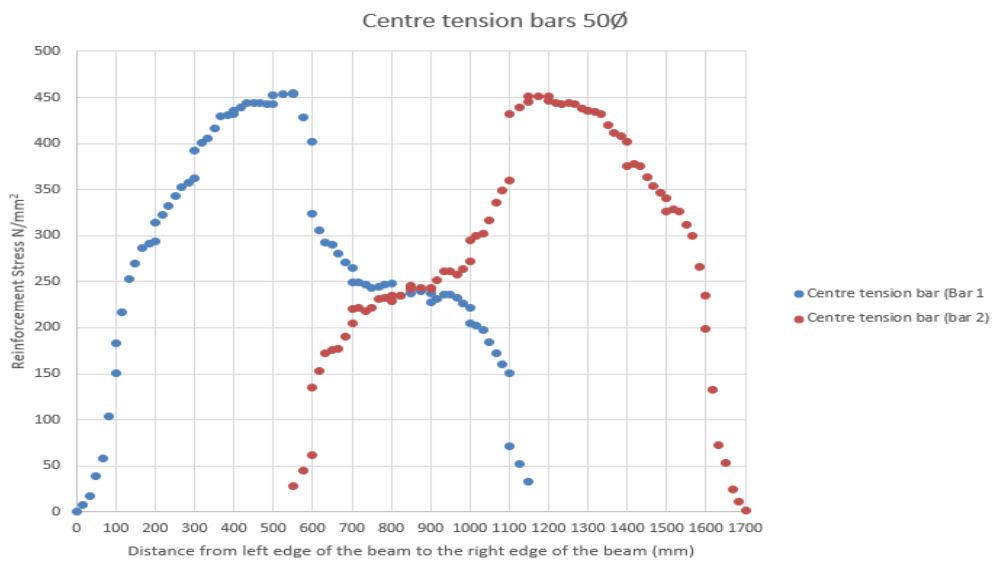
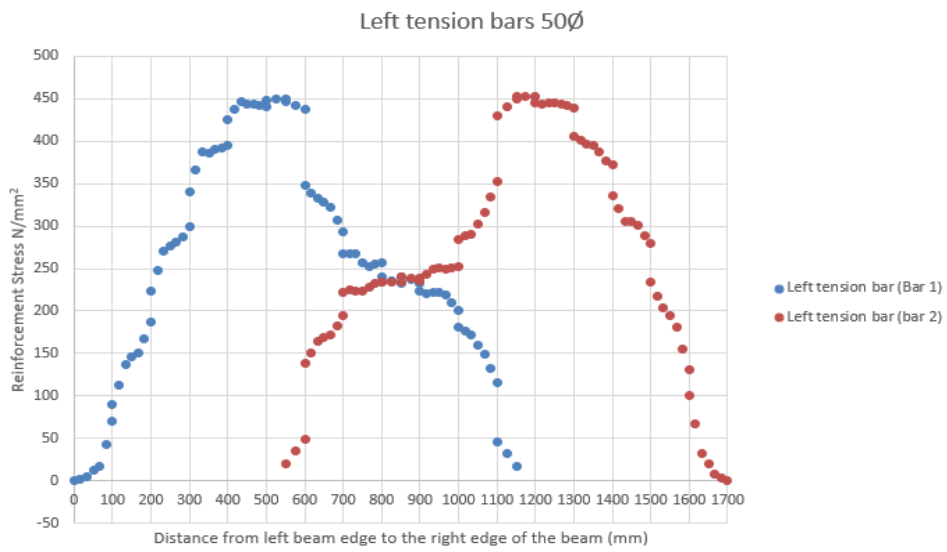


Figure 10.9. Reinforcement strain distribution sample 50Ø laps



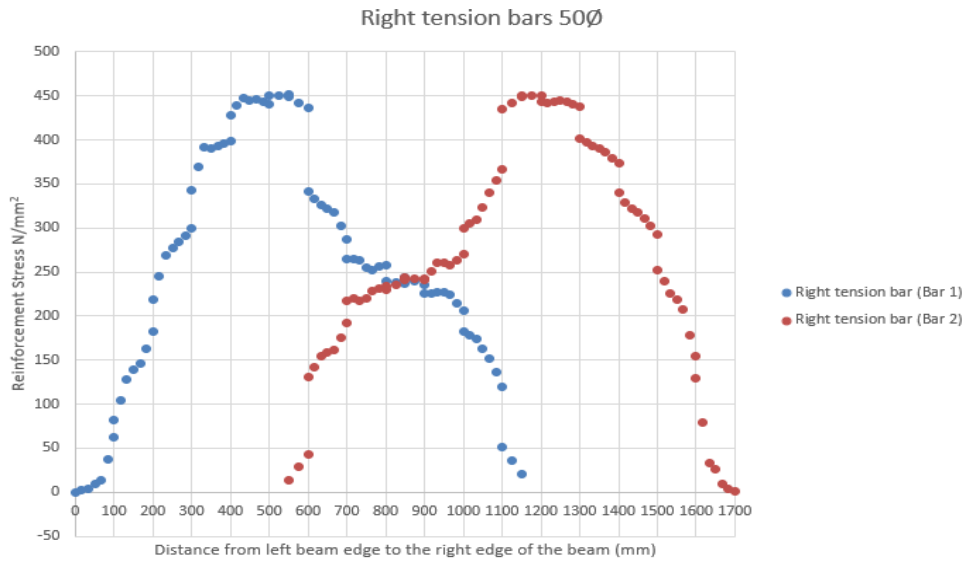
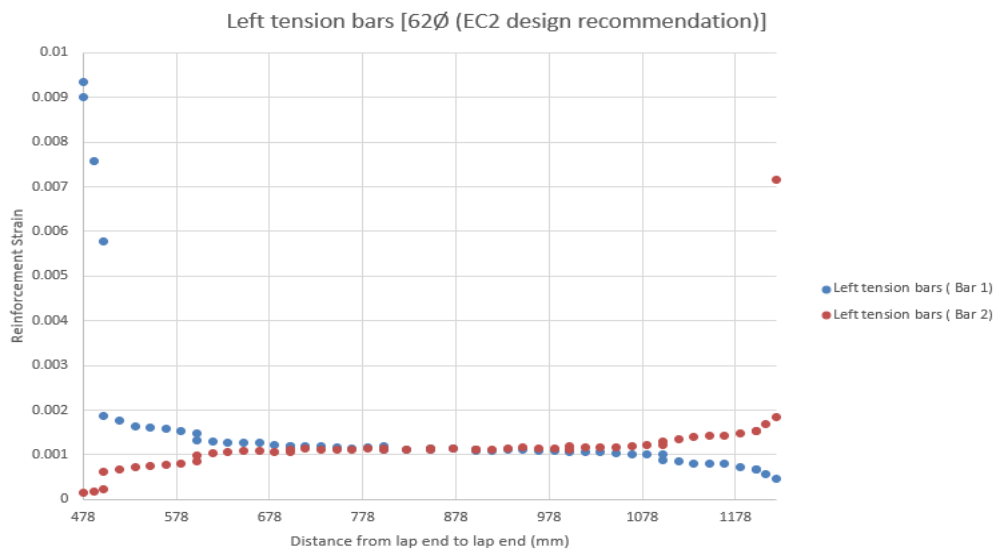


Figure 10.10. Reinforcement stress distribution sample 50Ø laps



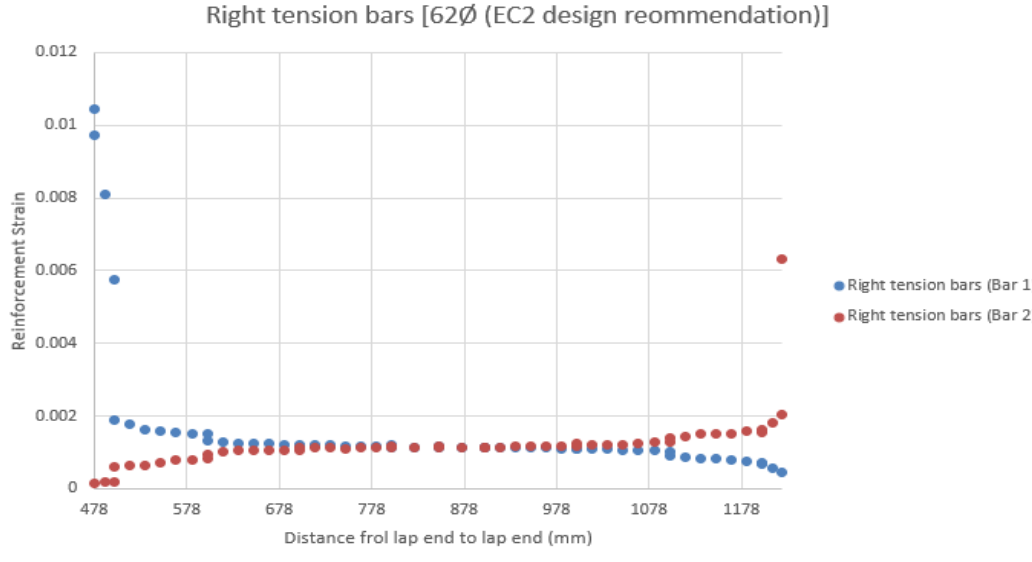
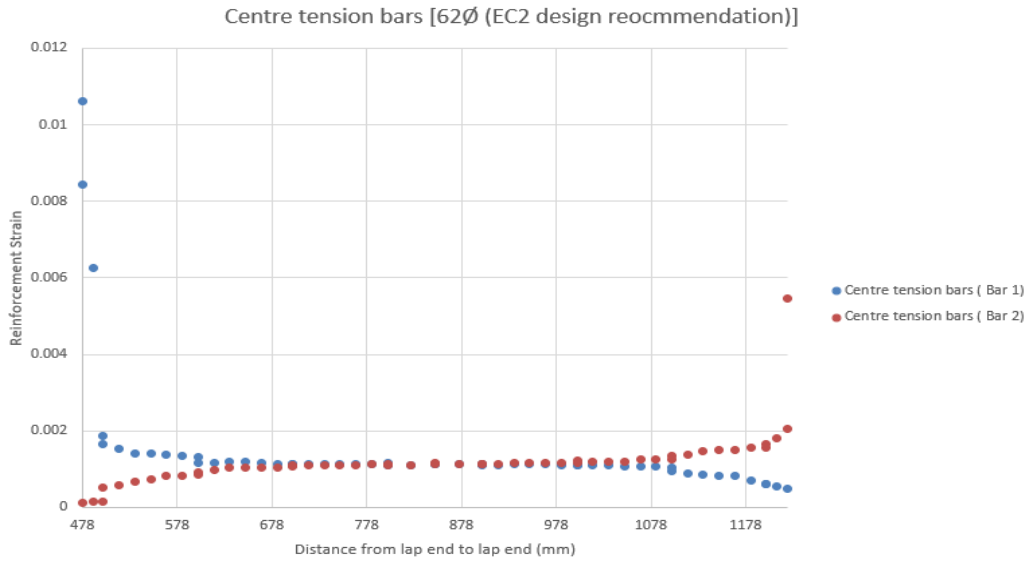


Figure 10.11. Rebar Strain Distribution Along Lap Specimen 62Ø[EC2 design recommendation]

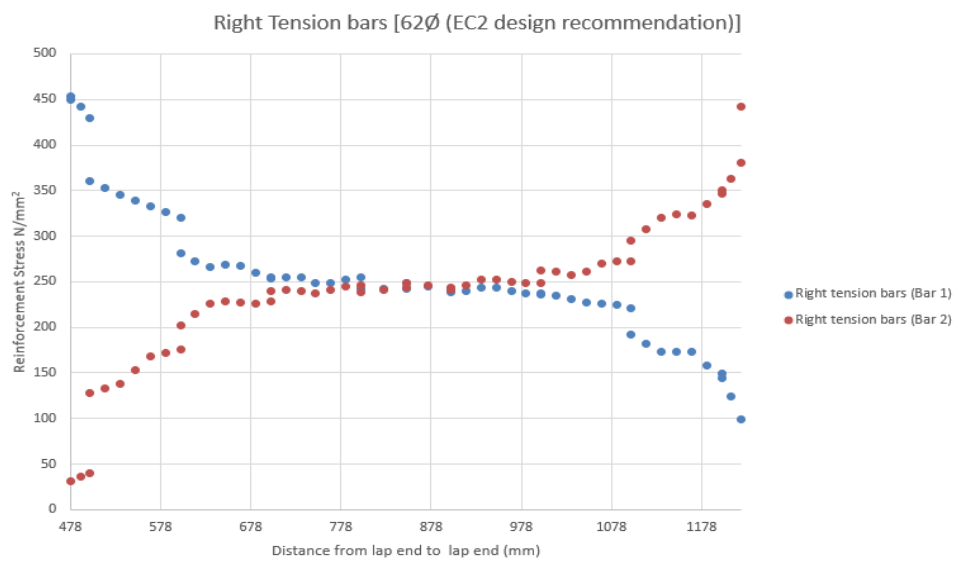
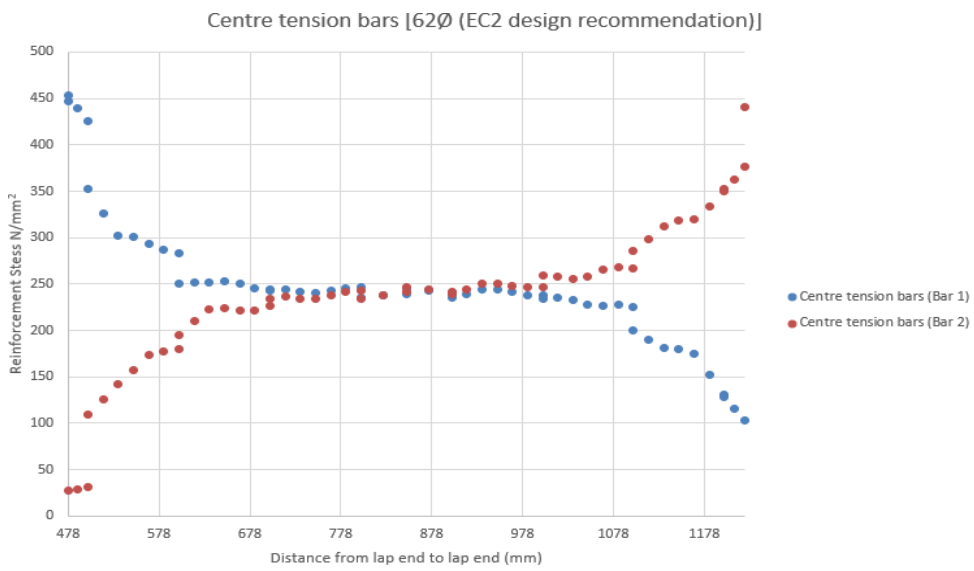
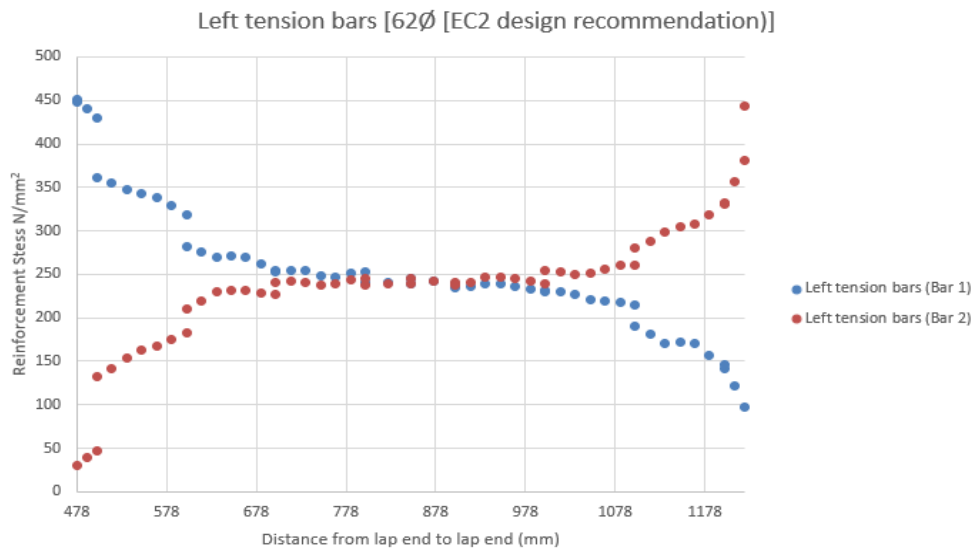


Figure 10.12. Rebar Stress Distribution Along Lap Specimen 62Ø[EC2 design recommendation]

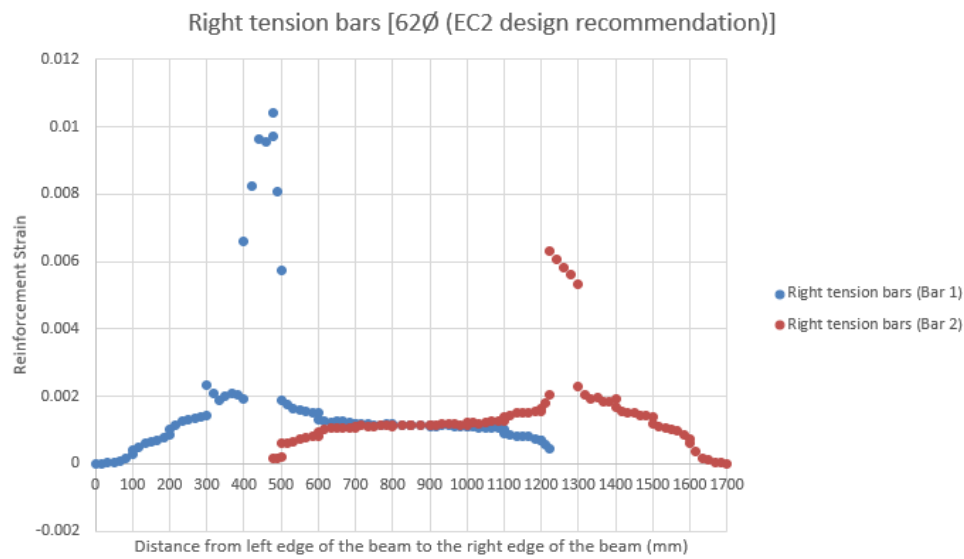
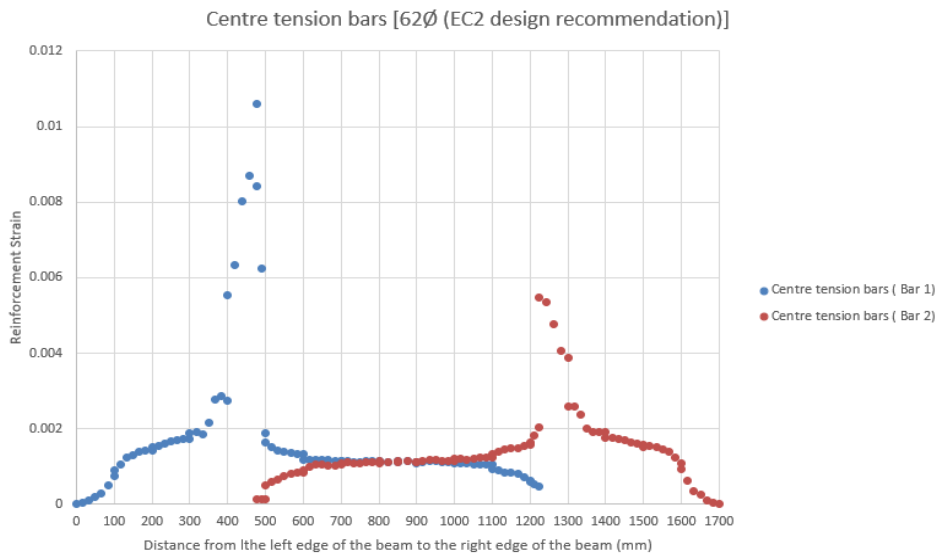
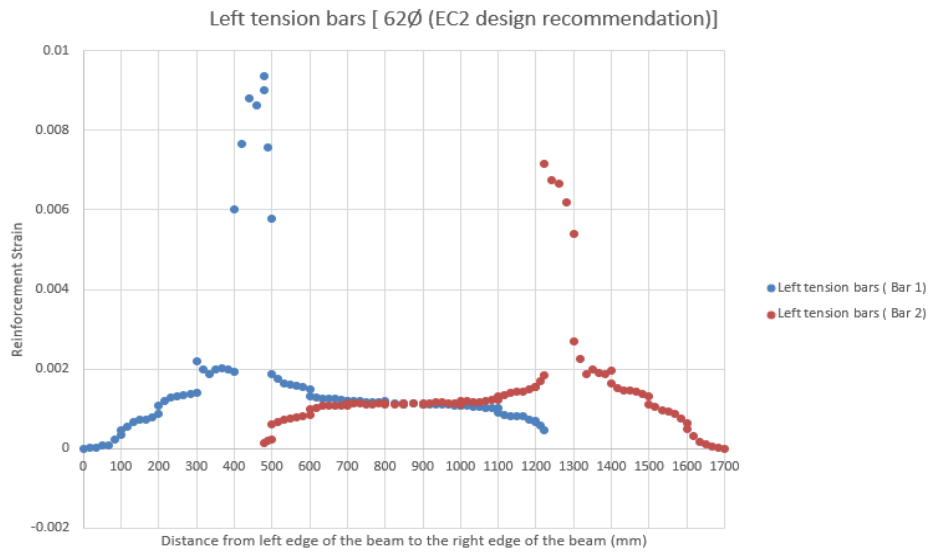


Figure 10.13. Reinforcement strain distribution sample 62Ø [EC2 design recommendation] laps

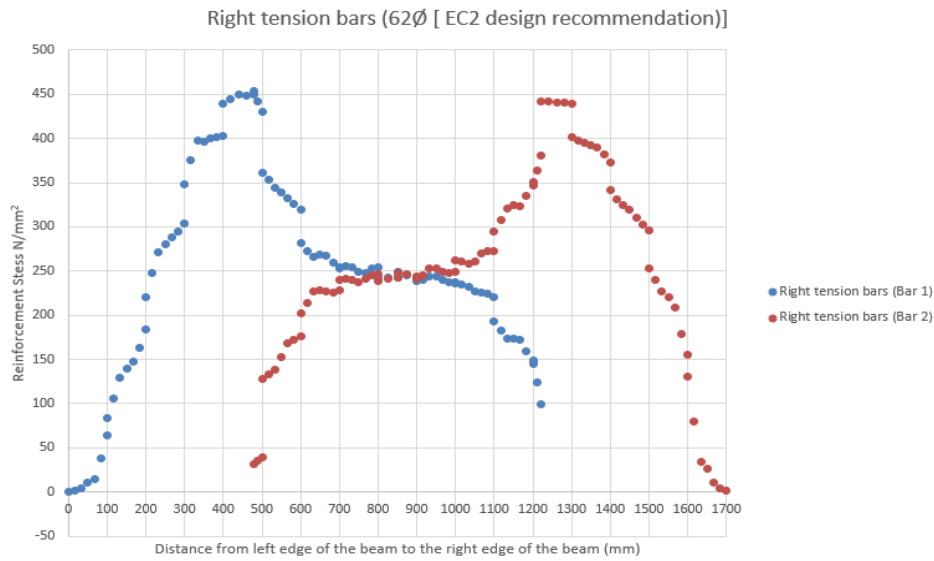
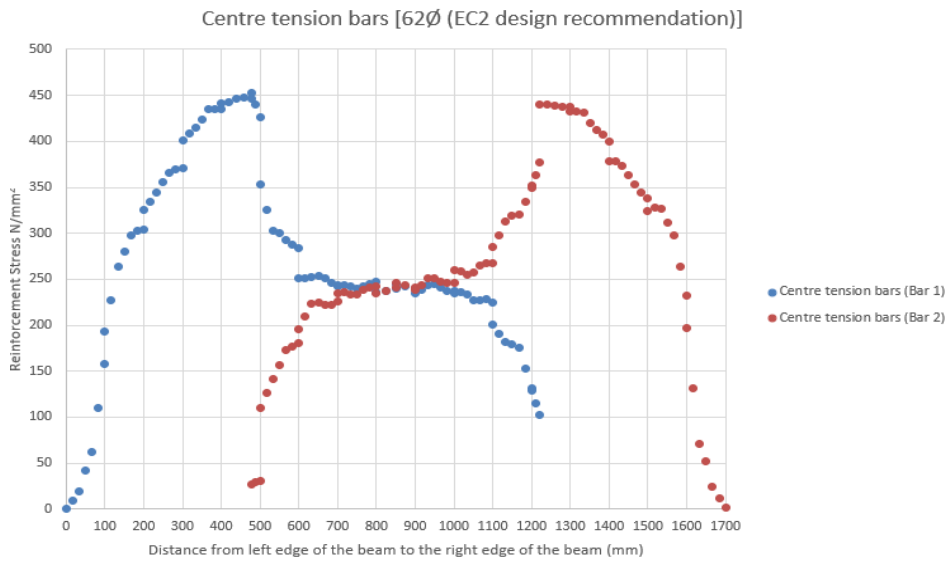
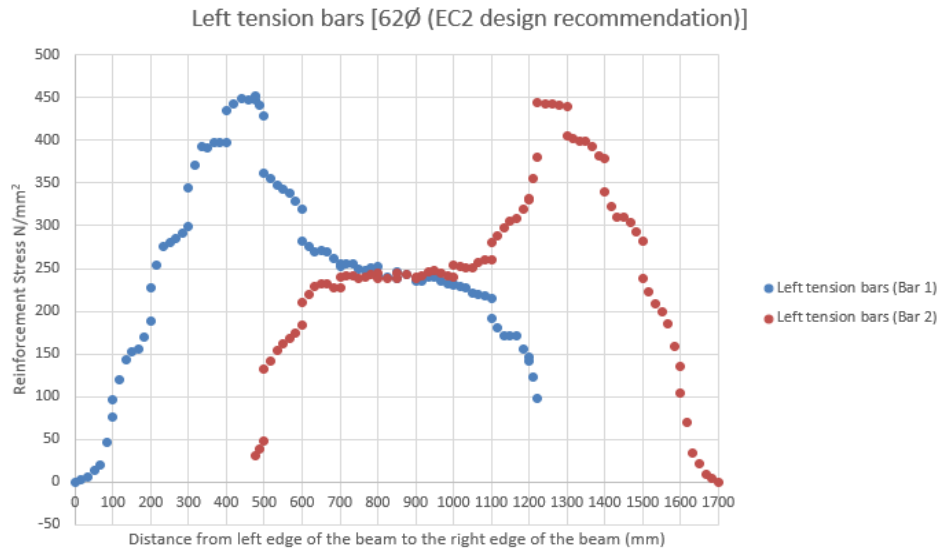


Figure 10.14. Reinforcement stress distribution sample 62Ø [EC2 design recommendation] laps

